Lanthanide Complexes as Chiral Probes Exploiting Circularly Polarized Luminescence

CARR, RACHEL

Durham University

Department of Chemistry

Lanthanide Complexes as Chiral Probes Exploiting Circularly Polarized Luminescence

Rachel Carr

A thesis submitted for the degree of Doctor of Philosophy

2014

Declaration

The work described herein was undertaken at the Department of Chemistry, Durham University between October 2010 and December 2013. All of the work is my own, except where specifically stated otherwise. No part has previously been submitted for a degree at this or any other university.

Statement of Copyright

ABSTRACT

A series of studies has been undertaken to facilitate the identification and development of chiral lanthanide complexes that are able to report on changes in their local environment through modulation of the circular polarization of their emission. Reports of such systems remain relatively rare in the literature, notwithstanding the prevalence and importance of chirality in biological systems.

The work described herein is separated into five chapters, the first of which comprises a discussion of relevant background information, along with a comprehensive review of responsive lanthanide-based CPL probes reported to date. A classification of these probes is built up, which informs the content of the following three chapters.

Chapter 2 describes work undertaken in the pursuit of a novel lanthanide-based system for use as a CPL probe for the detection of proteins. The synthesis of an enantiopure lanthanide complex was undertaken and characterisation of this system carried out with reference to a structurally related racemic complex. A series of comparative investigations designed to probe the relative protein binding capability of these complexes was subsequently performed, which revealed that the observation of induced CPL from racemic lanthanide systems may be brought about by a change in complex constitution. This is the first example of such an effect from a well-defined racemic lanthanide complex in solution. Chapter 3 goes on to detail studies undertaken to demonstrate the utility of this racemic lanthanide system as a probe for chiral detection.

Chapter 4 describes investigations carried out in an attempt to identify new systems exhibiting chiral quenching effects in solution. Initially, two pairs of enantiomeric electron-rich quenching species were assessed for their ability to quench the emission from an enantiopure DOTA-derived lanthanide complex differentially. Subsequently, investigations were focussed on examining the quenching of emission from novel enantiopure lanthanide complexes based on a 1,4,7-triazacyclononane framework, using cobalt complexes as the quenching species.

Finally, Chapter 5 contains experimental procedures for each compound synthesised, as well as general experimental procedures.

ACKNOWLEDGEMENTS

I would like to thank the following people, without whom the work presented in this thesis would not have been possible:-

My supervisor, Professor David Parker, for the wisdom he has shared, inspiration he has provided and encouragement he has offered throughout the years.

Members of the Durham analytical services teams for data they have collected on my behalf and for additional advice and assistance offered. Dr. Alan Kenwright, Catherine Heffernan, Ian McKeag and Dr. Juan Aguilar Malavia for NMR spectroscopy, Dr. Jackie Mosely, Dr. David Parker and Peter Stokes for mass spectrometry, Dr. Aileen Congreve, Dr. Ellie Hurst and Lenny Lauchlan for HPLC and Dr. Dmitry Yufit for crystal analysis.

Dr. Lars-Olof Palsson, Dr. Robert Pal and Robert Puckrin for the construction of a CPL spectrometer at Durham and Dr. Robert Peacock, at the University of Glasgow, for his assistance in collecting initial CPL spectroscopy data.

Dr Lorenzo Di Bari and Samuele Lo Piano, at the Università di Pisa, for induced CD data, and Lara Small, for her assistance in recording CD data at Durham.

Dr John Sanderson for protein structural alignment studies.

Dr Ilya Kuprov, at the University of Southampton, for DFT calculations.

Past and present members of CG27 who have ensured that the lab is a great place to work and have always been ready to share the benefit of their own experiences. Particular thanks go to Pete, Nick and Martina for their help with synthesis; Robek, Dave, James and Brian for their advice regarding luminescent titrations and Kanthi, Alex and Katie for their assistance with paramagnetic NMR spectroscopy.

My friends in Durham and further afield for their encouragement and for always being willing to lend an ear.

Dan for his love, prayers and for making me laugh.

Finally, a special thanks to my Mum, Dad and the rest of my family for their continued love and support, and for giving me the opportunity to achieve so much.

For Mum and Dad

TABLE OF CONTENTS

ABBREVIATIONS

(+)-hfbc	3-heptafluorobutyryl-(+)-camphorate
α_1-AAT	α_1-antitrypsin
α_1-AGP	α_1-acid glycoprotein
γ-Ig-G	γ-immunoglobulin-G
aq	aqueous
Arg	*L*-arginine
BET	back energy transfer
BMS	bulk magnetic susceptibility
br	broad
BSA	bovine serum albumin
CD	circular dichroism
conc.	concentrated
CPL	circularly polarized luminescence
CPZ	chlorpromazine
CSD	Cambridge Structural Database
cyclen	1,4,7,10-tetraazacyclododecane
d	doublet
dd	doublet of doublets
ddd	doublet of doublet of doublets
DFT	density functional theory
DNA	deoxyribonucleic acid
DO2A	1,7-di(carboxymethyl)-1,4,7,10-tetraazacyclododecane
DOPA	3,4,-dihydroxyphenylalanine
DOTA	1,4,7,10-tetraazacyclododecane-N',N",N"',N""-tetraacetic acid
DPA	pyridine-2,6-dicarboxylate
ECD	electronic circular dichroism
ESMS	electrospray mass spectrometry
ET	energy transfer
eT	electron transfer
EtOAc	ethyl acetate
EXSY	exchange spectroscopy
FATCAT	flexible structure alignment by chaining aligned fragment pairs allowing twists

FRET	Förster resonance energy transfer
GC	gas chromatography
Glu	*L*-glutamic acid
HBr	hydrobromic acid
HCl	hydrochloric acid
HEPES	4-(2-hydroxyethyl)-1-piperazineethanesulfonic acid
HPLC	high pressure liquid chromatography
HRMS	high resolution mass spectrometry
HSA	human serum albumin
IR	infra-red
ISC	intersystem crossing
LCMS	liquid chromatography-mass spectrometry
LMCT	ligand-to-metal charge-transfer
Ln	lanthanide
Lys	*L*-lysine
m	multiplet
MCPBA	meta-chloroperoxybenzoic acid
MDAP	mass directed auto preparation
MeCN	acetonitrile
MeOH	methanol
MOPS	3-(*N*-morpholino)propanesulfonic acid
NMR	nuclear magnetic resonance
O-P-Ser	*O*-phospho-*L*-serine
O-P-Tyr	*O*-phospho-*L*-tyrosine
PDB	Protein Data Bank
PEM	photoelastic modulator
phen	1,10-phenanthroline
PMT	photomultiplier tube
Q	quencher
QTOF	quadrupole time-of-flight
s	singlet
SAP	square antiprism
STD	saturation transfer difference
t	triplet

TFA	trifluoroacetic acid
THF	tetrahydrofuran
TL	total luminescence
TLC	thin layer chromatography
TR-CPL	time resolved circularly polarized luminescence
Tris	tris(hydroxymethyl)aminomethane
Trolox	6-hydroxy-2,5,7,8-tetramethylchroman-2-carboxylic acid
Trp	*L*-tryptophan
TSAP	twisted square antiprism
TQD	tandem quadrupole detector
UPLC	ultra performance liquid chromatography
UV	ultra-violet

CHAPTER ONE

INTRODUCTION

1.1 Overview

The word luminescence was coined in 1888 by Eilhardt Wiedemann, a German physicist[1] and can be defined as 'spontaneous emission of radiation from an electronically or vibrationally excited species not in thermal equilibrium with its environment'.[2] As such, the word luminescence is a hypernym and refers to various categories of emitted radiation, defined by the mode of excitation. The contents of this thesis focus on the discussion and demonstration of luminescence phenomena in relation to lanthanide complexes, arising specifically as a result of the absorption of photons. This is termed photoluminescence.

It should be noted at the outset that the applications of photoluminescence in science and technology are wide-ranging. For example, species which are able to absorb UV light and emit in the blue range of the visible spectrum are frequently employed as optical brighteners. Meanwhile, the use of photoluminescent inks in the printing of bank notes facilitates their authentication.[1] However, in the context of this thesis it is especially important to note that photoluminescence phenomena may also be exploited as an analytical tool. For example, luminescence imaging employs photoluminescent systems as emissive probes in the investigation of biological systems. Although many of these emissive probes act simply as cellular stains, others have been developed which are able to report on specific conditions within a cell, by modulation of their luminescence output.[3, 4] At present, the overwhelming majority of these responsive probes exploit changes in luminescence intensity or lifetime in order to report on their environment; the modulation of the circular polarization of the emitted light, otherwise known as circularly polarized luminescence (CPL), is rarely considered. The prevalence and importance of chirality in biological systems means that CPL probes could provide a rich source of information on their chiral environment that is yet to be fully exploited.

This review begins with a short discussion of CPL spectroscopy. The potential offered by luminescent lanthanide complexes in the development of chiral probes exploiting CPL is highlighted and the general principles that underpin the design of these complexes are considered. Finally, a brief consideration of the stereochemistry in representative lanthanide systems is followed by a discussion of examples of lanthanide complexes from the literature that have been found to modulate their CPL output as a response to change in their environment.

1.2 Circularly polarized luminescence

CPL spectroscopy is a technique, developed mainly in the 1970s, that is based on the measurement of the differential spontaneous emission of left and right circularly polarized light by luminescent systems.[5] As such, it is often described as the emission equivalent of circular dichroism (CD) spectroscopy, a more widespread chiroptical technique concerned with the differential absorption of left and right circularly polarized light. The two techniques are complimentary tools, which can be used to investigate the stereochemical and electronic structural properties of the emissive and ground states of luminescent systems respectively.

1.2.1 CPL spectroscopy - instrumentation

Due to the fact that CPL spectrometers have only recently become available commercially, the majority of CPL studies recorded in the literature to date have been performed using custom-built instruments, designed and developed by individual research groups.[6, 7] As is to be expected, each of these individually constructed spectrometers share common features, the most pertinent of which is the inclusion of a circular analyzer, located between the luminescent sample and the detector unit. In order to understand the function of the circular analyzer in the acquisition of CPL spectral data, it is worthwhile to first briefly recall the classical description of circularly polarized light and how it relates to light that is linearly polarized.

The classical description of light portrays it as a transverse wave with both an electric and a magnetic field component. These components oscillate in a fixed relationship to one another and are oriented perpendicular to each other and to the direction of propagation. When considering the polarization of light, it is conventional to describe only the electric field vector, which can itself be divided into two perpendicular components. It is important to note that, although these components oscillate with identical frequency, their phase and amplitude may differ. In the case of circularly polarized light, the components are of the same amplitude, but there is a phase difference that is exactly one quarter of the wavelength. Hence, when one component is zero, the other is at its maximum or minimum amplitude. Meanwhile, for linearly polarized light, the components may differ in amplitude but must be in phase.

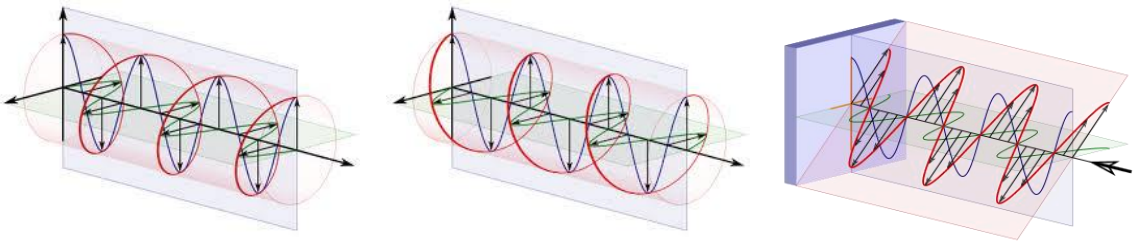

Figure 1.1: Representations of left and right circularly polarized light, shown alongside a representation of linearly polarized light. In each case, the separate components of the electric field vector are shown in blue and green. The overall evolution of the electric field vector is shown in red.

In a modern CPL spectrometer, the circular analyzer typically comprises two units, namely a photoelastic modulator (PEM) and a linear polarizer.[7] The modulator is driven, normally at a frequency of 50 kHz, such that it may act as an oscillating quarter-wave plate. On alternate cycles of the oscillation, it acts as a quarter-wave advancing and a quarter-wave retarding element, shifting the phase between the electric field vector components of the light. Hence, in accordance with the discussion above, the PEM serves to convert the left and right circularly polarized light emitted by the sample to linearly polarized light. This light is selected by the linear polarizer and may then be wavelength resolved by an emission monochromator and detected. The circular polarization of the luminescence is determined by analysis of differences in the measured intensity of the linear polarization in phase with the modulation. Although many of the first custom-built CPL spectrometers made use of a lock-in amplifier for detection, more recent instruments typically employ photon-counting detection. A schematic diagram depicting the full instrumental setup for a representative CPL spectrometer is shown in Figure 1.2.

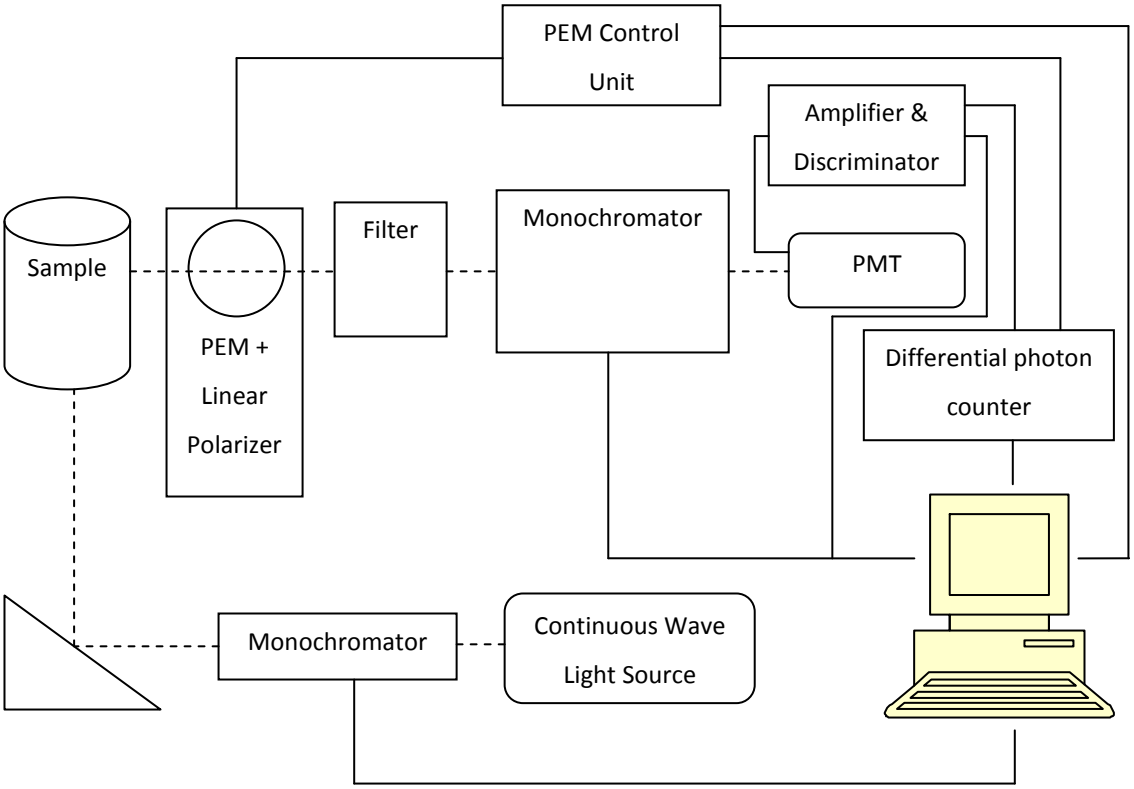

Figure 1.2: Block diagram of a custom-built CPL spectrometer. In the case of this instrument the excitation source may be an argon-ion laser, with or without a tunable dye laser, or a xenon arc lamp. The excitation monochromator is removed for laser excitation. Following conversion to linearly polarized light and wavelength resolution, the emission is detected by a photomultiplier tube (PMT), operating in photon-counting mode. Adapted from comprehensive chiroptical spectroscopy.[7]

It should be noted that variations on the basic instrumental set up described overleaf allow for a variety of less conventional and often highly informative CPL studies to be performed, many of which facilitate the observation of CPL from systems that do not have natural optical activity. For example, if a static magnetic field is applied along the direction of emission detection, then CPL may be observed from achiral luminescent species.[8] Such magnetically induced CPL has typically been used to elicit electronic structural information, rather than to acquire stereochemical information, and will not be discussed further in this review. A second adaptation, which has served to provide valuable information from systems not demonstrating natural CPL in the context of this review, is the use of circularly polarized excitation light.[9] This facilitates the study of CPL from racemic mixtures by achieving preferential excitation of one enantiomer. Provided that the rate of racemisation in the excited state is slower than the rate of emission, the emitted light will show partial circular polarization in steady-state measurements. This technique has found particular use in the verification of so-called

'outer sphere' effects leading to the induction of CPL in racemic systems, which will be discussed in Section 1.5.2.

An additional development that has proven particularly effective in the study of enantioselective quenching phenomena (Section 1.5.2.2) is the adaptation of instrumentation to facilitate the collection of time-resolved CPL spectral data.[10] This is achieved through the use of a pulsed excitation light source. Combination of the aforementioned methodologies has facilitated the study of the kinetics of excited state racemisation processes.[11, 12]

1.2.2 CPL spectroscopy - observables and parameters

Results of CPL investigations are commonly reported in terms of the emission dissymmetry factor, $g_{em}(\lambda)$, which was devised by Emeis and Oosterhoff as part of their pioneering studies into the observation of CPL from chiral molecules in solution.[13] The emission dissymmetry factor is defined using equation 1.

$$g_{\mathrm{em}}(\lambda) = \frac{2\Delta I(\lambda)}{I(\lambda)} \qquad \text{(eqn. 1)}$$

In this equation, $\Delta I(\lambda)$ is known as the emission circular intensity differential and is equal to the difference in intensities of the left and right circularly polarized components of the emitted radiation. Meanwhile, $I(\lambda)$ is the total intensity of emitted radiation and as such it is equal to the sum of its left and right circularly polarized components. Both of these quantities are observed experimentally. From equation 1 it can be deduced that the theoretical maximum value of g_{em} is ±2.

$$\Delta I(\lambda) = I_{\mathrm{L}}(\lambda) - I_{\mathrm{R}}(\lambda) \qquad \text{(eqn. 2)} \qquad\qquad I(\lambda) = I_{\mathrm{L}}(\lambda) + I_{\mathrm{R}}(\lambda) \qquad \text{(eqn. 3)}$$

For a given transition between two states, a and b, it is also possible to express the emission dissymmetry factor in terms of associated quantities. The rotatory strength, R_{ab}, of the transition is related to the sign and magnitude of the CPL associated with that transition, whilst the dipole strength, D_{ab}, is influential in determining the intensity of the total luminescence. The following equation is defined to express g_{em} in terms of these quantities.[14]

$$g_{\mathrm{em}}(\lambda) = \frac{4R_{\mathrm{ab}}}{D_{\mathrm{ab}}} \qquad \text{(eqn. 4)}$$

The rotatory and dipole strengths of the transition can in turn be expressed in terms of its magnetic and electric dipole moments, **m** and **μ**. This gives rise to another expression for g_{em}, where τ is the angle between the magnetic and electric transition dipole moments.

$$R_{ab} = \mathrm{Im}\,\boldsymbol{\mu}\,.\,\mathbf{m} \qquad \text{(eqn. 5)} \qquad\qquad D_{ab} = |\mathbf{m}|^2 + |\boldsymbol{\mu}|^2 \qquad \text{(eqn. 6)}$$

$$g_{em} = 4|\mathbf{m}||\boldsymbol{\mu}|(m^2 + \mu^2)^{-1}\cos\tau \qquad \text{(eqn. 7)}$$

Owing to the fact that magnetic dipole transition moments are typically much smaller than their electric dipole counterparts, the μ^2 term tends to dominate this expression, meaning it can be simplified further to give equation 8.

$$g_{em} = \frac{4|\mathbf{m}|}{|\boldsymbol{\mu}|}\cos\tau \qquad \text{(eqn. 8)}$$

Generally speaking, transitions which are electric dipole allowed and magnetic dipole forbidden will be associated with small values of g_{em}, whilst magnetic dipole allowed and electric dipole forbidden transitions will have the highest values of g_{em}.

1.2.3 Systems exhibiting CPL

As was previously mentioned, the first observations of CPL from chiral molecules in solution were made by Emeis and Oosterhoff in the late 1960s and early 1970s. In these experiments, the separated enantiomers of *trans-β*-hydrindanone and *trans-β*-thiohydrindanone were investigated, with results demonstrating the potential utility of CPL as a structural probe of emissive states.[15] Subsequent studies have demonstrated the observation of CPL for a variety of chiral molecules in solution, including organic systems, biomolecules and inorganic metal complexes.[16]

Generally speaking, it is apparent from the literature that CPL phenomena are best exemplified by chiral lanthanide complexes. These complexes not only act as pure spherical emitters, eliminating issues associated with anisotropy, but also tend to exhibit the highest values of g_{em}, typically two orders of magnitude greater than those observed for organic systems. In spite of this, it is worth highlighting one particular recent report of CPL in an organic system, before going on to discuss typical luminescence characteristics of lanthanide complexes and general principles underpinning their design.

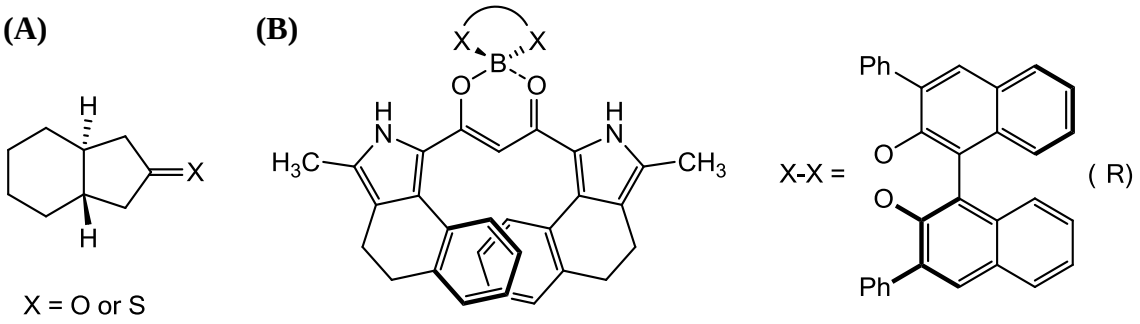

Figure 1.3: (A) *trans-β*-hydrindanone and *trans-β*-thiohydrindanone (*S*,*S*) enantiomer shown, **(B)** π-conjugated anion receptor.

The *π*-conjugated molecule depicted in Figure 1.3 has been shown to possess anion binding capabilities, which were recently demonstrated for both chloride and acetate.[17] With respect to anion-responsive chiroptical properties in particular, it was found that the circular polarization of the emission associated with the π-π^* transition of this molecule, occurring between roughly 500 and 600 nm, was increased significantly in the presence of both chloride and acetate. Whilst emission dissymmetry factors determined in the absence of either of these anions were negligible, values of around 4 x 10^{-3} were recorded in their presence.[18] The low values of g_{em} observed may be ascribed to a lack of magnetic dipole character in the π-π^* transition. It was suggested that the observed changes in the circularly polarized emission could be attributed to conformational changes of the *π*-conjugated system, induced by anion binding.

Although results such as those outlined in the preceding paragraph are noteworthy when considering systems exhibiting CPL, the authors' claim that the system described above is 'the first example of chemical-stimuli-responsive CPL properties'[17] is somewhat exaggerated. As will be demonstrated in Section 1.5 of this review, there exist several examples of lanthanide-based systems exhibiting such an effect.

1.3 Luminescent lanthanide complexes

When considering the design of chiral probes exploiting CPL as a signalling mechanism, there are a number of additional features of lanthanide luminescence which make the complexes of these ions particularly attractive. These features will be considered in the following sections of this review, which will also outline basic considerations in the design of emissive lanthanide complexes. It should be noted that, in the synthesis of lanthanide complexes for use as chiral probes exploiting CPL, particular concern should be given to maximising the emission quantum yield, Φ, i.e.

the ratio of the number of photons emitted by lanthanide luminescence to the number of photons absorbed. This is because the extent of circular polarization in the overall emission will always be small, so the observed signal must be maximised if such probes are to find use in biological systems.

1.3.1 Lanthanide ion luminescence

Excluding ytterbium and to some extent europium, the emission spectra of lanthanide complexes are characterised by sharp emission bands occurring at wavelengths virtually independent of the coordination environment. In addition, lanthanide luminescence is long-lived, with typical emission lifetimes falling in the micro- to millisecond range. This second feature facilitates the use of time-gated detection methods, which incorporate a delay between the excitation pulse and the measurement of lanthanide luminescence.[19] The use of these methods increases detection sensitivity and lowers detection limits, by generating images that are devoid of shorter-lived background fluorescence, with an improved signal-to-noise ratio.

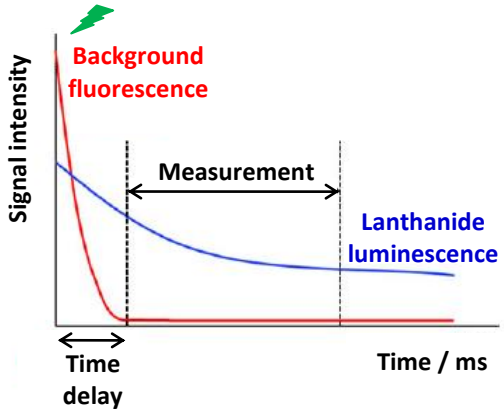

Figure 1.4: Illustration of the principle of a time-gated detection method.[19]

The intriguing luminescent properties offered by lanthanide ions may be extremely advantageous in the pursuit of chiral systems as responsive CPL probes. An explanation of these properties can be obtained by considering the electronic transitions to which the emission is attributed. Lanthanide ions show a distinct preference for the +3 oxidation state when in solution, with the energy expended in the removal of an f electron being offset by additional stabilisation associated with interactions of the triply charged ions.[20] It is apparent from consideration of the valence electronic configurations of the lanthanide ions in this oxidation state, shown in Table 1.1, that the observation of luminescence from lanthanide ion complexes results from the occurrence of 4f-4f intraconfigurational transitions. Hence, the appearance of the emission as sharp bands

may be attributed to the fact that the 4f shell is shielded by the filled 5s and 5p shells. This means that the energy levels of the $4f^n$ electronic configurations are largely unaffected by the ligand field. Meanwhile, the fact that intraconfigurational transitions are formally Laporte forbidden explains their long emission lifetimes. It should be noted that an additional consequence of this fact is that the transitions have low oscillator strengths. This will be discussed further in Section 1.3.3.

Table 1.1: Ground state valence electronic configurations of the lanthanide atoms and their ions. The Xenon core, [Xe], corresponds to $1s^2 2s^2 2p^6 3s^2 3p^6 3d^{10} 4s^2 4p^6 4d^{10} 5s^2 5p^6$.[20]

Atomic number	Name	Symbol	Valence configuration of element	Valence configuration of Ln^{III}
57	Lanthanum	La	$[Xe]5d^1 6s^2$	[Xe]
58	Cerium	Ce	$[Xe]4f^1 5d^1 6s^2$	$[Xe]4f^1$
59	Praseodymium	Pr	$[Xe]4f^3 6s^2$	$[Xe]4f^2$
60	Neodymium	Nd	$[Xe]4f^4 6s^2$	$[Xe]4f^3$
61	Promethium	Pm	$[Xe]4f^5 6s^2$	$[Xe]4f^4$
62	Samarium	Sm	$[Xe]4f^6 6s^2$	$[Xe]4f^5$
63	Europium	Eu	$[Xe]4f^7 6s^2$	$[Xe]4f^6$
64	Gadolinium	Gd	$[Xe]4f^7 5d^1 6s^2$	$[Xe]4f^7$
65	Terbium	Tb	$[Xe]4f^9 6s^2$	$[Xe]4f^8$
66	Dysprosium	Dy	$[Xe]4f^{10} 6s^2$	$[Xe]4f^9$
67	Holmium	Ho	$[Xe]4f^{11} 6s^2$	$[Xe]4f^{10}$
68	Erbium	Er	$[Xe]4f^{12} 6s^2$	$[Xe]4f^{11}$
69	Thulium	Tm	$[Xe]4f^{13} 6s^2$	$[Xe]4f^{12}$
70	Ytterbium	Yb	$[Xe]4f^{14} 6s^2$	$[Xe]4f^{13}$
71	Lutetium	Lu	$[Xe]4f^{14} 5d^1 6s^2$	$[Xe]4f^{14}$

Each lanthanide ion has a large number of electronic energy levels due to splitting of the $4f^n$ electronic configurations, primarily as a result of spin-orbit coupling.[21] These electronic energy levels may be represented in the form of term symbols, ${}^{2S+1}L_J$, derived using the Russell-Saunders coupling scheme. Here, $2S+1$ represents the multiplicity of the term, meanwhile L indicates the total orbital angular momentum quantum number and J the total angular momentum quantum number.[22] A partial energy level diagram for the lanthanide aqua ions is shown in Figure 1.5. The characteristic bands observed in lanthanide emission spectra can be attributed to transitions from the emissive state to the various electronic energy levels within the ground state manifold.

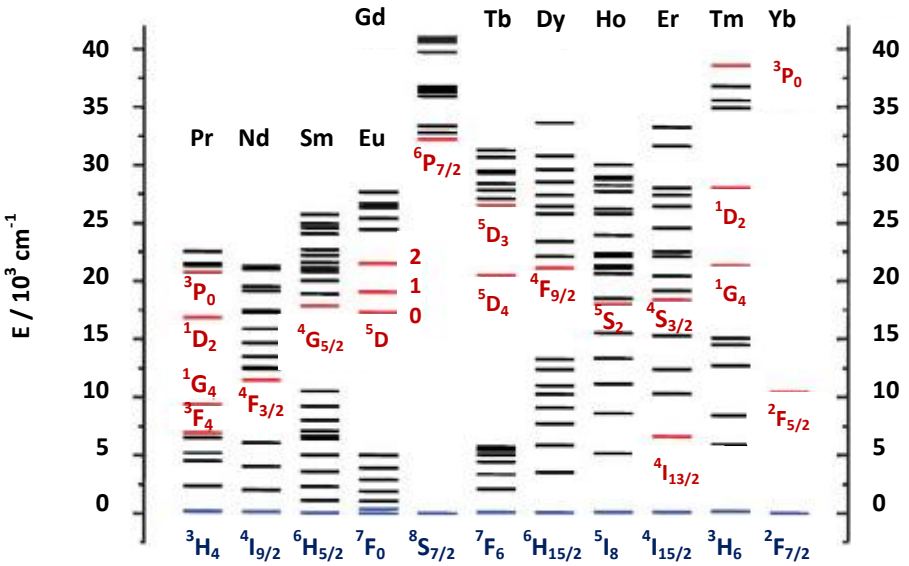

Figure 1.5: Partial energy level diagram for the lanthanide aqua ions showing emissive levels in red.[23]

With the exception of lanthanum and lutetium, which have no possible f-f transitions, all of the lanthanide ions are luminescent. For each of the emissive lanthanide ions, the efficiency of luminescence is indicated by its intrinsic quantum yield, Φ^{Ln}, which may be thought of as the quantum yield that would result from direct excitation of the lanthanide ion.[23] This can be defined by comparing the rate constant of radiative decay of the lanthanide ion, k_r, to the rate constants for all possible deactivation pathways, with k_{nr} denoting non-radiative processes.

$$\Phi^{Ln} = \frac{k_r}{k_r + k_{nr}} \qquad \text{(eqn. 9)}$$

For lanthanide luminescence, the intrinsic quantum yield is highly dependent on the energy gap between the emissive state and the highest lying electronic energy level of the ground state manifold.[23] A smaller gap will facilitate non-radiative deactivation processes, including coupling to solvent vibrational modes. It is clear from Figure 1.5 that the largest energy gaps are seen for Eu^{III}, Gd^{III} and Tb^{III}. The energy gaps for Eu^{III} and Tb^{III} are 12,300 ($^5D_0 \rightarrow {}^7F_6$) and 14,800 ($^5D_4 \rightarrow {}^7F_0$) cm^{-1} respectively, corresponding to emission in the visible region of the spectrum.[23] Meanwhile, the energy gap for Gd^{III} is much larger and corresponds to emission in the UV region of the spectrum. As was previously mentioned, when designing lanthanide complexes for use as chiral probes exploiting CPL, it is highly desirable to maximise the overall quantum yield of emission. Hence, the above analysis distinguishes Eu^{III} and Tb^{III} as the best ions to use in applications such as these.

1.3.2 Features of europium and terbium emission

As is the case for all of the luminescent lanthanide ions, the emission spectra of europium and terbium complexes are composed of a series of sharp bands, corresponding to electronic transitions from the emissive state to the various possible energy levels of the ground manifold. In the case of europium, the commonly observed bands are due to the $^5D_0 \rightarrow {}^7F_J$ (J = 0 - 4) transitions, with the emissive state lying at roughly 17,200 cm^{-1}.[24] Meanwhile for terbium the emissive state is $^5D_4$ and lies at 20,400 cm^{-1}, the bands are due to the $^5D_4 \rightarrow {}^7F_J$ (J = 6 - 3) transitions. It should be noted that the transitions are often referred to by the associated change in the total angular momentum quantum number, J.

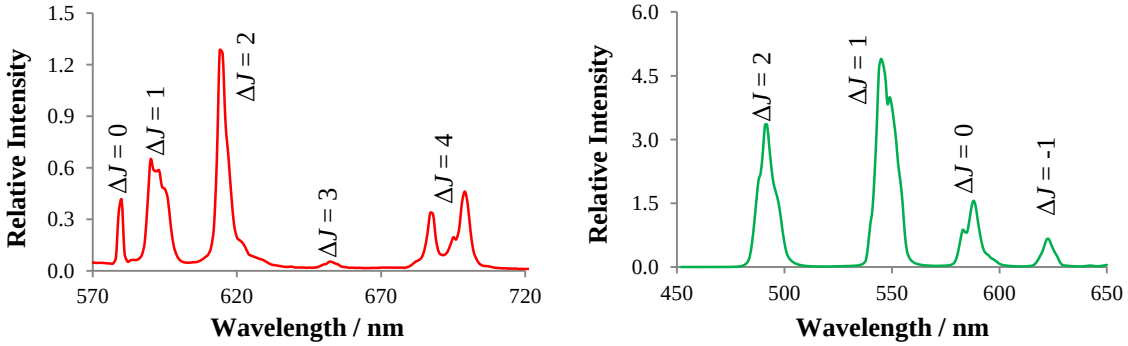

Figure 1.6: Representative emission spectra for europium (left) and terbium (right) complexes in aqueous solution.

As is apparent from Figure 1.6, fine structure can arise within each emission band due to the weak influence of the ligand environment.[25] This fine structure is particularly evident for complexes of europium, due to the fact that the emissive $^5D_0$ state is non-degenerate and cannot be split by the ligand field.[26] This means that the number of possible transitions within a band is limited to $2J$+1, where J is the total angular momentum of the electronic energy level to which the transition is occurring. Hence, analysis of the ΔJ = 0 band ($^5D_0 \rightarrow {}^7F_0$ transition) of a europium emission spectrum can be used to diagnose the presence of more than one chemically distinct europium-containing species in solution, provided they are not undergoing exchange on the emission timescale. The general characteristics of emission spectra for europium and terbium complexes in aqueous solution are summarised in Table 1.2.

Table 1.2: Transitions from the emissive states of europium and terbium.[27]

Transition		Spectral region (nm)	Relative intensity	Comments
Terbium				
$^5D_4$	$\rightarrow {}^7F_6$	485-500	Medium-strong	Moderate sensitivity to ligand environment
	$\rightarrow {}^7F_5$	540-555	Strongest	Best probe transition
	$\rightarrow {}^7F_4$	580-595	Medium	Moderate sensitivity to ligand environment
	$\rightarrow {}^7F_3$	615-625	Medium-weak	Some structure under high resolution
Europium				
$^5D_0$	$\rightarrow {}^7F_0$	578-580	Weak	Non-degenerate, appears as a single sharp line
	$\rightarrow {}^7F_1$	585-600	Strong	Sharp and structured under high resolution; up to 3 transitions observed
	$\rightarrow {}^7F_2$	610-630	Strong	Exhibits *hypersensitivity* to ligand environment
	$\rightarrow {}^7F_3$	645-660	Weak	Strictly forbidden, always very weak
	$\rightarrow {}^7F_4$	680-705	Weak	Exhibits *hypersensitivity* to ligand environment

As is highlighted in Table 1.2, an additional characteristic of europium luminescence is the apparent high sensitivity of certain emission bands to the local environment. For a given europium complex, variations in the coordination environment of the metal ion typically lead to changes in the form and relative intensity of the electric-dipole allowed $\Delta J = 2$ and $\Delta J = 4$ bands, which are described as being hypersensitive. This sensitivity has been exploited in the development of a number of europium-based probes for ratiometric analyses, where the ratio of emission intensity for one or more pairs of spectral bands is monitored in order to deduce information about the local environment. Ratiometric measurements are typically more reliable than those of total intensity, as they are independent of probe concentration, meaning results are unaffected by factors such as uneven distribution or susceptibility to photobleaching and quenching.[28]

For europium complexes derived from a ligand framework based on 1,4,7,10-tetraazacyclododecane (cyclen), the structure of which will be discussed in Section 1.4.2 of this review, particular sensitivity in the emission spectral form has been linked to changes in the nature and polarizability of the axial donor.[29, 30] The complex $[Eu.\mathbf{L^1}]^-$, which was developed as a ratiometric sensor for monitoring changes in intracellular pH, serves to illustrate this.[31] For this complex, an intense transition was observed at 680 nm in the emission spectrum obtained at pH 8, the relative intensity of which decreased as the pH was lowered. Overall, an 80% change in the ratio of the emission at 680 nm

compared to that at 587 nm was observed when the pH was varied from 4.5 to 8. In accordance with these results, it was postulated that this band could be attributed to axial N ligation at high pH.

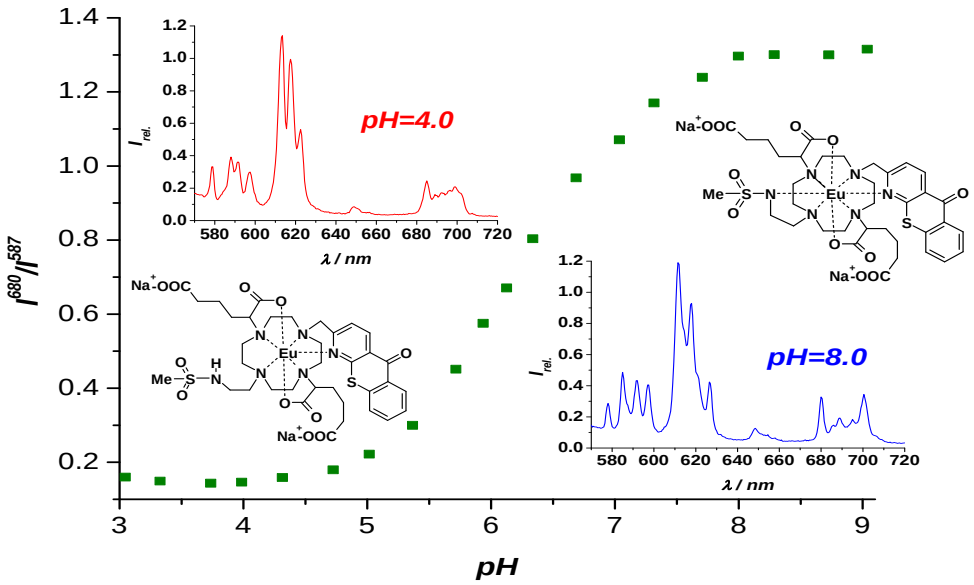

Figure 1.7: Plot of the intensity ratio vs. pH for [Eu.**L**^{1}]$^-$ (295 K, 0.1 M NaCl). The structures of the europium species at the limiting ratios are highlighted, along with their emission spectra.[31]

As is to be expected, the characteristics of the circularly polarized emission of europium and terbium complexes are broadly similar to those of the total emission. However, it should be noted that in many cases CPL is effective in providing spectral simplification within bands. One reason for this is because the polarization of adjacent transitions may differ, thus allowing them to be distinguished more easily. The total emission and CPL spectra of [Eu.**L**^{2}] (Figure 1.8) serve to illustrate this point, with the resolution of the $\Delta J = 3$ and $\Delta J = 4$ bands being particularly clear in the CPL spectrum.[32]

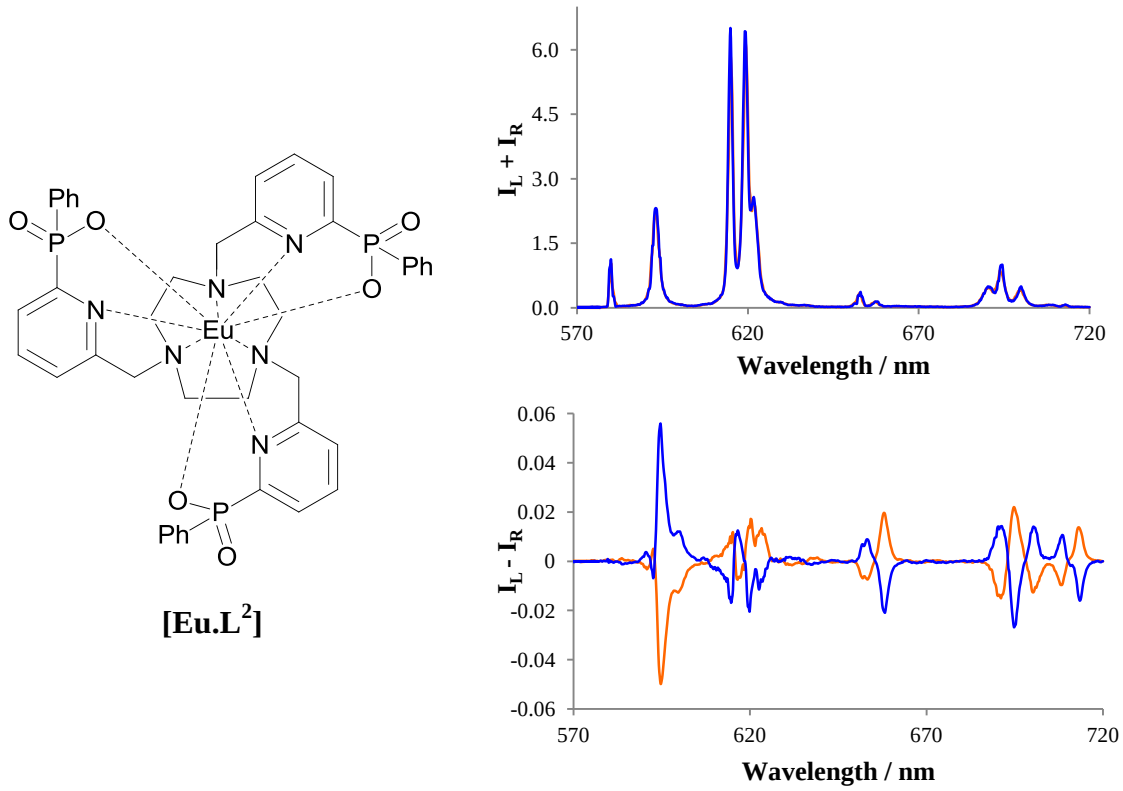

Figure 1.8: The structure of [Eu.**L**^{2}] is shown alongside total emission (top) and CPL (bottom) spectra recorded for its Δ (blue) and Λ (orange) enantiomers in aqueous MeOH (295 K).[32]

When considering CPL spectra of europium and terbium complexes, it is apparent that certain transitions tend to be associated with higher emission dissymmetry factors than others.[33] This observation can be explained fairly easily if the relationships outlined in Section 1.2.2 are taken into consideration. The analysis presented in this section leads to the deduction that transitions which are magnetic dipole allowed and electric dipole forbidden will have the highest values of g_{em}. On the basis of the first part of this statement, it can be deduced that for europium complexes the $^5D_0 \rightarrow {}^7F_1$ transition is expected to be associated with the largest value of g_{em}. Similarly, for terbium complexes the largest values of g_{em} are anticipated for the $^5D_4 \rightarrow {}^7F_J$ (J = 5 - 3) transitions. This is because these are the transitions which do not break the formal selection rules relating to the total angular momentum quantum number, J (i.e. $\Delta J = 0, \pm 1$ excluding $0 \leftrightarrow 0$), and are therefore magnetic dipole allowed. It should be noted that in practice g_{em} values for the $^5D_4 \rightarrow {}^7F_5$ transition of terbium complexes at around 545 nm are commonly found to be significantly greater than those associated with the other magnetic dipole allowed transitions.[33]

1.3.3 Sensitised emission

For the emission discussed in the preceding sections to occur, it is first necessary to promote the lanthanide ion to an excited state. The Laporte forbidden nature of the 4f-4f transitions means that their associated molar absorption coefficients are very low (~ 5 - 10 $M^{-1}cm^{-1}$) and direct excitation does not lead to efficient population of the lanthanide excited states.[34] This issue is typically overcome by designing complexes such that indirect excitation of the lanthanide ion may be achieved *via* a sensitising chromophore. This 'antenna effect' was discovered in 1942 by Weissman, who noted that, for certain compounds, europium luminescence could be observed following irradiation with light that was only absorbed by the organic constituents.[35]

An advantage associated with the use of sensitised emission is that there is a large Stokes' shift between the absorption of the sensitiser and the lanthanide luminescence. This can aid in distinguishing the lanthanide emission from background fluorescence and means there are no problems associated with concentration dependent self-absorption. The key processes involved in the sensitisation pathway may be illustrated with a Jablonski diagram (Figure 1.9).

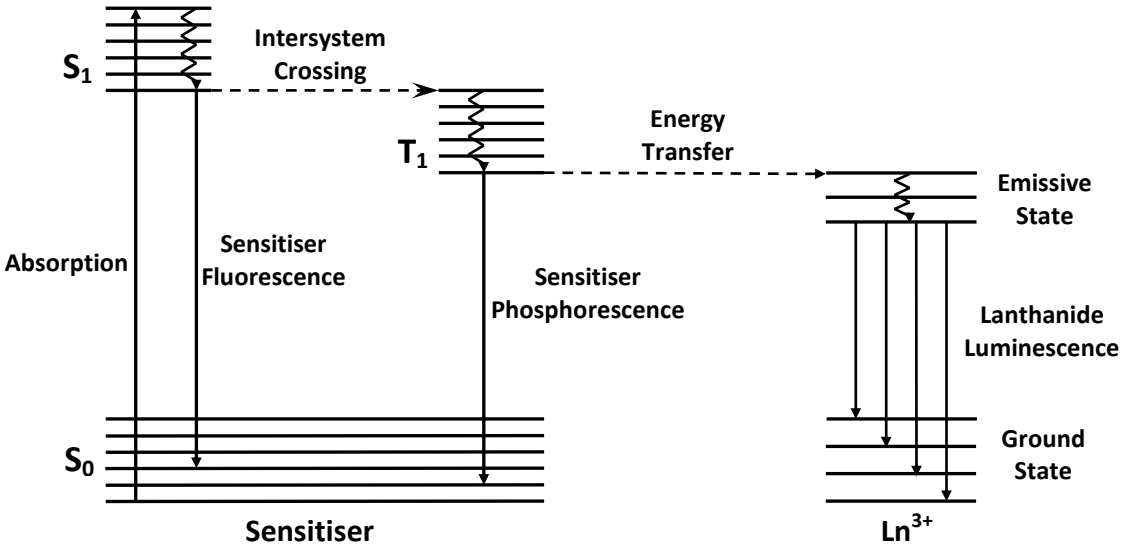

Figure 1.9: Simplified Jablonski diagram representing the key processes involved in the indirect excitation of a lanthanide ion.

The absorption of a photon leads to the excitation of the sensitiser to a vibrationally excited singlet state, S_n (n = 2, 3...), which will rapidly undergo vibrational relaxation and internal conversion to populate a high vibrational level within the S_1 manifold. Further vibrational relaxation then occurs so only the lowest vibrational level of the S_1

state is populated. This is in accordance with Kasha's rule, which was proposed in 1950 and states that 'the emitting level of a given multiplicity is the lowest excited level of that multiplicity'.[36] From the S_1 state, the sensitiser may decay radiatively by fluorescence, or alternatively, intersystem crossing can occur, transferring the energy to the triplet excited state of the sensitiser. It is suggested that the efficiency of this second, spin forbidden process is enhanced in lanthanide complexes because there is a sizeable amount of spin-orbit coupling due to the heavy atom effect of the lanthanide ion.[34] Finally, if the lanthanide excited state is lower in energy than the triplet state of the sensitiser then it may become populated by energy transfer and subsequently relax to its ground state, yielding the characteristic lanthanide luminescence. Alternatively, the T_1 state of the sensitiser may decay radiatively by phosphorescence.

For a sensitised lanthanide complex, the overall luminescence quantum yield, Φ, can be calculated according to the following equation, where η_{ISC} and η_{ET} are the efficiencies of the intersystem crossing and ligand to lanthanide energy transfer processes respectively.[37] Meanwhile, Φ^{Ln} is the intrinsic quantum yield of the lanthanide ion, which was defined and discussed in Section 1.3.1.

$$\Phi = \eta_{ISC}\eta_{ET}\Phi^{Ln} \qquad \text{(eqn. 10)}$$

It is clear from this expression that, in order to synthesise lanthanide complexes with high quantum yields, it is key to not only incorporate lanthanide ions with high intrinsic quantum yields, but also to identify ligands and sensitisers that will facilitate efficient intersystem crossing and energy transfer processes.

1.3.4 Luminescence deactivation pathways

In order to gain a thorough understanding of the dependence of the overall luminescence quantum yield for a sensitised lanthanide complex on the efficiency of intersystem crossing and energy transfer, time should be taken to appreciate the various luminescence deactivation pathways that may quench each of the excited states involved in the sensitisation pathway. Scheme 1.1 shows the unwanted competitive deactivating pathways associated with the process of sensitised emission.

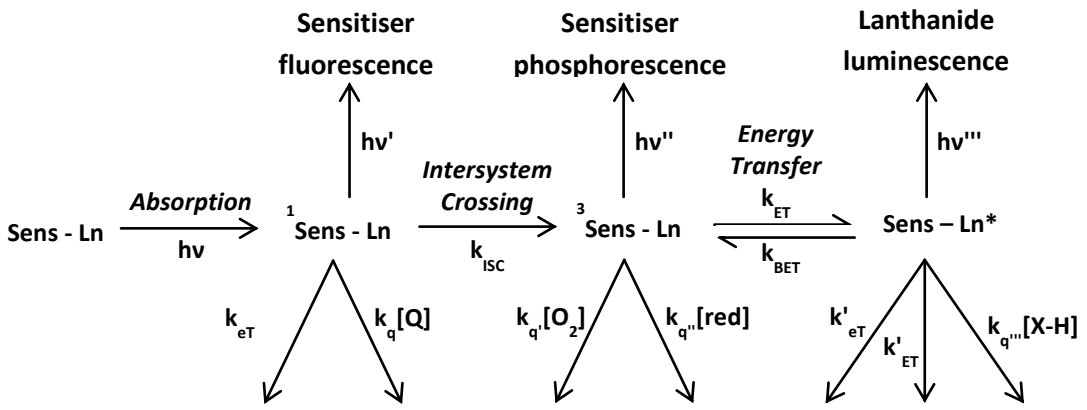

Scheme 1.1: Deactivating pathways following excitation of the sensitiser (k_{ET} is the rate constant for energy transfer, k_{eT} is the rate constant for electron transfer).

As is apparent, each of the excited states involved in the sensitisation pathway is susceptible not only to the radiative deactivation processes mentioned in the previous discussion, but also to non-radiative quenching.

1.3.4.1 Quenching of the sensitiser singlet state

The singlet excited state of the sensitiser has been found to be particularly vulnerable to non-radiative deactivation by electron transfer. This was demonstrated in a study carried out in 1998, which examined the quenching of europium and terbium complexes by halide anions.[38] Titrations were carried out in which the variation in emission intensity of both the ligand fluorescence and metal-based luminescence were monitored as a function of halide ion concentration. For the complexes examined it was found that the extent of the quenching effect observed at a given anion concentration could be correlated to the ease of oxidation of the halide, supporting the hypothesis of an electron transfer quenching mechanism. Meanwhile, at a given concentration of added anion, the ligand fluorescence was typically found to be quenched to a greater extent than the metal-based luminescence and no change in the lifetime of the metal-based emission was detected. These observations are consistent with a quenching mechanism affecting the sensitiser singlet state.

1.3.4.2 Quenching of the sensitiser triplet state

The triplet excited state of the sensitiser is especially susceptible to quenching by molecular oxygen. Several examples of this effect have appeared in the literature and in some cases it has been exploited to develop responsive systems.[39-43] Recently it was

demonstrated that the production of singlet oxygen associated with this quenching effect may be employed in the induction of regioselective cell death.[44]

A second mechanism by which the triplet excited state may be deactivated non-radiatively was hypothesised in 2007, on the basis of results from a study concerned with examining the quenching of europium and terbium systems by urate, ascorbate, iodide and several catechol derivatives.[45] It was anticipated that these species would yield a reduction in emission intensity as a result of direct quenching of the lanthanide excited state by electron transfer; a collisional process that is thermally activated. However, in the case of urate, ascorbate and the catechols, it was found that the efficiency of the observed quenching effect diminished as the temperature was increased, suggesting that this was not the case for these species. It was proposed that the quenching effect observed in the presence of these electron-rich reductants occurred via formation of an exciplex, involving the triplet excited state of the chromophore. This hypothesis was verified by a later study, which showed that no quenching of the lanthanide luminescence was observed in the presence of these species if the lanthanide ion was excited directly using a high-powered laser, and gathered evidence in support of the existence of an exciplex.[46]

At this point it should be noted that for a given terbium complex, its europium analogue will typically prove to be less sensitive to quenching with respect to processes operating by deactivation of the triplet excited state of the chromophore. This is because the energy of the $^5D_4$ emissive state in terbium is higher than that of the $^5D_0$ emissive state in europium meaning that, for a common ligand, it will be closer in energy to the triplet excited state of the chromophore. Hence, back energy transfer from the lanthanide excited state will occur more readily in terbium complexes meaning there is increased repopulation of the triplet state of the sensitising chromophore and more quenching of this state may occur. The complex $[Ln.\mathbf{L^3}]^{3-}$ has been developed as a potential urate sensor, in accordance with this principle.[47] It has been shown that a mixture of $[Eu.\mathbf{L^3}]^{3-}$ and $[Tb.\mathbf{L^3}]^{3-}$ can be used to assess the concentration of urate in solution by considering the intensity ratio of terbium emission at 546 nm to europium emission at 616 nm.

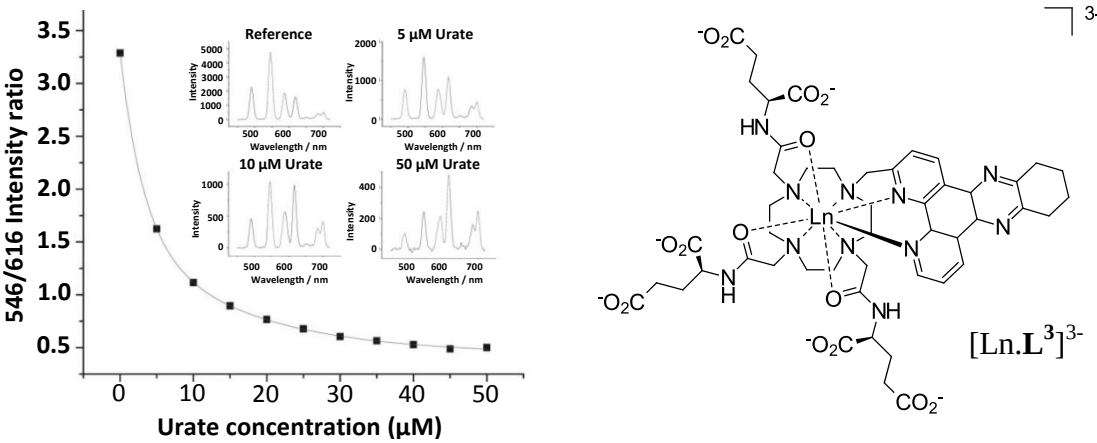

Figure 1.10: Variation of the Tb (546 nm) to Eu (616 nm) emission ratio as a function of the concentration of sodium urate (295 K, 0.1 M HEPES, pH 7.4). The inserts show spectra recorded at varying concentrations of urate. It can clearly be seen that the terbium emission at 546 nm is quenched more efficiently by urate than the europium emission at 616 nm.[47]

1.3.4.3 Quenching of the lanthanide excited state

The lanthanide excited state itself is prone to deactivation by several non-radiative pathways. For example, lanthanide complexes have been developed for FRET applications based on intermolecular energy transfer from the lanthanide excited state to an energy-matched proximal acceptor group.[48] Meanwhile, direct quenching of this state has in some cases been attributed to an electron transfer process, 'driven' by the free energy it possesses. In the 2007 study outlined in the previous section, the quenching of europium and terbium luminescence by iodide was shown to occur via this mechanism.[45] In contrast to the other species examined, quenching of the lanthanide luminescence by iodide was found to be more effective at higher temperature.

When considering the use of sensitised lanthanide complexes to probe aqueous media, it is particularly pertinent to consider an additional non-radiative deactivation pathway relating to the lanthanide excited state (Scheme 1.1). As was mentioned in Section 1.3.1, vibrational energy transfer from the lanthanide excited state to X-H oscillators (X = O, N, C) can lead to a reduction in luminescence intensity and lifetime.[49] Although in many situations it is considered advantageous to maximise the luminescence quantum yield of a given lanthanide complex, there are numerous examples of responsive systems which utilise this quenching effect to their advantage. By intentionally designing complexes such that when in aqueous solution the lanthanide ion must complete its coordination sphere with bound water molecules, the possibility of luminescence modulation and therefore analyte sensing by their displacement is

realised.[50-53] Conversely, responsive systems have also been reported where the hydration state is increased in the presence of the target analyte, also resulting in modulation of the luminescence output.[54]

It should be noted that the determination of the hydration state of a given europium or terbium complex is possible by comparison of the excited state lifetimes in H_2O and D_2O.[55] The quenching of lanthanide luminescence is less efficient in D_2O, due to the fact that O-D oscillators possess lower stretching frequencies than their corresponding O-H equivalents. This means that coupling of the excited states can only occur with higher vibrational overtones, where the Franck-Condon overlap factor is less favourable. It has been shown that for europium complexes, quenching by X-D oscillators is at least 200 times less effective compared to X-H oscillators.[56] Similar reasoning can be used to explain why terbium complexes typically show greater resistance to quenching by O-H oscillators than their europium analogues. As can be seen from Figure 1.11, for europium complexes coupling of the excited state occurs to the third vibrational overtone of proximate O-H oscillators. Hence, the Franck-Condon overlap factor is more favourable than for terbium complexes, where coupling is to the fourth vibrational overtone.

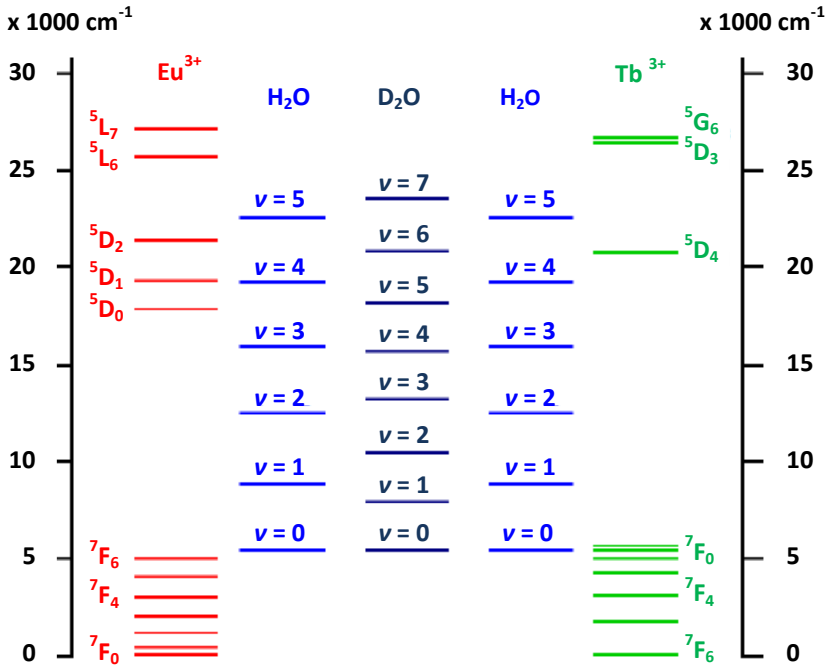

Figure 1.11: Partial energy level diagram for europium and terbium electronic energy levels, compared to idealised vibrational energy levels of O-H and O-D oscillators.

1.3.5 Design criteria for highly emissive lanthanide complexes

As was discussed in the previous section, the various quenching phenomena affecting the excited states involved in the sensitisation pathway can be exploited to great effect. However, it is evident that, in order to synthesise lanthanide complexes with high quantum yields, it is key to minimise time spent in the singlet and triplet excited states and therefore avoid their radiative and non-radiative deactivation. This explains the dependence of the overall luminescence quantum yield on the efficiency of both the intersystem crossing and energy transfer processes, which was first mentioned in Section 1.3.3.

Concerning the sensitising chromophore, it is clear that a small singlet-triplet energy gap is required in order to facilitate efficient intersystem crossing and minimise deactivation of the singlet state by competitive pathways. Similarly, the energy of the triplet excited state in relation to the lanthanide excited state is of high importance, with a smaller energy gap being optimum for efficient energy transfer. However, in this case the avoidance of thermally-activated back energy transfer is also necessary and it has been suggested that a gap of at least 1,700 cm^{-1} is therefore required.[57] It is thought that the energy transfer step of the sensitised emission pathway occurs via either a Förster or Dexter mechanism, which are both distance dependent.[58, 59] Hence, efficient energy transfer may also be promoted by ensuring the sensitising chromophore is located in close proximity to the lanthanide ion. In all cases efficient absorption of light is obviously advantageous, so it is beneficial to incorporate sensitising chromophores with high extinction coefficients.

With respect to the ligand, the design must be such that the number of accessible binding sites offered to the lanthanide ion is sufficient and completion of the coordination sphere by binding small molecules such as water is not necessary. It should be noted that the coordination chemistry of the lanthanide ions is dominated by coordination numbers falling in the range 7-9.[60]

Several additional considerations relating specifically to the development of systems for use in biological applications may also be outlined. Regarding the chromophore, the excitation wavelength should be in excess of 340 nm, such that absorption of excitation light by common biomolecules is avoided.[61] Meanwhile, toxicity associated with

premature metal decomplexation should be minimised by ensuring that complexes are both kinetically and thermodynamically stable.

Over the years, a variety of lanthanide-based systems has been developed which fulfil the criteria outlined above to varying degrees. Some of these may be considered as modular systems, where the chromophore is synthesised separately and then appended to a macrocylic ligand scaffold. In other cases, such as helical assemblies and many linear multidentate systems, the chromophore forms a more integral part of the ligand framework. Examples of both types of system will be presented in the following section, which focuses on a consideration of the stereochemistry in representative complexes.

1.4 Understanding the origin of chirality in lanthanide complexes

It is important to note that only the 4f-4f transitions of complexes in which the lanthanide ion is located in a chiral environment will demonstrate natural optical activity. In such complexes the presence of dissymmetry in the ligand field means that the electric and magnetic dipole moments associated with the transitions are non-orthogonal and therefore optical activity can be observed.[62] This is in accordance with equation 8, defined in Section 1.2.2.

1.4.1 Selected examples of chiral lanthanide complexes

The chiral environment of a lanthanide ion in a complex may arise in a number of ways, one of which is due to a chiral arrangement of the ligand molecules. When the tridentate ligand pyridine-2,6-dicarboxylate (DPA) binds to a lanthanide ion, an anionic tris chelate complex with trigonal dihedral symmetry is formed.[63] The arrangement of the ligands around the lanthanide is often described as resembling a three-bladed propeller, which can either be left (Λ) or right (Δ) handed about the trigonal symmetry axis. The helical arrangement of the chelate rings about the lanthanide centre therefore yields two enantiomeric species, which exist as a racemic mixture in water at room temperature.

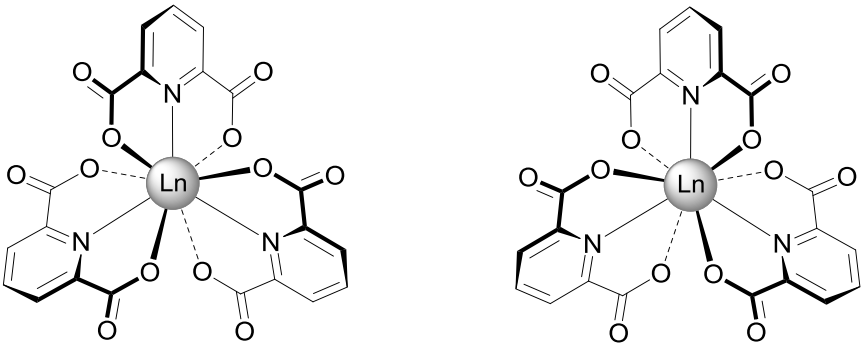

Figure 1.12: Representation of the D_3 symmetric species Δ-$[Ln(DPA)_3]^{3-}$ (left) and its enantiomer, Λ-$[Ln(DPA)_3]^{3-}$ (right), viewed along the trigonal symmetry axis.

It should be noted that the examination of racemic systems such as $[Ln(DPA)_3]^{3-}$ using standard CPL techniques (i.e. unpolarized excitation light) will not lead to the observation of optical activity under normal conditions. However, in the presence of chiral additives an induced CPL effect may occur, therefore facilitating their use as responsive CPL probes. As will be outlined later in this introduction, the vast majority of studies in this area have made use of the complex described above. In contrast, when it comes to current examples of responsive lanthanide-based CPL probes based on enantiopure systems, there are a number of different complexes that have been identified.

The synthesis of enantiopure complexes is typically achieved by the inclusion of asymmetric centres in the ligand molecules.[64, 65] This is illustrated in the case of the tris chelate lanthanide complexes derived using the tridentate ligand **L**$^{\mathbf{4}}$.[66, 67] As is apparent from Figure 1.13, this ligand is closely related to DPA in terms of its core structure and it is therefore not surprising that the ligands have been found to arrange around the lanthanide centre in a three bladed 'propeller-like' manner when used in complex formation. However, in this case the formation of a single complex enantiomer has been found to be favoured in solution, provided the ligand molecule is synthesised such that the two chiral centres had the same relative stereochemistry, i.e. (*S*,*S*)-**L**$^{\mathbf{4}}$ or (*R*,*R*)-**L**$^{\mathbf{4}}$. Crystal structures obtained for $[Eu((R,R)\text{-}\mathbf{L}^{\mathbf{4}})_3]^{3+}$ and $[Eu((S,S)\text{-}\mathbf{L}^{\mathbf{4}})_3]^{3+}$ showed that these complexes favour a left (Λ) and right (Δ) handed arrangement of the ligands respectively in the solid state. Meanwhile, CPL spectra recorded in solution showed a mirror image relationship between the signals observed for the two complexes, implying that they are enantiomeric. Emission dissymmetry factors of ±0.19 and ±0.18 were calculated for the emission at 590.5 and 595.3 nm within the $\Delta J = 1$ manifold. It

has been suggested that these complexes may find use in the development of lanthanide CPL spectra-structure correlations.[67]

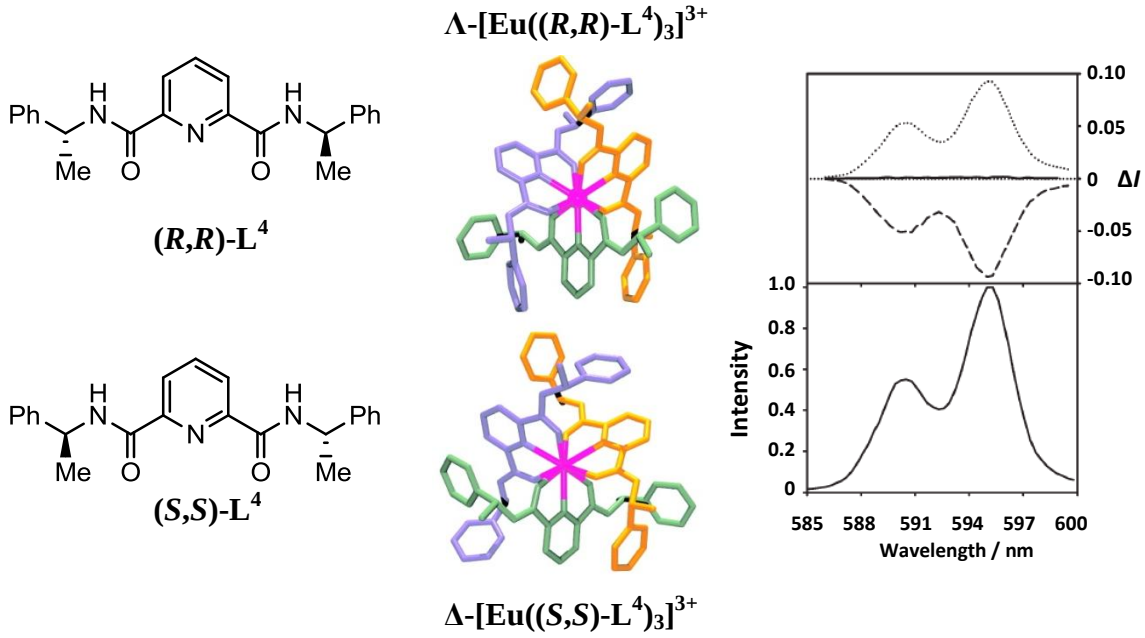

Figure 1.13: Structures of (*R*,*R*) and (*S*,*S*)-**L**^{4} and their Λ and Δ europium complexes alongside the total luminescence (bottom) and CPL (top) spectra of the Δ*J* = 1 band for the tris chelate complexes in MeCN at 295 K. CPL traces for the Λ and Δ complexes are shown by dashed and dotted lines respectively. Meanwhile, the solid lines represents CPL recorded for a tris chelate europium complex formed using (*R*,*S*)-**L**$^{1.4}$.[66, 67]

The fact that the chirality of the ligand may be effective in determining the overall configuration of a complex has also been demonstrated for systems of many other architectures. For instance, the synthesis and chiroptical properties of a pair of enantiomeric, dinuclear triple-stranded europium helicates has recently been reported.[68] As can be seen from Figure 1.14, the two metal binding sites incorporated into each ligand were comprised of the same tridentate chelating group as found in **L**^{4}. Evidence for the helical nature of the structures formed was gathered through the use of ^{1}H NMR spectroscopy and investigations into the hydration state of the metal centres, which suggested the formation of species of high symmetry in which each europium ion was in a nine-coordinate environment. The enantiomeric nature of the helicates was confirmed by several methods including CPL spectroscopy, which gave mirror image spectra for the two species. Emission dissymmetry factors calculated for the emission within the Δ*J* = 1 manifold were comparable in sign and magnitude to those found for the mononuclear complexes of **L**^{4}. For example, at 593 nm the emission dissymmetry factor was found to be -0.23 for the helicate derived from (*R*,*R*)-**L**^{5}.

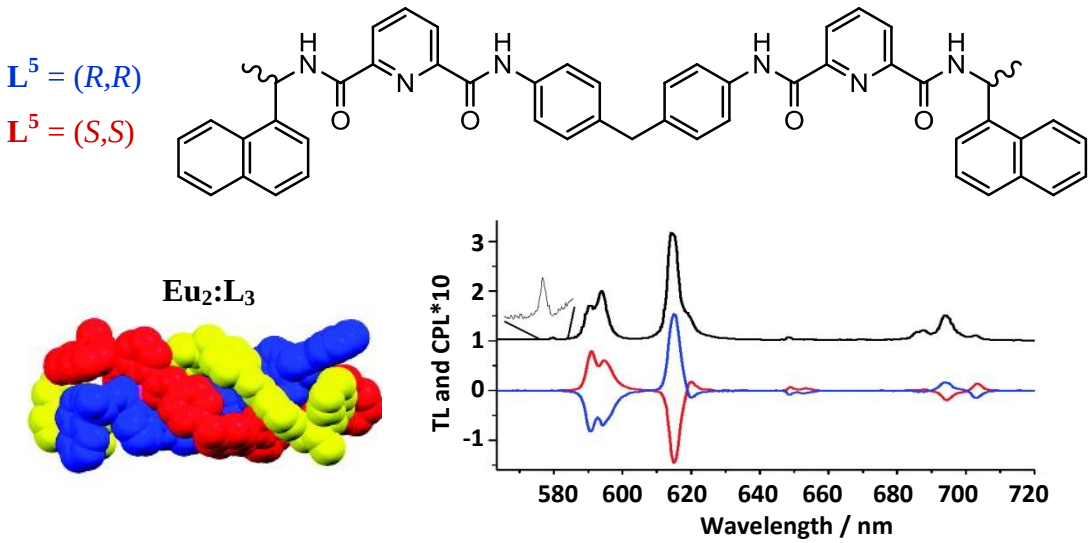

Figure 1.14: Structure of the chiral ligands, $\mathbf{L}^5$ and $\mathbf{L}^5$, used in the synthesis of enantiopure dimetallic helicates, shown with a representation of the overall helicate structure. Total luminescence (top) and CPL (bottom) spectra are also presented for Eu_2:$\mathbf{L}^5{}_3$ (blue) and Eu_2:$\mathbf{L}^5{}_3$ (red) in MeOH.[68]

Further examples of lanthanide systems in which a chiral environment has been created by the inclusion of asymmetric atoms in the coordinating ligands include the europium and terbium complexes of $\mathbf{L}^6$ and $\mathbf{L}^7$ respectively.[69] Both of these enantiopure, octadentate ligands incorporate stereogenic centres in their backbones. In the case of $\mathbf{L}^6$, four asymmetric centres can be found in the tetrapodal arms, whilst for $\mathbf{L}^7$, there are two stereogenic centres located in the central region of the oligoamine backbone. Both the europium complex, [Eu($\mathbf{L}^6$)(H_2O)], and the terbium complex, [Tb($\mathbf{L}^7$)], have been found to exhibit CPL in aqueous solution at pH 7.4, with results of ^{1}H NMR studies and luminescence lifetime measurements suggesting the presence of only one dominant emitting species in solution. It should be noted that, while the terbium complex in particular has been found to exhibit an impressive luminescence quantum yield in aqueous solution (Φ = 0.57), the CPL activity of these complexes was found to be relatively modest, with emission dissymmetry factors not exceeding ±0.12.[69] Recent attempts to synthesise analogues of these complexes in which exceptional luminescence quantum yields are combined with higher degrees of optical activity have been of mixed success.[70, 71] Of the chelating units examined, only one has been identified which conserves all the desirable photophysical and structural properties associated with [Tb($\mathbf{L}^7$)], whilst also roughly doubling the observed g_{em} values.

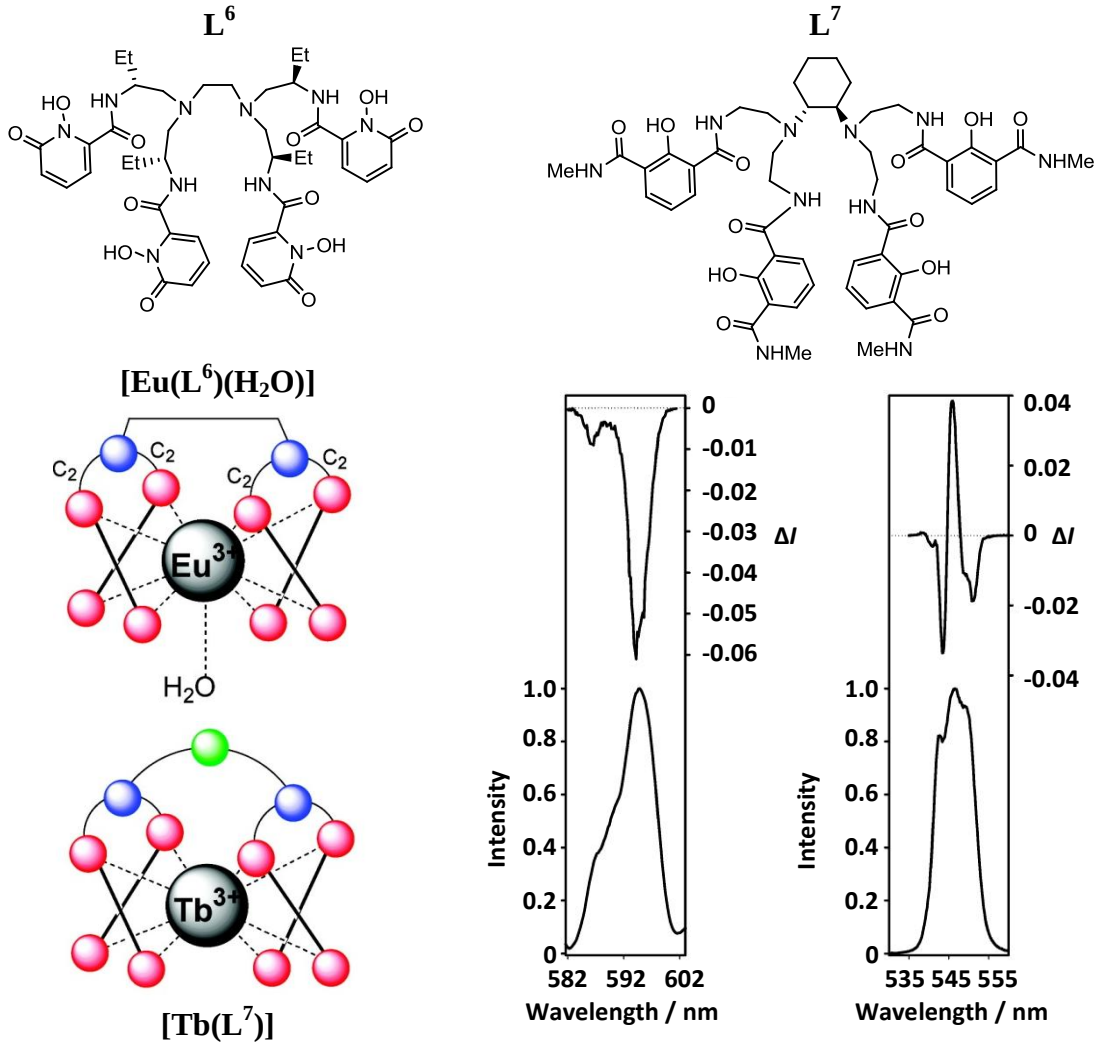

Figure 1.15: Structure of $\mathbf{L}^6$ and $\mathbf{L}^7$ shown with a schematic representation of the design principle for each ligand. Red and blue spheres denote oxygen and nitrogen respectively. In the case of the terbium complex, the green sphere is representative of the location of the chiral information in the ligand framework. The total luminescence (bottom) and CPL (top) spectra of the $\Delta J = 1$ bands of [Eu($\mathbf{L}^6$)(H_2O)] (left) and [Tb($\mathbf{L}^7$)] (right) are also shown (295 K, 0.1 M Tris buffer, pH 7.4).[69, 70]

A final example of this so-called chirality transfer effect which is worth highlighting concerns a lanthanide complex that has been shown to exhibit exceptional optical activity. Whilst values of g_{em} for the majority of enantiopure lanthanide complexes described in the literature fall in the range ±0.1 - 0.5, much larger values have been reported for the complex Cs[Eu((+)-hfbc)$_4$]; a g_{em} value of +1.38 has been observed at 595 nm when the complex is in chloroform.[72] Studies of this complex have revealed that the high degree of circular polarization in the emission may be attributed to the occurrence of dynamic coupling between the f-f transitions and the ligand-centred π-π^* transition.[73] On the basis of exciton CD measurements and ^{19}F NMR data, a solution state structure was proposed for this complex and several of its analogues.[74, 75] In this

structure, the coordination of the lanthanide ion by the four bidentate 3-heptafluorobutylryl-(+)-camphorate ligands occurs in such a manner that the eight oxygen donor atoms define two square bases. The wrapping of the ligands gives rise to a Δ helicity and the caesium ion is encapsulated, with weak interactions of this metal ion with the fluorocarbon moieties of the ligand molecules having been alleged.[72, 75]

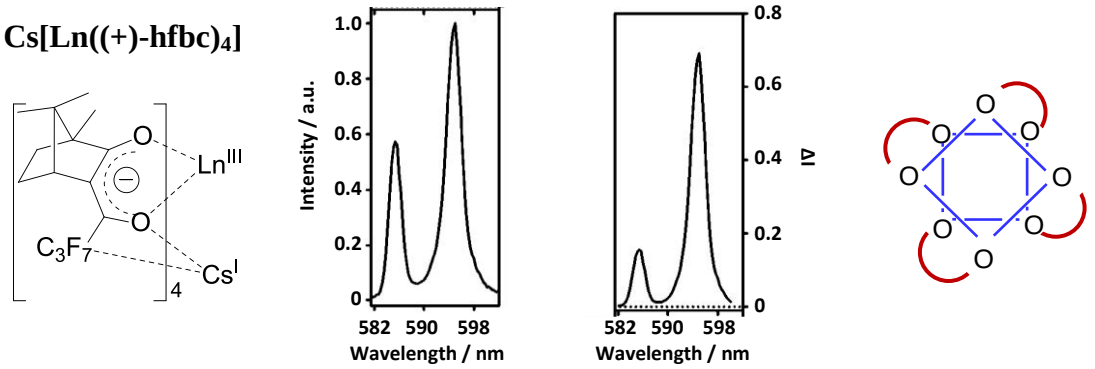

Figure 1.16: Ligand structure and representation of overall complex structure for Cs[Ln((+)-hfbc)$_4$]. Total emission (left) and CPL (right) spectra are shown for the $\Delta J = 1$ transition of Cs[Eu((+)-hfbc)$_4$] in $CHCl_3$ at 295 K.[72, 75]

1.4.2 Examining the stereochemistry of macrocylic systems

It is important to note that, while the use of CPL has been fundamental in the characterisation of all of the enantiopure systems discussed up to this point, for most of them no results have yet been reported concerning the modulation of their CPL output in response to changes in their environment. Indeed, a survey of the literature reveals that the majority of lanthanide-based systems which have been identified as showing such an effect are derived from a common macrocyclic framework, namely that of 1,4,7,10-tetraazacyclododecane-1,4,7,10-tetraacetic acid (DOTA).

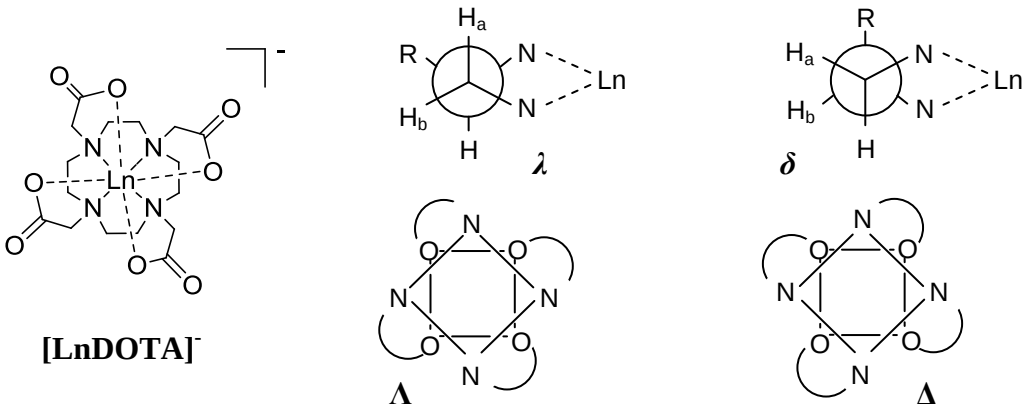

Figure 1.17: The structure of [LnDOTA]$^-$ shown alongside diagrams depicting the limiting orientations of the cyclen ring and possible lay-outs of the acetate arms.

The geometry of the complex $[LnDOTA]^-$ can be described in terms of two torsion angles. Firstly, the N-C-C-O angle of the acetate arms, which can be $+30^o$ or -30^o (Δ and Λ respectively), and secondly the N-C-C-N angle of the macrocyclic ring, which can be $+60^o$ or -60^o (δ and λ respectively).[76] The different possible combinations of these two structurally independent elements of chirality give rise to the four stereoisomers depicted in Figure 1.18, which are related as two enantiomeric pairs.[77] When in solution it is possible for the four stereoisomers to interconvert via ring inversion ($\delta \leftrightarrow \lambda$) and cooperative arm rotation ($\Delta \leftrightarrow \Lambda$), yielding a racemic mixture which will exhibit no CPL if examined using a standard experimental procedure.

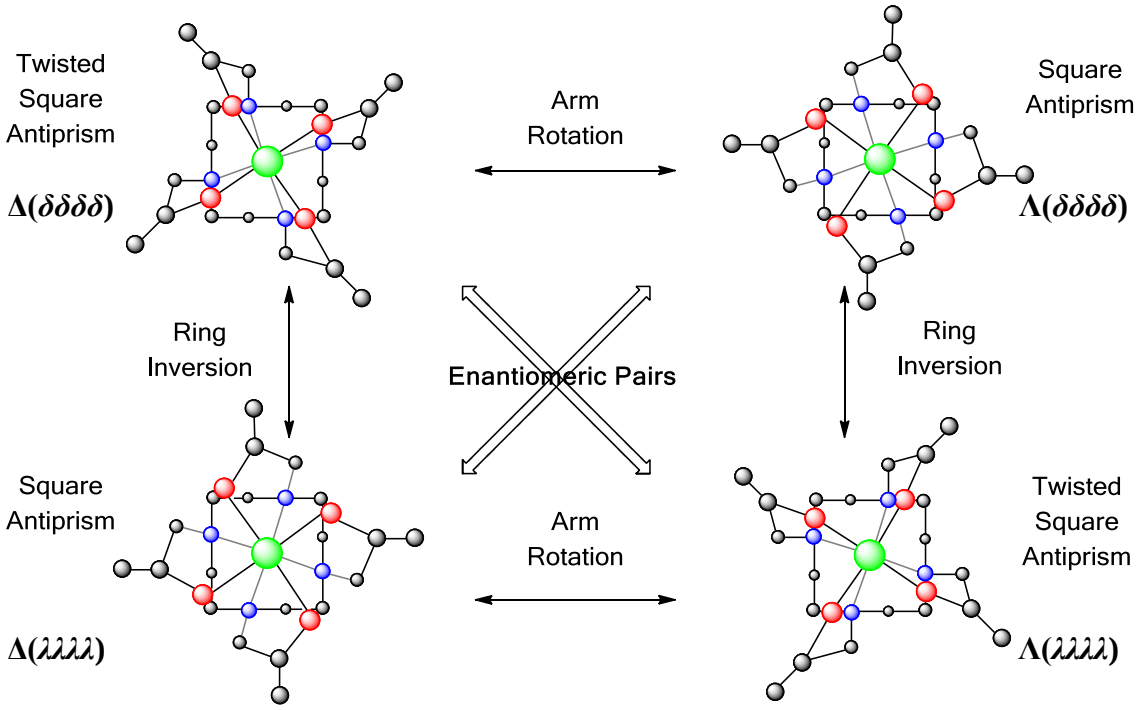

Figure 1.18: Schematic representation of the four stereoisomers of $[LnDOTA]^-$.

As is apparent from this representation of the stereoisomers, the geometry adopted by the $\Lambda(\delta\delta\delta\delta)/\Delta(\lambda\lambda\lambda\lambda)$ enantiomeric pair in solution differs to that observed for the $\Delta(\delta\delta\delta\delta)/\Lambda(\lambda\lambda\lambda\lambda)$ pair. In each case, the coordination polyhedron is defined by two square bases, one comprising the four nitrogen atoms of the macrocylic ring and the other the four oxygen donor atoms of the pendant arms. The two geometries may be distinguished by the angle between these square bases, which is roughly 40^o in the case of the former pair, and 15^o for the latter.[77] The geometries are commonly referred to as square antiprismatic (SAP) and twisted square antiprismatic (TSAP) respectively and have slightly different characteristics. For example, the coordination polyhedron is typically more compressed in a SAP structure and the 'bite angle' wider. It should be

noted that a given lanthanide DOTA complex will typically favour either a SAP or TSAP geometry and therefore exist as a major and a minor enantiomeric pair in solution.

As was shown to be the case for the lanthanide architectures discussed previously, it has been found that the inclusion of asymmetric centres in the ligand framework of complexes derived from DOTA-based ligands may yield the formation of enantiopure complexes in solution. Typically, the incorporation of stereogenic centres directly on the macrocycle will suppress the rate of ring inversion.[78, 79] Meanwhile, the integration of chirality into the pendant arms will generally inhibit arm rotation.[80-82] Due to the fact that all lanthanide complexes derived from a DOTA framework will show preference towards either a SAP or TSAP geometry, the implementation of only one of the strategies outlined above will normally lead to the preferential formation of a single stereoisomer in solution. For example, NMR studies have shown that the europium complex of the enantiopure octadentate ligand (*S*)-**L**[9] exists in solution as Λ(*δδδδ*) and Δ(*δδδδ*) stereoisomers, in a ratio of 12:1 i.e. the ring is effectively locked and a SAP geometry is favoured.[83]

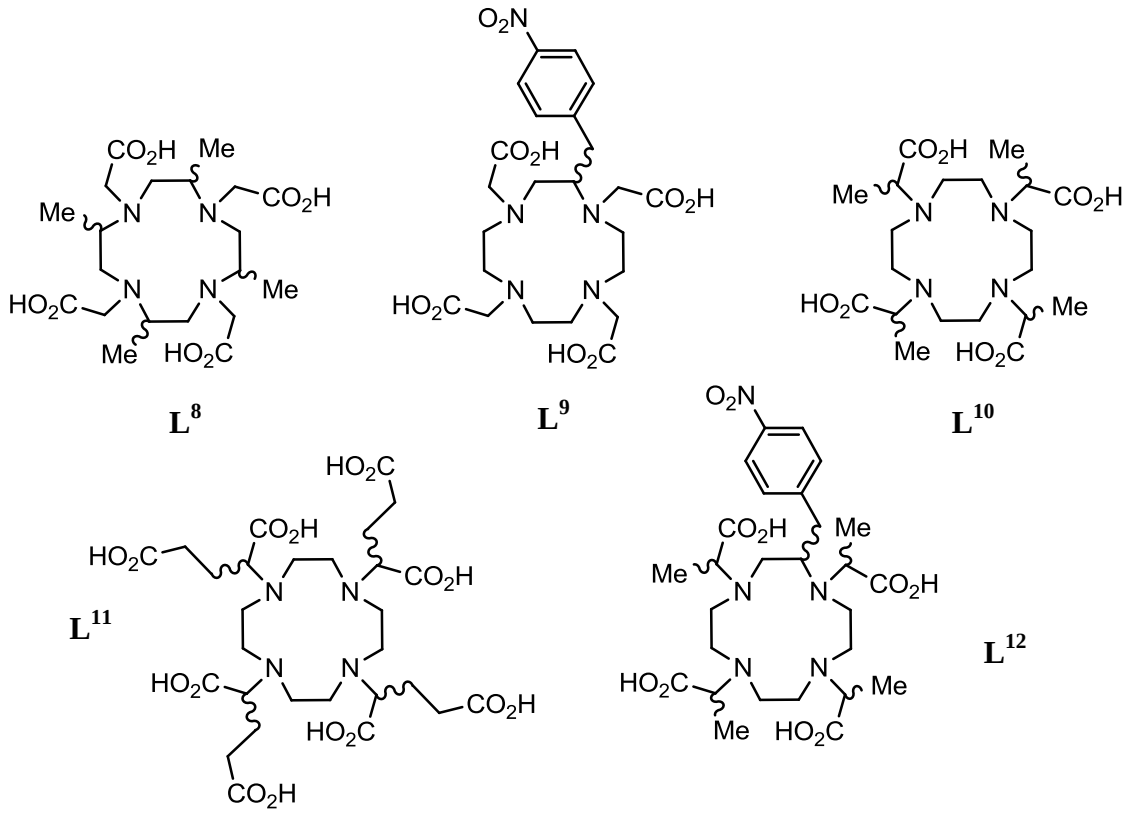

Scheme 1.2: Selected chiral ligands employed in the preferential synthesis of single stereoisomers.

In some cases it has been found that the incorporation of asymmetry solely into the pendant arms is effective in achieving exclusively the formation of a single stereoisomer.[84-86] For example, the europium complex of the C_4-symmetric tetraamide ligand (*RRRR*)-**L**^{13}, in which a chiral centre is incorporated into each of the pendant arms in a position δ to the ring nitrogen, has been shown by ^{1}H NMR spectroscopy to exist as solely one stereoisomer in solution.[87, 88] Well-defined CPL spectra have been reported for both terbium and europium complexes of this ligand, with enantiomeric complexes giving rise to mirror image spectra. For the europium complex derived from (*RRRR*)-**L**^{13}, emission dissymmetry factors of -0.12 and +0.18 were reported for the two bands observed within the $\Delta J = 1$ manifold.

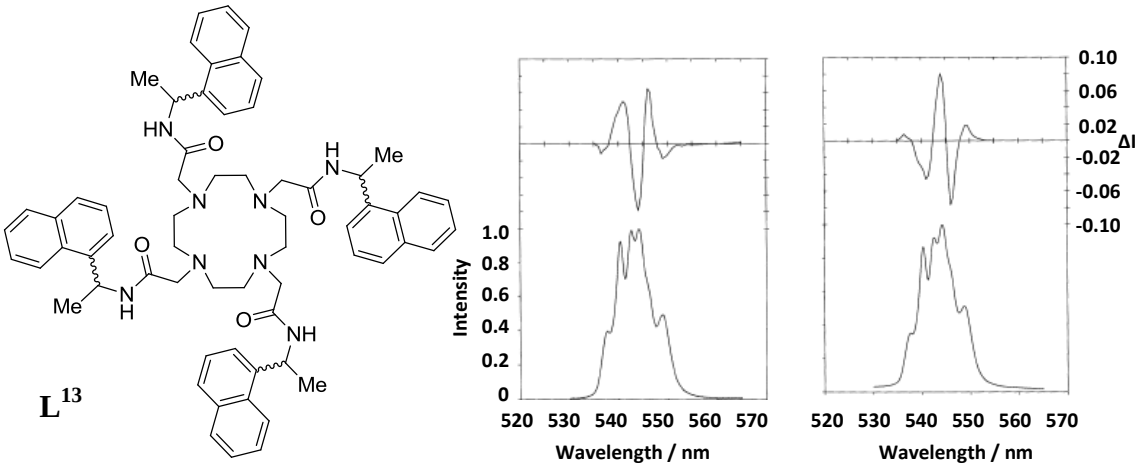

Figure 1.19: Structure of the tetraamide ligand **L**^{13} accompanied by the total luminescence and circularly polarized luminescence spectra for the $\Delta J = 1$ band of the two enantiomers of [Tb.**L**^{13}]$^{3+}$ (293 K, degassed MeCN).[88]

In accordance with the discussion above, it may be deduced that the best way to ensure the sole existence of only one stereoisomer in solution is through the use of ligands in which asymmetry is incorporated in both the macrocyclic ring and the pendant arms. However, it should be noted that whilst this method has been demonstrated successfully with ligands such as **L**^{12}, recent studies involving complexes of this ligand have reported the presence of two species in solution.[89-91] NMR experiments have shown that these species may be thought of as regioisomers, with their existence being attributed to the fact that it is possible for the ring substituent to be located in one of two non-equivalent positions (Figure 1.20).

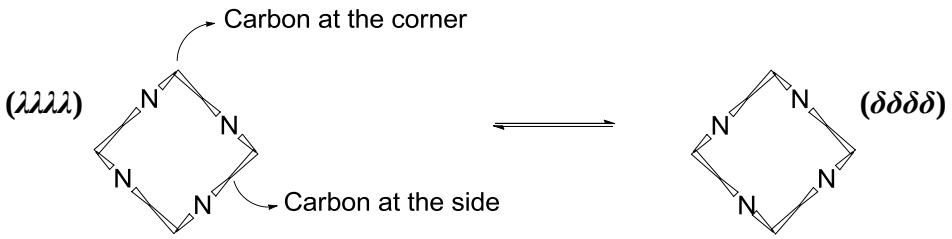

Figure 1.20: Possible locations of a ring substitution for a given conformation of tetraazacyclododecane.[77]

Before going on to discuss examples of responsive lanthanide-based CPL probes from the literature, it is first worth mentioning that, although in general spectra-structure correlations for lanthanide complex CPL are not well understood, some effort has been made with regard to identifying the factors that determine the sign and magnitude of g_{em} for lanthanide complexes based on substituted DOTA ligands. It has been suggested that for such complexes changes in the angle of twist about the principal axis and variations in the local ligand field (particularly the polarizability of any axial donor) will both lead to modulation of the total emission and/or CPL output and therefore changes in observed g_{em} values.[92] In particular, the CPL is predicted to follow a sin4θ dependence for such complexes, where θ is the angle of twist about the principal axis. Hence, a twist angle of 0^o or 45^o will result in no CPL, whilst CPL will be at its highest when $\theta = \pm 22.5^o$. From this it may be implied that higher CPL may in theory be expected for complexes adopting a TSAP geometry, whose twist angles are typically closer to this idealised value than their SAP analogues.

Speaking more generally, an additional factor which plays a key role in determining the size and magnitude of g_{em} for any given lanthanide complex is its conformational rigidity. As was discussed in Section 1.2.2, g_{em} is dependent on the angle between the electric and magnetic transition dipoles, τ, with large values being expected if these dipoles are parallel or antiparallel (i.e. $\tau = 0^o$ or 180^o). Therefore, restriction of any conformational exchange processes which lead to perturbation of this angle as a function of time is necessary if a given lanthanide complex is to find use as a responsive CPL probe. It is important to note that, while in some cases τ may be correlated to the aforementioned twist angle θ, there does not necessarily exist any explicit relationship between these two angles for a given lanthanide complex.

1.5 Responsive lanthanide-based CPL probes

When considering the development of lanthanide systems that are able to report on changes in their environment through modulation of their CPL output, it is clear that only systems where a reasonable understanding of the origin of the observed CPL modulation can be attained will ever show promise with regard to their use in real-world applications. In accordance with this, early examples of responsive CPL behaviour, from so-called 'mixed ligand' solutions, will not be presented in the following sections of this review, which aim to provide a comprehensive overview of well-defined lanthanide complexes that show modulation of their CPL output in response to environmental change.

A classification of systems fitting the description given above may be built up in accordance with first the complex stereochemistry (achiral, racemic or enantiopure) and second the manner by which the change in CPL is brought about. The discussion in the following sections is arranged according to this classification. In each case, examples of systems belonging to the given category are presented and a consideration of their practical utility as responsive CPL probes is undertaken. Before embarking on a detailed discussion in accordance with this outline, it is informative to first draw attention to a recent example of responsive lanthanide-based CPL reported in the literature that will not be considered again later.

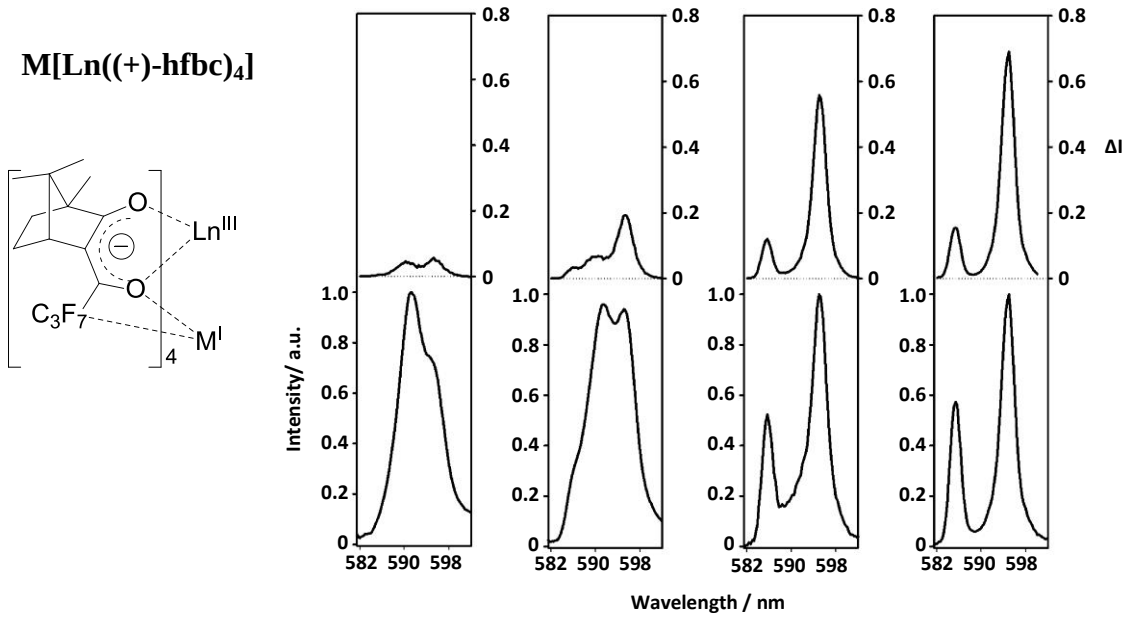

Figure 1.21: Ligand structure for complexes of the general formula M[Ln((+)-hfbc)$_4$], whose solution structure was discussed in Section 1.4.1. Total emission (bottom) and CPL (top) spectra are shown for the ΔJ = 1 transition of M[Eu((+)-hfbc)$_4$], where M = Na^+, K^+, Rb^+, Cs^+ (left to right) (295 K, 2 mM $CHCl_3$ solution).[93]

Modulation of the CPL output from the complex $Cs[Eu((+)\text{-hfbc})_4]$, was observed to occur in both ethanol and chloroform solution when the caesium metal ion was substituted for a different alkali metal ion.[93] The emission dissymmetry factor at 595 nm was determined for $M^I = Na^+$, K^+, Rb^+ and Cs^+ and found to vary in accordance with the size of the metal ion. For example, in chloroform solution the emission dissymmetry factor at this wavelength was reported to take values ranging between +0.15 ($M^I = Na^+$) and +1.38 ($M^I = Cs^+$). Without further evidence, it would be tempting to attribute this variation in optical activity to a change in polarizability in the primary coordination environment of the complex associated with the various alkali metal ions. However, in the case of this system, it was subsequently shown that the observed modulation of the CPL output may be attributed to a change in complex constitution, with NMR studies revealing competitive dissociation of the $M^I[Eu((+)\text{-hfbc})_4]$ complexes to give the neutral tris-chelated complex, $Eu(hfbc)_3$, in the case of Na^+, K^+ and Rb^+.[73] Notwithstanding the fact that this lanthanide system is inherently unsuitable for application in biological systems due to a lack of aqueous solubility, this example helps to illustrate the importance of gaining as much understanding as possible of the origin of observed CPL modulation in systems that are to be developed for use as optical probes.

1.5.1 Exploring the use of achiral lanthanide systems

In cases where the complexation of a lanthanide ion by achiral ligands does not result in a chiral structure, the complex itself will be achiral and therefore exhibit no CPL if examined under standard conditions. There exist two examples in the literature of achiral lanthanide systems in which a CPL signal is apparently induced in the presence of a chiral additive.

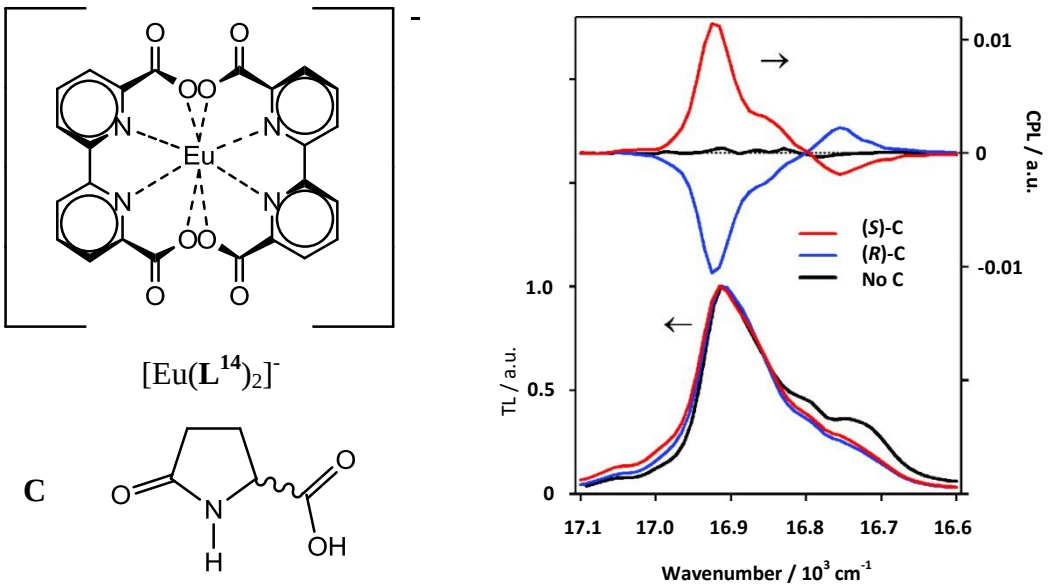

Figure 1.22: Structures of $[Eu(\mathbf{L}^{14})_2]^-$ and **C** shown alongside the total luminescence (bottom) and CPL (top) spectra of the $\Delta J = 1$ band for $[Eu(\mathbf{L}^{14})_2]^-$ in aqueous solution in the presence and absence of both enantiomers of the chiral additive.[94]

The europium complex, $[Eu(\mathbf{L}^{14})_2]^-$, is known to adopt an achiral structure of D_{2d} symmetry in the solid state.[95, 96] A recent study has shown that in solution this complex exhibits CPL in the presence of the chiral amino acid derivative, **C**.[94] It was demonstrated that mirror image CPL spectra could be generated by the addition of (*S*)- and (*R*)-**C** to aqueous solutions of $[Eu(\mathbf{L}^{14})_2]^-$. The maximum values of g_{em} associated with the interaction were approximately ±0.03, roughly an order of magnitude smaller than those typically observed for lanthanide-based systems. Various investigations were carried out in an attempt to identify the mechanism by which this induced CPL arose, with the authors concluding that the amino acid derivative is able to bind to the europium centre in the complex, giving rise to chiral species of the general formula $[Eu(\mathbf{L}^{14})_2(\mathbf{C})]^-$ in solution.

A critical analysis of the results presented for this system may however conclude that the diminutive values of g_{em} determined are more consistent with the observed CPL being attributed to only one component of a more complex mixture of emissive species present in solution. There is precedent for such a hypothesis, with several early studies of CPL from lanthanide species formed in 'mixed ligand' solutions having been later questioned on the basis of the fact that the CPL active species was shown to account for only part of the total emission observed.[97, 98] In the example presented here, it is likely that the observed CPL may be attributed to the formation of complexes of the formula

$[Eu(\mathbf{L^{14}})(\mathbf{C})]^+$, which are in turn outnumbered in solution by more emissive achiral complexes of the original composition.

The second example of this induced CPL effect reported for an achiral lanthanide systems pertains to a europium-containing polymer, which has been found to exhibit CPL when in the presence of the amino acid proline.[99] Approximately mirror image spectra were recorded in the presence of enantiomerically pure samples of *D*- and *L*-proline, with particularly large emission dissymmetry factors apparent in the $\Delta J = 1$ emission band ($g_{em} \approx \pm 0.4$ at 596 nm). The authors suggest that specific orientation of the guest-molecule may be encouraged by the well-defined structure of the conjugated polymer, however, no further comment is offered regarding the exact nature of the interaction between the polymer and the amino acid.

1.5.2 Sensing through perturbation of a dynamically racemic complex

As was discussed in Section 1.4, lanthanide complexes derived from achiral ligands will typically exist in solution as a racemic mixture, provided complexation yields a chiral structure. The induction of a CPL effect for such systems is possible in the presence of a chiral additive and has been demonstrated to occur via two mechanisms, which will be described and exemplified below. As was mentioned in Section 1.4.1, the vast majority of work carried out in this area has examined the induction of CPL by perturbation of Δ- and Λ-$[Ln(DPA)_3]^{3-}$ in solution. In accordance with this, only results pertaining to this system will be considered here.

1.5.2.1 Disruption of the ground state equilibrium: The Pfeiffer effect

One way in which the introduction of a chiral additive to a solution containing a racemic mixture of Δ- and Λ-$[Ln(DPA)_3]^{3-}$ can lead to optical activity is by perturbation of the ground-state equilibrium. For this to be achieved, outer sphere association of the complex with the optically active chiral additive first need occur. This leads to a build up of an enantiomeric excess in the ground state because the formation of one diastereomeric outer sphere association complex is more energetically favourable than that of the other. As long as other chiral effects, such as enantioselective excited state quenching, are absent then the enantiomeric excess in the excited state will be equal to that of the ground state, leading to the observation of optical activity.

This so-called 'Pfeiffer effect' was discovered in the 1930s and first demonstrated with regard to the observation of induced CPL from $[Ln(DPA)_3]^{3-}$ (Ln = Eu^{3+} and Tb^{3+}) systems roughly 50 years later.[100-102] It should be noted that although the binding constants of DPA for lanthanide ions are of such a magnitude that added chiral species should not be able to compete for coordination to the metal centre,[103] the importance of verifying the origin of an observed induced CPL signal has been highlighted in many studies of this effect. That the induced signal does not occur as a result of a change in the primary lanthanide coordination environment is supported in general by the fact that, for a given lanthanide-DPA complex, the CPL spectral form has been found to be identical across reported instances of the Pfeiffer effect. The absence of change in the primary coordination environment has also been verified in some cases by other methods, such as comparison of the CPL spectrum obtained from a Pfeiffer-perturbed system with that of the 'pure' enantiomer (see Section 1.2.1).[104, 105] It should be noted that evidence has also been gathered to support the ascribing of the Pfeiffer effect to the formation of outer-sphere association complexes. This has been achieved through ^1H NMR studies examining the upfield shift of amino acid resonances induced in the presence of $[Eu(DPA)_3]^{3-}$.[106]

Over the years, the Pfeiffer effect has been demonstrated for $[Ln(DPA)_3]^{3-}$ complexes with a number of different chiral additives including vitamin B_{12} derivatives,[107] sugars[108] and, most recently, amino-acid based ionic liquids.[109] Observations made over the course of these studies have led to the implication of a wide range of non-covalent interactions in the formation of the outer-sphere association complexes, from hydrogen bonding to electrostatic and hydrophobic effects. With such a range of interactions involved in the formation of these complexes, it is perhaps unsurprising that the sign and magnitude of the induced CPL observed in these studies frequently appears to show no meaningful correlation to the specific structural characteristics of the added substrate.

It is unlikely that the Pfeiffer effect will ever find employment in the selective detection of a desired chiral substrate in a complex mixture. However, it does show great promise with regard to its ability to distinguish enantiomers of a given analyte in solution. Otherwise unpublished results outlined in a review written by Muller have demonstrated a clear correlation between the measured CPL signal from $[Tb(DPA)_3]^{3-}$ in aqueous solution and the nature and amount of serine present (Figure 1.23).[110] Although

intriguing, it is important to take into account the preliminary nature of these results, given that Muller does not provide any evidence verifying the origin of this observed induced CPL signal.

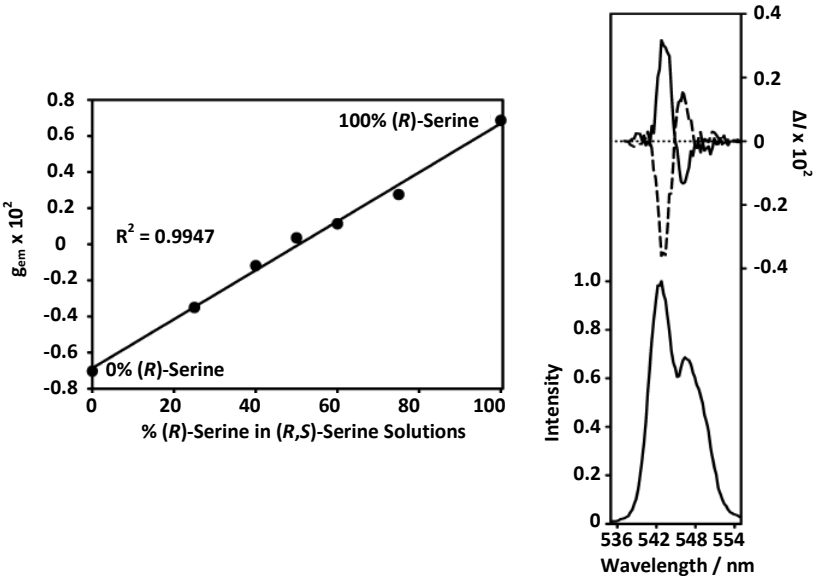

Figure 1.23 Left: Plot of g_{em} values at 543 nm for 0.01 M $[Tb(DPA)_3]^{3-}$ in the presence of (*R*)- and (*S*)-serine, as a function of the percentage of (*R*)-serine present (total serine concentration 0.40 M). **Right:** CPL spectra for the $\Delta J = 1$ transition of 0.01 M $[Tb(DPA)_3]^{-}$ in the presence of 0.40 M (*S*)- and (*R*)-serine (top, dashed and solid lines respectively) and the corresponding total luminescence spectrum (bottom) (295 K, pH 7).

1.5.2.2 Enantioselective excited state quenching

The second mechanism by which a chiral additive may lead to the induction of a CPL signal from a solution containing a racemic mixture of Δ- and Λ-$[Ln(DPA)_3]^{3-}$ is by chiral discrimination in the excited state. Although racemisation of $[Ln(DPA)_3]^{3-}$ occurs too quickly to allow chemical separation of the enantiomers, it is slow compared to the rate of radiative decay (for example, for $[Eu(DPA)_3]^{3-}$ the racemisation lifetime in aqueous solution at approximately 31 ^{o}C is 17.7 ms, whilst the emission lifetime is 1.60 ms).[12] This means that in the presence of a chiral quencher, an enantiomeric excess will be generated in the excited state over time, if the ΛL^* - *Q* and ΔL^* - *Q* quenching rates differ. The occurrence of such stereoselective energy transfer or preferential charge transfer will therefore lead to an induced CPL signal.

Induction of CPL from a $[Ln(DPA)_3]^{3-}$ system via this mechanism was first observed in 1989.[10] In this first study it was shown that CPL could be observed from solutions containing a racemic mixture of 10 mM $[Tb(DPA)_3]^{3-}$ when enantiomerically resolved samples of the trigonal dihedral transition metal complex $[Ru(phen)_3]^{2+}$ were present at

a concentration of just 5 μM. The origin of the effect was inferred through the performance of several additional experiments. Firstly, the ground-state population of the lanthanide complex was probed by CD, with the measurements revealing a lack of optical activity in this state. This confirmed that the racemic equilibrium in the ground state of $[Tb(DPA)_3]^{3-}$ was unperturbed by the presence of $[Ru(phen)_3]^{2+}$ so the optical activity observed could not be attributed to a Pfeiffer effect. Meanwhile, disruption of the primary coordination sphere of the lanthanide ion was ruled out by comparison of the observed CPL spectral form for the $^5D_4 \rightarrow {}^7F_5$ transition to that recorded for the 'pure' enantiomer. Finally, the variation in g_{em} at 543 nm as a function of the ratio of the transition metal to terbium complex concentration was recorded and found to be non-linear. This observation led to the deduction that the effect must be attributed to a dynamic mechanism, as opposed to a static ion-pairing mechanism. On the basis of this evidence it was concluded that the induction of CPL could be ascribed to a 'chiral quenching' effect, where a single transition metal complex was able to quench the emission of several terbium complexes during the lifetime of the excited state. Quantification of the extent of this effect was made possible by the measurement of time-resolved CPL data, which was used to estimate differential rate constants for the quenching of Δ- and Λ-$[Tb(DPA)_3]^{3-}$ by Λ-$[Ru(phen)_3]^{2+}$.

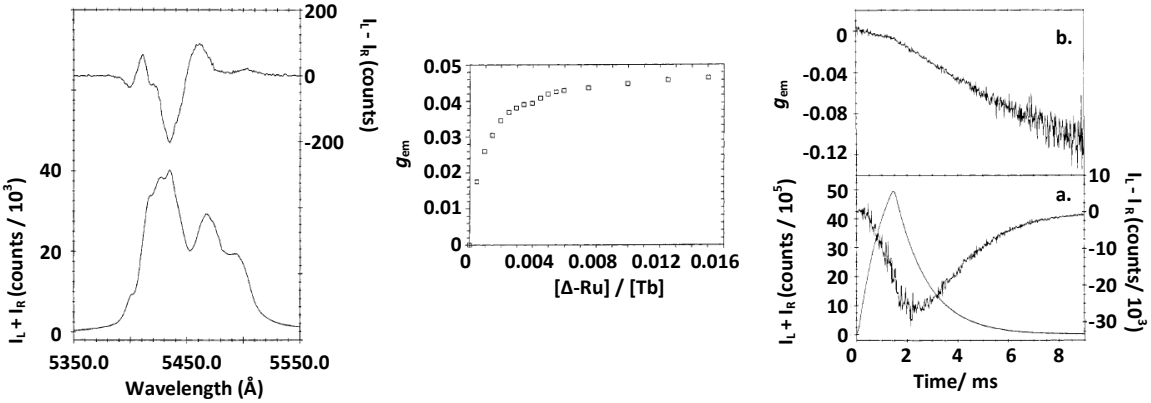

Figure 1.24 Left: CPL (top) and TL (bottom) for the $^5D_4 \rightarrow {}^7F_5$ transition of $[Tb(DPA)_3]^{3-}$ (10 mM) in the presence of $[Ru(phen)_3]^{2+}$ (5 μM). **Middle:** Variation in g_{em} at 543 nm as a function of the ratio of the transition metal to terbium complex concentration. **Right:** Time-resolved CPL (noisy trace) and TL (smooth trace) as a function of time after excitation at 543.5 nm (bottom) and variation in g_{em} as a function of time (top).[10]

The majority of studies of this effect have employed transition metal complexes in the role of the chiral quencher and, generally speaking, the use of time-resolved CPL spectroscopy in the identification and characterisation of the degree and sense of

enantioselective quenching is typical. The associated theory and measurement methodology for TR-CPL studies was further developed soon after the initial publication described above,[111] and, using transition metal-based quenchers, investigations have been carried out into the effect of variation in the electronic and stereochemical structures of the interacting species on quenching rates and enantioselectivity.[112-115] In addition, the effect of sample variables such as solvent, temperature, pressure and ionic strength has also been assessed.[116-120] Results observed in all of these studies have been analysed on the basis that quenching occurs via an energy transfer process, typically assumed to involve diastereomeric Ln^{*} - Q encounter complexes, which have non-identical relative stabilities and energy transfer efficiencies.[121]

It is important to highlight that a number of metalloproteins and vitamin B_{12} derivatives have also been found to be capable of inducing a CPL signal from $[Ln(DPA)_3]^{3-}$ in solution via this mechanism.[122-124] In the case of the corrinoid vitamin B_{12} and its derivatives, the observation of an enantioselective quenching effect has been attributed to energy transfer in a hydrogen-bonded encounter complex.[125] It has been demonstrated that these enantioselective quenching effects can be exploited to provide information about the accessibility of this chromophore and therefore may be used to investigate and monitor processes such as its binding to proteins.[126] Results such as this serve to demonstrate the potential utility of this effect with regard to the development of responsive lanthanide-based CPL probes.

1.5.3 Lanthanide complexes containing chiral ligands

As was discussed in Section 1.4, lanthanide complexes derived from chiral ligands will typically exist in solution as one major stereoisomer if complexation yields a chiral structure. The modulation of the CPL output from such enantiopure complexes in the presence of a chosen analyte may be induced via one of two mechanisms, both of which will be described and exemplified below.

1.5.3.1 Sensing through a change in the primary coordination environment

The first mechanism by which modulation of the CPL output may occur for an enantiopure lanthanide system is through a change in the primary coordination environment of the lanthanide ion. Such a change may comprise the displacement of a weakly bound primary ligand donor or coordinated water molecule, typically yielding

an alteration in the hydration state of the given lanthanide complex. Alternatively, the modulation of the CPL output may be brought about by a more subtle change in the primary coordination environment, such as an alteration of the strength of interaction or polarizability of a primary ligand donor. As was discussed in Section 1.3.4.3, the former of these approaches has been employed to great effect in the development of ratiometric lanthanide-based systems, where changes in the total luminescence output are exploited to signal the presence of a target analyte. It is therefore perhaps unsurprising that all of the enantiopure systems for which CPL modulation has been demonstrated as a result of change in the primary coordination environment are also based on this well-explored principle.

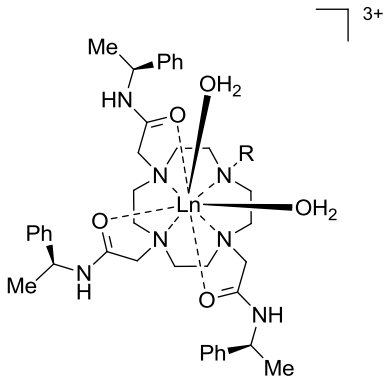

(*SSS*)-[Ln.**L**^{15}$(OH_2)_2]^{3+}$ R = H
(*SSS*)- [Ln.**L**^{16}$(OH_2)_2]^{3+}$ R = Me

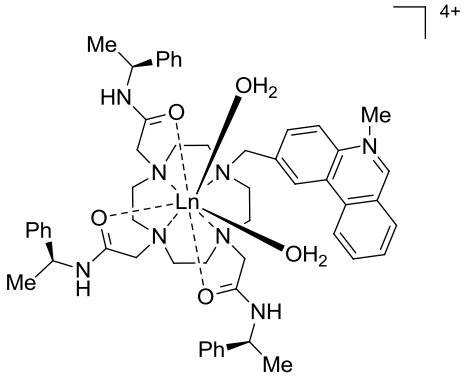

(*SSS*)-[Ln.**L**^{17}$(OH_2)_2]^{4+}$

The earliest example in the literature of an 'enantiopure' lanthanide-based system where an alteration of the observed CPL spectral signature has been demonstrated in the presence of a chosen analyte was published in 1998.[53] In this study, the analyte binding capabilities of the complex (*SSS*)-[Ln.**L**^{15}$(OH_2)_2]^{3+}$ (Ln = Eu^{3+} or Tb^{3+}) were evaluated. Following its synthesis, the speciation of this complex was determined using NMR spectroscopy, with spectra revealing that it exists in solution as a mix of four stereoisomers, in a ratio of 3.5 : 1 : 0.5 : 0.25. Although at this time no effort was made to assign the helicity of the major stereoisomer in solution, a later study involving this complex suggested that a Δ configuration was adopted.[50] This conclusion was made on the basis of a comparison of the CPL spectral fingerprint recorded for (*SSS*)-[Ln.**L**^{15}$(OH_2)_2]^{3+}$ in the absence of additives to the CPL spectrum of a related tetraamide complex, whose absolute configuration had been verified by X-ray crystallography.

Preliminary experiments monitoring changes in hydration state and total emission spectral form of (*SSS*)-[Ln.$\mathbf{L}^{\mathbf{15}}$$(OH_2)_2]^{3+}$ in the presence of a number of anions were reported as part of the 1998 study.[53] These experiments revealed that HCO_3^- and CO_3^{2-} were distinctive in their ability to form a chelated adduct with the lanthanide ion centre, with the presence of this adduct being confirmed by ESMS. CPL measurements were used to probe the excited state structure of (*SSS*)-[Eu.$\mathbf{L}^{\mathbf{15}}$$(OH_2)_2]^{3+}$, both in the presence and absence of 40 mM HCO_3^- and 10 mM HPO_4^{2-}. In both cases results showed a modulation of the CPL output compared to that observed for the free complex. In the case of HCO_3^-, the intensity of the circularly polarized transitions was roughly halved. Meanwhile, for HPO_4^{2-} the CPL intensity was unchanged but the form of the $\Delta J = 1$ manifold was altered, with an additional component becoming distinguishable.

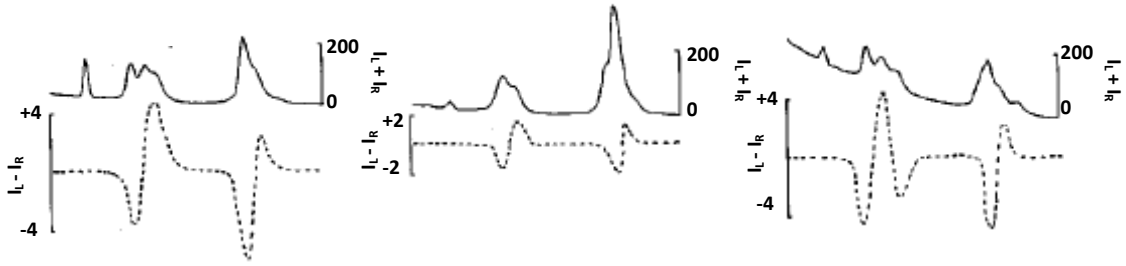

Figure 1.25: Total emission (top) and CPL (bottom) spectra for (*SSS*)-[Eu.$\mathbf{L}^{\mathbf{15}}$$(OH_2)_2]^{3+}$ alone (left; 293 K, 0.1 M MES, pD 6.9) and with 40 mM HCO_3^- (middle) and 10 mM HPO_4^{2-} (right).[53]

Additional investigations into the anion binding behaviour of both enantiomers of [Ln.$\mathbf{L}^{\mathbf{15}}$$(OH_2)_2]^{3+}$ and its N-alkylated analogues [Ln.$\mathbf{L}^{\mathbf{16}}$$(OH_2)_2]^{3+}$ and [Ln.$\mathbf{L}^{\mathbf{17}}$$(OH_2)_2]^{4+}$ were published in 2000.[50] As part of this study, further CPL spectra were obtained for both enantiomers of [Eu.$\mathbf{L}^{\mathbf{15}}$$(OH_2)_2]^{3+}$ in the presence of 10 equivalents of added HCO_3^-, HPO_4^{2-}, lactate and malonate.[50] Although the binding of both lactate and malonate to the metal centre had been verified by other methods, only the former two anions caused significant perturbation of the observed CPL signal in comparison to the spectrum obtained for the complex in the absence of anion. For the N-alkylated complexes the binding of these two anions to the metal centre was also examined using both total emission and CPL spectroscopic techniques. While little change in form was observed for either complex with HPO_4^{2-}, a noticeable variation was apparent with HCO_3^-. It should be noted that, for a given enantiomer, the N-alkylated complexes [Eu.$\mathbf{L}^{\mathbf{16}}$$(OH_2)_2]^{3+}$ and [Eu.$\mathbf{L}^{\mathbf{17}}$$(OH_2)_2]^{4+}$ have identical CPL spectra and therefore identical helicity. However, the CPL spectral fingerprint of these complexes differs significantly in both the sign and relative intensity of the $\Delta J = 1$ and $\Delta J = 2$ bands in

comparison to [Eu.$\mathbf{L}^{\mathbf{15}}(OH_2)_2]^{3+}$. An emission spectrum of [Eu.$\mathbf{L}^{\mathbf{17}}(OH_2)_2]^{4+}$ was subsequently obtained in a solution designed to simulate an extracellular anionic environment.[50] The form of the spectrum was seen to mimic that of the carbonate adduct, suggesting preferential binding of this species under these conditions. In accordance with this result, a titration was performed in a mixed anionic background where the change in the emission dissymmetry factor at 614 nm was measured as a function of added HCO_3^- concentration. The binding curve generated was in good agreement with those produced using total intensity or intensity ratio data.

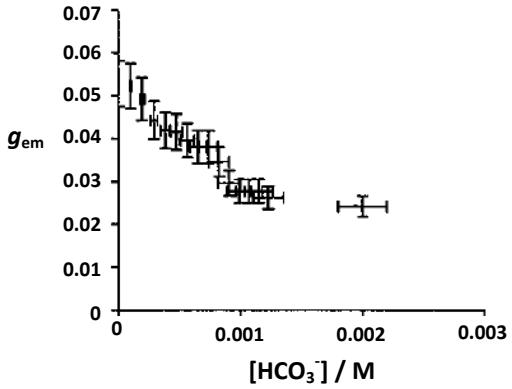

Figure 1.26: Variation in the emission dissymmetry factor measured at 614 nm for the complex (*SSS*)-[Eu.$\mathbf{L}^{\mathbf{17}}(OH_2)_2]^{4+}$ as a function of added $NaHCO_3$ (pH 7.4, 100 mM NaCl, 0.9 mM Na_2HPO_4, 0.13 mM sodium citrate, 2.3 mM sodium lactate).[50]

On the basis of preliminary ^{1}H NMR studies of the complex [Eu.$\mathbf{L}^{\mathbf{15}}(OH_2)_2]^{3+}$ in the presence and absence of 10 equivalents of HCO_3^- it was suggested that binding of this anion to the metal centre causes a change in complex geometry, from a square-antiprismatic structure to a twisted square-antiprismatic structure.[50] The modulation of the CPL output was therefore tentatively attributed to a change in twist angle. However, this conclusion was later discounted following a subsequent study in which a variety of anion adducts of the complex [Yb.$\mathbf{L}^{\mathbf{15}}(OH_2)_2]^{3+}$ were prepared and crystal structures obtained, therefore allowing the emission dissymmetry factors of the ternary complexes to be correlated to the nature of the most likely axial donor.[127] It was hypothesised that the variation in the circular polarization and ^{1}H NMR spectra of the chelated adducts can be attributed to a change in the axial donor polarizability, rather than an alteration of the helicity around the lanthanide centre.

It should be noted that the modulation of the CPL output of the complexes discussed above has also been demonstrated with a number of other analytes. For example, a CPL experiment using (*SSS*)-[Eu.$\mathbf{L}^{\mathbf{16}}(OH_2)_2]^{3+}$ has shown that the binding interactions of a

variety of phosphate anions with this complex may be distinguished on the basis of subtle differences in the CPL spectral fingerprints.[128] Meanwhile, CPL spectroscopic techniques have also been exploited in studies concerned with examining the DNA binding capabilities of [Eu.$\mathbf{L}^{\mathbf{17}}(OH_2)_2]^{4+}$.[129] On the basis of comparison of CPL spectral data obtained in the presence of DNA and that obtained with HPO_4^{2-}, it was deduced that the binding interaction between this complex and DNA constituted the formation of an adduct in which the europium centre was coordinated to an oligonucleotide phosphate group. Further exploitation of this complex as a DNA binding probe was unfortunately prohibited due to the occurrence of substantial charge transfer quenching of the intermediate phenanthridinium singlet excited state.

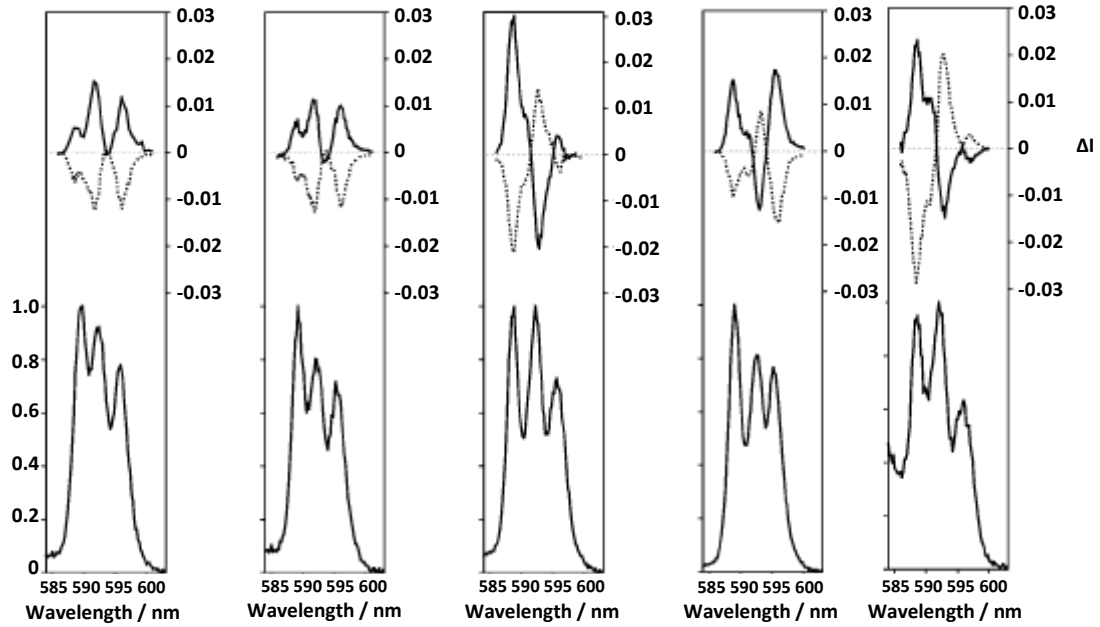

Figure 1.27: Total emission (bottom) and CPL (top) spectra for (*RRR*)-Λ (bold) and (*SSS*)-Δ-[Eu.$\mathbf{L}^{\mathbf{16}}(OH_2)_2]^{3+}$ (dashed) in the presence of 10 equivalents of *N*-acetyl-*O*-phospho-*L*-tyrosine, a phosphorylated hexapeptide, *D*-glucose-6-phosphate, *O*-phospho-*L*-tyrosine and HPO_4^{2-} (left to right) (293 K, 0.1 M MOPS, pH 7.4).[128]

An additional example of a coordinatively unsaturated lanthanide system displaying modulation of its CPL output in response to bicarbonate binding has been described in the literature more recently.[130] In contrast to the work described above, where changes in the CPL spectral signature were only investigated for europium based systems, this work describes modulation of the CPL output for both europium and terbium analogues of the complex (*SS*)-[Ln.$\mathbf{L}^{\mathbf{18}}(OH_2)_2]^{3+}$ when in the presence of bicarbonate. In doing this, it highlights the way in which the use of systems that report on changes in their environment via CPL modulation, as opposed to ratiometric measurements of total

intensity, can better facilitate the exploitation of terbium-based complexes as responsive probes.

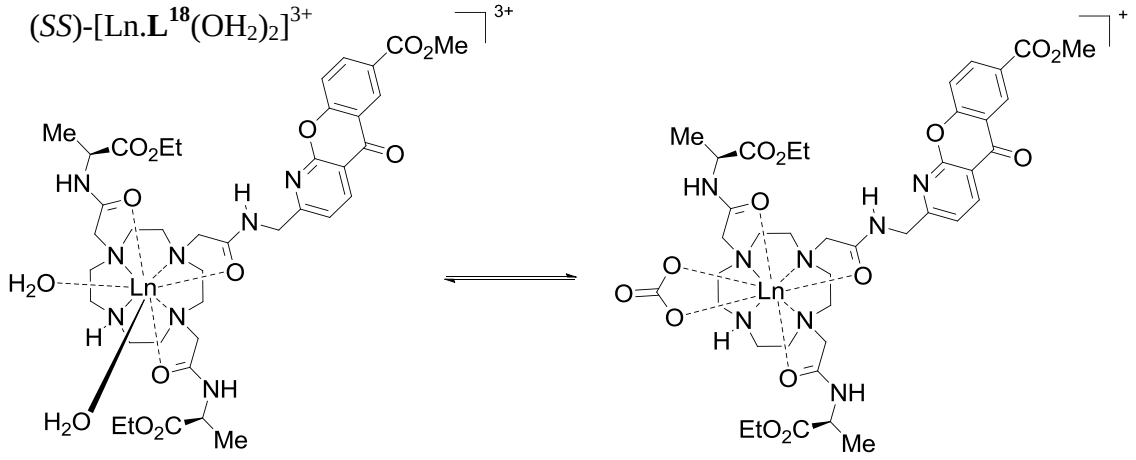

As for the systems that have previously been described in this section, the mechanism by which CPL modulation is brought about involves the displacement of coordinated water molecules from the lanthanide ion centre by the target analyte. Changes in the CPL spectral fingerprint for (*SS*)-[Eu.$\mathbf{L}^{\mathbf{18}}(OH_2)_2]^{3+}$ in the presence of bicarbonate were most pronounced in the $\Delta J = 1$ and $\Delta J = 2$ manifolds of the spectrum, with the relative sign of the two transitions observed in the $\Delta J = 1$ manifold becoming inverted. In the case of (*SS*)-[Tb.$\mathbf{L}^{\mathbf{18}}(OH_2)_2]^{3+}$, the CPL spectrum in the presence of bicarbonate showed most change within the $\Delta J = 1$ (545 nm) manifold and an increased intensity in the $\Delta J = -1$ (630 nm) manifold. Generally speaking, emission dissymmetry values were seen to increase in the presence of bicarbonate, in contrast to behaviour observed for the triamide based systems. It was suggested that the observed changes in the CPL fingerprint could be attributed to an altered local helicity at the lanthanide centre in the ternary complex, with a different twist angle and more rigid coordination geometry. It should be noted that the CPL spectral signature for (*SS*)-[Tb.$\mathbf{L}^{\mathbf{18}}(OH_2)_2]^{3+}$ was also recorded in the presence of citrate but no significant change in form was apparent in comparison to the unbound complex.

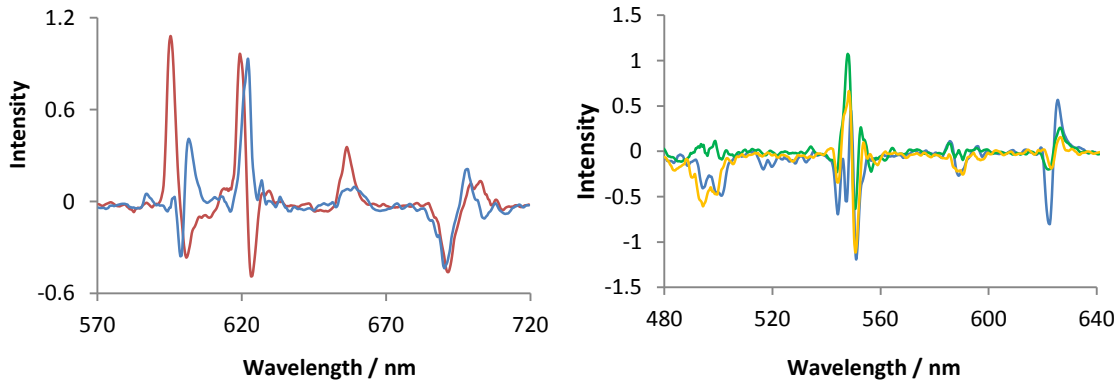

Figure 1.28 Left: CPL spectra of (*SS*)-[Eu.**L**^{18}$(OH_2)_2]^{3+}$ in the presence (blue) and absence (red) of 30 mM sodium bicarbonate (295 K, 0.1 M NaCl). **Right:** CPL spectra of (*SS*)-[Tb.**L**$^{1.18}$$(OH_2)_2]^{3+}$ (green); in the presence of 30 mM sodium bicarbonate (blue) and in the presence of 2 mM sodium citrate (yellow) (295 K, 0.1 M NaCl).[130]

The structurally related complex, (*SS*)-[Eu.**L**^{19}$(OH_2)]^{3+}$, also recently reported in the literature, provides an example of a system in which a change in primary coordination environment as a result of the reversible displacement of one of the ligand donors leads to an altered CPL output.[131] In this system, a sulphonamide moiety is incorporated into the ligand framework, which is deprotonated at high pH and able to bind to the lanthanide centre. However, at low pH this is not the case and the coordination sphere is instead completed by a bound water molecule. This pH dependent change in the primary coordination environment of the europium complex is signalled by alterations in the CPL fingerprint. At higher pH larger emission dissymmetry factors are apparent, perhaps indicative of a rigidified structure in which the angle between the electric and magnetic transition dipole vectors is subject to less variation over time in comparison to the structure at low pH. It was shown that variation in the emission dissymmetry factor with pH could be used to calculate a protonation constant for the complex, which was in good agreement with the value derived using total emission spectral changes.

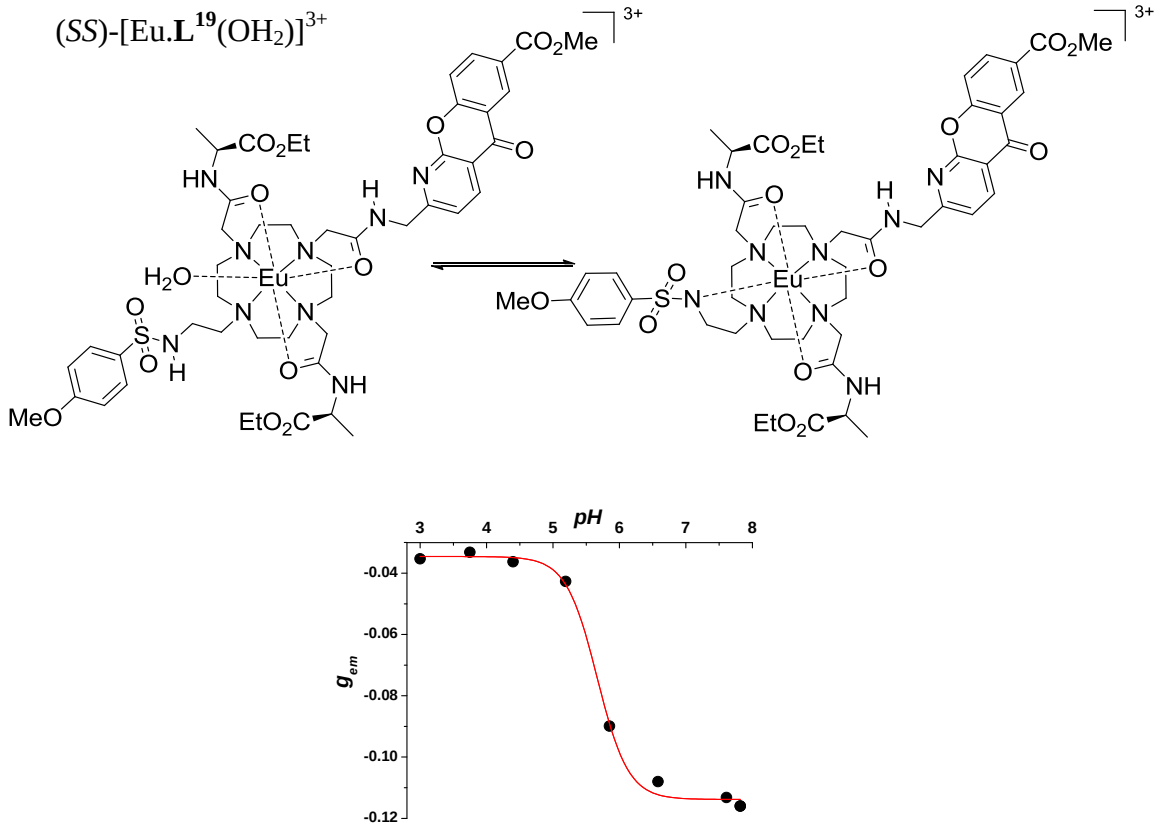

Figure 1.29: Schematic showing structural changes accompanying alteration in solution pH for (*SS*)-[Eu.**L**^{19}(OH$_2$)]$^{3+}$. These changes result in alteration of both the total emission and CPL spectral signature, giving rise to changes in g_{em}. The variation in the emission dissymmetry factor at 632 nm as a function of pH is shown (pK_a = 5.65 (± 0.04), 295 K, 0.1 M NaCl).[131]

1.5.3.2 Sensing through a change in complex configuration

The second mechanism by which modulation of the CPL output may occur for an enantiopure lanthanide system is through a change in complex configuration. Such a change may comprise concerted arm rotation or an alternative rearrangement of the coordination polyhedron, both of which will lead to an altered CPL output.

At present, there is only one example in the literature of a lanthanide-based system in which the modulation of the CPL output is brought about through a change in the complex configuration. In this system, (*SSS*)-[Ln.**L**^{20}]$^{3+}$, the ligand framework incorporates three chiral arms and a tetraazatriphenylene sensitising moiety and may be thought of as being derived from DOTA. Comparison of the CPL spectral form for this complex to that of related systems in which the absolute configuration has been verified by X-ray crystallography has allowed the identification of the major stereoisomer as one adopting a square antiprismatic $\Delta(\lambda\lambda\lambda\lambda)$ configuration.[84, 132] As is expected, the (*RRR*)

analogue of this complex adopts an enantiomeric Λ(*δδδδ*) configuration, verified by the observation of mirror image CPL spectra.

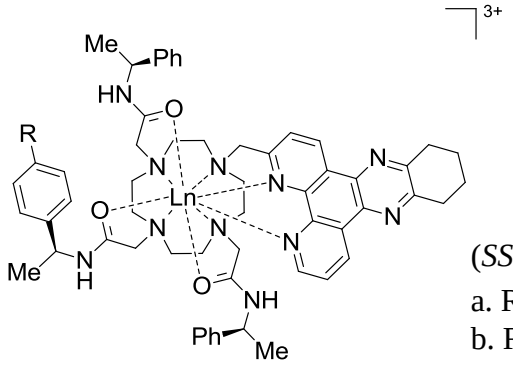

(*SSS*)-Δ-[Ln.**L**^{20}]$^{3+}$
a. R = H
b. R = CO_2Me

The modulation of the CPL output from (*SSS*)-Δ-[Ln.**L**^{20}]$^{3+}$ was observed as part of a study in which the binding of this complex and its enantiomer by the protein serum albumin was examined using a variety of methods.[133] Whilst no significant change in CPL spectral form was observed for the (*RRR*)-Λ stereoisomer, for (*SSS*)-Δ-[Ln.**L**^{20}]$^{3+}$ it was found that a dramatic modulation of the CPL output was induced in the presence of the protein serum albumin (Figure 1.30). The sign of the CPL signal was found to be inverted for the majority of transitions when the (*SSS*)-Δ complex was in the presence of this protein, for both the europium and terbium analogues. It was suggested that this observation was consistent with the preferential stabilisation of the Δ complex isomer as a Λ complex when in the presence of serum albumin.

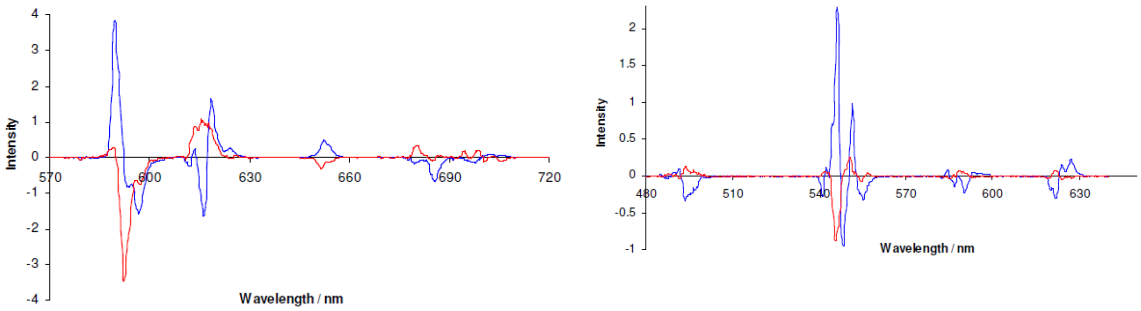

Figure 1.30: CPL spectra of (*SSS*)-[Ln.**L**^{20}]$^{3+}$ (left = Eu^{3+}, right = Tb^{3+}) in the presence (red) and absence (blue) of 15 μM bovine serum albumin (D_2O, 295 K).[134]

In a later publication, distinct similarity was noted between the CPL spectral form of (*SSS*)-[Eu.**L**^{20}]$^{3+}$ in the presence of serum albumin and the CPL spectrum recorded for a structurally related lanthanide complex, (*SSS*)-Λ-[Eu.**L**^{21}]$^{3+}$, in the absence of any additive.[135] On the basis of this observation, it was concluded that the configurations adopted by these systems under the conditions mentioned above must be identical. Due

to the fact that CPL inversion was noted for these systems in comparison to (*SSS*)-Δ-[Ln.**L**^{20}]$^{3+}$ it was suggested that they favour a square antiprismatic Λ-(*δδδδ*) configuration in solution, therefore implying that both cooperative arm rotation and ring inversion are induced in (*SSS*)-Δ-[Ln.**L**^{20}]$^{3+}$ when in the presence of serum albumin. Additional evidence to support the adoption of a Λ-(*δδδδ*) configuration by (*SSS*)-Λ-[Ln.**L**^{21}]$^{3+}$ in solution was provided by ^{1}H NMR data, which showed a reduced dipolar shift for (*SSS*)-Λ-[Eu.**L**^{21}]$^{3+}$ in comparison to (*SSS*)-Δ-[Eu.**L**^{20}]$^{3+}$, seemingly consistent with the proposed structural differences between the complexes. An alternative and perhaps more likely interpretation of this data would be that the reduced dipolar shift is indicative of the predominance of a twisted square antiprismatic stereoisomer in solution for (*SSS*)-Λ-[Ln.**L**^{21}]$^{3+}$. This hypothesis is supported by the fact that the splitting within the Δ*J* = 1 band of the total emission spectrum is smaller for (*SSS*)-Λ-[Eu.**L**^{21}]$^{3+}$ in comparison to (*SSS*)-Δ-[Eu.**L**^{20}]$^{3+}$. Taking into account the comparative CPL spectra, this revised interpretation of the data implies that (*SSS*)-Λ-[Ln.**L**^{21}]$^{3+}$ exists predominantly as the twisted square antiprismatic Λ-(*λλλλ*) stereoisomer in solution. Hence, the presence of serum albumin induces concerted arm rotation for (*SSS*)-Δ-[Ln.**L**^{20}]$^{3+}$ in solution and likely additional polyhedral distortion, but the configuration of the ring may be thought of as being conserved. Given the nature of the observed changes in the CPL spectral signature of (*SSS*)-[Ln.**L**^{20}]$^{3+}$, it must be the case that the structural changes induced in the presence of protein lead to alteration of the rotatory strength of the transitions, perhaps implying that in this case some relationship does exist between the twist angle around the principal axis, θ, and the angle between the magnetic and electric transition dipoles, τ.

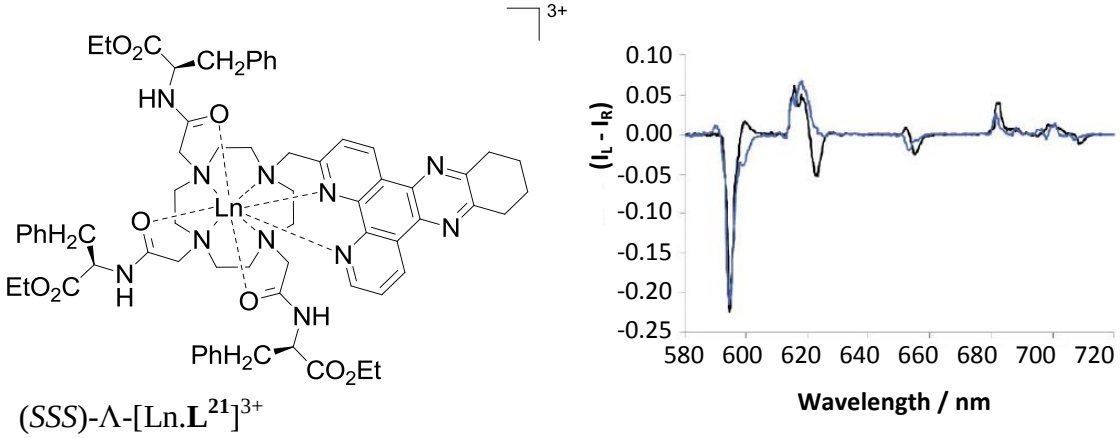

Figure 1.31: Comparison of the CPL spectral signature of (*SSS*)-[Eu.**L**^{20}]$^{3+}$ (blue) in the presence of added BSA (30 μM) with that observed for (*SSS*)-Λ-[Eu.**L**^{21}]$^{3+}$ (black) in the absence of any additive (295 K, 0.1 M HEPES, pH 7.4, 15 μM complex).[135]

The nature of the interaction between (*SSS*)-[Ln.$\mathbf{L}^{\mathbf{20}}$]$^{3+}$ and serum albumin in solution has been probed using saturation transfer difference (STD) NMR techniques as well as via competitive binding studies and DFT modelling and docking simulations.[136] These experiments have revealed that the formation of (*SSS*)-Λ-[Ln.$\mathbf{L}^{\mathbf{20}}$]$^{3+}$ involves non-covalent interactions between the ligand sensitising moiety and the hydrophobic pocket in drug-site(II) of serum albumin. The phenylmethyl pendant arms were also shown to be implicated in the primary protein binding interaction, therefore providing some enlightenment with regard to the lack of CPL modulation observed for the (*RRR*)-Λ stereoisomer.

Although further experiments exploiting the responsive CPL properties of (*SSS*)-Δ-[Ln.$\mathbf{L}^{\mathbf{20}}$]$^{3+}$ have yet to be reported in the literature, it may be envisaged that instrumental advances could yet facilitate the exploitation of this complex in the intracellular mapping of serum albumin.

1.6 Project aims

As outlined in the preceding sections of this chapter, there exists in the literature a number of examples of lanthanide systems exploiting modulation of their CPL output to report on aspects of their environment, such as the presence of a chosen analyte. Notwithstanding these reports, it remains the case that the overwhelming majority of responsive lanthanide-based probes developed to date utilise changes in luminescence intensity or lifetime in order to convey information. In light of this fact, the aim of the work described in this thesis is to identify and develop new lanthanide-based systems where the presence of a given analyte is indicated by changes in the observed CPL output. The following chapters detail research conducted in pursuit of this aim. Chapter 2 outlines the discovery of a novel mechanism through which CPL modulation can be brought about, and explores the possibility of its application to the sensing of acute phase proteins. Meanwhile, Chapter 3 builds on this work, demonstrating the way in which this mechanism may also be exploited for the determination of enantiomeric excess in solutions containing a known concentration of a chosen chiral analyte. Finally, Chapter 4 focuses on work carried out with a view to the identification of macrocyclic lanthanide systems with potential utility in chiral quenching studies.

CHAPTER TWO

A CHIRAL PROBE FOR ACUTE PHASE PROTEINS

2.1 Introduction

The contents of this chapter detail work undertaken in the pursuit of a novel lanthanide-based system for use as a responsive CPL probe. The initial focus of the work described herein was the synthesis and characterisation of an enantiopure complex, derived from a chiral ligand framework. The synthetic target was chosen following consideration of work detailed in a communication published in 2010, concerning the racemic complex $[Ln.\mathbf{L}^{\mathbf{22}}]^+$.[137] In this communication it was reported that the emission spectral fingerprint of $[Eu.\mathbf{L}^{\mathbf{22}}]^+$ underwent a dramatic change in form when in the presence of the protein serum albumin, showing a large increase in the relative intensity of the $\Delta J = 2$ transition and changes in the splitting of the $\Delta J = 1$ manifold. As was outlined in Section 1.3.2 of Chapter 1, changes in the emission spectral profile of a europium complex such as these are typically indicative of an alteration in the metal ion coordination environment.

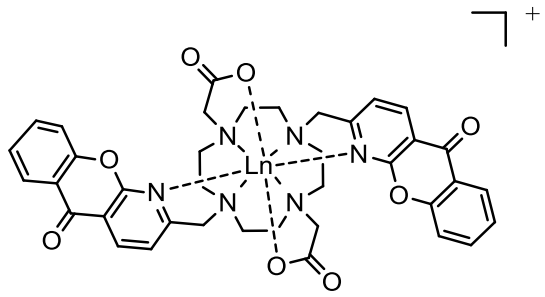

$[Ln.\mathbf{L}^{\mathbf{22}}]^+$

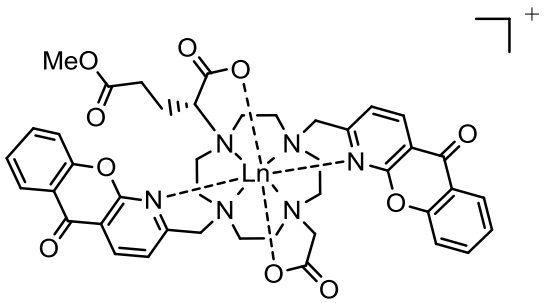

(*R*)-$[Ln.\mathbf{L}^{\mathbf{23}}]^+$

Ln = Eu^{3+}, Tb^{3+}

As was illustrated in the previous chapter, the circularly polarized emission of a given enantiopure lanthanide complex is also typically sensitive to changes in the metal ion coordination environment. Hence, it was proposed that by synthesising an analogue of $[Ln.\mathbf{L}^{\mathbf{22}}]^+$ containing a chiral ligand framework, it would be possible to create a responsive probe where interactions with chiral species, such as serum albumin, were not only signalled by changes in the emission spectral form but also by variations in the CPL fingerprint.

On the basis of the fact that the introduction of a stereogenic centre α to the ring nitrogen has been observed to impart rigidity into lanthanide complexes, leading to one diastereomeric form being favoured in solution, the complex (*R*)-$[Ln.\mathbf{L}^{\mathbf{23}}]^+$ was chosen as the synthetic target.[80] It was hoped that the small alteration to the ligand framework would not affect the analyte binding abilities of the enantiopure complex, in comparison to $[Ln.\mathbf{L}^{\mathbf{22}}]^+$.

2.2 Synthetic aspects

2.2.1 Synthesis of the chromophore

The azaxanthone chromophore was synthesised according to previously described methods.[138] The synthetic pathway is shown in Scheme 2.1.

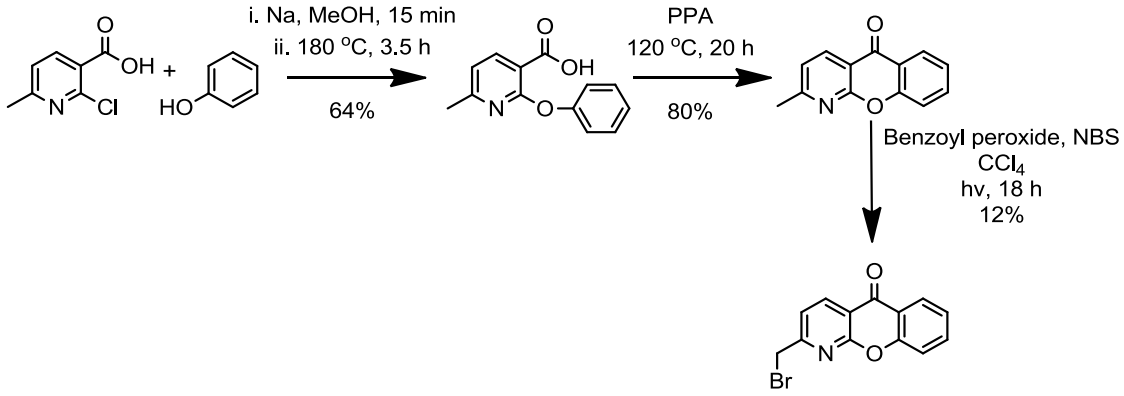

Scheme 2.1: Chromophore synthesis.

Reaction of 2-methyl-1-azaxanthone with N-bromosuccinimide, using dibenzoyl peroxide as a radical initiator yielded a mixture of the unreacted reagent, along with the mono- and di-brominated products. The mono-brominated product was isolated for use by column chromatography on silica gel and is characterised by the presence of a singlet at ~ 4.6 ppm in its ^{1}H NMR spectrum, corresponding to the methylene group protons.

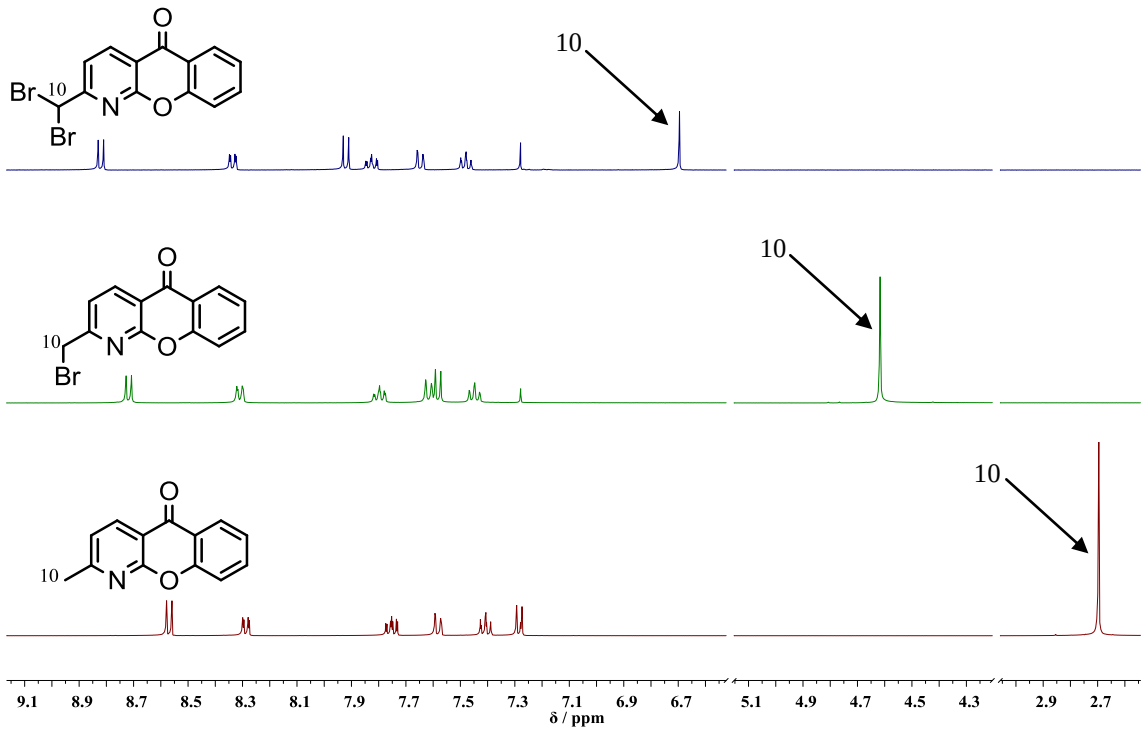

Figure 2.1: Comparison of ^{1}H NMR spectra for 2-methyl-1-azaxanthone (1) and its mono- (2) and di-brominated (3) analogues ($CDCl_3$, 295 K, 400 MHz).

2.2.2 Synthesis of the chiral pendant arm

In previous instances, the incorporation of an enantiomerically pure glutarate arm into a cyclen based complex has been achieved by the use of either (*S*)-2-bromopentanedioic acid 5-benzyl ester 1-*tert*-butyl ester or its 1,5-dimethyl ester analogue.[139, 140] Taking into account the nature of the target complex it may at first seem intuitive to attempt the synthesis of (*S*)-2-bromopentanedioic acid 5-methyl ester 1-*tert*-butyl ester. However, the preparation of this species from the commercially available precursor, (*S*)-glutamic acid 5-methyl ester, via the established procedure used in the synthesis of the 5-benzyl ester analogue mentioned above (Scheme 2.2) is precluded. The methyl ester would be likely to undergo hydrolysis under the acidic conditions used in the first stage of this synthesis, yielding a species in which neither of the carboxylate groups are protected. (*S*)-2-Bromopentanedioic acid 5-benzyl ester 1-*tert*-butyl ester was therefore prepared in accordance with Scheme 2.2. In this derivative, the two carboxylate groups are protected in an orthogonal manner, facilitating their selective removal at different stages of the subsequent synthetic procedure.

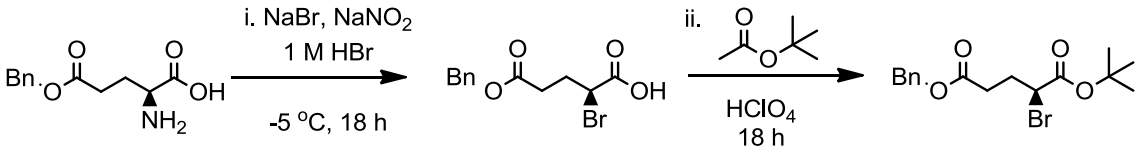

Scheme 2.2: Synthetic pathway for the preparation of (*S*)-2-bromopentanedioic acid 5-benzyl ester 1-*tert*-butyl ester. The overall yield was 13%.

In the initial step of the reaction, a solution of aqueous sodium nitrite was added dropwise to a solution of the glutamic acid based starting material and sodium bromide salt in 1 M HBr. The temperature of the reaction solution was maintained at -5 ^{o}C over the course of the addition. The combination of sodium nitrite and the mineral acid HBr leads to the in situ generation of nitrous acid, which induces the formation of a diazonium salt from the starting material. The diazo group is easily displaced by bromide in two successive S_N2 reactions, in this case yielding (*S*)-2-bromopentanedioic acid 5-benzyl ester. This species was isolated and used without purification in the next step of the reaction, which involved the protection of the carboxylate functionality as a *tert*-butyl ester. In order to achieve the esterification, the glutamic acid derivative was dissolved in *tert*-butyl acetate which was then acidified using perchloric acid. The solution was left to stir at room temperature overnight and, following work up, the product was purified by column chromatography.

2.2.3 Synthesis of the ligand

In order to accomplish the synthesis of the target ligand, $\mathbf{L}^{23}$, it was first necessary to produce 1,4,7,10-tetraaza-cyclododecane-1,7-dicarboxylic acid dibenzyl ester, **1**, a protected cyclen derivative. This was achieved using a published procedure and gave the desired product in reasonable yield.[141] The full ligand synthesis is shown in Scheme 2.3.

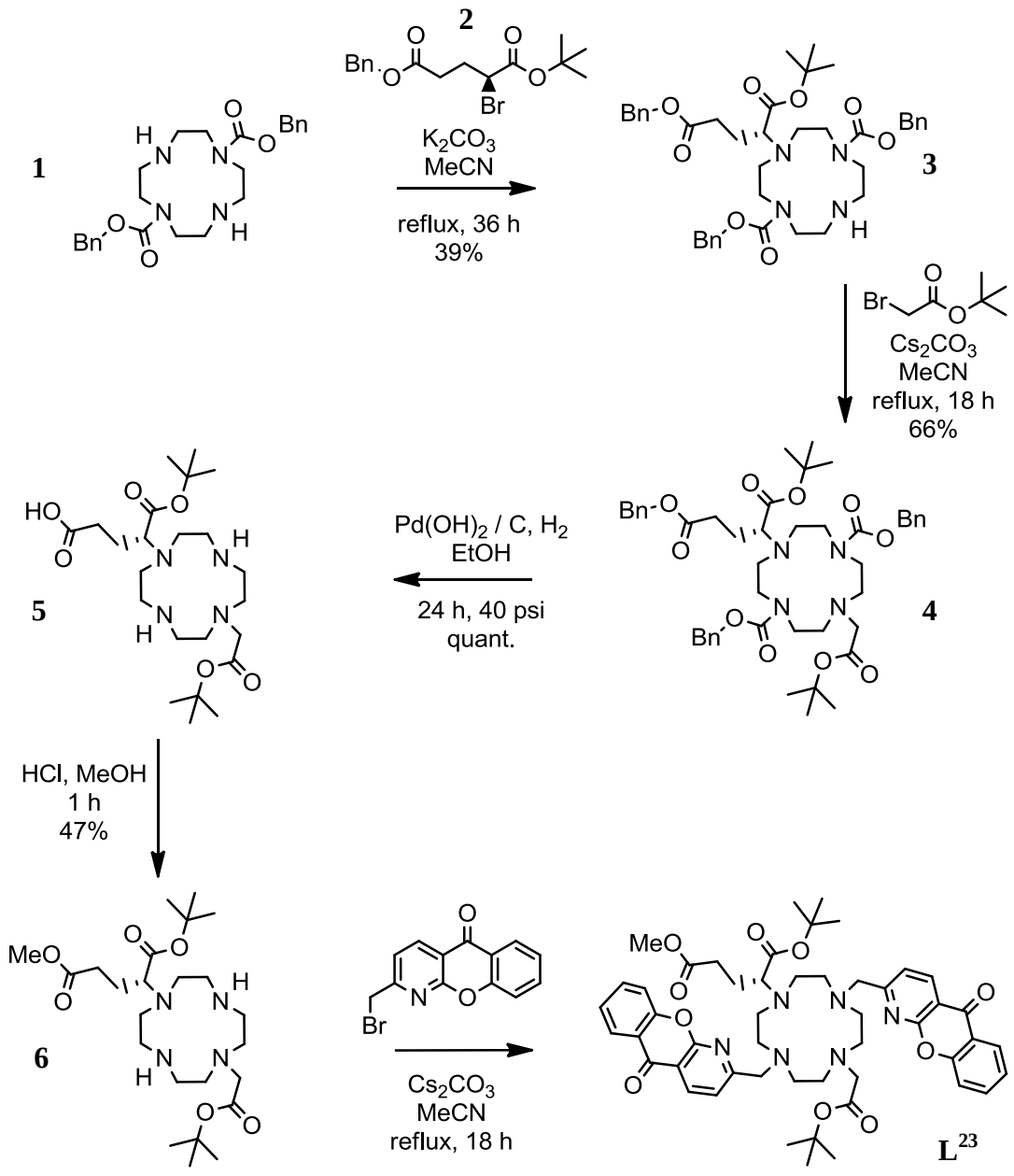

Scheme 2.3: Complete synthesis of $\mathbf{L}^{23}$.

The initial step in the synthetic scheme outlined above involved the mono-alkylation of the protected cyclen derivative, **1**. It was decided that the best way to proceed would be via the mono-alkylated species **3**. This is because it is known that di-alkylation of **1** with *tert*-butyl bromoacetate is facile, with the reaction between these two species being

utilised in the synthesis of a frequently used cyclen derivative known as DO2A.[141] Hence, preferential formation of the mono-alkylated species would require extremely well-tuned reaction conditions. It was thought that the comparatively increased steric bulk of the glutarate derivative **2** may facilitate selective formation of a mono-alkylated species. The chiral arm was therefore introduced under standard conditions (CH_3CN, K_2CO_3), with the S_N2 nucleophilic substitution reaction giving **3** in moderate yield. Competitive formation of the di-alkylated species did not appear to be yield-limiting and in a subsequent attempt at this reaction, it was found that the yield was not improved if the reaction was left for a longer time period.

Following purification of **3** by column chromatography, the second alkylation was carried out with *tert*-butyl bromoacetate. The reaction was carried out in a small volume of acetonitrile in order to maximise the rate and extent of reaction. The benzyl protecting groups were subsequently cleaved by hydrogenolysis using a heterogeneous catalyst, which was removed from the product, **5**, by filtration through celite. Before the azaxanthone chromophores could be coupled onto the cyclen ring it was necessary to reprotect the carboxylate group of the chiral pendant arm, this time as a methyl ester. This was achieved in an acid-catalysed reaction in methanol, which was monitored by mass spectrometry. The final step in the preparation of $\mathbf{L}^{\mathbf{23}}$ involved another alkylation reaction. This time, 2-bromomethyl-1-azaxanthone was coupled onto the cyclen ring twice, again via an S_N2 nucleophilic substitution reaction carried out under standard conditions. The reaction was checked by TLC to confirm that the brominated starting material had been completely consumed, before being worked up.

An attempt was made to purify the crude product $\mathbf{L}^{\mathbf{23}}$ by column chromatography on silica gel. However, it did not prove possible to achieve the separation of the desired product using this method. The decision was made to continue with the synthesis of (*R*)-[Ln.$\mathbf{L}^{\mathbf{23}}$]$^+$ using the crude sample of $\mathbf{L}^{\mathbf{23}}$, anticipating that (*R*)-[Ln.$\mathbf{L}^{\mathbf{23}}$]$^+$ could later be purified by preparative HPLC.

2.2.4 Lanthanide complex formation and purification

Formation of the lanthanide complex required two further steps (Scheme 2.4).

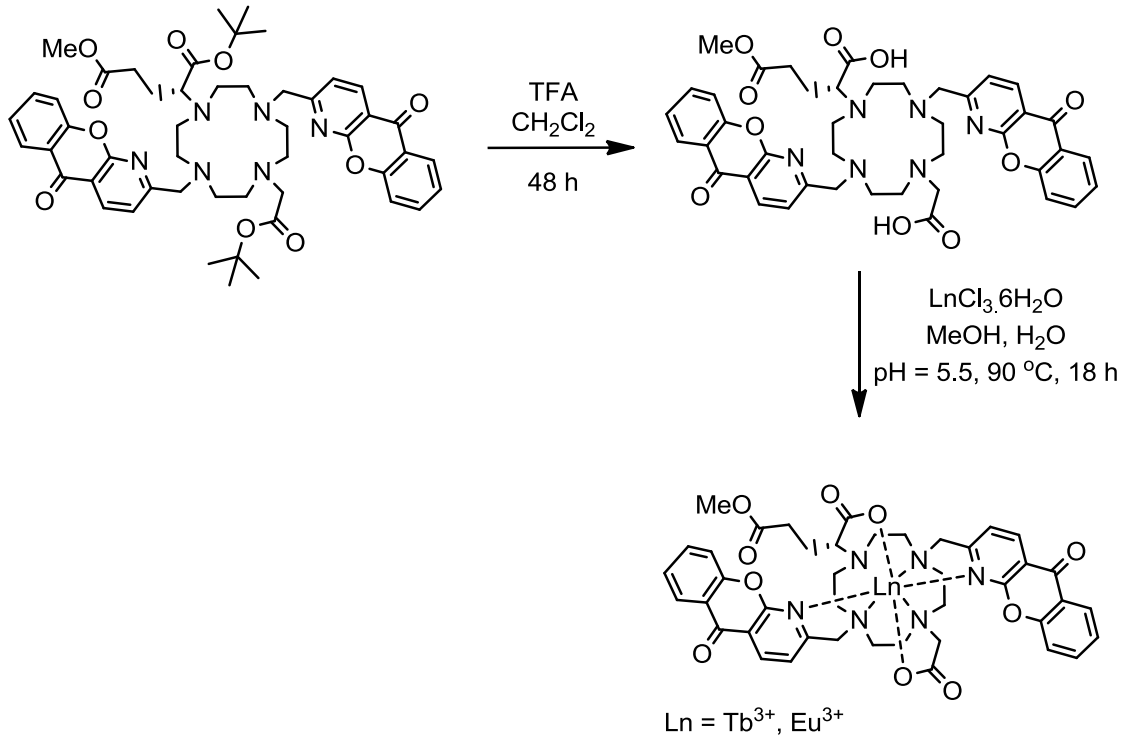

Scheme 2.4: Formation of the lanthanide complex, (*R*)-[Ln.**L**^{23}]$^{+}$.

Initially, attempts were made to monitor the removal of the *tert*-butyl protecting groups using TFA by ^{1}H NMR spectroscopy. However, solubility issues in both MeOD and $CDCl_3$ hampered these attempts. This problem was resolved by instead using LCMS to monitor the progress of the deprotection reaction. Once the cleavage was complete, it was possible to proceed to the second stage of the reaction scheme. Metal complexation was confirmed, prior to isolation of each of the complexes, by removing a sample of the reaction mixture and obtaining its emission spectrum in water. In each case, the characteristic emission spectra expected for europium and terbium were visible, following excitation of the azaxanthone chromophore at 336 nm.

Once the complexes had been isolated, samples were submitted for HPLC. For both the europium and terbium complexes, this analysis revealed the presence of two major luminescent species in roughly equal abundance. Further analysis using LCMS revealed the identity of these luminescent species, with both of the samples being found to be mainly comprised of a mixture of the desired complex and its hydrolysed analogue, (*R*)-[Ln.**L**^{24}].

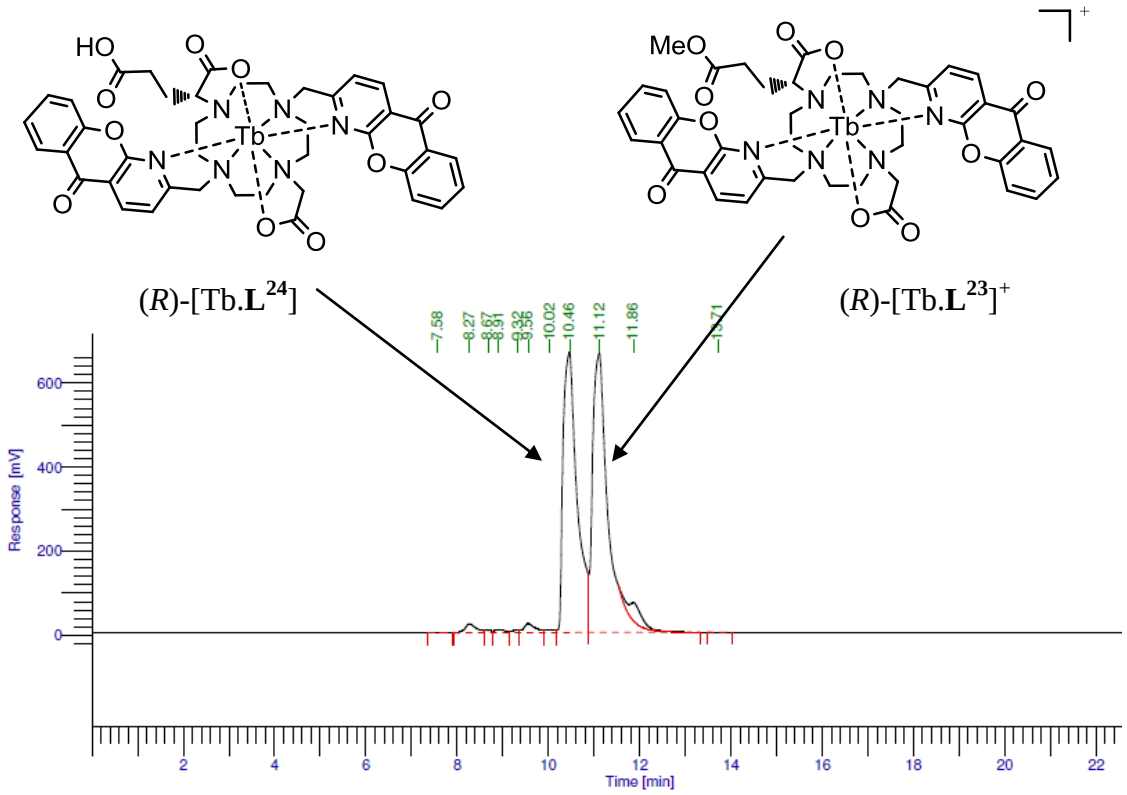

Figure 2.2: HPLC trace obtained for (*R*)-[Tb.$\mathbf{L}^{23}$]$^{+}$ following complexation of crude $\mathbf{L}^{23}$.

Since there was no evidence of the ligand $\mathbf{L}^{24}$ being present in the crude ligand sample used for complexation, it was inferred that the hydrolysis of the methyl ester occurred during the complexation procedure. This is not an unreasonable theory as both acidic and basic conditions were used at different stages of this procedure, potentially leading to hydrolysis. Preparative HPLC was used to obtain pure samples of (*R*)-[Ln.$\mathbf{L}^{23}$]$^{+}$ and (*R*)-[Ln.$\mathbf{L}^{24}$] (Ln = Tb^{3+}, Eu^{3+}).

2.3 Characterisation and structural analysis

The purified europium and terbium complexes of $\mathbf{L}^{23}$ were characterised using various techniques, some of which served simply to verify the identity of the isolated complexes. For example, high resolution mass spectrometry allowed the determination of accurate masses. Due to the fact that inner sphere water molecules are typically not observed in mass spectrometric analyses, it was necessary to employ emission spectroscopic techniques to estimate the hydration state of the complexes, q'. The results of this characterisation are discussed in the following section.

2.3.1 Estimation of the complex hydration state, q'

For a given europium or terbium complex, the diminution of the metal-based emission intensity over time will always occur more slowly in D_2O than in water, reflecting the poorer efficiency of energy transfer from the lanthanide excited state to XD oscillators, in comparison to XH oscillators.[55] The excited state decay data presented in Figure 2.3[i] serves to illustrate this.

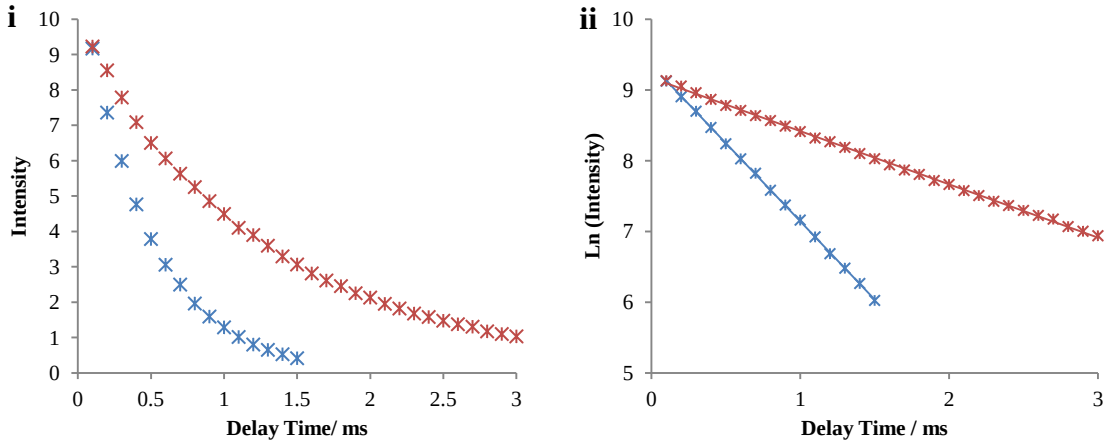

Figure 2.3: Excited state decay profiles for europium emission at 620 nm from solutions of (*R*)-[Eu.$\mathbf{L}^{23}$]$^+$ as a function of delay time in D_2O (red) and H_2O (blue). The gradient of Ln(intensity) vs. delay time gives the radiative decay constant. It should be noted that the lifetime of the emission is the reciprocal of this value.

As is shown in Figure 2.3[ii], manipulation of the excited state decay data collected for a given lanthanide complex can allow determination of rate constants for the depopulation of the excited state in both water and D_2O. If determination of such rate constants is possible, the number of water molecules bound to the metal centre when a europium or terbium complex is in solution may be estimated using equations 11 and 12, where *n* is the number of proximate carbonyl-bound amide groups.[55]

$$q'_{Eu} = 1.2\left(\left(k_{H_2O} - k_{D_2O}\right) - 0.25 - 0.075\,n\right) \qquad \text{(eqn. 11)}$$

$$q'_{Tb} = 5\left(\left(k_{H_2O} - k_{D_2O}\right) - 0.06\right) \qquad \text{(eqn. 12)}$$

In order to calculate the q' value of the europium and terbium complexes of $\mathbf{L}^{23}$ the decay of the intensity of the lanthanide emission was initially recorded in water. Next, following lyophilisation, the complex samples were re-dissolved in D_2O and left overnight to facilitate the displacement of any coordinated water molecules by D_2O

molecules. Finally, the D_2O was removed under vacuum and replaced with fresh D_2O before the emission decay was again measured. In each case, a monoexponential decay was observed, meaning the rate constants for the depopulation of the lanthanide excited state could be calculated for each complex in both of these media. Appropriate substitution of the values obtained into equations 11 and 12 allowed estimation of the hydration state for each of the complexes.

Table 2.1: Experimentally determined radiative rate constants and derived values of q' (± 20%) for europium and terbium complexes of $\mathbf{L^{23}}$ (295 K, pH 5.5).

Complex	k_{H_2O} / ms^{-1}	k_{D_2O} / ms^{-1}	q'
(*R*)-[Eu.$\mathbf{L^{23}}$]$^+$	2.13	0.75	1.36
(*R*)-[Tb.$\mathbf{L^{23}}$]$^+$	0.55	0.32	0.85

As can be seen from Table 2.1, analysis of the data obtained in the measurements outlined above led to the conclusion that there is one water molecule located in the inner coordination sphere of the europium and terbium complexes of $\mathbf{L^{23}}$. This was an unexpected result, as the q' value given in the literature for the racemic parent complex [Ln.$\mathbf{L^{22}}$]$^+$ was ~ 0 for both the europium and terbium analogues.[137] The reproducibility of this literature result was subsequently investigated; using the methodology outlined for the complexes of $\mathbf{L^{23}}$, appropriate rate constants were determined and the hydration state of the europium and terbium complexes of $\mathbf{L^{22}}$ was estimated using these values (Table 2.2).

Table 2.2: Experimentally determined radiative rate constants and derived values of q' (± 20%) for europium and terbium complexes of $\mathbf{L^{22}}$ (295 K, pH 5.5). Literature data is taken from reference 137.

Complex	Literature data			Experimental data		
	k_{H_2O} / ms^{-1}	k_{D_2O} / ms^{-1}	q'	k_{H_2O} / ms^{-1}	k_{D_2O} / ms^{-1}	q'
[Eu.$\mathbf{L^{22}}$]$^+$	1.02	0.65	0.14	2.08	0.61	1.46
[Tb.$\mathbf{L^{22}}$]$^+$	0.43	0.36	0.05	0.66	0.48	0.60

As can be seen from the data presented in Table 2.2, the experimentally determined rate constants for the depopulation of the lanthanide excited state of the complexes of $\mathbf{L^{22}}$ were not found to be in agreement with the literature data. A hydration state of ~ 1 was calculated for both the europium and terbium complexes. The agreement of the experimentally determined values with those observed for complexes of $\mathbf{L^{23}}$ suggests

that the k_{H_2O} and k_{D_2O} values given in the literature for europium and terbium complexes of **L**[22] may be erroneous. It was concluded that the lanthanide complexes adopt the structures shown below when in solution.

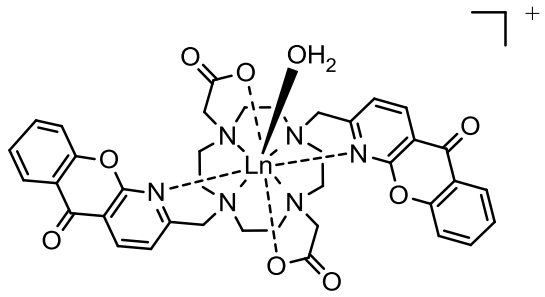

[Ln.**L**[22](OH$_2$)]$^+$

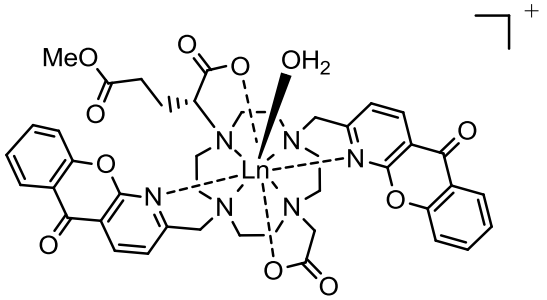

(*R*)-Ln.**L**[23](OH$_2$)]$^+$

Ln = Eu^{3+}, Tb^{3+}

Having determined the hydration state of the europium and terbium complexes of **L**[23], a number of other characterisation techniques were employed to facilitate the completion of a detailed structural analysis of these complexes. This structural analysis was carried out with reference to data collected for the racemic parent system and is discussed in detail in the following sections, which focus on individual methods of characterisation and highlight relevant observations and conclusions.

2.3.1 Emission spectroscopy

Emission spectra were obtained for [Ln.**L**[22](OH$_2$)]$^+$ and (*R*)-[Ln.**L**[23](OH$_2$)]$^+$ (Ln = Tb^{3+}, Eu^{3+}) in aqueous solution (Figure 2.4). In each case, minimal ligand fluorescence was seen, consistent with observations made previously for other cyclen-based lanthanide complexes including 1-azaxanthone derivatives as the sensitising moiety.[138] The emission spectral profile observed for the two europium complexes was extremely similar, with slight differences apparent in the relative intensity of the various emission bands, particularly within the hypersensitive $\Delta J = 2$ and $\Delta J = 4$ manifolds. Meanwhile, for the terbium complexes, the spectral form of the metal-based emission was found to show a striking resemblance. These observations suggested that the coordination environment of the lanthanide ion bears a high degree of similarity in complexes of both **L**[22] and **L**[23]. It was therefore anticipated that the analyte binding capabilities initially observed for [Eu.**L**[22](OH$_2$)]$^+$ in the presence of HSA would be preserved in this newly synthesised analogue.

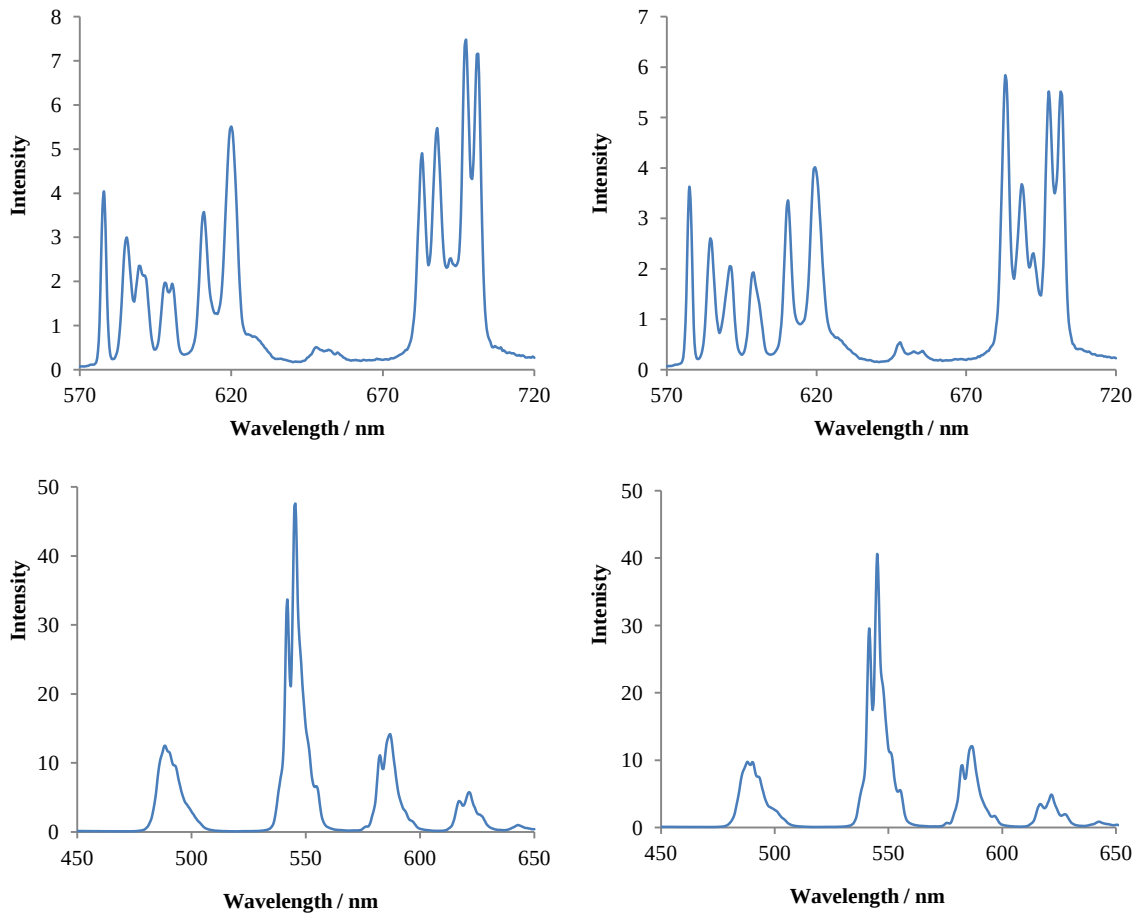

Figure 2.4: Emission spectra of [Ln.**L**^{22}(OH$_2$)]$^+$ (left) and (*R*)-[Ln.**L**^{23}(OH$_2$)]$^+$ (right) in water after excitation at 336 nm. Europium spectra are shown at the top and terbium at the bottom (295 K, pH 7.4, 0.1 M NaCl).

Inspection of the form of the ΔJ = 1 manifold within the emission spectra obtained for [Eu.**L**^{22}(OH$_2$)]$^+$ and (*R*)-[Eu.**L**^{23}(OH$_2$)]$^+$ revealed further information about the solution structures of the two complexes. Due to the fact that the $^5D_0$ excited state of europium is singly degenerate, a maximum of three bands should be visible within this manifold if there is only one luminescent species present in solution, corresponding to A_1-A_2, A_1-E_1 and A_1-E_2 transitions.[26] Within this limit, the number of separate bands observed is influenced by the symmetry of the complex. For europium complexes of high symmetry, such as C_n, simpler emission spectra with fewer bands within each manifold are typically observed. With respect to the ΔJ = 1 manifold the three transitions mentioned above are typically closer or identical in energy for complexes of higher symmetry, leading to the observation of less than three bands in this manifold. In cases where two or three bands are observed within the ΔJ = 1 manifold, it is possible to calculate the splitting between the A_1-A_2 and A_1-$E_{1,2}$ components, which is directly proportional to the second-order crystal field coefficient, B_0^2.[142] Given that this

parameter is determined primarily by the local symmetry and donor polarizability, analysis of the splitting between the A_1-A_2 and A_1-$E_{1,2}$ components of the $\Delta J = 1$ manifold can prove informative in the comparison of lanthanide complexes derived from structurally related ligands.

The $\Delta J = 1$ manifold of both [Eu.$\mathbf{L}^{\mathbf{22}}$$(OH_2)]^+$ and (*R*)-[Eu.$\mathbf{L}^{\mathbf{23}}$$(OH_2)]^+$ was found to be composed of three main bands, implying that both complexes adopt structures of low symmetry in solution. For the racemic complex [Eu.$\mathbf{L}^{\mathbf{22}}$$(OH_2)]^+$, the second and third bands visible within the $\Delta J = 1$ manifold appeared to show further splitting, implying the presence of multiple luminescent species in solution. Meanwhile, for (*R*)-[Eu.$\mathbf{L}^{\mathbf{23}}$$(OH_2)]^+$ no such additional splitting was evident and the splitting between the A_1-A_2 and A_1-$E_{1,2}$ components was determined as approximately 308 cm^{-1}.

If it is assumed that the multiple species present in solution in the case of [Eu.$\mathbf{L}^{\mathbf{22}}$$(OH_2)]^+$ are different stereoisomers of the complex (i.e. SAP and TSAP species), then these observations lend support to the idea that the inclusion of a stereogenic centre in the ligand framework of (*R*)-[Ln.$\mathbf{L}^{\mathbf{23}}$$(OH_2)]^+$ favours the existence of a single diastereomer in solution. Additional methods of structural analysis were subsequently employed in order to gain more information with regard to the number and identity of species present in solution for both [Ln.$\mathbf{L}^{\mathbf{22}}$$(OH_2)]^+$ and (*R*)-[Ln.$\mathbf{L}^{\mathbf{23}}$$(OH_2)]^+$.

2.3.2 ^{1}H NMR spectroscopy

The utility of ^{1}H NMR spectroscopy in the structural analysis of cyclen-based lanthanide complexes is well recognised, with this method of analysis having been found to be of value in determining the relative distribution of SAP and TSAP stereoisomers in solution for a given DOTA-derived lanthanide complex (see Section 1.4.2 of Chapter 1). Generally speaking, the chemical shift range of the resonances arising as a result of the presence of the SAP stereoisomer in solution will be larger than that of the TSAP stereoisomer, for such complexes.[30]

In light of the facts outlined above, it was decided that ^{1}H NMR studies could prove valuable in the gathering of more information about the number and identity of species present in solution for both [Ln.$\mathbf{L}^{\mathbf{22}}$$(OH_2)]^+$ and (*R*)-[Ln.$\mathbf{L}^{\mathbf{23}}$$(OH_2)]^+$. Owing to the fact that line broadening is typically more apparent for terbium complexes than their europium analogues, ^{1}H NMR spectra were obtained for [Eu.$\mathbf{L}^{\mathbf{22}}$$(OH_2)]^+$ and (*R*)-[Eu.$\mathbf{L}^{\mathbf{23}}$$(OH_2)]^+$ only. Spectra were recorded in D_2O at 400 MHz.

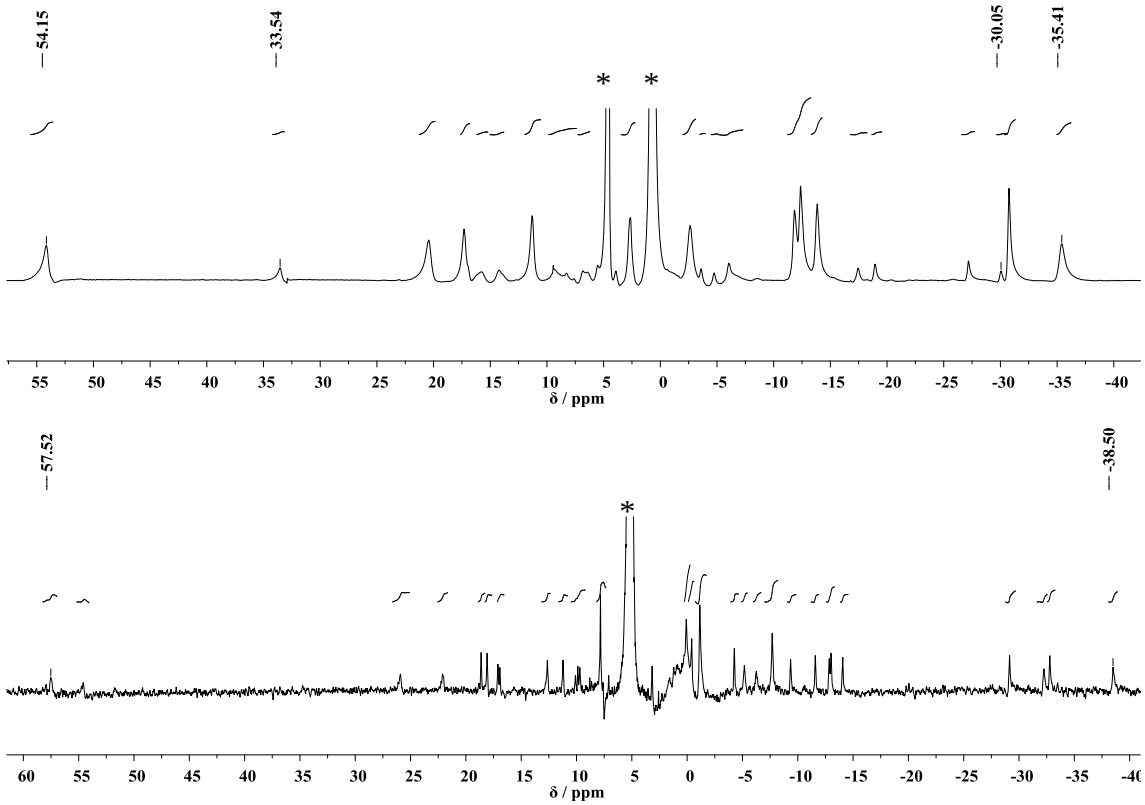

Figure 2.5: ^{1}H NMR spectra obtained for [Eu.$\mathbf{L}^{22}$(OH$_2$)]$^{+}$ (top) and (*R*)-[Eu.$\mathbf{L}^{23}$(OH$_2$)]$^{+}$ (bottom) (D$_2$O, 295 K, 400 MHz), * indicates solvent resonances.

Two sets of proton resonances were clearly discernible in the ^{1}H NMR spectrum obtained for [Eu.$\mathbf{L}^{22}$(OH$_2$)]$^{+}$, consistent with the presence of multiple species in solution. The relative intensity of the observed sets of resonances was roughly 4:1. For the major species, the chemical shift range extended from around +54 ppm, for the most shifted axial ring resonance, to -35 ppm. Meanwhile, the chemical shift range was smaller for the minor species, extending from approximately +34 to -30 ppm. It was concluded that the observed sets of resonances were most likely indicative of a 4:1 distribution of 9-coordinate SAP and TSAP stereoisomers in solution, each with one inner sphere water molecule. Unfortunately, the linewidth of the ^{1}H NMR signals observed for [Eu.$\mathbf{L}^{22}$(OH$_2$)]$^{+}$ was found to be too broad for any 2D NMR studies to be carried out, even when the sample was cooled down to 273 K. This precluded verification of the above hypothesis by methods such as EXSY. It should be noted that, although the observation of such a large change in chemical shift range is unusual for complexes of this type, it is not without precedent, having been observed in europium complexes of tetra-glutarate ligands.[81]

In the case of (*R*)-[Eu.$\mathbf{L}^{23}$(OH$_2$)]$^{+}$ only a small amount of material was available, meaning that the quality of the ^{1}H NMR spectrum obtained was relatively poor.

Importantly, the appearance of the spectrum was consistent with the presence of only one species in solution. The range of chemical shifts for the observed resonances stretched from roughly +58 to -39 ppm, indicating that the species present in solution adopted the same SAP geometry as the major species visible in the ^{1}H NMR spectrum of $[Eu.\mathbf{L}^{22}(OH_2)]^{+}$.

2.3.3 CPL spectroscopy

CPL spectra for $[Ln.\mathbf{L}^{22}(OH_2)]^{+}$ and (*R*)-$[Ln.\mathbf{L}^{23}(OH_2)]^{+}$ (Ln = Tb^{3+}, Eu^{3+}) in D_2O were recorded with the assistance of Dr R. D. Peacock at Glasgow University. As anticipated, no circularly polarized emission was observed for $[Ln.\mathbf{L}^{22}(OH_2)]^{+}$, providing confirmation of the fact that this complex exists as a racemic mixture in solution. In contrast, the presence of circularly polarized emission for (*R*)-$[Ln.\mathbf{L}^{23}(OH_2)]^{+}$ provided further evidence for the theory that the introduction of a stereogenic centre at a position α to the ring N in this complex leads to the formation of one diastereomeric species in solution.

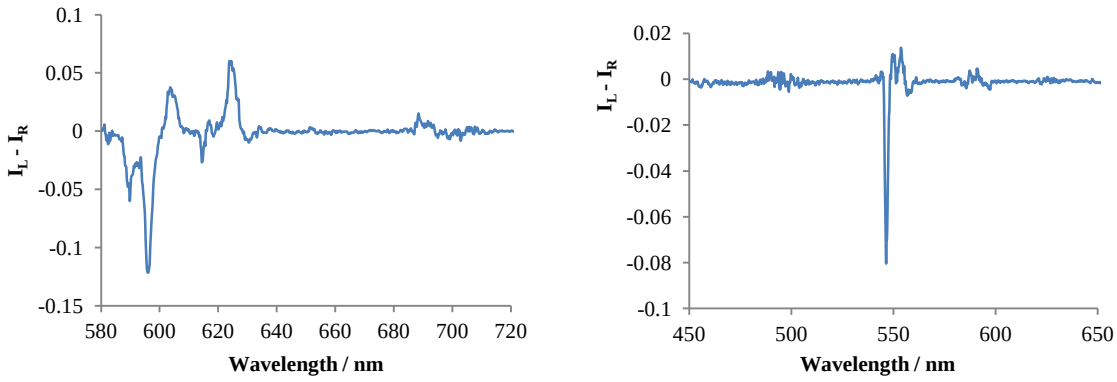

Figure 2.6: Representative CPL spectra showing the circularly polarized emission of (*R*)-$[Eu.\mathbf{L}^{23}(OH_2)]^{+}$ (left) and (*R*)-$[Tb.\mathbf{L}^{23}(OH_2)]^{+}$ (right) in D_2O (295 K).

As was outlined in Section 1.2.2 of Chapter 1, a quantitative assessment of the information contained in CPL spectra is possible by calculation of emission dissymmetry factors, which were devised by Emeis and Oosterhoff and can be defined using equation 1.[13]

$$g_{em}(\lambda) = \frac{2\Delta I(\lambda)}{I(\lambda)} \qquad \text{(eqn. 1)}$$

Emission dissymmetry factors for selected transitions in the spectra displayed in Figure 2.6 are given overleaf in Table 2.3.

Table 2.3: Selected emission dissymmetry factors for (*R*)-[Eu.**L**^{23}(OH$_2$)]$^+$ and (*R*)-[Tb.**L**^{23}(OH$_2$)]$^+$ calculated using the data shown in Figure 2.6.

	g_{em}			
Complex	$\Delta J = 1$ (λ)		$\Delta J = 2$ (λ)	
(*R*)-[Eu.**L**^{23}(OH$_2$)]$^+$	-0.17 (597)	+0.04 (605)	+0.03 (624)	-0.04 (631)
	$\Delta J = 1$ (λ)			
(*R*)-[Tb.**L**^{23}(OH$_2$)]$^+$	-0.09 (546)	+0.03 (554)	-0.04 (559)	

In terms of the sign and sequence of the transitions, the CPL signature of (*R*)-[Eu.**L**^{23}(OH$_2$)]$^+$ is similar to the spectrum previously reported for (*RRR*)-[Eu.**L**^{25}]$^{3+}$.[132] The absolute configuration of this complex was assigned based on the similarities of its CPL spectrum to that of (*RRRR*)-[Eu.**L**^{26}]$^{3+}$, whose absolute configuration has been verified by X-ray crystallography.[86] This suggests that (*R*)-[Eu.**L**^{23}(OH$_2$)]$^+$ adopts a square antiprismatic Λ(*δδδδ*) configuration, with a right-handed ring conformation and left-handed helicity in the layout of the pendant arms. This conclusion is in agreement with the hypothesis made previously on the basis of ^{1}H NMR spectral data obtained for this complex in solution.

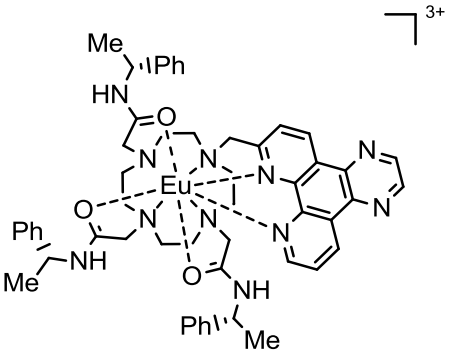

(*RRR*)-[Eu.**L**^{25}]$^{3+}$

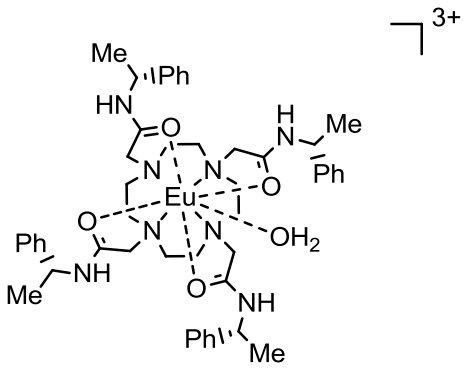

(*RRRR*)-[Eu.**L**^{26}]$^{3+}$

2.4 Preliminary investigations into interactions with proteins

Having completed a thorough structural analysis of the newly synthesised complex (*R*)-[Ln.**L**^{23}(OH$_2$)]$^+$ and confirmed that it appears to adopt a similar structure in solution to [Ln.**L**^{22}(OH$_2$)]$^+$, attention was turned to carrying out an assessment of the potential of this enantiopure complex as a responsive CPL probe. In order for a complex to be of any utility in such a role, it must show selectivity for the desired analyte in a competitive environment. Hence, it was decided that the binding of the complexes

$[Ln.\mathbf{L}^{22}(OH_2)]^+$ and (*R*)-$[Ln.\mathbf{L}^{23}(OH_2)]^+$ with a selection of proteins should be investigated. A total of six proteins were chosen, all of which are relatively abundant in human serum.[143] Table 2.4 gives the normal range of these proteins in human serum, along with their pI values. It is important to note that several of the proteins selected belong to a class of proteins known as 'acute phase proteins'. These proteins can be defined as those whose plasma concentration increases (positive acute-phase proteins) or decreases (negative acute-phase proteins) by more than 25% in response to inflammation.[144] Both α_1-AGP and α_1-AAT can be described as positive acute phase proteins, whilst serum albumin and transferrin are negative acute phase proteins. The pI value of a protein is the pH at which it will carry an overall neutral surface charge.

Table 2.4: Abundance and pI values for the six selected serum proteins.

Protein	Normal Range / μM	pI
Serum albumin	500-750	4.7 – 5.1
γ-Immunoglobulin-G	50-120	6.4 - 9
α_1 -Antitrypsin	40-80	4.9 – 5.1
apo-Transferrin	25-40	6.5
α_1 -Acid glycoprotein	12-32	2.7 – 3.1
Fibrinogen	6-14	5.6

At this point it may also be noted that of the proteins selected, both serum albumin and α_1-AGP are known to be important drug-binders.[145, 146] It may therefore be anticipated that both complexes should demonstrate an ability to bind to α_1-AGP, with the binding event likely to be indicated by well-defined changes in spectral form, as was previously noted for $[Eu.\mathbf{L}^{22}(OH_2)]^+$ in the presence of HSA.

2.4.1 Examining changes in emission spectral form

Six pairs of titrations were carried out monitoring the luminescence emission intensity of $[Eu.\mathbf{L}^{22}(OH_2)]^+$ and (*R*)-$[Eu.\mathbf{L}^{23}(OH_2)]^+$ in gradually increasing amounts of each protein. These initial investigations utilised the europium complexes rather than their terbium analogues because for europium the emissive $^5D_0$ excited state is non-degenerate, meaning that the emission spectra are comparatively simple and their interpretation relatively straightforward.[147] In addition, as has been outlined previously, the emission spectra of europium complexes are more sensitive to changes in the lanthanide coordination environment than their terbium counterparts.

Incremental additions of protein were made to 1 mL samples of each complex, which had been dissolved in aqueous solution at pH 7.4 containing 0.1 M NaCl, to give solutions where the concentration of complex was 30 μM. Additions were halted when the relevant physiological concentrations of the proteins had been reached. The pH, temperature and ionic strength of the samples were kept constant for each experiment, with pH adjustment being carried out after each addition of protein, using conc. $HCl_{(aq)}$ and conc. $NaOH_{(aq)}$. The emission spectral profile was recorded between 400 nm and 720 nm. This allowed changes in the intensity of fluorescence from the azaxanthone chromophore, a broad band between roughly 400 and 500 nm, to be monitored, along with metal-based emission.

In every case, some increase in the fluorescent emission intensity in the region between 400 and 550 nm was apparent. The most considerable change in fluorescence in this region was observed in the case of HSA and γ-immunoglobulin-G, which were examined at higher concentrations than the other proteins due to their higher abundance in human serum. It is therefore reasonable to attribute this to fluorescence from the protein itself, which contains fluorescent moieties, such as the amino acids tyrosine and tryptophan. Meanwhile, in terms of the metal-based emission, a variety of responses were observed. Figure 2.7 shows the variation in the metal-based emission of $[Eu.\mathbf{L}^{\mathbf{22}}(OH_2)]^+$ upon addition of α_1-AGP.

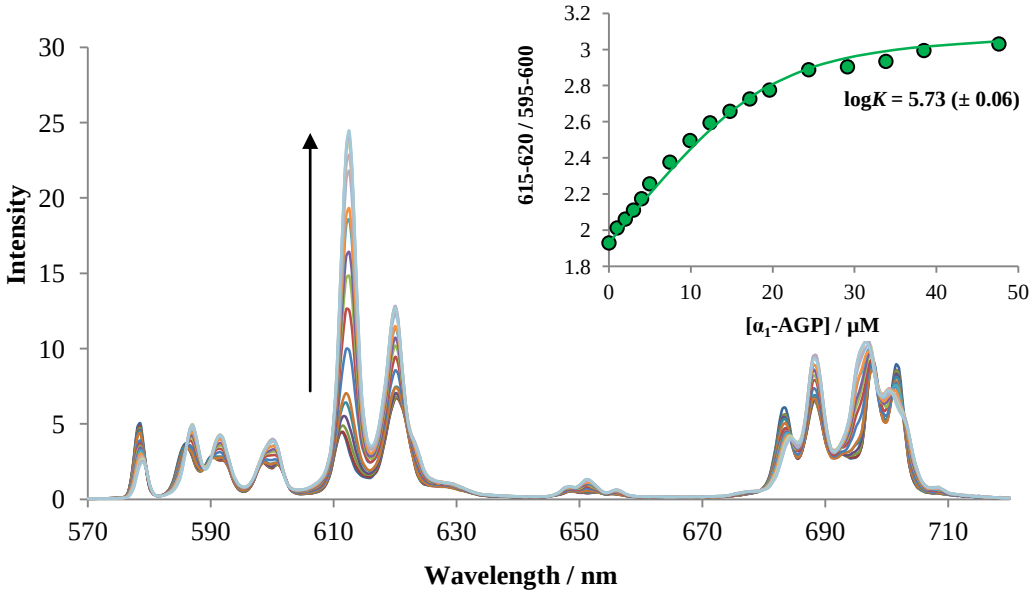

Figure 2.7: Variation of the emission spectral profile of [Eu.$\mathbf{L}^{22}$(OH$_2$)]$^+$ upon addition of α_1-AGP (295 K, pH 7.4, 0.1 M NaCl, 30 μM complex). Inset: Calibration curve showing variation of the observed emission intensity versus [α_1-AGP]. The line shows the fit to the experimental data obtained using a non-linear least squares fitting algorithm, assuming 1:1 binding stoichiometry.

Although some alteration of spectral form was observed in the majority of cases, the dramatic changes in the emission profile that are apparent in Figure 2.7 were not typical of every system examined. When considering changes in the metal-based emission, apo-transferrin proved particularly exceptional. Neither complex showed any significant change in its spectral fingerprint when in the presence of this protein, although some quenching of the emission intensity was apparent. Meanwhile for fibrinogen, significant quenching of the emission intensity was observed for each complex. This was accompanied by minor changes in spectral form, which were more apparent for the complex [Eu.$\mathbf{L}^{22}$(OH$_2$)]$^+$ and were only induced when the concentration of protein was at the upper limit of its normal range in human serum. These observations are perhaps unsurprising, as neither of these proteins is known to exhibit drug-binding characteristics.

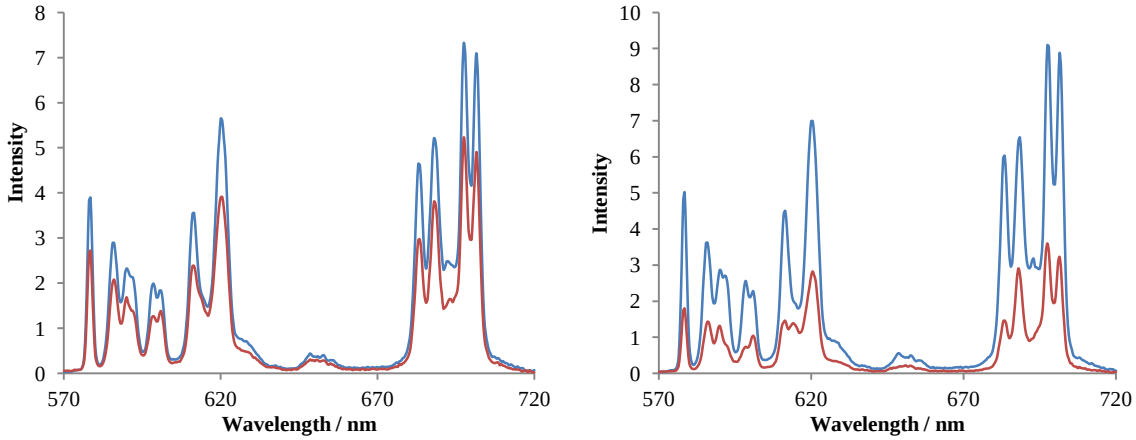

Figure 2.8: Europium emission spectral changes following addition of human apo-transferrin (left, 40 μM) and bovine fibrinogen (right, 15 μM) to [Eu.**L**^{22}(OH$_2$)]$^+$ (blue = initial, red = final, 295 K, 0.1 M NaCl, pH 7.4, 30 μM complex).

The remaining proteins gave more significant changes in spectral form, meaning that a 1:1 binding isotherm could be fitted to the data collected using non-linear least squares iterative analysis. By doing this it was possible to estimate the binding affinity (Table 2.5). It is important to note that the values given in Table 2.5 can only be treated as estimates of the binding affinity, as the stoichiometry of the binding interaction was not determined experimentally. Nevertheless, it is still useful to quantify the binding interactions in this manner as it enhances the comparative analysis that can be carried out for the systems studied.

Table 2.5: Comparison of the experimentally determined apparent binding constants for [Eu.**L**^{22}(OH$_2$)]$^+$ and (*R*)-[Eu.**L**^{23}(OH$_2$)]$^+$. Standard deviation errors associated with data fitting are shown in brackets.

Complex	log*K*			
	HSA	α$_1$-AGP	α$_1$-AAT	γ-Ig-G
[Eu.**L**^{22}(OH$_2$)]$^+$	4.00 (± 0.02)	5.73 (± 0.06)	4.72 (± 0.01)	3.91 (± 0.02)
(*R*)-[Eu.**L**^{23}(OH$_2$)]$^+$	3.91 (± 0.01)	5.84 (± 0.05)	4.58 (± 0.01)	3.58 (± 0.03)

In the case of HSA, α$_1$-AGP and α$_1$-AAT, well-defined spectral transformations were observed over the physiological range for each complex, with limiting spectra being attained. For γ-immunoglobulin-G the spectral fingerprint remained relatively unchanged over the physiological range of protein, particularly in the case of the complex (*R*)-[Eu.**L**^{23}(OH$_2$)]$^+$. More significant variation in the emission spectral form was apparent at concentrations exceeding the normal range. The limiting spectra for

each complex in the presence of HSA, α_1-AGP and α_1-AAT are shown below, along with the originally recorded emission spectra.

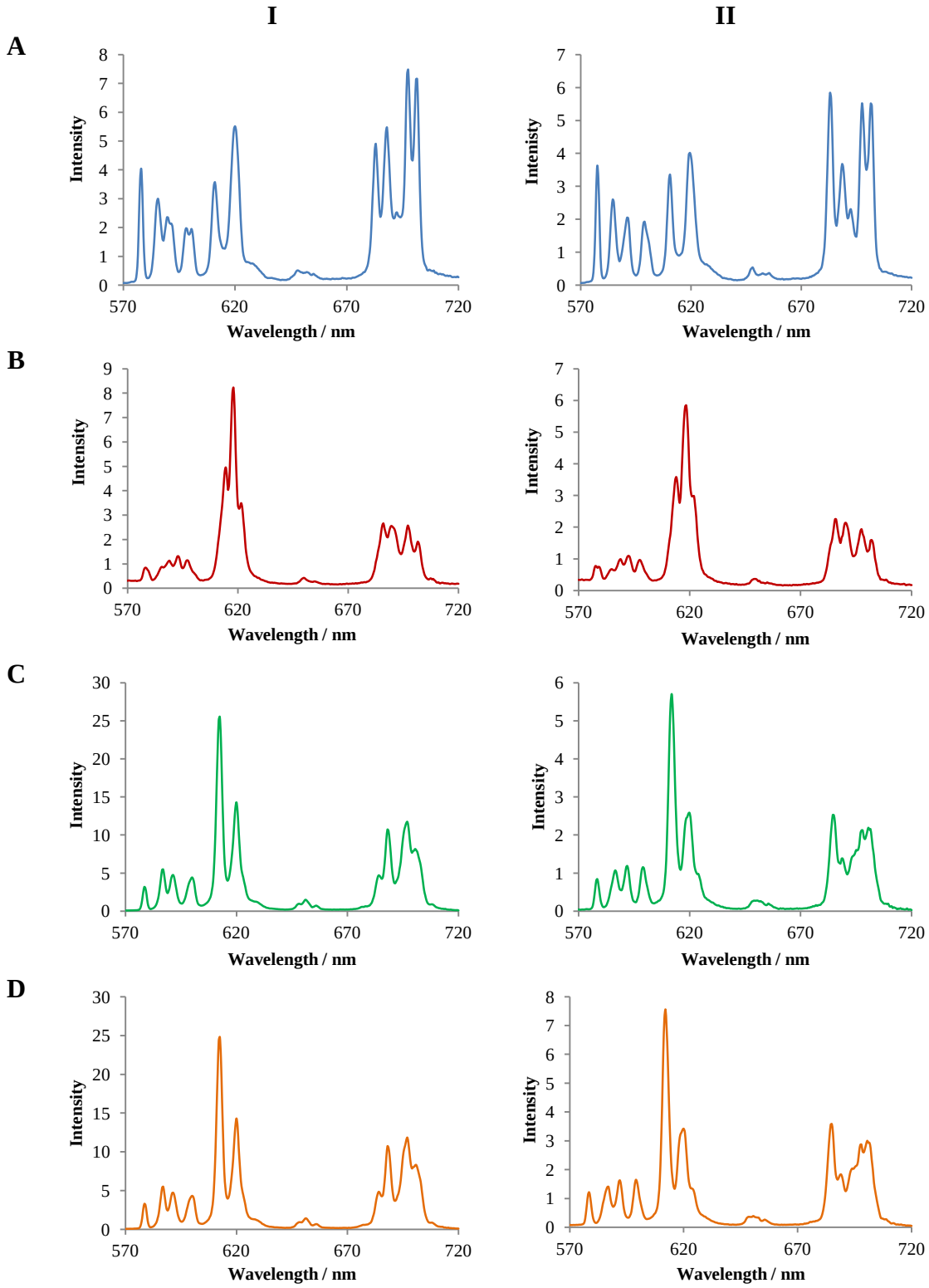

Figure 2.9: Representative emission spectra showing the metal-based emission of [Eu.$\mathbf{L}^{22}$(OH_2)]$^+$ (I) and (*R*)-[Eu.$\mathbf{L}^{23}$(OH_2)]$^+$ (II): (A) complex only; (B) complex + 0.7 mM HSA; (C) complex + 0.03 mM α_1-AGP; (D) complex + 0.07 mM α_1-AAT (295 K, pH 7.4, 0.1 M NaCl, 30 µM complex).

As can be seen from the spectra presented in Figure 2.9 and the values given in Table 2.5, the complexes tended to mimic each other's behaviour in the presence of protein. The appearance of the limiting spectra in the presence of HSA is almost identical and the spectra obtained in the presence of α_1-AGP and α_1-AAT show a marked similarity, with minor differences occurring in the hypersensitive $\Delta J = 2$ and $\Delta J = 4$ bands. Meanwhile, the equilibrium binding constants are comparable in each of these cases. These results suggest that the protein binding interactions do not involve the ligand glutarate substituent.

In each of the cases depicted in Figure 2.9, the addition of protein to the aqueous samples of the complexes led to a dramatic change in spectral form. The emission spectra obtained in the presence of these proteins are characterised by a large increase in the relative intensity of the $\Delta J = 2$ band, suggesting a change in the axial donor polarizability. This may be attributed to the replacement of a neutral N donor with a polarizable charged oxygen donor, which could take the form of an aspartic or glutamic acid side chain carboxylate group. It is interesting to note that in some cases the metal-based emission intensity was found to show an overall increase when in the presence of protein. For example, the quantum yield of $[Eu.\mathbf{L}^{\mathbf{22}}(OH_2)]^+$ was found to double when in the presence of α_1-AGP at a concentration of 50 μM, increasing from 4% to 8%.

Although the general changes discussed above are characteristic of all three of these proteins, it is apparent that the more detailed form of the limiting spectra seems to depend on the protein that is present. It is interesting to note that closer inspection of the limiting spectra shown in Figure 2.9 reveals that for both complexes in the presence of HSA there are two components visible within the $\Delta J = 0$ band. Meanwhile, for the α_1-AGP and α_1-AAT bound species only one component is visible within this band. The number of components in this band correlates directly to the number of chemically distinct emissive species that are present, which are not undergoing exchange on the millisecond timescale. Additional differences exist in the pattern of splitting within the $\Delta J = 1$ manifold. In the presence of HSA there are at least four components visible within this manifold, whilst for the α_1-AGP and α_1-AAT bound species three well-defined components are visible. The presence of more than three components within this manifold is another indicator that there is more than one chemically distinct species present in the HSA-bound sample.

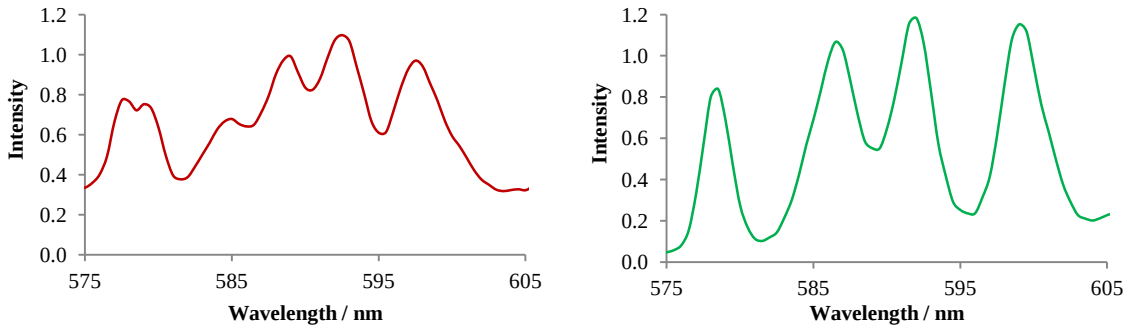

Figure 2.10: Representative emission spectra showing the $\Delta J = 0$ and $\Delta J = 1$ manifolds of the europium emission for (*R*)-[Eu.$\mathbf{L}^{23}$(OH_2)]$^+$ in the presence of 0.7 mM HSA (left) and 0.03 mM α_1-AGP (right) (295 K, pH 7.4, 0.1 M NaCl, 30 μM complex).

At this point it is important to note that significant differences exist between the structures and known drug binding characteristics of HSA and α_1-AGP. For example, studies have indicated that human serum albumin has multiple sites for ligand binding whilst α_1-AGP has a single ligand binding site. A crystal structure obtained for α_1-AGP has shown that there is one ligand pocket, which has three separate lobes.[146] Two of these lobes are negatively charged and smaller in size than the deep main lobe, which is completely nonpolar. In contrast, the two major binding sites in serum albumin are known to have cationic residues near the surface, including Arg257, Arg222, Lys199 and Lys195.[148] Taking these differences into consideration, it is perhaps unsurprising that the complexes appear to be bound in a different manner by these two proteins.

In contrast to HSA and α_1-AGP, α_1-AAT is not a known drug binder and the dramatic changes in spectral form that were observed for each complex in the presence of this protein were therefore somewhat unexpected. The identical nature of the emission spectra obtained for each complex in the presence of α_1-AGP and α_1-AAT is intriguing and suggests identical coordination environments around the metal centres. Although some homology does exist in the DNA sequence of the genes coding for these proteins, the only conserved region is located in the 5'-untranslated region and therefore does not yield any homology in the amino-acid sequences.[149]

The identical nature of the emission spectra for each complex in the presence of α_1-AGP and α_1-AAT, which are both characterised by a large increase in the relative intensity of the $\Delta J = 2$ band, prompted an investigation into the structural similarity of these two proteins. Protein structural alignment studies were carried out by Dr J. Sanderson (Durham University) using the FATCAT algorithm for representative PDB entries for α_1-AGP (3KQ0) and α_1-AAT (9API).[150, 151] It became apparent that although there was

very little overall structural similarity between the two proteins, some common features were present. Of particular significance was the location of two sets of glutamic acid residues. Firstly Glu-36, which is located over the entrance to the binding pocket in α_1-AGP, was found to be in close proximity to Glu-152 of α_1-AAT in the modelled structure. In addition, Glu-64, which is located in the hydrophobic binding pocket of α_1-AGP, was found to lie in close proximity to Glu-206 of α_1-AAT. These results support the hypothesis that the binding event is associated with the coordination of a polarizable charged oxygen donor to the metal centre in an axial position.

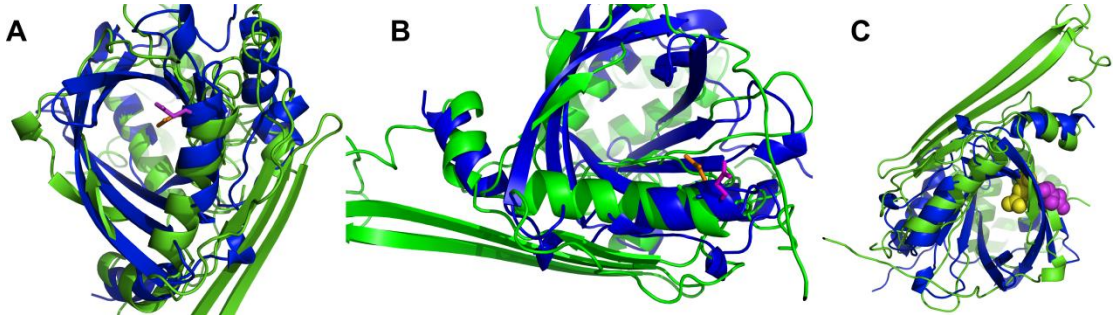

Figure 2.11: Structural superposition using FATCAT. In each case, α_1-AGP (3KQ0) is shown in blue, α_1-AAT (9API) is shown in green. (A) and (B), orthogonal views of the superposition of E36 of α_1-AGP (magenta) with E152 of α_1-AAT (orange); (C), showing the position of E64 of α_1-AGP (yellow) and E206 of α_1-AAT (magenta).

2.4.2 Determining the hydration state of the protein-bound complexes

In order to provide more insight into the mode of protein binding, studies were carried out to determine q' values for the protein-bound complexes, using an analogous method to that outlined in Section 2.3.1. In the case of the HSA-bound complexes, the presence of multiple species in solution gave rise to a biexponential decay of the emission intensity over time. Hence, it was not possible to determine rate constants for the depopulation of the europium excited state for either complex in the presence of this protein.

Table 2.6: Experimentally determined radiative rate constants and derived values of q' (± 20%) for europium complexes (295 K, pH 5.5) and in the presence of α_1-AAT (0.1 mM) and α_1-AGP (0.05 mM) (295 K, pH 7.4, 0.1 M NaCl, 30 μM complex).

Complex	Protein	k_{H_2O} / ms^{-1}	k_{D_2O} / ms^{-1}	q'
[Eu.**L**^{22}(OH$_2$)]$^+$	-	2.08	0.61	1.46
	α_1-AAT	1.19	0.70	0.29
	α_1-AGP	0.96	0.70	0.01
(*R*)-[Eu.**L**^{23}(OH$_2$)]$^+$	-	2.13	0.75	1.36
	α_1-AAT	0.98	0.74	0
	α_1-AGP	1.09	0.89	0

In each of the cases for which data is shown in Table 2.6, it was found that the rate of decay of the excited state of the complexes in water was decreased in the presence of protein. Meanwhile, no significant change occurred in the rate of decay of the excited state emission recorded in D_2O. Generally speaking, it is normally the case that for 9-coordinate complexes possessing one bound water molecule it is very difficult to substitute the water molecule in aqueous media.[63] However, in this case the q' value was consistently calculated to tend to zero in the presence of protein. Hence, it can be concluded that in each of these instances, protein binding is accompanied by the displacement of the bound water molecule from the metal centre.

2.4.3 Probing the mode of protein binding for α_1-AGP

In the case of α_1-AGP further investigations into the mode of protein binding were carried out. Both the emission spectral form and lifetime data suggest the presence of one major species in solution for each complex when in the presence of this protein. In addition, the binding affinity for the interaction between α_1-AGP and each complex was determined to be an order of magnitude higher than any of the other proteins that were considered.

2.4.3.1 Considering a structurally similar complex

The complex [Eu.**L**^{27}(OH$_2$)]$^+$ is an isomer of [Eu.**L**^{23}(OH$_2$)]$^+$, differing only in the constitution of the tricyclic sensitising group. A control experiment was performed in which the emission spectrum of a 1 mL sample of [Eu.**L**^{27}(OH$_2$)]$^+$ was recorded in the presence and absence of α_1-AGP.

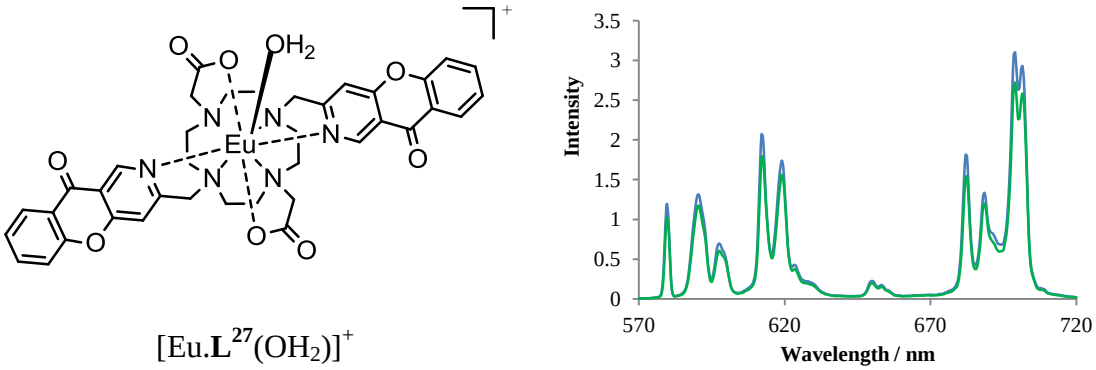

$[Eu.\mathbf{L}^{27}(OH_2)]^+$

Figure 2.12: Europium emission spectral variation following addition of human α_1-AGP (50 μM) to $[Eu.\mathbf{L}^{27}(OH_2)]^+$ (blue = initial, green = final, 295 K, 0.1 M NaCl, pH 7.4, 20 μM complex).

As can be seen from Figure 2.12, the behaviour observed differed completely to that found for the other two complexes in the presence of this protein. Namely, the addition of α_1-AGP to the solution containing $[Eu.\mathbf{L}^{27}(OH_2)]^+$ resulted in neither a change in spectral form nor any variation in lifetime, consistent with retention of the metal coordination environment and hydration state of the complex. This observation suggests that the protein binding interaction of $[Eu.\mathbf{L}^{22}(OH_2)]^+$ and (*R*)-$[Eu.\mathbf{L}^{23}(OH_2)]^+$ with α_1-AGP must involve the azaxanthone chromophore.

It is apparent from the emission spectral form observed for $[Eu.\mathbf{L}^{27}(OH_2)]^+$ in aqueous solution that the ligand field of this complex is somewhat different to that of $[Eu.\mathbf{L}^{22}(OH_2)]^+$ and (*R*)-$[Eu.\mathbf{L}^{23}(OH_2)]^+$. Only two bands are visible in the $\Delta J = 1$ manifold suggesting that this complex adopts a structure of higher symmetry in solution. In addition, the splitting between the A_1-A_2 and A_1-$E_{1,2}$ components of this manifold is smaller, at only 198 cm^{-1}. As was previously stated, the splitting between these components of the $\Delta J = 1$ manifold is influenced by the second-order crystal field coefficient, B_0^2. This is also true of the range of chemical shifts observed for a given lanthanide complex in its ^1H NMR spectrum. Hence, the existence of differences in the ligand field between $[Eu.\mathbf{L}^{27}(OH_2)]^+$ and $[Eu.\mathbf{L}^{22}(OH_2)]^+$ is also apparent if comparison is made between their ^1H NMR spectra, the former of which has been published in the literature.[152] As for $[Eu.\mathbf{L}^{22}(OH_2)]^+$, this complex was found to exist in solution as a mixture of SAP and TSAP stereoisomers. However, the range of chemical shifts observed for the resonances associated with the two isomers were very similar, with all resonances falling between +28 and -25 ppm. This is in agreement with the observation of a reduced splitting between the A_1-A_2 and A_1-$E_{1,2}$ components of the $\Delta J = 1$ manifold in the emission spectrum of $[Eu.\mathbf{L}^{27}(OH_2)]^+$, outlined above.

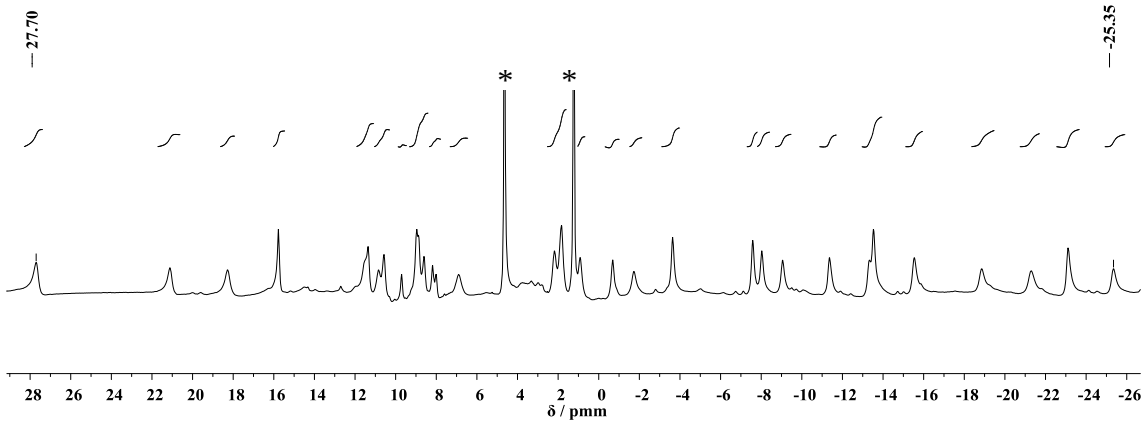

Figure 2.13: ^{1}H NMR spectrum obtained for [Eu.$\mathbf{L}^{27}$(OH$_2$)]$^+$ (D$_2$O, 295 K, 400 MHz), * indicates solvent resonances.[152]

When considering the origin of these differences in ligand field between [Eu.$\mathbf{L}^{27}$(OH$_2$)]$^+$ and [Eu.$\mathbf{L}^{22}$(OH$_2$)]$^+$, it may be observed that the constitution of the azaxanthone chromophore in the complex [Eu.$\mathbf{L}^{27}$(OH$_2$)]$^+$ leads to a reduced steric demand around the metal centre in comparison to [Eu.$\mathbf{L}^{22}$(OH$_2$)]$^+$. In addition, the pyridyl nitrogen is a weaker donor in the case of [Eu.$\mathbf{L}^{22}$(OH$_2$)]$^+$ due to its location in an α-position relative to the σ-polarizing oxygen. Hence, in the case of [Eu.$\mathbf{L}^{22}$(OH$_2$)]$^+$ and (*R*)-[Eu.$\mathbf{L}^{23}$(OH$_2$)]$^+$, an interaction may be envisaged in which protein binding is not only accompanied by displacement of the coordinated water molecule, but also by dissociation of one of the coordinated azaxanthone chromophores.

2.4.3.2 Studies using circular dichroism

As was previously mentioned, α_1-AGP is an important drug binding protein, showing particular affinity for apolar and basic drugs.[153-155] Up until recently, the X-ray crystal structure of this protein had not been resolved,[146] meaning that it was necessary to use alternative methods to attempt to characterise the drug binding interactions. Circular dichroism spectra induced by the binding of achiral drug molecules to the asymmetric binding site of α_1-AGP have proven useful in this respect.[156] Hence, it was suggested that it may be possible to exploit circular dichroism as a tool to probe in absorption the chiral environment of the azaxanthone chromophore for the complex [Eu.$\mathbf{L}^{22}$(OH$_2$)]$^+$ in the presence and absence of α_1-AGP. Circular dichroism studies were carried out by Samuele Lo Piano under the supervision of Dr Lorenzo Di Bari (Università di Pisa).

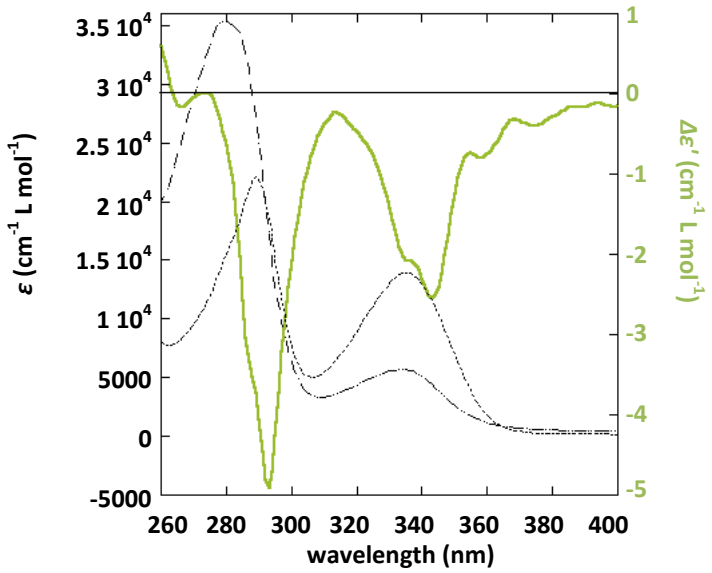

Figure 2.14: UV absorption spectra for [Eu.$\mathbf{L}^{22}$(OH_2)]$^+$ (41 μM) in the absence (dotted) and presence (dashed) of 1 equivalent of α_1-AGP. The ECD spectrum in the presence of 1 equivalent of bovine α_1-AGP is also shown (green). The ECD spectrum was normalised (Δε') to the total concentration of complex.

The absorption spectrum of the azaxanthone chromophore in the absence of protein was found to show two main bands, centred at 290 and 330 nm. In the presence of one equivalent of α_1-AGP, it was still possible to discern the two absorption bands, which showed a marked variation in their relative intensity. As was anticipated, the complex exhibited no electronic circular dichroism (ECD) signal in the absence of protein. In contrast to this, a strong ECD signal was recorded for the complex in the presence of 1 equivalent of protein, confirming the formation of a stereodefined adduct between the protein and complex. The signal consists of two negative Cotton effects, each associated with one of the main transitions of the azaxanthone chromophore. Partially resolved fine structure is apparent, typical of a relatively rigid environment with little or no solvation dynamics. Closer inspection of the induced ECD spectrum reveals the presence of two partially resolved CD bands within each transition, implying that the two azaxanthone chromophores may be in slightly different local chiral environments. This lends support to the hypothesis that the protein binding interaction involves displacement of one of the azaxanthone chromophores from the europium centre, whilst the other remains coordinated.

In order to gather further information about the site of the binding interaction and origin of the induced ECD signal, competition experiments were carried out using three known AGP-binders: progesterone, chlorpromazine and amitriptylene. A recent publication has described the computational docking of progesterone into the ligand binding pocket of

α_1-AGP, whilst X-ray crystal structures of the latter two species co-crystallised with α_1-AGP were recently published.[146, 157] Initial experiments were attempted in which the emission from a sample containing the α_1-AGP bound complex $[Eu.\mathbf{L}^{22}(OH_2)]^+$ was monitored as a function of increasing amounts of each competitive binder. It was hypothesised that displacement of the europium complex from its binding site on the protein by any one of these species would result in a change of spectral form, ultimately regenerating the emission spectrum observed in the absence of protein. The addition of progesterone and amitriptylene was found to cause no variation in the emission spectral signature of the protein-bound species. In contrast, the addition of chlorpromazine appeared to yield some alteration of the spectral form, although an apparent quenching of the emission intensity made it difficult to discern the exact nature of the variation. To clarify this result a second circular dichroism experiment was carried out, based on a similar premise to the luminescence experiment outlined above.

Incremental addition of chlorpromazine (0 to 1.25 equivalents) to a sample containing the α_1-AGP bound complex $[Eu.\mathbf{L}^{22}(OH_2)]^+$ (1:1, 21 µM) was found to result in a progressive reduction of the induced CD signal associated with the azaxanthone chromophore, suggesting the displacement of the europium complex from its protein binding site. Prior CD studies examining the binding of chlorpromazine to α_1-AGP have attributed the observation of an induced CD signal (a positive band, centred around 258 nm) to an exciton coupling interaction with the electric-dipole allowed transitions of a proximate tryptophan residue (Trp-25).[156]

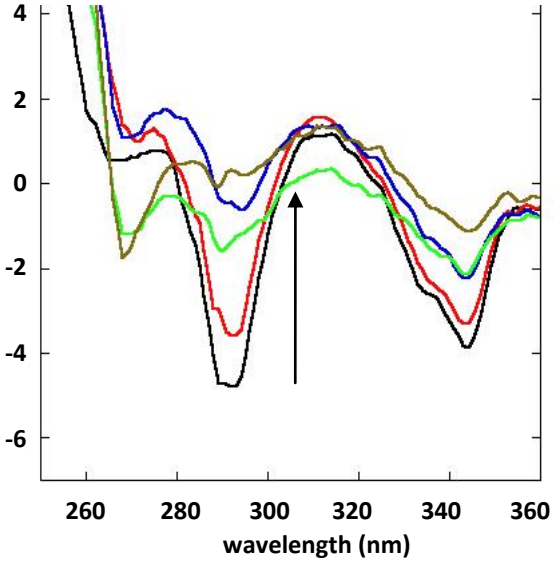

Figure 2.15: Variation in the induced ECD spectrum of $[Eu.\mathbf{L}^{22}(OH_2)]^+$ (21 µM) in the presence of 1 equivalent of α_1-AGP upon addition of CPZ (up to 1.25 equivalents).

2.4.3.3 A proposed mode of binding

Based on the information outlined in the preceding sections of this discussion, it is possible to propose a tentative model for the structure of the α_1-AGP-bound complexes, involving the displacement of one chromophore and the coordinated water molecule from the metal centre. Taking into account the nature of the observed emission spectral changes and the results of the FATCAT structural analysis, which aimed to discern the apparently identical mode of binding for the europium complexes in the presence of α_1-AGP and α_1-AAT, it seems probable that the binding interaction involves coordination of a polarizable charged oxygen donor to the metal centre in the axial position; this could take the form of a glutamic acid side chain carboxylate group (e.g. Glu 64 for α_1-AGP). The enhanced binding affinity of both complexes for α_1-AGP in comparison to the other proteins examined can be attributed to favourable hydrophobic interactions between the azaxanthone sensitising moiety and the protein drug-binding pocket.

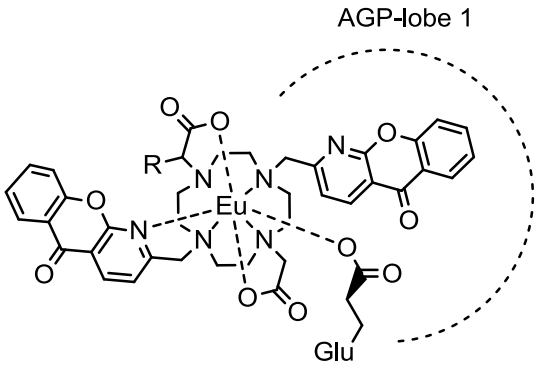

Relaxivity studies utilising the gadolinium analogue of the complex $[Ln.\mathbf{L}^{\mathbf{22}}(OH_2)]^+$ provided support for the proposed α_1-AGP bound structure. The gadolinium complex was synthesised according to previously described methods.[137] Complexation was confirmed by mass spectrometry prior to working up the reaction. The complex was then purified by preparative HPLC and isolated as an off-white solid.

In order to facilitate the preparation of samples of an exact concentration for use in relaxivity studies, the concentration of gadolinium in the isolated sample was determined using a method demonstrated by Peters *et al*.[158] A sample of the complex $[Gd.\mathbf{L}^{\mathbf{22}}(OH_2)]^+$ was dissolved in an aqueous 1% *tert*-butyl alcohol solution and 300 µL was placed in an NMR tube. An inner reference tube containing aqueous 1% *tert*-butyl alcohol solution was inserted into the NMR tube. Using ^{1}H NMR spectroscopy, it was possible to observe two resonance signals from the methyl protons of the *tert*-butyl

alcohol. The frequency shift of these two resonance signals represents the bulk magnetic susceptibility shift caused by the presence of the paramagnetic gadolinium complex.

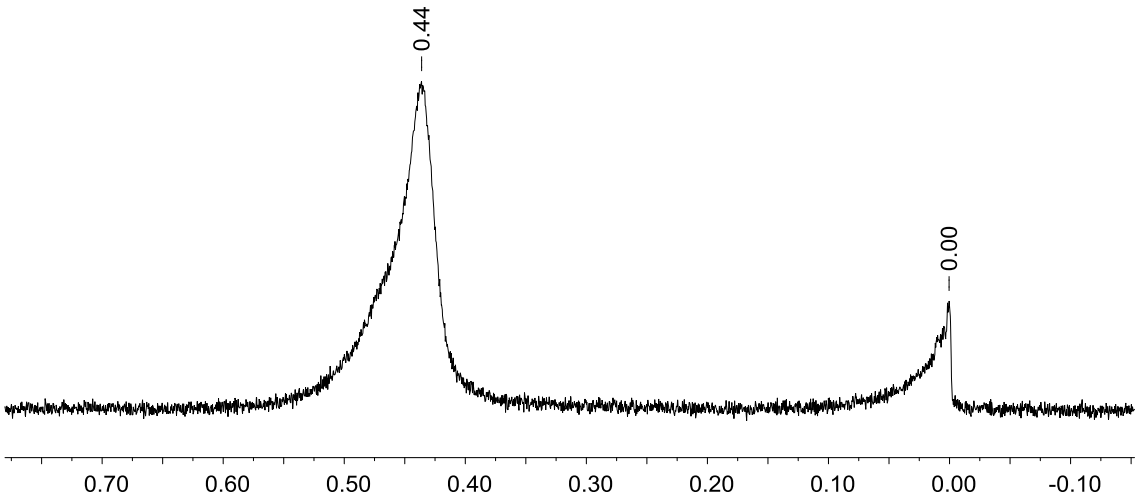

Figure 2.16: ^{1}H NMR spectrum showing the frequency shift between two resonance signals from the methyl protons of the tert-butyl alcohol induced by the presence of [Gd.$\mathbf{L}^{22}$(OH$_2$)]$^+$.

The observed BMS shift is related to the concentration of the gadolinium complex, *c*, by equation 13 where *s* is a constant dependent on the shape of the sample and its position in the magnetic field, *T* is the absolute temperature and μ_{eff} is the effective magnetic moment of the lanthanide in question.

$$\Delta_x = \frac{4\pi cs}{T}\left(\frac{\mu_{eff}}{2.84}\right)^2 \times 10^3 \qquad \text{(eqn. 13)}$$

Having determined the concentration of the bulk solution by this method, it was possible to prepare a 0.5 mmol solution of the complex in 0.1 M NaCl by dilution. Titrations were conducted using samples of this 0.5 mmol solution monitoring the longitudinal relaxation time, T_1, of the bulk water as a function of α_1-AGP and HSA concentration at 37 ^{o}C. Incremental additions of protein were made to 500 µL samples of the solution, which were adjusted to pH 7.4. Additions were halted when a limiting value of T_1 appeared to have been reached. The pH of the sample was monitored over the course of each titration and adjustments carried out using conc. $HCl_{(aq)}$ and conc. $NaOH_{(aq)}$ when necessary. Using the data gathered it was possible to calculate relaxivity data.

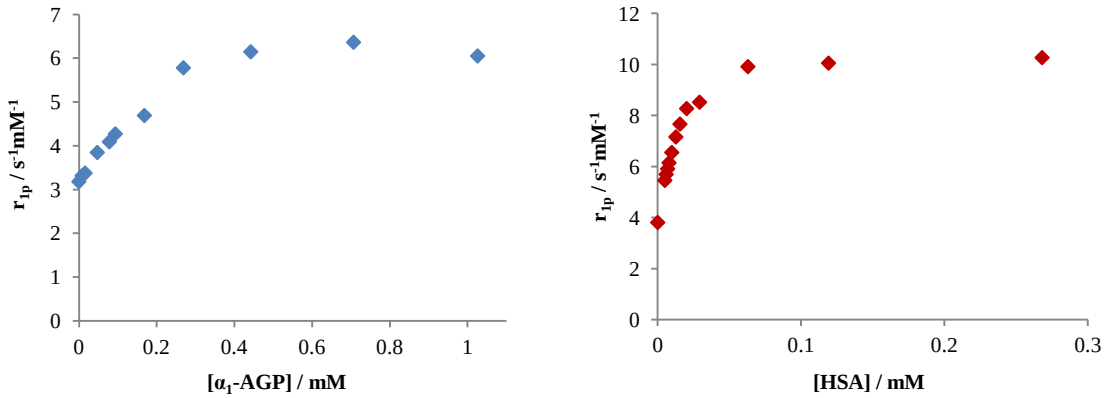

Figure 2.17: Variation in relaxivity as a function of added protein for an aqueous solution of [Gd.$\mathbf{L}^{22}$$(OH_2)]^+$ (0.5 mmol complex, 0.1 M NaCl, pH 7.4, 310 K).

As can be seen from Figure 2.17, the addition of protein to the sample caused an increase in relaxivity for both α_1-AGP and HSA. In the case of α_1-AGP, the increase in relaxivity was relatively modest, with a limiting value being reached in the presence of roughly 1 equivalent of α_1-AGP. This result suggests specifically that only one complex is binding per protein. Meanwhile, in the presence of HSA the increase in relaxivity was larger and a limiting value was reached at a much lower concentration of added protein, supporting a hypothesis that the binding of the complex by this protein occurs at multiple sites.

The large increase in relaxivity observed in the presence of HSA is in keeping with the results of analogous studies detailed in the literature.[134] This effect can be attributed to the large molecular size of the protein adduct resulting in a slowing down of the molecular motion and elongation of the rotational correlation time, τ_r, which is a limiting factor in the relaxivity of small Gd(III) chelates.[159] Meanwhile, the modest enhancement in relaxivity that was observed in the presence of α_1-AGP can be rationalised as a mixture of two opposing effects. For the α_1-AGP adduct it appears that the paramagnetic effect is not transmitted towards the bulk solvent as well as it is for HSA, an effect which on its own would be expected to cause a decrease in r_1. The observed changes in relaxivity are therefore consistent with a model of protein binding in which the coordinated water molecule is displaced and bulk water is excluded more effectively from the site where the complex is bound for α_1-AGP than for HSA. This supports the theory that the binding of [Ln.$\mathbf{L}^{22}$$(OH_2)]^+$ by α_1-AGP occurs within a relatively hydrophobic drug-binding pocket.

2.5 CPL spectroscopy studies

The original hypothesis suggested in this work was that the synthesis of an analogue of $[Ln.\mathbf{L}^{\mathbf{22}}(OH_2)]^+$ based on an enantiomerically pure ligand framework may yield a complex for which the binding of an analyte could be probed by CPL spectroscopic techniques. However, in accordance with the discovery that it was possible to record an induced circular dichroism spectrum for the complex $[Eu.\mathbf{L}^{\mathbf{22}}(OH_2)]^+$ in the presence of α_1-AGP, it was envisaged that the protein binding interactions that have been discussed in this work may also be coupled to a new phenomenon, namely induced CPL caused by a change in the constitution of a racemic complex. Therefore, the utility of both $[Ln.\mathbf{L}^{\mathbf{22}}(OH_2)]^+$ and (*R*)-$[Ln.\mathbf{L}^{\mathbf{23}}(OH_2)]^+$ as responsive CPL probes was investigated in a series of CPL spectroscopy studies.

CPL spectra were initially obtained for the europium analogues of $[Ln.\mathbf{L}^{\mathbf{22}}(OH_2)]^+$ and (*R*)-$[Ln.\mathbf{L}^{\mathbf{23}}(OH_2)]^+$ in the presence of HSA, γ-immunoglobulin-G, α_1-AGP and α_1-AAT. Appropriate concentrations of protein were chosen on the basis of the preliminary results outlined in the preceding sections. The spectra obtained in the presence of these proteins are shown in Figure 2.18, along with those recorded in the absence of any additive. For a given complex, the CPL spectral signature in the presence of α_1-AGP and α_1-AAT was found to be almost identical, in agreement with observations made previously. Therefore, only the CPL spectral fingerprints for $[Eu.\mathbf{L}^{\mathbf{22}}(OH_2)]^+$ and (*R*)-$[Eu.\mathbf{L}^{\mathbf{23}}(OH_2)]^+$ in the presence of α_1-AAT are shown.

As is apparent from the data presented in Figure 2.18, it was indeed possible to observe the induction of circularly polarized emission through protein binding for $[Eu.\mathbf{L}^{\mathbf{22}}(OH_2)]^+$. The CPL spectra recorded for this complex in the presence of HSA, α_1-AAT/α_1-AGP and globulin were found to differ in form, suggesting that the observed signal cannot simply be attributed to a perturbation of the racemic equilibrium either in the ground or excited state. Instead, it appears that the helicity at the metal centre is being determined by the manner of protein binding and not the inherent conformation of the complex. This is consistent with the formation of an adduct in which the coordination environment around the metal centre is altered and is therefore in agreement with previously discussed results. For (*R*)-$[Eu.\mathbf{L}^{\mathbf{23}}(OH_2)]^+$ the CPL spectral signature was found to be altered in the presence of each protein, also suggesting an altered metal coordination environment. Particularly well defined spectra were obtained in the presence of HSA and α_1-AAT/α_1-AGP.

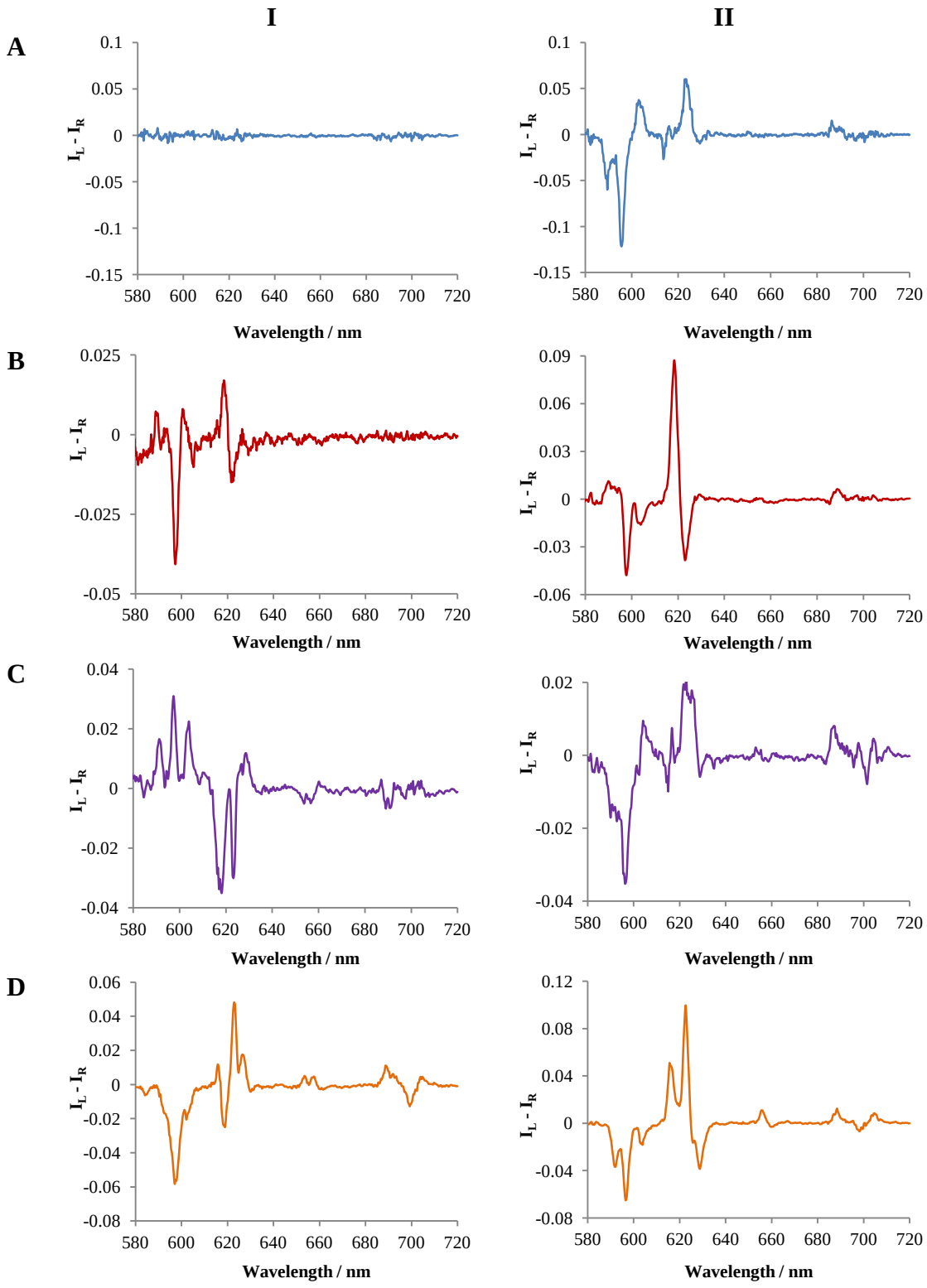

Figure 2.18: Representative CPL spectra showing the circularly polarized emission of [Eu.$\mathbf{L}^{22}$$(OH_2)]^+$ (I) and (*R*)-[Eu.$\mathbf{L}^{23}$$(OH_2)]^+$ (II): (A) complex only (295 K, pH 5.5); (B) complex + 0.7 mM HSA; (C) complex + 0.3 mM γ-immunoglobulin-G; (D) complex + 0.1 mM α_1-AAT (295 K, pH 7.4, 0.1 M NaCl, 30 μM complex).

Emission dissymmetry factors for selected transitions in the various spectra displayed in Figure 2.18 are given overleaf in Table 2.7.

Table 2.7: Selected emission dissymmetry factors calculated using the data displayed in Figure 2.18.

		g_{em}				
Complex	Protein	$\Delta J = 1$ (λ)	$\Delta J = 2$ (λ)		$\Delta J = 3$ (λ)	$\Delta J = 4$ (λ)
$[Eu.\mathbf{L}^{22}(OH_2)]^+$	-	0	0	0	0	0
	HSA	-0.13 (598)	+0.03 (619)	-0.02 (624)	0	0
	γ-Ig-G	+0.04 (598)	-0.02 (619)	-0.02 (624)	-0.05 (657)	-0.02 (691)
	α_1-AAT	-0.21 (599)	-0.03 (619)	+0.05 (623)	+0.10 (658)	+0.04 (692)
	α_1-AGP	-0.23 (598)	-0.02 (618)	+0.05 (623)	+0.08 (657)	+0.02 (690)
(*R*)-$[Eu.\mathbf{L}^{23}(OH_2)]^+$	-	-0.17 (597)	0 (619)	+0.03 (624)	0	+0.02 (688)
	HSA	-0.16 (598)	+0.07 (619)	-0.02 (624)	0	+0.03 (689)
	γ-Ig-G	-0.07 (598)	0 (619)	+0.02 (624)	-0.02 (658)	+0.01 (689)
	α_1-AAT	-0.22 (597)	+0.04 (619)	+0.12 (623)	+0.15 (656)	+0.03 (689)
	α_1-AGP	-0.07 (597)	+0.04 (619)	+0.07 (623)	+0.14 (656)	+0.02 (690)

It is apparent from the data shown in Table 2.7 that in all cases the largest emission dissymmetry factor was associated with the $\Delta J = 1$ transition, occurring between 585 and 600 nm. This is in agreement with established theory on the topic of lanthanide-based CPL phenomena, which allows the emission dissymmetry factor to be related to size and relative orientations of the electric and magnetic dipole transition moments, **μ** and **m**, associated with a given transition (see Section 1.2.2).[92] This relationship is expressed in equation 8, where τ is the angle between the magnetic and electric transition dipole moments.

$$g_{\mathrm{em}} = \frac{4|\mathbf{m}|}{|\boldsymbol{\mu}|} \cos\tau \qquad \text{(eqn. 8)}$$

This relationship suggests that the largest dissymmetry factors will be associated with magnetic-dipole allowed transitions that also have weak electric-dipole character. For europium, the $^5D_0 \rightarrow {}^7F_1$ transition is the only transition that obeys the formal selection rules relating to the total angular momentum quantum number, J (i.e. $\Delta J = 0, \pm 1$ excluding $0 \leftrightarrow 0$), and therefore it is the only transition that is strictly magnetic-dipole

allowed. Hence, the largest emission dissymmetry factor can be expected to be associated with this transition.

The data presented in Figure 2.18 and Table 2.7 reveals that protein binding does not appear to affect the enantiopure complex (*R*)-[Eu.$\mathbf{L}^{\mathbf{23}}$(OH_2)]$^+$ in such a manner as to induce a significant change in the helicity at the metal centre. Generally speaking, the emission dissymmetry factor at a selected wavelength for the protein-bound adduct was found to retain its sign in comparison with the complex in absence of protein. This was particularly true of the circularly polarized emission associated with the magnetic dipole allowed $\Delta J = 1$ transition. These results are in contrast to a previous example from the literature, where it was found that the helicity of a DOTA-based lanthanide complex became inverted upon binding to serum albumin.[133] In addition, it was also noted that in many cases the emission dissymmetry factors characterising the emission from (*R*)-[Eu.$\mathbf{L}^{\mathbf{23}}$(OH_2)]$^+$ were diminished in the presence of protein. From these observations it may be inferred that the dynamically racemic complex, [Ln.$\mathbf{L}^{\mathbf{22}}$(OH_2)]$^+$, may actually prove to be of more use as a chiral probe exploiting CPL than its analogue (*R*)-[Ln.$\mathbf{L}^{\mathbf{23}}$(OH_2)]$^+$.

In order to further characterise the binding of [Ln.$\mathbf{L}^{\mathbf{22}}$(OH_2)]$^+$ by α_1-AGP, a titration was carried out in which the 'switching on' of the CPL signal from the europium analogue of this dynamically racemic system was monitored in the presence of increasing amounts of bovine α_1-AGP. The method employed was analogous to that used for the titrations previously described, in which the total emission spectral change was monitored. It is important to note that the changes in total emission spectral form in the presence of bovine α_1-AGP had been found to be extremely similar to those observed with human α_1-AGP, which have been presented earlier in this report. In agreement with this, the CPL spectral signature of [Eu.$\mathbf{L}^{\mathbf{22}}$(OH_2)]$^+$ in the presence of 50 μM bovine α_1-AGP was also found to mimic the form of the CPL spectrum in the presence of 50 μM human α_1-AGP, with some difference in the hypersensitive $\Delta J = 2$ band around 620 nm.

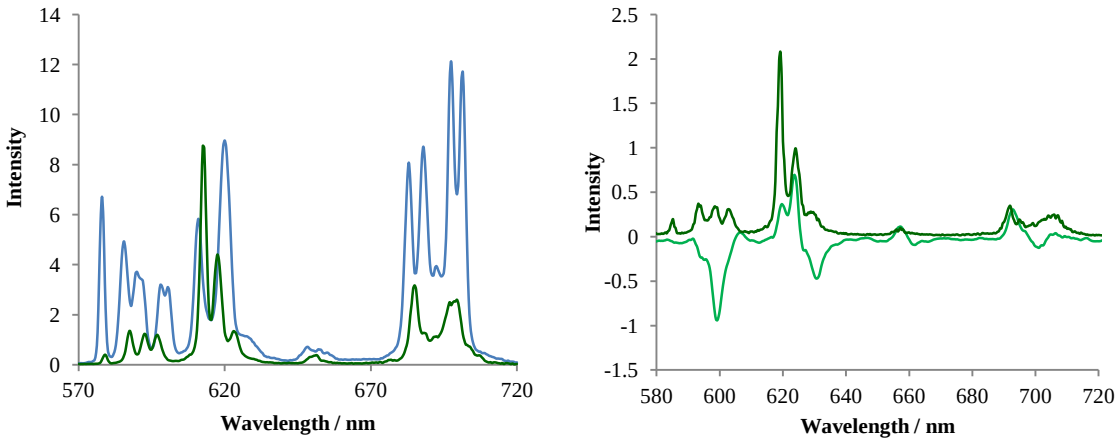

Figure 2.19: Europium emission spectral changes following addition of bovine α_1-AGP (left, 50 µM) to [Eu.$\mathbf{L}^{22}$(OH$_2$)]$^+$ (blue = initial, dark green = final) shown alongside the europium emission spectrum (dark green) and CPL spectrum (light green) of [Eu.$\mathbf{L}^{22}$(OH$_2$)]$^+$ in the presence of 50 µM bovine α_1-AGP. The scale used in the CPL figure refers to (I_L+ I_R) and is on a scale of x 40 with respect to (I_L - I_R). (295 K, 0.1 M NaCl, pH 7.4, 40 µM complex). CPL spectra are not red corrected.

By plotting the variation in the magnitude of the emission dissymmetry factor at 600 nm as a function of the concentration of added protein it was possible to estimate a binding constant for the association between [Eu.$\mathbf{L}^{22}$(OH$_2$)]$^+$ and bovine α_1-AGP. A 1:1 binding isotherm was fitted to the data using non-linear least squares iterative analysis, giving a value of log$K$ = 5.9 (± 0.1). This was in fairly good agreement with the estimate made on the basis of total emission spectral changes.

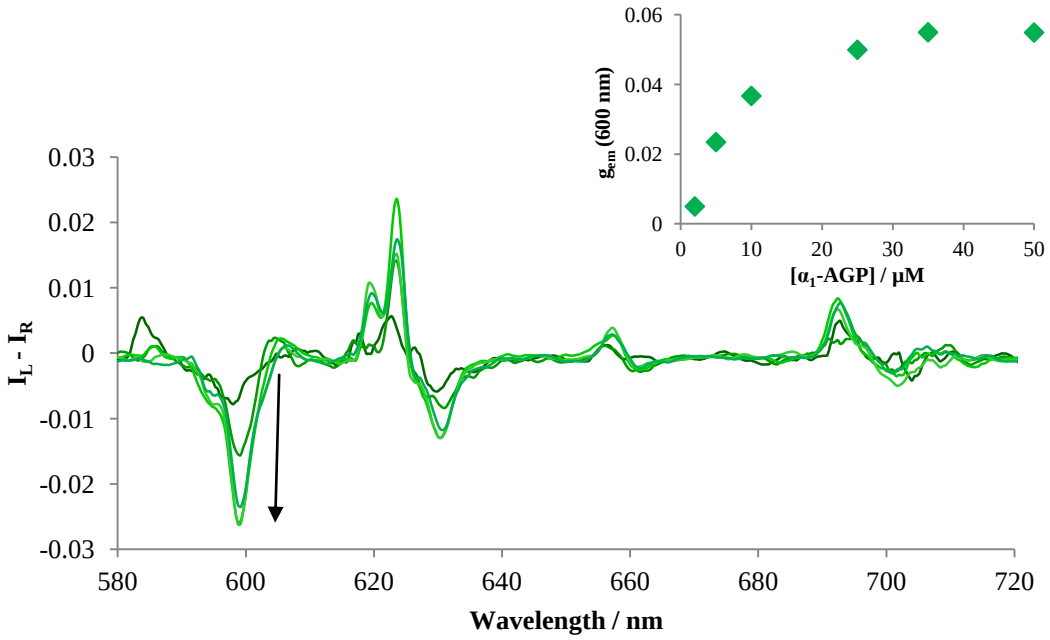

Figure 2.20: CPL spectral changes following addition of bovine α_1-AGP to [Eu.$\mathbf{L}^{22}$(OH$_2$)]$^+$. Inset: Variation in g_{em} at 600 nm with concentration of bovine α_1-AGP (295 K, 0.1 M NaCl, pH 7.4, 40 µM complex).

The CPL spectra of [Tb.$\mathbf{L}^{22}(OH_2)]^+$ in the presence of HSA, γ-immunoglobulin-G, α_1-AGP and α_1-AAT were also recorded. Preliminary studies monitoring the variation in total emission intensity and form of the terbium spectra in the presence of HSA, γ-Immunoglobulin-G, α_1-AGP and α_1-AAT revealed quenching of the emission intensity in each case but no significant change in spectral form. In the case of HSA and γ-Ig-G this quenching effect was particularly significant, with an overall loss of more than 90% of the signal intensity in the presence of 0.5 mM HSA and 80% in the presence of 0.5mM γ-immunoglobulin-G. The measurement of CPL for the terbium complex in the presence of either of these proteins yielded only poor quality spectra, presumably due to lack of signal intensity. In the case of HSA, it was found that a slightly better quality spectrum could be obtained at lower concentrations of added protein. A spectrum was collected at [HSA] = 0.2 mM as changes in the europium emission spectral form had previously been observed to manifest themselves at this concentration. For α_1-AGP and α_1-AAT slightly more of the signal intensity was retained in the presence of protein and CPL spectra of higher quality were obtained.

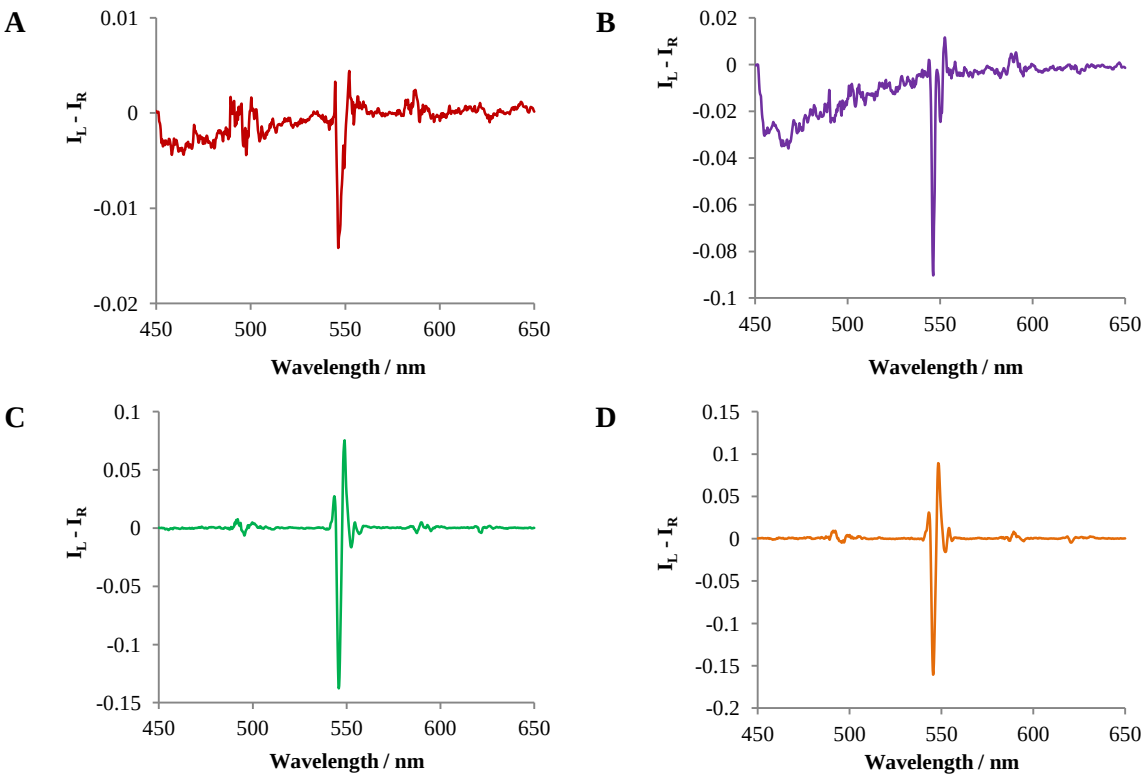

Figure 2.21: Representative CPL spectra showing the circularly polarized emission of [Tb.$\mathbf{L}^{22}(OH_2)]^+$: (A) complex + 0.2 mM HSA; (B) complex + 0.3 mM γ-immunoglobulin-G; (C) complex + 0.05 mM α_1-AGP; (D) complex + 0.1 mM α_1-AAT (295 K, pH 7.4, 0.1 M NaCl, 30 μM complex).

As can be seen from Figure 2.21, the CPL spectra recorded for [Tb.$\mathbf{L}^{\mathbf{22}}$(OH$_2$)]$^+$ in the presence of protein all took on the same general form; a large CPL signal was associated with the $^5D_4 \rightarrow {}^7F_5$ transition, whilst no substantial circular polarization was associated with any of the other transitions. As would be expected from the results already obtained with the europium analogue of this complex, the CPL spectral signature of [Tb.$\mathbf{L}^{\mathbf{22}}$(OH$_2$)]$^+$ in the presence of α_1-AGP and α_1-AAT was identical. Emission dissymmetry factors were calculated and are displayed in Table 2.8.

Table 2.8: Selected emission dissymmetry factors calculated using the data displayed in Figure 2.21.

Complex	Protein	g_{em} $\Delta J = 1$ (λ)			
[Tb.$\mathbf{L}^{\mathbf{22}}$(OH$_2$)]$^+$	HSA	0	-0.03 (546)	0	+0.01 (552)
	γ-Ig-G	0	-0.04 (546)	-0.01 (550)	+0.01 (552)
	α_1-AAT	+0.06 (543)	-0.13 (546)	+0.05 (549)	-0.02 (552)
	α_1-AGP	+0.06 (544)	-0.13 (547)	+0.05 (549)	-0.03 (553)

Much of the current research in the area of lanthanide complexation chemistry is focussed on the development of emissive europium complexes as ratiometric probes for biological analytes.[31, 131, 160, 161] The sensitivity of the europium emission spectral form to the metal coordination environment is key to these advances and terbium is often overlooked. This example illustrates nicely how the use of CPL spectroscopy may be able to facilitate the use of terbium complexes as emissive probes, where changes in g_{em} at a given wavelength could be used to indicate the presence of a given analyte.

2.6 Investigating protein binding in a background of human serum

As was previously stated, for a complex to be of any utility as a responsive CPL probe, it must show selectivity for the desired analyte in a competitive biological environment. Hence, it was decided that the binding of the complex [Ln.$\mathbf{L}^{\mathbf{22}}$(OH$_2$)]$^+$ to the acute phase protein α_1-AGP should be investigated in a background of human serum. Serum contains a complex mixture of proteins, along with electrolytes and a variety of other biomolecules such as antibodies and antigens.

In order to allow for the construction of a calibration curve to characterise the spectral response of the complex in the presence of increasing amounts of α_1-AGP, it was first necessary to assess the α_1-AGP content of the human serum sample. This was achieved using a commercially available solid-phase ELISA assay, purchased from R&D

systems. A stock solution of the serum sample was created by carrying out a 10,000-fold dilution of a raw sample. The concentration of α_1-AGP present in this sample was then estimated by comparison with a series of standard solutions, having α_1-AGP concentrations ranging between 200 and 3.13 ng/mL.

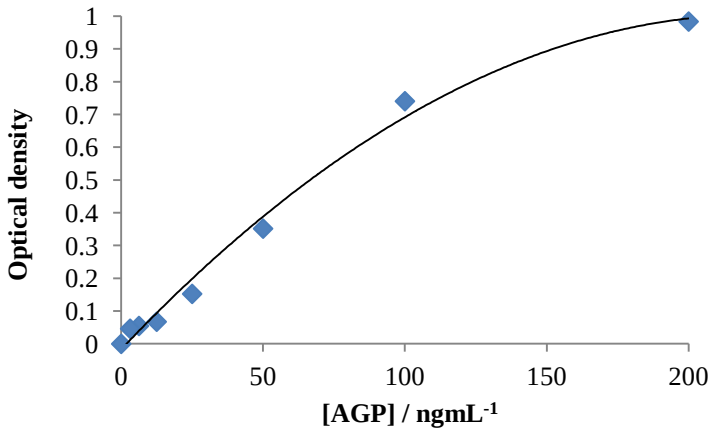

Figure 2.22: A standard curve generated to facilitate calculation of the α_1-AGP concentration in a sample of human serum.

Using the standard curve that was generated, it was possible to estimate the concentration of α_1-AGP in the human serum sample as being 0.62 mg/mL (≈ 15 μM), which is at the lower end of the normal concentration range in plasma.[162] Having estimated the concentration of α_1-AGP present in the serum sample, a preliminary titration was carried out in which incremental additions of a concentrated α_1-AGP stock solution were made to a sample of the complex $[Eu.\mathbf{L}^{22}(OH_2)]^+$ that had been dissolved in human serum. Associated spectral changes were monitored using total emission spectroscopy.

As was previously mentioned, serum albumin is the most abundant plasma protein and on this basis it may have been anticipated that the initial spectral form of the complex in serum would resemble the HSA-bound species. However, as was shown previously, the binding affinity that characterised the interaction between the complex and serum albumin was actually surpassed by other proteins, even within the relatively small sample size of 6 proteins. Hence, it was presumed likely that the initial spectral form in serum would not mimic any of the spectra recorded to date. This was indeed found to be the case, with the initial spectral form bearing some resemblance to that of the HSA-bound complex suggesting that although a mixture of adducts are present when the complex is dissolved in serum, this is the major contributor to the speciation.

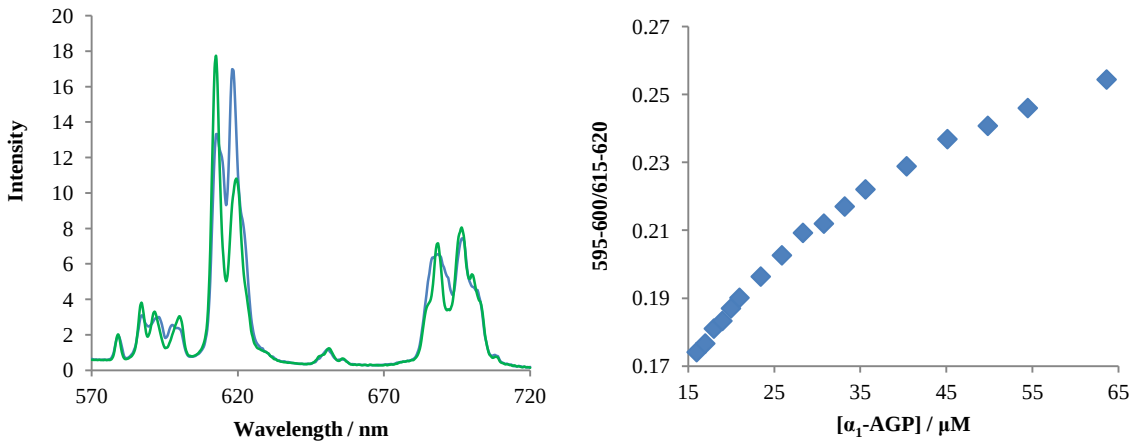

Figure 2.23: Europium emission spectral changes following addition of α_1-AGP (left, 50 μM) to [Eu.**L**^{22}(OH$_2$)]$^+$ in human serum (blue = initial, green = final) shown alongside a calibration curve depicting the variation in the emission intensity ratio of selected europium emission bands over the course of the titration (295 K, pH 7.4).

Over the course of the titration the emission spectral signature was found to change, eventually reaching a limiting form which bore close resemblance to that observed for the α_1-AGP bound complex. A total of 50 μM of α_1-AGP was added to the serum sample, reflecting a four-fold increase in the initial serum concentration in order to mimic an inflammatory response. Analysis of the change in the emission intensity ratio comparing the integrated emission intensity over part of the $\Delta J = 2$ band in comparison to part of the $\Delta J = 1$ band from the total emission spectrum allowed a calibration curve to be generated, which is shown in Figure 2.23.

A control experiment was carried out in order to assess the effect of α_1-AAT addition on the total emission spectral form observed from the serum sample. As was shown in Section 2.4.1, the complex [Eu.**L**^{22}(OH$_2$)]$^+$ was also found to have a higher affinity for this protein than for HSA. It is therefore perhaps unsurprising that an analogous titration carried out with this protein gave rise to changes in spectral form and an increase in the emission intensity ratio that was similar to that induced by α_1-AGP. It can be concluded that the elevation in serum levels of either of these acute phase proteins may be used to signal the onset of inflammation in biologically relevant systems through the use of the dynamically racemic complex [Eu.**L**^{22}(OH$_2$)]$^+$.

Attempts were subsequently made to record the CPL spectrum of [Eu.**L**^{22}(OH$_2$)]$^+$ in samples of human serum with and without added α_1-AGP. As was expected on the basis of the results outlined above, the spectral form of the CPL signal for the complex in serum in the absence of added α_1-AGP was not found to resemble that of any one of the

protein-bound species. When 50 μM of bovine α_1-AGP was added to the serum sample a modulation of the CPL output was induced, with the resulting spectral fingerprint bearing some resemblance to that recorded for the α_1-AGP adduct in a non-competitive media. Unfortunately, these changes in CPL spectral form were much less well-defined than those observed in total emission and a high background signal meant that the generation of a calibration curve that could be used for determining α_1-AGP concentration in biologically relevant samples was not possible using CPL data.

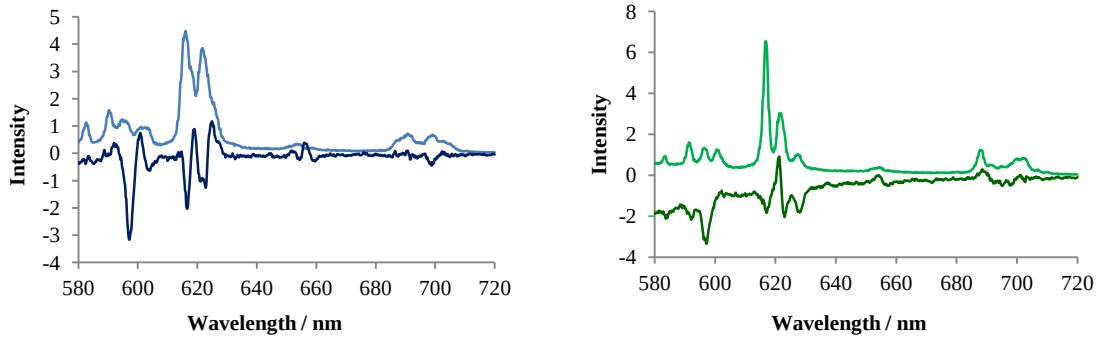

Figure 2.24: The europium emission spectrum and CPL spectrum of [Eu.$\mathbf{L}^{22}$$(OH_2)]^+$ in human serum in the absence (left) and presence (right) of 50 μM added bovine α_1-AGP (295 K, pH 7.4). The scale used on the y axis refers to $(I_L + I_R)$ and is on a scale of x 40 with respect to $(I_L - I_R)$. Spectra are not red corrected.

2.7 Conclusions

A chiral lanthanide complex, (*R*)-[Ln.$\mathbf{L}^{23}$$(OH_2)]^+$ was synthesised and characterised and a structural analysis carried out in comparison to the related complex [Ln.$\mathbf{L}^{22}$$(OH_2)]^+$. The emission spectral form of the europium complexes was examined and found to be similar in general. Slight differences in the splitting of the $\Delta J = 1$ band suggested that [Eu.$\mathbf{L}^{22}$$(OH_2)]^+$ existed in solution as a mixture of species. Proton NMR studies gave further evidence for this, revealing the presence of two species in solution, in a ratio of 4:1. It was proposed that the complex was present in solution as a mixture of SAP and TSAP stereoisomers. Further NMR studies were hindered by broad linewidths. In the case of (*R*)-[Eu.$\mathbf{L}^{23}$$(OH_2)]^+$ the amount of material available for study limited the scope of the NMR studies. A ^{1}H NMR spectrum was obtained (D_2O, 295 K, 400 MHz) and appeared to show the presence of only one species in solution. The range of chemical shifts observed was similar to that seen for the major isomer of [Eu.$\mathbf{L}^{22}$$(OH_2)]^+$, suggesting that (*R*)-[Ln.$\mathbf{L}^{23}$$(OH_2)]^+$ adopts a SAP geometry in solution. CPL spectra obtained for the two complexes confirmed that although [Ln.$\mathbf{L}^{22}$$(OH_2)]^+$ exists in solution as a racemic mixture, this is not the case for (*R*)-[Ln.$\mathbf{L}^{23}$$(OH_2)]^+$. For this complex, the inclusion of an asymmetric carbon centre in a position α to a ring nitrogen

yielded the predominant formation of what is tentatively assigned as a (*R*)-Λ(*δδδδ*) diastereoisomer.

Comparative investigations were carried out to assess the effect of protein binding on the emission profile of [Eu.$\mathbf{L}^{\mathbf{22}}$$(OH_2)]^+$ and (*R*)-[Eu.$\mathbf{L}^{\mathbf{23}}$$(OH_2)]^+$. A total of six proteins were investigated, chosen on the basis of their abundance in human serum. In the case of fibrinogen and apo-transferrin, no significant change in emission spectral form was noted for either complex and no further analysis was carried out using these proteins. Meanwhile, changes in the total emission spectral fingerprint were noted for both complexes in the presence of HSA, α_1-AGP, α_1-AAT and γ-Ig-G. This suggests that a binding interaction is able to occur between the complexes and each of these proteins, involving a change in complex constitution. Apparent binding constants were calculated for these interactions based on the assumption of 1:1 association.

It was found that for both complexes the most well-defined spectral response over the physiological concentration range of protein was observed in the case of HSA, α_1-AGP and α_1-AAT. In every case, the total emission spectrum of the complex in the presence of protein had the same general form, with the relative intensity of the $\Delta J = 2$ band found to be much larger in comparison to spectra obtained in the absence of protein. This suggests that a binding interaction is occurring in which the complex constitution is changed in such a manner that the axial donor polarizability is increased. In some cases, the metal-based emission intensity was found to show an overall increase when in the presence of protein, suggesting very effective exclusion of quenching XH oscillators from the primary and secondary coordination spheres.

In the case of each of these three proteins, the complexes were found to mimic each other's behaviour, both in terms of observed changes in emission spectral form and calculated affinity constants. In samples containing HSA the observation of multiple components in the $\Delta J = 0$ band implies the presence of more than one chemically distinct lanthanide containing species. For α_1-AGP and α_1-AAT similar analysis suggests the presence of only one species. It can be concluded that the complexes occupy more than one binding site on HSA, with a different local coordination environment at europium. With α_1-AGP and α_1-AAT one binding site is occupied.

For both europium complexes, observed changes in spectral form in the presence of α_1-AAT were identical to those seen in the presence of α_1-AGP. The origin of this result

was probed by carrying out protein structural alignment studies on representative PDB entries for α_1-AGP and α_1-AAT. Although very little overall structural similarity was apparent for the two proteins, some commonality was found in the location of two sets of glutamic acid residues. This supports a hypothesis that the binding event is associated with the coordination of a polarizable charged oxygen donor from a glutamic acid side chain to the metal centre in an axial position.

It was possible to estimate the inner sphere hydration number for the systems where the form of the emission spectrum indicated the presence of only one major emissive species in solution. In all cases, q' was found to tend to zero in the presence of protein. This was consistent with previous observations of changes in the metal-based emission intensity in the presence of protein, which suggested very effective exclusion of quenching XH oscillators from the primary and secondary coordination spheres.

The nature of the interaction between the complexes and α_1-AGP was investigated more thoroughly using a variety of techniques. The emission spectral form of the complex $[Eu.\mathbf{L}^{27}(OH_2)]^+$, an isomer of $[Eu.\mathbf{L}^{22}(OH_2)]^+$ in which the constitution of the azaxanthone chromophore is altered, showed no change in the presence of α_1-AGP. This indicates that the interaction of $[Eu.\mathbf{L}^{22}(OH_2)]^+$ and (*R*)-$[Eu.\mathbf{L}^{23}(OH_2)]^+$ with α_1-AGP must involve the sensitising moiety. Further investigations were carried out using CD spectroscopy, with the observation of a strong induced ECD signal for $[Eu.\mathbf{L}^{22}(OH_2)]^+$ in the presence of α_1-AGP suggesting the formation of a stereodefined adduct between the protein and complex. The presence of two partially resolved CD bands within each observed transition supports a hypothesis that the two azaxanthone chromophores may be in slightly different local chiral environments in the protein adduct. The site of protein binding was also probed in a series of competitive binding studies with known α_1-AGP drug binders. It was concluded that the protein binding interaction involves displacement of one of the azaxanthone chromophores from the europium centre, whilst the other remains coordinated.

Taking into account all of the observations outlined above, a tentative model for the structure of the α_1-AGP-bound complexes was proposed, involving the displacement of one chromophore and the coordinated water molecule from the metal centre. It was also concluded that the binding interaction involves coordination of a polarizable charged oxygen donor to the metal centre in the axial position. It was suggested that this could take the form of a glutamic acid side chain carboxylate group (e.g. Glu 64 for α_1-AGP).

The enhanced binding affinity of both complexes for α_1-AGP in comparison to the other proteins examined was attributed to favourable hydrophobic interactions between the azaxanthone sensitising moiety and the protein drug-binding pocket. Relaxivity studies carried out using $[Gd.\mathbf{L}^{\mathbf{22}}(OH_2)]^+$ supported these conclusions.

Further assessment of the protein binding interactions was carried out using CPL spectroscopy. For HSA, α_1-AGP, α_1-AAT and γ-Ig-G protein binding caused a helical structure to be adopted by $[Eu.\mathbf{L}^{\mathbf{22}}(OH_2)]^+$, resulting in strong induced CPL. In the case of (*R*)-$[Eu.\mathbf{L}^{\mathbf{23}}(OH_2)]^+$ some change in the CPL spectral signature was observed in the presence of each protein but it was apparent from comparison of g_{em} values that protein binding did not cause a major change in the helicity at the metal centre in any case. It was concluded that the racemic complex, $[Ln.\mathbf{L}^{\mathbf{22}}(OH_2)]^+$, showed more promise with respect to its development as a responsive CPL probe. For $[Ln.\mathbf{L}^{\mathbf{22}}(OH_2)]^+$ (Ln = Eu^{3+} or Tb^{3+}) CPL spectra obtained in the presence of α_1-AGP and α_1-AAT were identical. This was in agreement with observations of the changes exhibited in total emission, detailed above. A titration was carried out in which the 'switching on' of a CPL signal from the dynamically racemic complex $[Eu.\mathbf{L}^{\mathbf{22}}(OH_2)]^+$ was monitored in the presence of incremental amounts of bovine α_1-AGP. It was shown that by monitoring changes in g_{em} a binding constant for the interaction could be calculated which was in agreement with the binding constant calculated using total emission data. It was concluded that $[Ln.\mathbf{L}^{\mathbf{22}}(OH_2)]^+$ showed potential for development as a chiral probe for the acute phase proteins α_1-AGP and α_1-AAT.

A titration in which incremental amounts of α_1-AGP were added to a solution of $[Eu.\mathbf{L}^{\mathbf{22}}(OH_2)]^+$ in human serum was carried out. Spectral changes remained well defined in total emission, with the limiting spectral form mimicking that observed in 0.1 M NaCl. This allowed a calibration curve to be generated. In addition, it was shown that identical changes in the emission spectral fingerprint could be generated by addition of α_1-AAT to the serum solution. Unfortunately, the same could not be said for the CPL spectral response. Hence, although this complex does show promise as a probe for these acute phase proteins in biological media, it seems unlikely that it will be possible to signal the presence of these proteins by CPL methods.

CHAPTER THREE

INDUCED CPL FOR CHIRAL DETECTION

3.1 Introduction

The work described in Chapter 2 demonstrated the induction of circular polarization in the luminescence output of the racemic lanthanide system $[Ln.\mathbf{L}^{\mathbf{22}}(OH_2)]^+$ as a result of a change in complex constitution. Although the induction of CPL from a racemic lanthanide system via this mechanism has not before been exemplified in the literature, the observation of induced CPL from such a system is in itself not a new phenomenon; such an effect has previously been demonstrated for $[Ln(DPA)_3]^{3-}$ complexes. As was discussed in Chapter 1, the detection of induced CPL from these complexes has been achieved in the presence of a variety of chiral additives, with the observation of the effect generally being attributed in part to the occurrence of outer sphere associative mechanisms.

Several studies conducted using $[Ln(DPA)_3]^{3-}$ complexes have highlighted the fact that the observation of induced CPL from these systems typically allows discrimination between enantiomeric compounds and therefore may facilitate the determination of enantiomeric excess in mixtures of pure enantiomers.[110] Owing to the abundance of chirality in nature and its importance in the manufacture of pharmaceuticals, the development of techniques aiding chiral analysis is of great significance. At present, discrimination between enantiomeric compounds is typically achieved using methods such as NMR spectroscopy, HPLC or GC. The former method employs chiral shift solvating or derivatising agents and the latter two require the use of a chiral stationary phase, which is often derived from a complex biomolecule.[163-165] Each of these methods is relatively time-consuming and requires the use of expensive and complex instrumentation. The discovery of alternative methods, by which chiral detection can be achieved, therefore has great appeal.

This chapter describes investigations carried out in order to assess the utility of racemic lanthanide systems based on macrocylic ligands for chiral detection, in which an induced CPL effect is observed as a result of a change in complex constitution. The work presented concerns studies carried out using $[Ln.\mathbf{L}^{\mathbf{22}}(OH_2)]^+$ (Ln = Eu^{3+}, Tb^{3+}). Although the induction of circular polarization in the luminescence output of this complex was only demonstrated in the presence of proteins in Chapter 2, it was envisaged that the binding of a number of other chiral substrates to the lanthanide centre may also be coupled to a change in complex constitution, and therefore could yield further induced CPL effects.

3.2 Preliminary investigations into anion binding

Owing to the fact that there exist many chiral anions where both enantiomers are readily-available, it was decided that these species were promising substrates for use in the investigations. The binding of anionic species by lanthanide complexes derived from ligands based on a DOTA framework is a well-recognised phenomenon, with the mechanism of binding typically involving the displacement of bound water molecules from a coordinatively unsaturated lanthanide centre.[166] Many examples of anion responsive systems exist in the literature based on such a framework, including the bicarbonate responsive complexes discussed in Section 1.5.3.1 of Chapter 1. As has been previously noted (Section 2.4.2, Chapter 2), the displacement of the single water molecule from the primary coordination sphere of a monohydrated lanthanide complex derived from an octadentate ligand has typically been found to be prohibited. In accordance with this, it would be reasonable to predict that the binding of anions at the lanthanide centre in $[Ln.\mathbf{L}^{\mathbf{22}}(OH_2)]^+$ should not be possible. However, it was anticipated that such binding may be facilitated for this complex by the weakness of the binding interaction with the pyridine nitrogens of the azaxanthone chromophores.

3.2.1 Verifying the occurrence of anion binding at the lanthanide centre

As was shown in Chapter 2, the sensitivity of europium emission to the metal coordination environment allows any binding event occurring at the metal centre to be easily visualised and a binding affinity to be calculated. Hence, in order to verify the hypothesis that anion binding may occur at the lanthanide centre in $[Ln.\mathbf{L}^{\mathbf{22}}(OH_2)]^+$, a preliminary titration was carried out in which the emission intensity of $[Eu.\mathbf{L}^{\mathbf{22}}(OH_2)]^+$ was monitored in the presence of gradually increasing amounts of the achiral chelating anion bicarbonate. The binding of bicarbonate to a coordinatively unsaturated lanthanide centre is a well-known phenomenon and is thought to occur in a stepwise manner, ultimately yielding a complex in which the anion acts as a bidentate ligand.

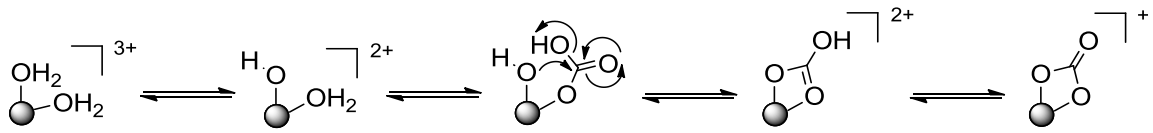

Figure 3.1: Schematic diagram of a plausible mechanism of hydrogencarbonate chelation at a coordinatively unsaturated lanthanide centre.[57]

Incremental additions of a freshly prepared, concentrated sodium bicarbonate stock solution were made to a 1 mL sample of [Eu.$\mathbf{L}^{22}$(OH$_2$)]$^+$, which had been dissolved in aqueous solution at pH 7.4 containing 0.1 M NaCl, to give a solution where the concentration of complex was 30 μM. The pH of the sample was allowed to rise over the course of the titration, such that the concentration of bicarbonate could be accurately known, and the experiment was halted when the concentration of bicarbonate in solution was 29 mM. Figure 3.2 shows the variation in europium emission upon addition of the stock solution, along with separate plots showing the initial and limiting spectral signatures. Ratiometric analysis of the data gathered generated values to which a 1:1 binding isotherm could be fitted, therefore allowing the binding affinity to be estimated. The binding interaction between [Eu.$\mathbf{L}^{22}$(OH$_2$)]$^+$ and bicarbonate was found to be characterised by a value of log$K$ = 2.42 (± 0.02).

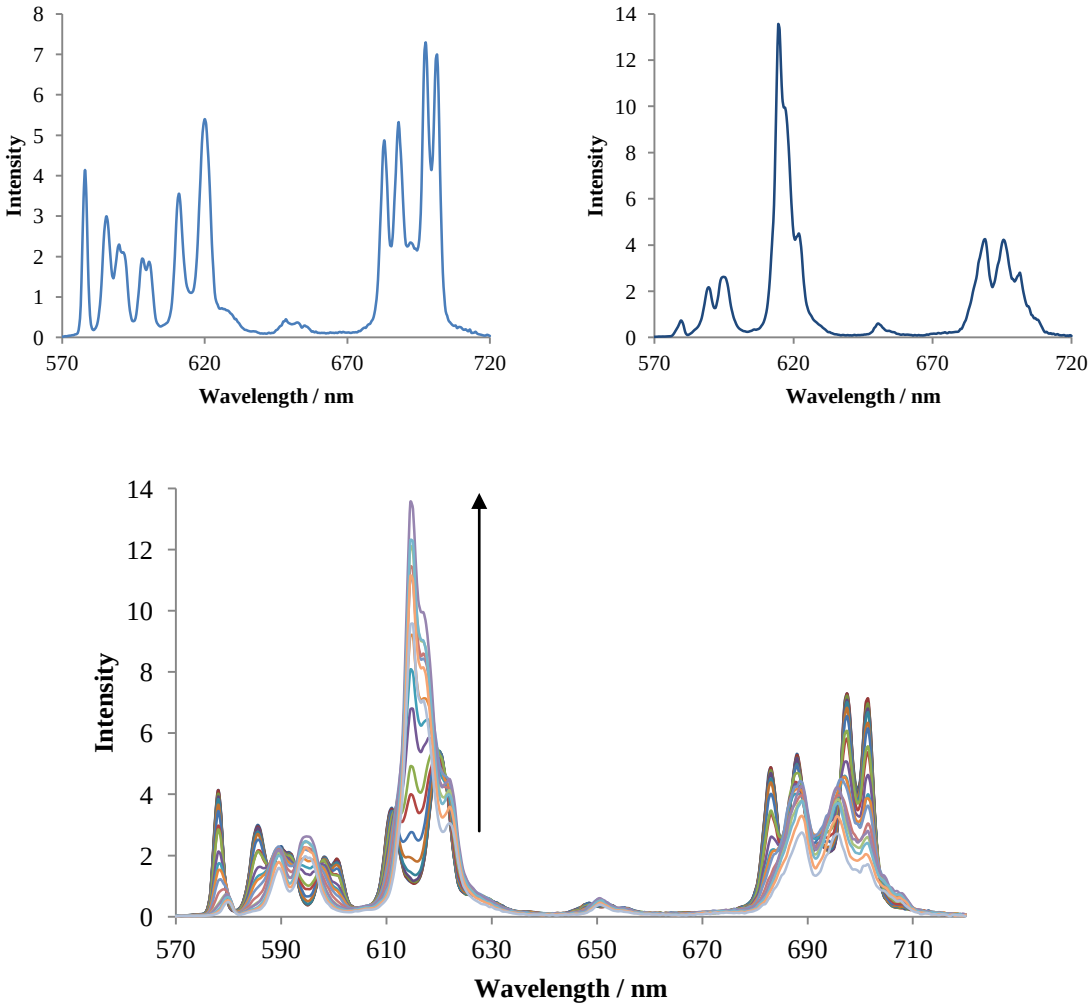

Figure 3.2: Variation of the emission spectral profile of [Eu.$\mathbf{L}^{22}$(OH$_2$)]$^+$ upon addition of bicarbonate. The initial spectral form and limiting spectral form (10 mM bicarbonate) are highlighted in separate plots (295 K, pH 7.4, 0.1 M NaCl, 30 μM complex).

The dramatic change in spectral form observed upon addition of bicarbonate was reminiscent of that observed previously in the presence of protein, consistent with the occurrence of a binding interaction between the anion and the lanthanide centre, involving a similar change in the constitution of the complex. Again, a large increase in the relative intensity of the $\Delta J = 2$ band was apparent, suggesting a change in the axial donor polarizability.[29, 30] As before, this could possibly be attributed to the replacement of the neutral N donor of the azaxanthone chromophore with a polarizable charged oxygen donor from the chelating anion. Meanwhile, using an analogous method to that outlined in Section 2.3.1 of Chapter 2, the hydration state of the complex in the presence of 29 mM bicarbonate was found to be reduced in comparison to the free complex (Table 3.1), suggesting displacement of the coordinated water molecule from the lanthanide centre. Overall these results are consistent with a mode of binding involving displacement of both the coordinated water molecule and one of the azaxanthone chromophores from the lanthanide centre.

Table 3.1: Experimentally determined radiative rate constants and the derived value of q' (± 20%) for $[Eu.\mathbf{L}^{\mathbf{22}}(OH_2)]^+$ (295 K, pH 5.5) and in the presence of sodium bicarbonate (29 mM) (295 K, 0.1 M NaCl).

Complex	Anion	k_{H_2O} / ms^{-1}	k_{D_2O} / ms^{-1}	q'
$[Eu.\mathbf{L}^{\mathbf{22}}(OH_2)]^+$	-	2.08	0.61	1.46
	Bicarbonate	1.51	0.72	0.65

The reversibility of the binding interaction between $[Eu.\mathbf{L}^{\mathbf{22}}(OH_2)]^+$ and bicarbonate was probed in a simple experiment. Firstly, a 1 mL sample of $[Eu.\mathbf{L}^{\mathbf{22}}(OH_2)]^+$ was prepared, as outlined above, and a sample of concentrated sodium bicarbonate stock solution was added to give a bicarbonate concentration of 29 mM. The pH of the sample was then gradually lowered and the total emission output monitored. Upon acidification of the sample, the emission spectral form changed. The experiment was halted at pH 3 and argon was bubbled through the sample in order to facilitate the removal of carbonic acid as carbon dioxide. The spectral fingerprint observed at this pH bore close resemblance to that of the starting aqua complex, suggesting that the binding interaction and associated changes in complex constitution are indeed reversible.

3.2.2 Examining changes in emission spectral form

Having verified that reversible anion binding is able to occur at the lanthanide centre in $[Ln.\mathbf{L}^{\mathbf{22}}(OH_2)]^+$, several additional investigations were carried out to assess and characterise the binding of a number of chiral anions. It was anticipated that such an analysis would allow the identification of the chiral anions that would be most suitable for use in CPL studies, aimed at demonstrating the scope and utility of $[Ln.\mathbf{L}^{\mathbf{22}}(OH_2)]^+$ in chiral detection.

Titrations were carried out in which the emission intensity of $[Ln.\mathbf{L}^{\mathbf{22}}(OH_2)]^+$ (Ln = Eu^{3+} or Tb^{3+}) was monitored in the presence of a gradually increasing amount of each chosen anion. In every case, incremental additions of a freshly prepared, concentrated anion stock solution were made to a 1 mL sample of $[Ln.\mathbf{L}^{\mathbf{22}}(OH_2)]^+$ (Ln = Eu^{3+} or Tb^{3+}), which had been dissolved in aqueous solution at pH 7.4 containing 0.1 M NaCl. The pH of each anion stock solution was adjusted to 7.4 using conc. $HCl_{(aq)}$ and conc. $NaOH_{(aq)}$ prior to additions being carried out, in order to minimise changes in the pH of the lanthanide complex solution over the course of each titration. Generally speaking, it was found that changes in spectral form for $[Eu.\mathbf{L}^{\mathbf{22}}(OH_2)]^+$ only occurred at relatively high concentrations of added anion. In accordance with this, the titrations were typically carried out over the concentration range 0 - 75 mM for both the europium and terbium analogues of the complex, unless significant quenching of signal intensity was found to occur or a limiting spectral form was attained prior to this endpoint. Representative structures of the anions investigated are shown below.

Phosphorus(v) oxy-anions:

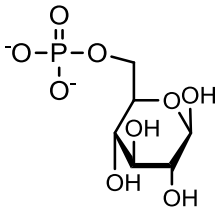

D-Glucose-6-phosphate

pKa's: 0.94, 6.11[167]

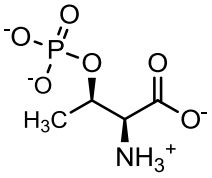

O-Phospho-*L*-threonine

<1, 2.08, 5.65, 9.74[168]

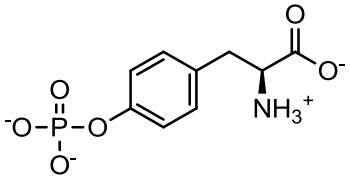

O-Phospho-*L*-tyrosine

1.6, 2.02, 5.65, 9.20[168]

α-Hydroxy acids:

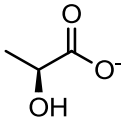

L-Lactate

3.86[169]

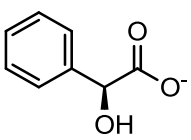

L-Mandelate

3.41[170]

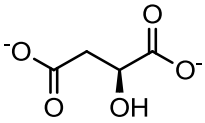

L-Malate

3.40, 5.20[169]

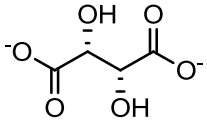

L-Tartrate

2.99, 4.40[169]

In the case of the chiral phosphorus(v) oxy-anions, very little change in spectral form was observed upon addition of the anion stock solution to 1 mL samples of $[Eu.\mathbf{L}^{22}(OH_2)]^+$. For *D*-glucose-6-phosphate and *O*-phospho-*L*-threonine, slight variations in the emission spectral fingerprint first became apparent when the concentration of added anion was in excess of roughly 5 mM. These changes were similar in nature for the two anions and were particularly evident within the hypersensitive $\Delta J = 2$ manifolds of the emission spectra. Each titration was halted when the concentration of added anion reached roughly 75 mM, at which point a limiting spectrum was still not attained. In the case of *O*-phospho-*L*-tyrosine, quenching of signal intensity meant that the analogous titration was halted when the concentration of added anion was roughly 46 mM. No significant change in spectral form was observed for $[Eu.\mathbf{L}^{22}(OH_2)]^+$ in the presence of this anion. Analogous titrations carried out with $[Tb.\mathbf{L}^{22}(OH_2)]^+$ showed only quenching of the signal intensity, which was particularly pronounced in the case of *O*-phospho-*L*-tyrosine, as was expected on the basis of the results obtained with $[Eu.\mathbf{L}^{22}(OH_2)]^+$.

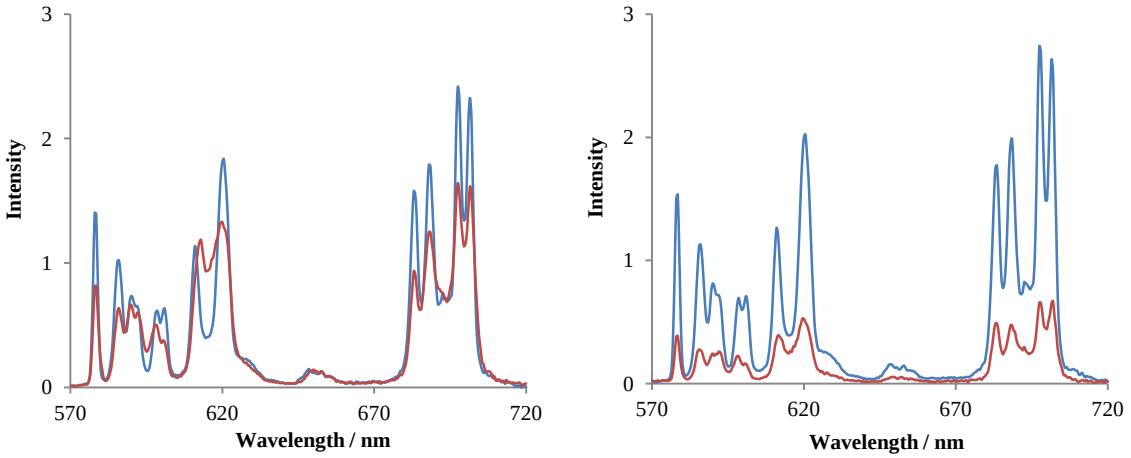

Figure 3.3: Europium emission spectral changes following addition of *O*-phospho-*L*-threonine (left, 75 mM) and *O*-phospho-*L*-tyrosine (right, 46 mM) to $[Eu.\mathbf{L}^{22}(OH_2)]^+$ (blue = initial, red = final, 295 K, 0.1 M NaCl, pH 7.4, 15 µM complex).

The observations outlined above were very different to the dramatic changes in spectral form observed for $[Eu.\mathbf{L}^{22}(OH_2)]^+$ in the presence of bicarbonate, and provided limited evidence to support a mode of anion binding involving a change in complex constitution. Binding affinities were estimated where possible by fitting 1:1 binding isotherms to the data gathered using non-linear least squares iterative analysis. For each anion, the binding interaction with $[Eu.\mathbf{L}^{22}(OH_2)]^+$ was found to be characterised by a value of $\log K \leq 1.0$ (± 0.1). Taking this into account, it is unsurprising that the changes

in spectral form observed in the presence of the phosphorus(v) oxy-anions were less dramatic than those seen with bicarbonate (log*K* = 2.42 (± 0.02)). Previous studies examining the binding of phosphorus(v) oxy-anions by coordinatively unsaturated lanthanide complexes have revealed that these anions tend to bind to the lanthanide centre of europium complexes in a monodentate manner.[50, 128] This is in contrast to the chelating manner known to be favoured by bicarbonate (see Figure 3.1) and could perhaps in part explain the weaker affinity observed.

In contrast to the results obtained with the phosphorus(v) oxy-anions, well-defined and dramatic changes in the emission spectral form were found to occur for [Eu.**L**^{22}(OH$_2$)]$^+$ in the presence of the α-hydroxy acids lactate, mandelate and malate. For the structurally-related chiral anion tartrate, some change in form was observed but the variation appeared incomplete over the concentration range examined. Limiting spectra attained in the presence of the former three anions are shown in Figure 3.4, along with the initially recorded emission spectrum.

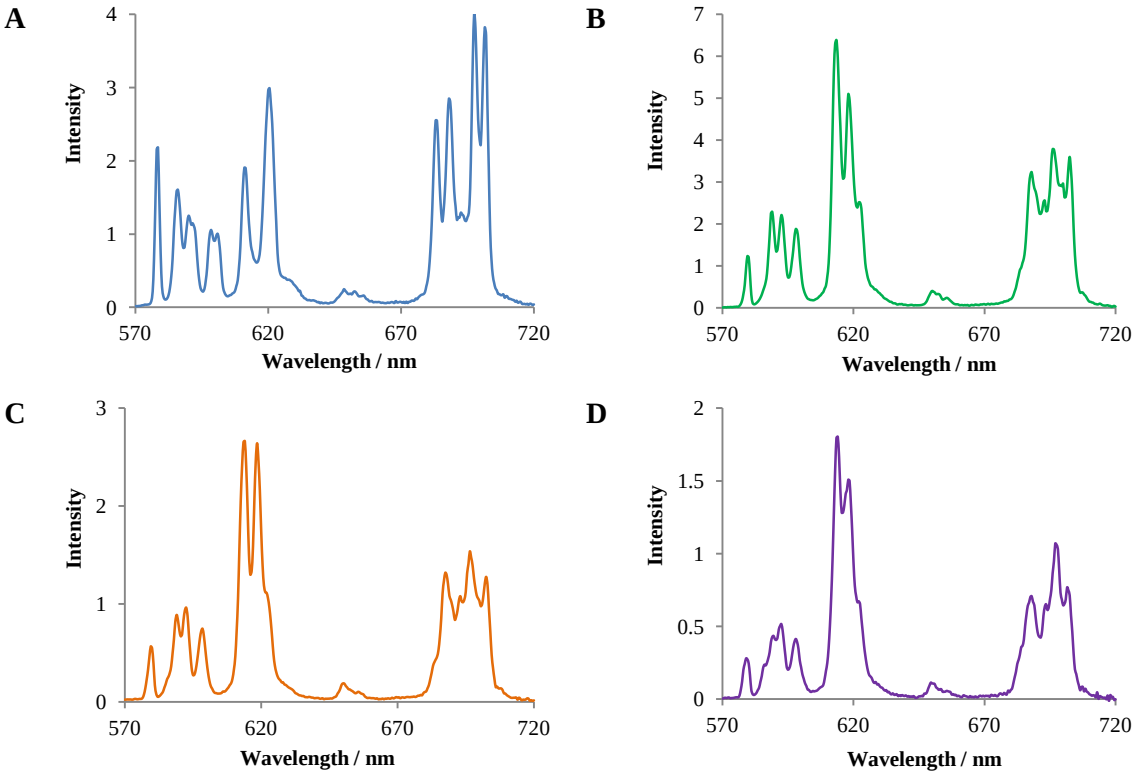

Figure 3.4: Representative emission spectra showing the metal-based emission of [Eu.**L**^{22}(OH$_2$)]$^+$: (A) complex only; (B) complex + 69 mM *L*-lactate; (C) complex + 34 mM *D*-mandelate; (D) complex + 61 mM *L*-malate (295 K, pH 7.4, 0.1 M NaCl, 15 μM complex).

As can be seen from Figure 3.4, the limiting spectral fingerprint of the complex in the presence of lactate, mandelate and malate was very similar in form, suggesting a near

identical mode of binding at the lanthanide centre. In each case, a large increase in the relative intensity of the $\Delta J = 2$ band was apparent in comparison to the free complex, mimicking the variation which had previously been observed with bicarbonate. On the basis of this observation, it may be hypothesised that the mode of coordination of these α-hydroxy acids at the lanthanide centre again involves displacement of both the coordinated water molecule and one azaxanthone pyridine nitrogen from the lanthanide centre. In the presence of lactate, an overall increase in the emission intensity was observed, suggesting particularly efficient exclusion of quenching XH oscillators from the primary and secondary coordination spheres. For lactate and mandelate close inspection of the $\Delta J = 1$ manifold within the limiting emission spectral fingerprint revealed the presence of only three bands, consistent with the presence of a single emissive species in solution. In contrast, a similar analysis of the spectral fingerprint obtained in the presence of malate suggested the existence of multiple emissive species in solution, implying the presence of several different ternary complexes in solution (see Section 3.3.1 for further discussion).

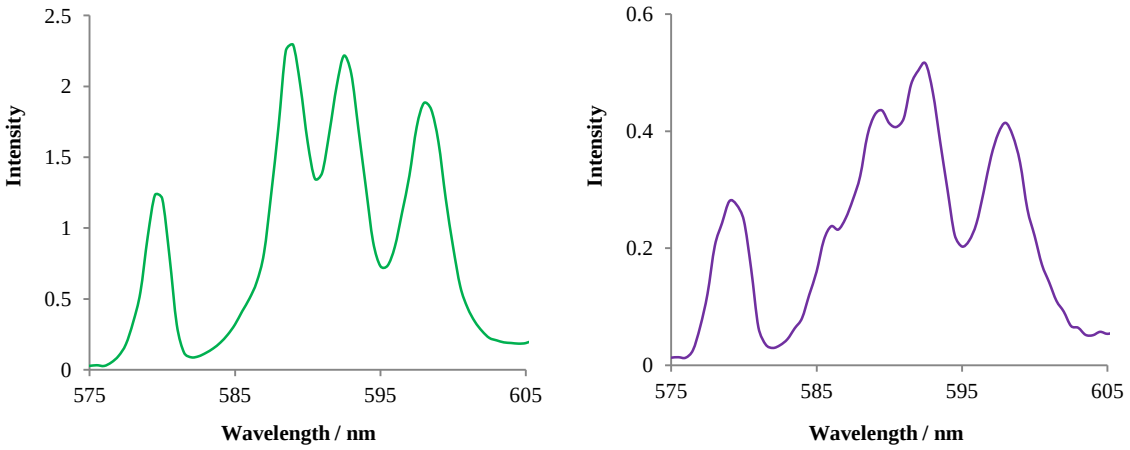

Figure 3.5: Representative emission spectra showing the $\Delta J = 0$ and $\Delta J = 1$ manifolds of the europium emission for [Eu.$\mathbf{L}^{22}$(OH$_2$)]$^+$ in the presence of 69 mM *L*-lactate (left) and 61 mM *L*-malate (right) (295 K, pH 7.4, 0.1 M NaCl, 15 μM complex).

As expected, for [Tb.$\mathbf{L}^{22}$(OH$_2$)]$^+$ the changes in spectral form observed in the presence of the chiral α-hydroxy acids discussed above were much less pronounced. Generally speaking, for this complex the overall emission intensity was found to decrease in the presence of each anion, with no significant variation in the relative intensity of the emission within the various manifolds. Substantial quenching of the emission intensity was observed in the presence of mandelate and the titration was halted when the concentration of added anion was 17 mM. In every other case, less quenching was

observed and the titrations were carried out over the concentration range 0 - 75 mM. The variation in metal-based emission of [Tb.$\mathbf{L}^{22}(OH_2)]^+$ upon addition of lactate is shown in Figure 3.6.

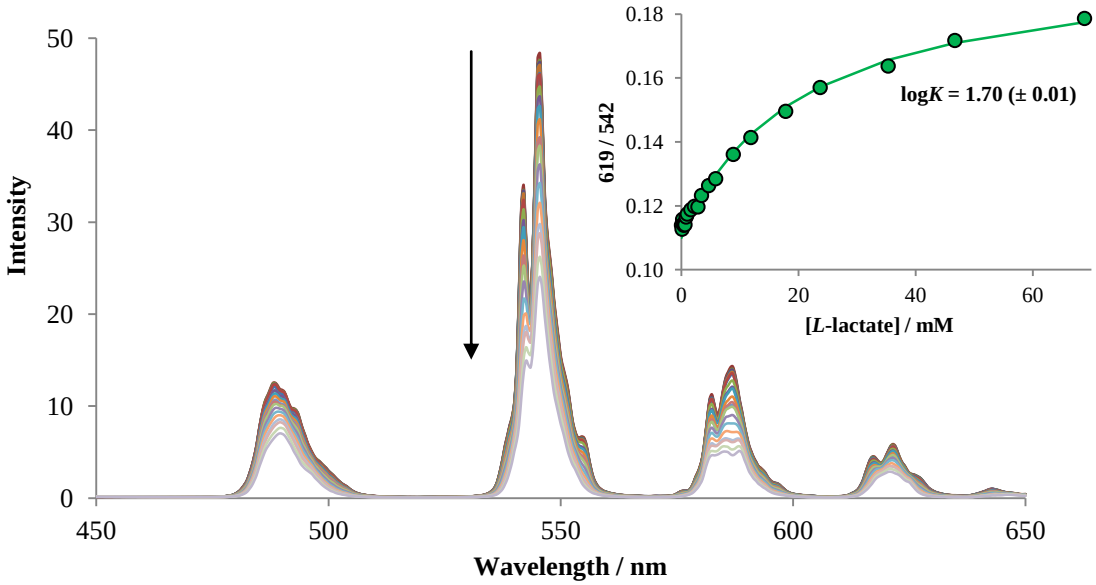

Figure 3.6: Variation of the emission spectral profile of [Tb.$\mathbf{L}^{22}(OH_2)]^+$ upon addition of *L*-lactate. Inset: Calibration curve showing variation of the observed emission intensity versus [*L*-lactate] (295 K, pH 7.4, 0.1 M NaCl, 30 µM complex).

Attempts were made to estimate binding affinities for each of the α-hydroxy chiral anions with [Ln.$\mathbf{L}^{22}(OH_2)]^+$ (Ln = Eu^{3+}, Tb^{3+}). First, a ratiometric analysis of the data collected at each concentration of added anion was carried out. A 1:1 binding isotherm was then fitted to the resulting data points using non-linear least squares iterative analysis, allowing the determination of binding constants. For the titrations carried out using the europium complex, the ratiometric analysis of the data generated was carried out by comparing the integrated emission intensity of the $\Delta J = 2$ band to that of the $\Delta J = 1$ band. As is evident from the data presented in Table 3.2, the binding constant associated with the interaction between [Eu.$\mathbf{L}^{22}(OH_2)]^+$ and tartrate was much weaker than those characterising the interaction between this complex and the other α-hydroxy acids. Meanwhile, of the other three anions, the highest binding constant was associated with the interaction between [Eu.$\mathbf{L}^{22}(OH_2)]^+$ and mandelate. In light of previous studies of interactions between coordinatively unsaturated DOTA-derived lanthanide complexes and phosphorus(v) oxy-anions, which demonstrated a chemoselectivity for (*O*-P-Tyr)$^{2-}$ over (*O*-P-Ser)$^{2-}$, this latter result was not unexpected and may reasonably be attributed to the lower degree of hydration experienced by mandelate in aqueous media, in comparison to lactate and malate.[128, 171]

Table 3.2: Comparison of the experimentally determined binding constants for $[Eu.\mathbf{L}^{\mathbf{22}}(OH_2)]^+$ in the presence of various anions. Standard deviation errors associated with data fitting are shown in brackets.

Complex	log*K*			
	Lactate	Mandelate	Malate	Tartrate
$[Eu.\mathbf{L}^{\mathbf{22}}(OH_2)]^+$	1.94 (± 0.02)	2.39 (± 0.03)	1.81 (± 0.01)	0.88 (± 0.01)

Attempts to perform ratiometric analyses of the data obtained over the course of titrations carried out with $[Tb.\mathbf{L}^{\mathbf{22}}(OH_2)]^+$ using a method of the type described above did not generate data that was amenable to further analysis. By instead analysing the variation in emission intensity at a pair of individual emission wavelengths a set of data points to which a 1:1 binding isotherm could be fitted was generated in the case of lactate, and an affinity constant of log*K* = 1.70 (± 0.01) was calculated. This was a surprising result, owing to the fact that terbium is slightly more charge dense than europium and one may therefore anticipate that for a given anion a higher affinity constant is expected to be associated with its interaction with the terbium analogue of a chosen complex.

3.2.3 Determining the hydration state of the anion-bound complexes

In order to gain further evidence in support of the hypothesis that the binding of lactate, mandelate and malate to $[Ln.\mathbf{L}^{\mathbf{22}}(OH_2)]^+$ (Ln = Eu^{3+}, Tb^{3+}) is associated with the displacement of both the coordinated water molecule and one of the azaxanthone chromophores from the lanthanide centre, experiments were undertaken to facilitate the determination of the hydration state, q', of the complex in the presence of these anions. The method used was analogous to that outlined in Section 2.3.1 of Chapter 2, with suitable concentrations of each anion being decided on the basis of previously obtained results. In all cases, a mono-exponential decay of the emission intensity was observed in both H_2O and D_2O, facilitating the determination of radiative rate constants and derivation of q' values.

Table 3.3: Experimentally determined radiative rate constants the derived value of the hydration state, q' (± 20%), for [Ln.**L**^{22}(OH$_2$)]$^+$ (295 K, pH 5.5) and in the presence of lactate (106 mM), mandelate (44 mM for Eu^{3+}, 17 mM for Tb^{3+}) and malate (96 mM) (295 K, 0.1 M NaCl).

Complex	Anion	k_{H_2O} / ms^{-1}	k_{D_2O} / ms^{-1}	q'
[Eu.**L**^{22}(OH$_2$)]$^+$	-	2.08	0.61	1.46
	Lactate	1.32	0.69	0.46
	Mandelate	1.38	0.72	0.49
	Malate	1.26	0.66	0.42
[Tb.**L**^{22}(OH$_2$)]$^+$	-	0.66	0.48	0.60
	Lactate	0.56	0.42	0.40
	Mandelate	0.72	0.59	0.35
	Malate	0.57	0.46	0.25

As can be seen from the data presented in Table 3.3, the hydration state of both the europium and terbium complexes of **L**^{22} was consistently found to tend towards zero in the presence of each added anion. The results obtained are therefore in support of the hypothesis that binding of lactate, mandelate and malate to [Ln.**L**^{22}(OH$_2$)]$^+$ (Ln = Eu^{3+}, Tb^{3+}) is associated with the displacement of both the coordinated water molecule and one of the azaxanthone chromophores from the lanthanide centre. It is interesting to note that, whilst in all other cases the rate of radiative decay of the lanthanide emission in water was found to decrease in the presence of anion, [Tb.**L**^{22}(OH$_2$)]$^+$ proved exceptional to this when in the presence of mandelate.

3.3 CPL studies

On the basis of the results outlined in the preceding sections, lactate, mandelate and malate were selected for use in a series of experiments aimed at evaluating the utility of [Ln.**L**^{22}(OH$_2$)]$^+$ (Ln = Eu^{3+}, Tb^{3+}) for chiral detection. In comparison to the proteins examined in Chapter 2, these chiral anions are much smaller entities and offer no possibility of secondary coordination effects, such as the inclusion of the azaxanthone sensitiser into the ligand binding pocket which was noted for α_1-AGP. Hence, although it was clear from the results discussed previously that these chiral α-hydroxy acids are able to bind to the lanthanide centre in [Ln.**L**^{22}(OH$_2$)]$^+$ in a manner that is coupled to a change in complex constitution, it remained to be seen whether this would lead to the observation of an induced CPL effect in any of these cases. All CPL spectra reported in

this chapter were recorded at Durham University on a custom built spectrometer, which employed a laser driven light source with a spectral range of 170 to 2100 nm.

3.3.1 Preliminary studies using $[Tb.\mathbf{L}^{22}(OH_2)]^+$

An initial study was undertaken to establish whether any circular polarization was induced in the emission output of $[Tb.\mathbf{L}^{22}(OH_2)]^+$ in the presence of lactate, mandelate or malate. A preliminary titration was performed in an attempt to monitor the 'switching on' of CPL in the emission output of this racemic complex, in the presence of gradually increasing amounts of *L*-lactate. The method employed was analogous to that used for the titrations previously described, in which the total emission spectral change was monitored. Unfortunately, the complex $[Tb.\mathbf{L}^{22}(OH_2)]^+$ was found to be extremely susceptible to photobleaching under the experimental conditions. The observed decrease in emission intensity presumably occurred as a result of photoreduction of the carbonyl group, facilitated by the high power of the laser driven excitation light source. This meant that the signal intensity was progressively depleted over the course of the titration. The experimental method was subsequently revised such that for each anion examined a number of separate 1 mL samples of the terbium complex was prepared as outlined previously. The total emission spectrum of each sample was recorded prior to and immediately after the acquisition of CPL spectral data, such that the extent of photobleaching could be monitored. Typically, each sample was analysed for its CPL output in the presence of a chosen concentration of anion and then discarded. As before, additions of the anions were made from freshly prepared, concentrated stock solutions, which had been adjusted to pH 7.4 using conc. $HCl_{(aq)}$ and conc. $NaOH_{(aq)}$. Between four and six different concentrations of each anion were examined, with appropriate ranges chosen on the basis of previously obtained results.

In the case of both *L*-lactate and *L*-mandelate, the 'switching on' of a CPL signal was observed for $[Tb.\mathbf{L}^{22}(OH_2)]^+$ at various concentrations of added anion (Figure 3.7). As was anticipated based on the structural similarity of these anions, the spectral fingerprint of the induced CPL signal observed in the presence of their *L* enantiomers was identical in form. The CPL spectra were characterised by a large signal associated with the $^5D_4 \rightarrow {}^7F_5$ transition, whilst little circular polarization was associated with any of the other transitions. This was reminiscent of the behaviour previously exhibited by this complex in the presence of protein (see Section 2.5, Chapter 2).

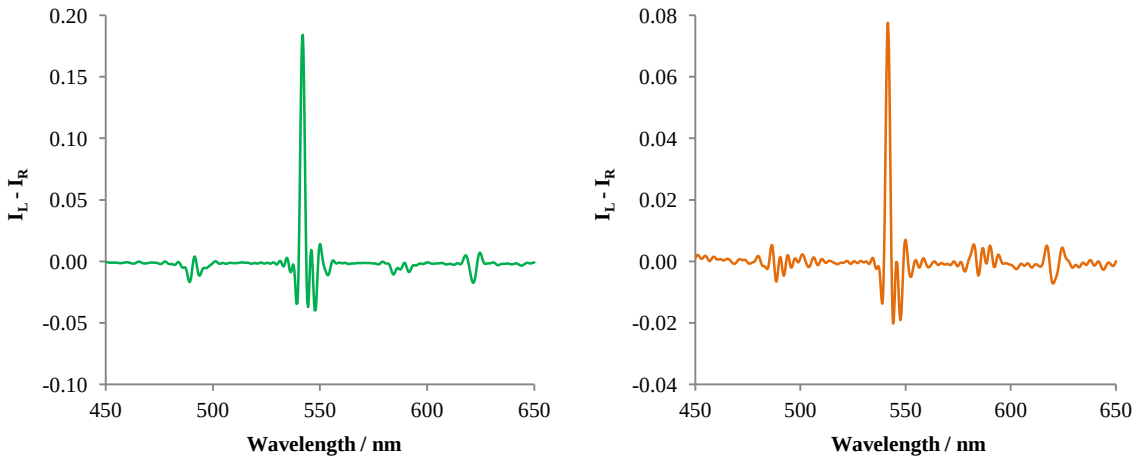

Figure 3.7: Representative CPL spectra showing the circularly polarized emission of [Tb.$\mathbf{L}^{22}$(OH$_2$)]$^+$ in the presence of 10 mM *L*-lactate (left) and 0.5 mM *L*-mandelate (right) (295 K, 0.1 M NaCl, pH 7.4, 15 μM complex).

In contrast to the results outlined above, CPL spectra recorded for [Tb.$\mathbf{L}^{22}$(OH$_2$)]$^+$ in the presence of *L*-malate did not show any circular polarization of the emission. Samples were analysed at 4 different concentrations of added anion, ranging between 5 and 45 mM. Unfortunately it was not possible to gather data at higher concentrations owing to quenching of signal intensity. The lack of induced CPL observed in the presence of malate provides clear evidence to support a hypothesis that the mode of binding of this anion at the metal centre in [Ln.$\mathbf{L}^{22}$(OH$_2$)]$^+$ differs to that of lactate and mandelate.

Previous studies examining the binding of lactate to lanthanide centres in complexes based on ligands derived from DOTA have shown that the binding of this anion typically occurs via the formation of a 5 membered chelate, involving the hydroxy group and the α-carboxylate.[127] However, it may be envisaged that the formation of a chelated adduct involving a lanthanide centre and this or other α-hydroxy acids may also occur via the carboxylate moiety, either exclusively or in part. In addition, for hydroxy acids such as malate where there is a second carboxylate moiety present in a β-position relative to the hydroxy group, a coordination mode involving cooperative carboxylate binding may be anticipated.

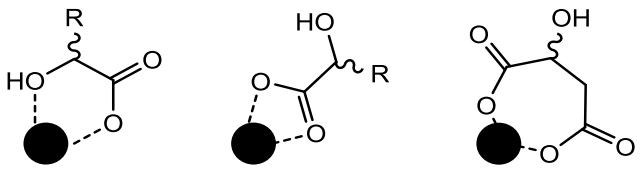

Scheme 3.1: Possible modes of chelation for α-hydroxy acids at a lanthanide centre.

A series of control titrations was carried out using an identical method to that outlined in the previous section, in an attempt to ascertain further information regarding the mode of binding of lactate, mandelate and malate at the europium centre in $[Eu.\mathbf{L}^{22}(OH_2)]^+$. The variation in the emission spectral output of $[Eu.\mathbf{L}^{22}(OH_2)]^+$ was examined in the presence of gradually increasing amounts of acetate, alanate, succinate and citrate. As before, titrations with these ions were halted when the concentration in solution reached roughly 75 mM. With citrate, significant quenching of the signal intensity was observed, which precluded analysis of changes in spectral form. Meanwhile, for alanate very little change in spectral form was found to occur, suggesting that this zwitterion is unable to form a ternary complex in solution with $[Eu.\mathbf{L}^{22}(OH_2)]^+$ over the concentration range examined. More significant changes in spectral form were seen with acetate and succinate. The observed variations in the emission spectral profile of $[Eu.\mathbf{L}^{22}(OH_2)]^+$ in the presence of these anions are shown in Figure 3.8. A limiting spectral form was not attained, in either case, over the concentration range examined, suggesting that the binding of lactate and mandelate to the europium centre in $[Eu.\mathbf{L}^{22}(OH_2)]^+$ must occur predominantly in a classical manner, via the formation of 5 membered chelates involving the hydroxy group.[127] Meanwhile, results obtained with succinate suggest that the ternary complexes formed by $[Eu.\mathbf{L}^{22}(OH_2)]^+$ in the presence of malate may involve coordination of the anion via one or both of the carboxylate moieties. The chiral centre is therefore located more remotely in relation to the lanthanide ion and induced CPL is not observed.

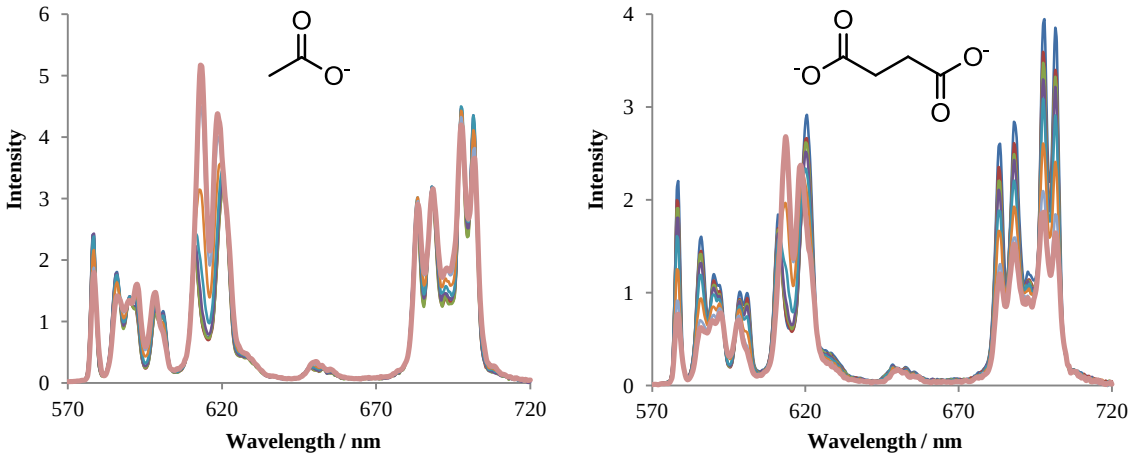

Figure 3.8: Europium emission spectral changes following addition of acetate (left, up to 80 mM) and succinate (right, up to 78 mM) to $[Eu.\mathbf{L}^{22}(OH_2)]^+$, shown with the structures of the anions (295 K, 0.1 M NaCl, pH 7.4, 15 µM complex). The emission spectrum obtained at the endpoint of each titration is shown in bold.

The CPL data gathered for [Tb.$\mathbf{L}^{\mathbf{22}}$(OH$_2$)]$^+$ in the presence of *L*-lactate and *L*-mandelate was used to determine emission dissymmetry factors in accordance with equation 1, as defined in Section 1.2.2 of Chapter 1.[13]

$$g_{\mathrm{em}}(\lambda) = \frac{2\Delta I(\lambda)}{I(\lambda)} \qquad \text{(eqn. 1)}$$

For both anions, the highest emission dissymmetry factor was found to be associated with the transition centred at 541.5 nm. Figure 3.9 shows a plot of the variation in the emission dissymmetry factor at this wavelength as a function of *L*-lactate concentration. For this anion the emission dissymmetry factor was found to reach its maximum between 6 and 10 mM. Meanwhile, in the case of mandelate it was found that a lower concentration of added anion was required in order for a maximal emission dissymmetry factor to be reached at 541.5 nm, with the highest value of g_{em} being obtained in the presence of between 0.5 and 1 mM *L*-mandelate. This was not unexpected given the relative affinity of [Eu.$\mathbf{L}^{\mathbf{22}}$(OH$_2$)]$^+$ for these anions, which had already been calculated on the basis of total emission spectral changes (see Table 3.2).

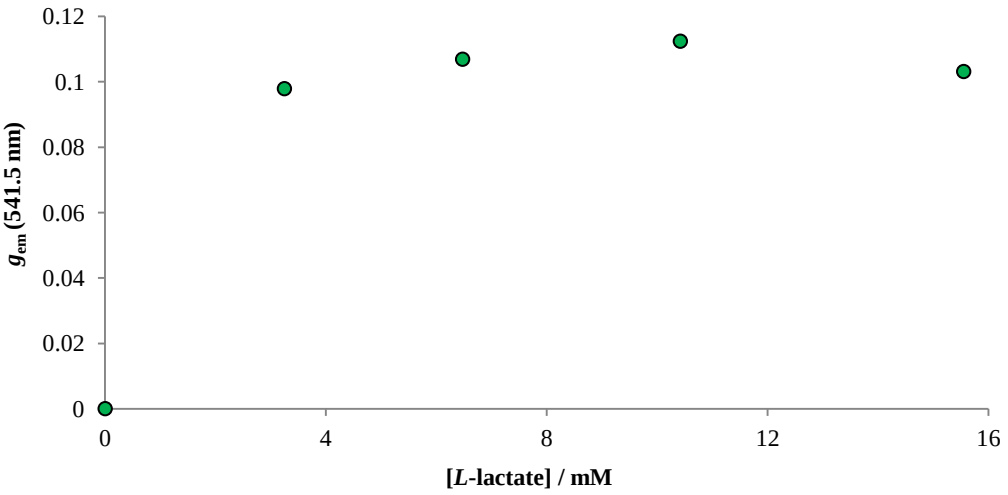

Figure 3.9: A plot of the variation in g_{em} at 541.5 nm with concentration of *L*-lactate for [Tb.$\mathbf{L}^{\mathbf{22}}$(OH$_2$)]$^+$ (295 K, 0.1 M NaCl, pH 7.4, 15 µM complex).

As can be seen from Figure 3.9, the CPL signal associated with the ternary complex formed between *L*-lactate and [Tb.$\mathbf{L}^{\mathbf{22}}$(OH$_2$)]$^+$ was characterised by a maximal g_{em} value of roughly +0.1 at 541.5 nm. Surprisingly, it was found that there was a significant difference in magnitude between this and the equivalent value observed in the presence of *L*-mandelate, with the latter figure being around +0.05. On the basis of these figures, it was concluded that the utility of [Tb.$\mathbf{L}^{\mathbf{22}}$(OH$_2$)]$^+$ for chiral detection would be best demonstrated in the presence of lactate, where it was hoped that the higher emission

dissymmetry factor would facilitate the collection of data for mixtures of stereoisomers containing only a slight excess of one enantiomer.

3.3.2 Demonstrating the utility of $[Tb.L^{22}(OH_2)]^+$ in chiral detection

Prior to undertaking further CPL studies aimed at demonstrating the utility of $[Tb.\mathbf{L}^{22}(OH_2)]^+$ in chiral detection, a preliminary titration was carried out monitoring the variation in total emission intensity of $[Eu.\mathbf{L}^{22}(OH_2)]^+$ as a function of *D*-lactate concentration. The data gathered facilitated the determination of a binding constant for the formation of a ternary complex between these species in accordance with the method outlined in Section 3.2.2. As was anticipated, the changes in spectral form observed in the presence of *D*-lactate were found to mimic those seen with the enantiomeric anion, and the binding affinity was found to be 1.97 (± 0.02) compared to 1.94 (± 0.02) for *L*-lactate, i.e. the same within error (Figure 3.10 and see also Table 3.2).

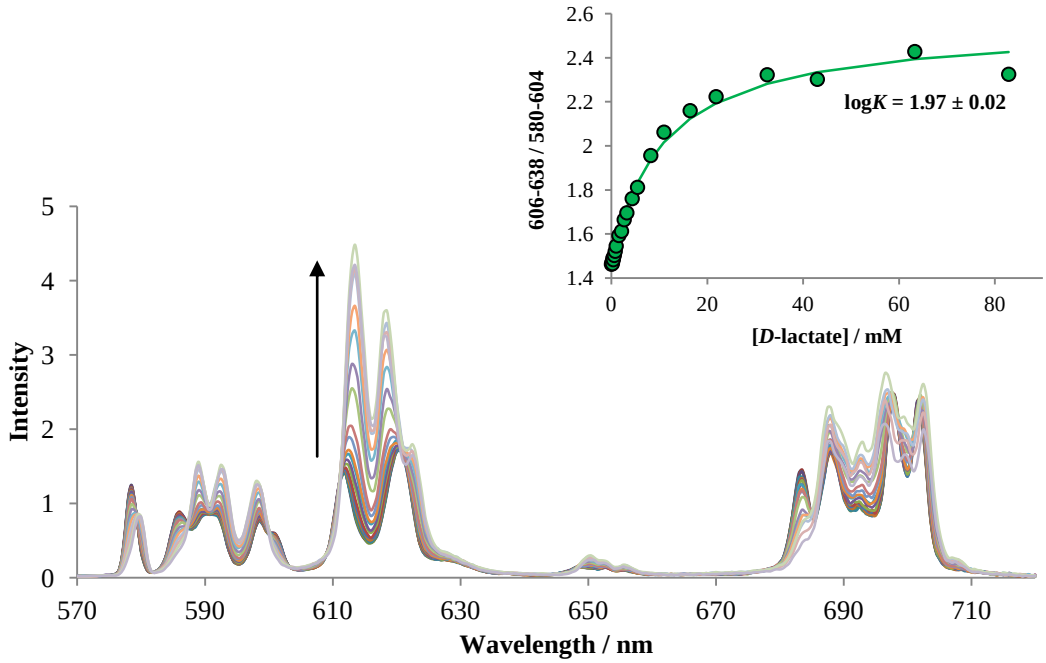

Figure 3.10: Variation of the emission spectral profile of $[Eu.\mathbf{L}^{22}(OH_2)]^+$ upon addition of *D*-lactate (295 K, pH 7.4, 0.1 M NaCl, 15 µM complex). Inset: Calibration curve showing variation of the observed emission intensity versus [*D*-lactate] and the fit (line) to the observed data.

Subsequent CPL experiments carried out using the methods outlined in the previous section demonstrated that the addition of *D*-lactate to a 1 mL sample of $[Tb.\mathbf{L}^{22}(OH_2)]^+$ in 0.1 M NaCl at pH 7.4 also led to the induction of circular polarization in the emission output of the complex. As expected, the form of the observed CPL spectral fingerprint

was a mirror image of that seen in the presence of *L*-lactate and the variation in g_{em} at 541.5 nm followed an identical pattern as the concentration of added anion was raised.

A final set of experiments was carried out in which scalemic samples of lactate of pre-determined enantiomeric composition were added to 1 mL samples of [Tb.$\mathbf{L}^{22}$(OH$_2$)]$^+$ in 0.1 M NaCl at pH 7.4 to give a series of solutions where the overall concentration of lactate was 10 mM. A CPL spectrum was recorded for each sample and the data generated was used to calculate emission dissymmetry factors. It was found that it was possible to calibrate the observed emission dissymmetry factor at 541.5 nm to the enantiomeric purity of the lactate sample, with an approximately linear relationship being observed between the two variables (Figure 3.11). Such a relationship could facilitate the determination of enantiomeric purity in samples containing an unknown composition of lactate.

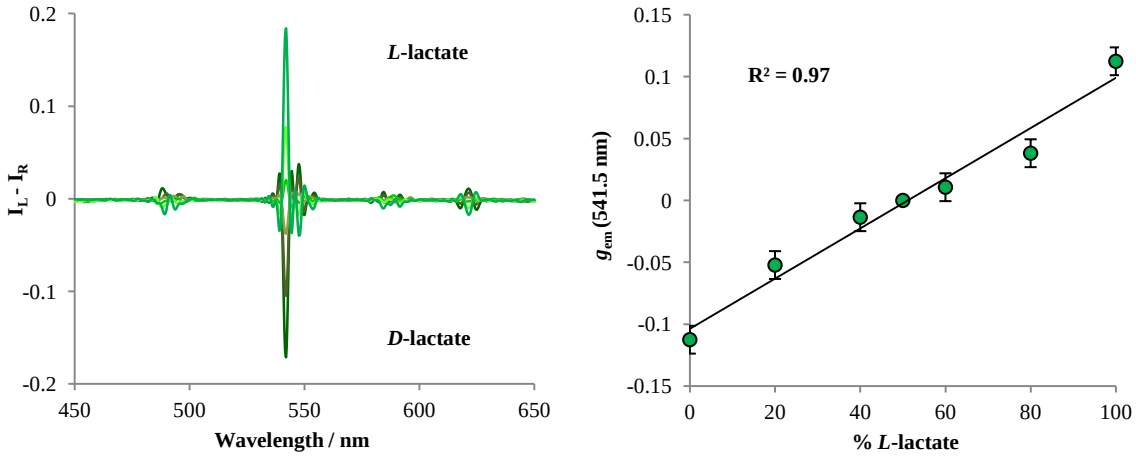

Figure 3.11: Representative CPL spectra showing the circularly polarized emission of [Tb.$\mathbf{L}^{22}$(OH$_2$)]$^+$ in the presence of 10 mM lactate of varying enantiomeric composition shown alongside a plot demonstrating the correlation between g_{em} at 541.5 nm and the enantiomeric composition of the solution (295 K, 0.1 M NaCl, pH 7.4, 15 µM complex).

3.3.3 Studies using [Eu.$\mathbf{L}^{22}$(OH$_2$)]$^+$ and an insight into the mechanism of binding

Having demonstrated the utility of [Tb.$\mathbf{L}^{22}$(OH$_2$)]$^+$ for the chiral detection of lactate, attempts were made to carry out an analogous study using the europium analogue of this complex. Firstly, a set of experiments was undertaken to determine if an induced CPL signal could be observed for this complex in the presence of various concentrations of enantiopure samples of *D*- and *L*-lactate. The same method was used for these experiments as had previously been employed in the initial analysis of induced CPL from samples of [Tb.$\mathbf{L}^{22}$(OH$_2$)]$^+$ described in Section 3.3.1. Again, the total emission

spectrum of each sample was recorded prior to and immediately after the acquisition of CPL spectral data, such that the extent of photobleaching could be monitored. For each enantiomer, a total of five concentrations of lactate were examined, ranging between 6 and 49 mM.

As expected on the basis of CPL data acquired for the terbium analogue of this complex, it did indeed prove possible to observe induced circular polarization in the emission of [Eu.$\mathbf{L}^{\mathbf{22}}$(OH$_2$)]$^+$ in the presence of enantiopure samples of *D*- and *L*-lactate. The signal was found not to be particularly well defined at concentrations lower than around 25 mM, which was somewhat surprising, given that this complex had been determined to have a higher affinity for lactate than its terbium analogue on the basis of previous analysis of changes in the total emission spectral output (see Section 3.2.2). Again, for a given concentration of *L*- or *D*-lactate mirror image spectra were observed, with differing degrees of circular polarization being associated with each of the transitions.

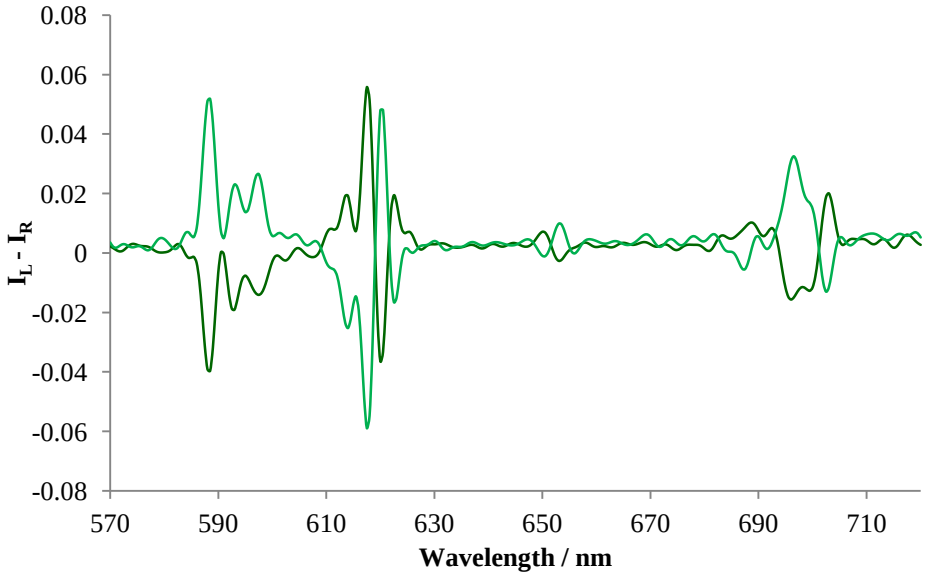

Figure 3.12: Representative CPL spectra showing the mirror image circularly polarized emission of [Eu.$\mathbf{L}^{\mathbf{22}}$(OH$_2$)]$^+$ in the presence of 49 mM of *D*- and *L*-lactate (295 K, 0.1 M NaCl, pH 7.4, 15 μM complex).

A more in depth analysis of the CPL data gathered at each concentration of lactate was facilitated by the calculation of emission dissymmetry factors, which were found to be at a maximum when the concentration of lactate was between 30 and 50 mM. As can be seen from the data presented in Table 3.4, relatively modest values of g_{em} were observed

in general, with the highest values occurring for transitions within the $\Delta J = 1$ and $\Delta J = 2$ manifolds.

Table 3.4: Selected emission dissymmetry factors calculated using the data displayed in Figure 3.12.

		g_{em}				
Complex	Anion	$\Delta J = 1$ (λ)		$\Delta J = 2$ (λ)		$\Delta J = 4$ (λ)
	-	0	0	0	0	0
$[Eu.\mathbf{L}^{22}(OH_2)]^+$	*L*-lactate	+0.04 (588)	-0.03 (618)	+0.04 (620)	-0.02 (623)	+0.02 (696)
	D-lactate	-0.04 (588)	+0.03 (618)	-0.04 (620)	+0.02 (623)	-0.02 (696)

An inspection of the total emission spectral data recorded prior to and following the CPL data collection for each sample revealed an unexpected result, with it being found that, for a given sample, differences in form were apparent between the two spectra. As can be seen from Figure 3.13, changes in form were more evident for samples where the concentration of added lactate was low. However, some variation was still noted in samples where lactate was present at a concentration of 49 mM. In particular, the $\Delta J = 1$ manifold appeared to become more well-defined, with the spectrum recorded following acquisition of CPL data clearly showing only three distinct bands within this manifold.

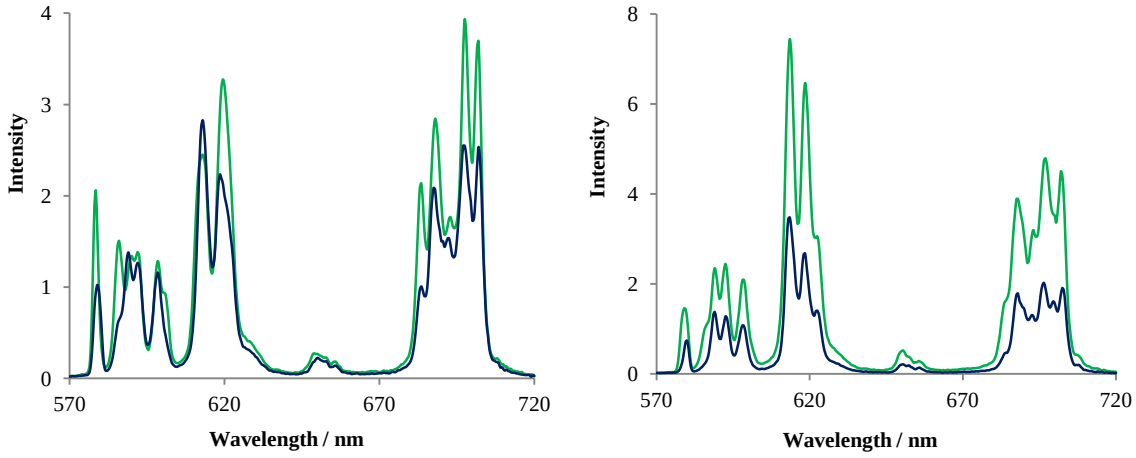

Figure 3.13: Europium emission spectra for $[Eu.\mathbf{L}^{22}(OH_2)]^+$ in the presence of 6 mM (left) and 49 mM (right) *L*-lactate. In each case, spectra recorded prior to (green) and following (blue) CPL data acquisition are shown (295 K, 0.1 M NaCl, pH 7.4, 15 μM complex).

Subsequent investigations were carried out in an attempt to determine the factors implicit in the observations outlined above. A 1 mL sample of $[Eu.\mathbf{L}^{22}(OH_2)]^+$ was prepared in 0.1 M NaCl at pH 7.4 and an aliquot of sodium *L*-lactate added from a freshly prepared stock solution in order to yield a sample in which the concentration of

anion was approximately 50 mM. The total emission of this sample was recorded twice, with a 30 minute interval between measurements. No significant difference in form was noted between the spectra generated by these measurements. In a separate experiment a second 1 mL sample of $[Eu.\mathbf{L}^{22}(OH_2)]^+$ in the presence of 50 mM *L*-lactate was prepared using an identical method. The total emission spectrum of this sample was recorded ten times over the space of a 30 minute time period, such that the sample was under frequent irradiation. In this case, it was found that the emission spectral form did change over the 30 minute time period, with the observed changes found to be largely conserved when the sample was subsequently left at room temperature for one hour, without further irradiation (Figure 3.14). Similar results were subsequently noted in analogous experiments carried out with bicarbonate, malate and mandelate, suggesting that the mechanism of binding of these anions at the lanthanide centre in $[Ln.\mathbf{L}^{22}(OH_2)]^+$ is photo-assisted, to some extent. It should be noted that, in the absence of added anion, no change in the emission spectral form of the complex was observed, under the experimental conditions outlined above.

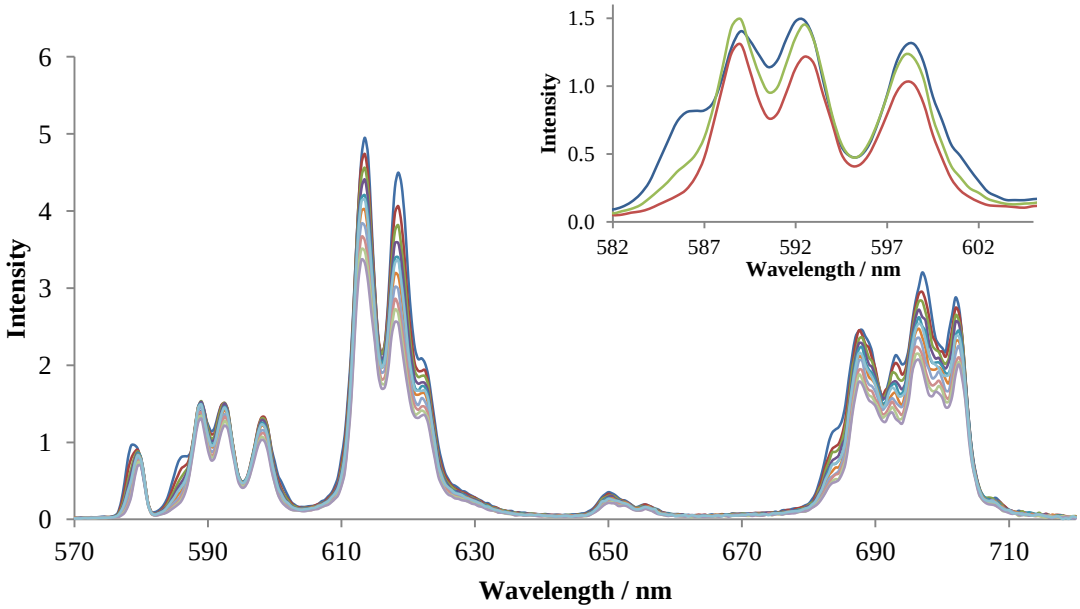

Figure 3.14: Europium emission spectral changes over the course of 30 minutes for $[Eu.\mathbf{L}^{22}(OH_2)]^+$ in the presence of 50 mM *L*-lactate when under constant irradiation. The inset shows the variation in spectral form within the $\Delta J = 1$ manifold, with the original spectrum depicted in blue and the final spectrum in red. The green spectrum was recorded 1 hour later (295 K, 0.1 M NaCl, pH 7.4, 15 µM complex).

A tentative hypothesis regarding the nature of the photo-assistance proposed above can be made, based on the assumption that the binding mechanism involves rate-limiting dissociation of the azaxanthone pyridine nitrogen, followed by fast anion binding.

Assuming this is the case, then the results outlined above suggest that the population of the triplet state of the chromophore leads to a weakening of the interaction between the lanthanide centre and the azaxanthone pyridine nitrogen, meaning anion binding is facilitated in the excited state.

A final set of CPL experiments was carried out in order to evaluate the utility of this europium complex for the chiral detection of lactate. Using an analogous method to that outlined for [Tb.$\mathbf{L}^{22}$(OH$_2$)]$^+$ a linear correlation between the emission dissymmetry factor at 620 nm and the enantiomeric purity of lactate was established for samples in which the overall lactate concentration was 50 mM. Again, it may be envisaged that such a relationship could facilitate the determination of enantiomeric purity in samples containing an unknown composition of lactate. However, it should be acknowledged that the larger values of g_{em} observed for the terbium analogue of this complex in the presence of *D*- or *L*-lactate mean that [Tb.$\mathbf{L}^{22}$(OH$_2$)]$^+$ is inherently better suited to such an application. In either case, additional experiments would first need to be undertaken to determine the reliability of such measurements, particularly in light of the apparent photo-assisted nature of the anion binding process.

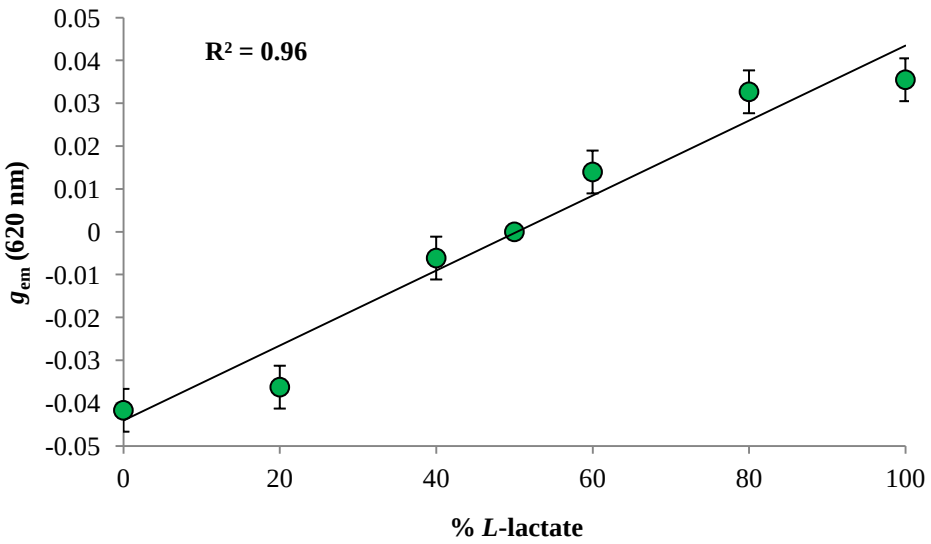

Figure 3.15: A plot demonstrating the correlation between g_{em} at 620 nm for [Eu.$\mathbf{L}^{22}$(OH$_2$)]$^+$ and the enantiomeric composition of a solution containing 50 mM lactate (295 K, 0.1 M NaCl, pH 7.4).

3.4 Conclusions and future work

The utility of the racemic europium and terbium complexes of $\mathbf{L}^{22}$ for chiral detection has been demonstrated through a series of experiments. Given their wide availability, chiral anions were identified as suitable targets in this proof of concept study.

Before undertaking any studies with chiral anions, the ability of [Ln.$\mathbf{L}^{\mathbf{22}}$(OH_2)]$^+$ to form ternary complexes with anionic species was first verified in an initial experiment, monitoring changes in the emission spectral output of [Eu.$\mathbf{L}^{\mathbf{22}}$(OH_2)]$^+$ in the presence of the achiral anion bicarbonate. Spectral changes were found to mimic those observed in the presence of protein and the hydration state of the complex was found to decrease in the presence of this anion, suggesting that anion binding is also accompanied by displacement of both the coordinated water molecule and one of the azaxanthone chromophores from the lanthanide centre.

Having confirmed the possibility of anion binding at the lanthanide centre in [Ln.$\mathbf{L}^{\mathbf{22}}$(OH_2)]$^+$, experiments were carried out monitoring the change in the emission spectral output of [Ln.$\mathbf{L}^{\mathbf{22}}$(OH_2)]$^+$ (Ln = Eu^{3+}, Tb^{3+}) in the presence of seven different chiral anions, three phosphorus(v) oxy-anions and four α-hydroxy acids. In the case of the phosphorus(v) oxy-anions, only minor changes in spectral form were observed for the emission spectral output of [Eu.$\mathbf{L}^{\mathbf{22}}$(OH_2)]$^+$ over the concentration range examined and binding affinities were found to be weak ($\log K \leq 1.0$ (±0.1)). The modest nature of the binding interaction observed with these anions was attributed to their preference for a monodentate binding mode. More dramatic changes in the emission spectral form of [Eu.$\mathbf{L}^{\mathbf{22}}$(OH_2)]$^+$ were generally observed in the presence of each of the chelating α-hydroxy acids, with a large increase in the relative intensity of the $\Delta J = 2$ band being observed in all cases. Emission spectral changes for [Tb.$\mathbf{L}^{\mathbf{22}}$(OH_2)]$^+$ were also monitored in the presence of these anions; although quenching of the signal intensity was consistently seen, no real change in spectral form was found to occur in any case.

On the basis of the results obtained in the total luminescence studies outlined above, lactate, mandelate and malate were selected for study in a series of CPL experiments aimed at demonstrating the utility of [Ln.$\mathbf{L}^{\mathbf{22}}$(OH_2)]$^+$ for chiral detection. Initially, an attempt was made to record an induced CPL spectrum for [Tb.$\mathbf{L}^{\mathbf{22}}$(OH_2)]$^+$ in the presence of each of these anions. Whilst well-defined CPL spectra were observed in the presence of *L*-lactate and *L*-mandelate, the induction of CPL was not found to be apparent with *L*-malate. It was suggested that the mode of binding at the lanthanide centre may differ for this anion, with coordination predominantly occurring through the carboxylate moieties rather than by the formation of a 5 membered chelate, involving the hydroxy group and the α-carboxylate oxygen. Therefore, for malate it was proposed that the chiral centre was placed further away from the lanthanide ion in the ternary

complex, thus leading to a lack of induced CPL. Evidence was gathered in support of this hypothesis through a series of control experiments examining the changes in total luminescence spectral form for $[Eu.\mathbf{L}^{\mathbf{22}}(OH_2)]^+$ in the presence of a number of achiral anions.

Owing to the fact that the CPL signal observed in the presence of lactate was associated with larger emission dissymmetry factors than that seen with mandelate, it was decided that the former anion was more suited to further study. A preliminary titration was undertaken in which changes in the total emission of $[Eu.\mathbf{L}^{\mathbf{22}}(OH_2)]^+$ were monitored in the presence of *D*-lactate, in order to verify that species was able to bind to the lanthanide centre in an identical manner to its enantiomer. This was indeed found to be the case. A final CPL study was then performed with $[Tb.\mathbf{L}^{\mathbf{22}}(OH_2)]^+$ in order to establish a correlation between the enantiomeric composition of an aqueous solution containing a known overall concentration of lactate and the emission dissymmetry factor at 541.5 nm. A linear relationship was observed between these variables, clearly demonstrating the utility of $[Tb.\mathbf{L}^{\mathbf{22}}(OH_2)]^+$ for analysis of enantiomeric purity and assignment of absolute configuration.

Similar CPL experiments carried out with $[Eu.\mathbf{L}^{\mathbf{22}}(OH_2)]^+$ also led to promising results, although emission dissymmetry factors were found to be lower in the case of this complex, meaning that the signal to noise was lower than for the terbium analogue. An unexpected insight into the mechanism of binding at the lanthanide centre was gained through undertaking these experiments. It was observed that, for a sample of the complex with a given concentration of lactate, the binding event appeared to be photo-assisted, with changes in spectral form being observed over the course of the CPL data acquisition. On the basis of these results, it was proposed that anion binding must occur via a mechanism involving rate-limiting dissociation of the azaxanthone pyridine nitrogen, which in turn must occur more readily in the excited state.

The work detailed in this chapter has clearly demonstrated the potential offered by racemic lanthanide complexes based on macrocyclic ligands for chiral detection. However, it should be highlighted that the photo-assisted nature of the binding mechanism observed for $[Ln.\mathbf{L}^{\mathbf{22}}(OH_2)]^+$ in the presence of anions perhaps does not lend itself to the development of this particular system as a reliable tool for such analyses. It may be envisaged that alternative racemic lanthanide systems could be developed based on heptadentate ligands derived from DOTA, where anion binding would simply

involve displacement of coordinated water molecules from the lanthanide centre. There are several examples of enantiopure lanthanide systems of this type in the literature, where anion binding has been demonstrated through monitoring changes in the total emission spectral output.[166] In addition, racemic lanthanide complexes of ligands derived from alternative macrocylic frameworks could be examined. For example, recent work carried out at Durham has demonstrated the potential offered by europium complexes derived from ligands based on a 1,4,7-triazacyclononane framework for anion sensing.[172] In this work it was shown that the complex, [Eu.$\mathbf{L}^{\mathbf{28}}$$(OH_2)]^+$ is able to bind lactate at the europium centre, with coordination occurring through the carboxylate moiety rather than via the formation of 5 membered chelates. A series of CPL experiments using this complex were carried out in parallel to the studies detailed in this chapter by Brian McMahon and Robert Pal. Results showed that the observation of induced CPL was possible in the presence of lactate, with emission dissymmetry factors an order of magnitude lower than those observed for [Tb.$\mathbf{L}^{\mathbf{22}}$$(OH_2)]^+$.[173] This is presumably a reflection of the differing coordination mode at the lanthanide centre, with the observation of the CPL signal made possible due to the exceptional quantum yield of the complex (in contrast to results obtained for [Tb.$\mathbf{L}^{\mathbf{22}}$$(OH_2)]^+$ in the presence of malate). For this complex, a linear correlation was also established between the average emission dissymmetry factor at 621.5 nm and the enantiomeric purity of lactate.

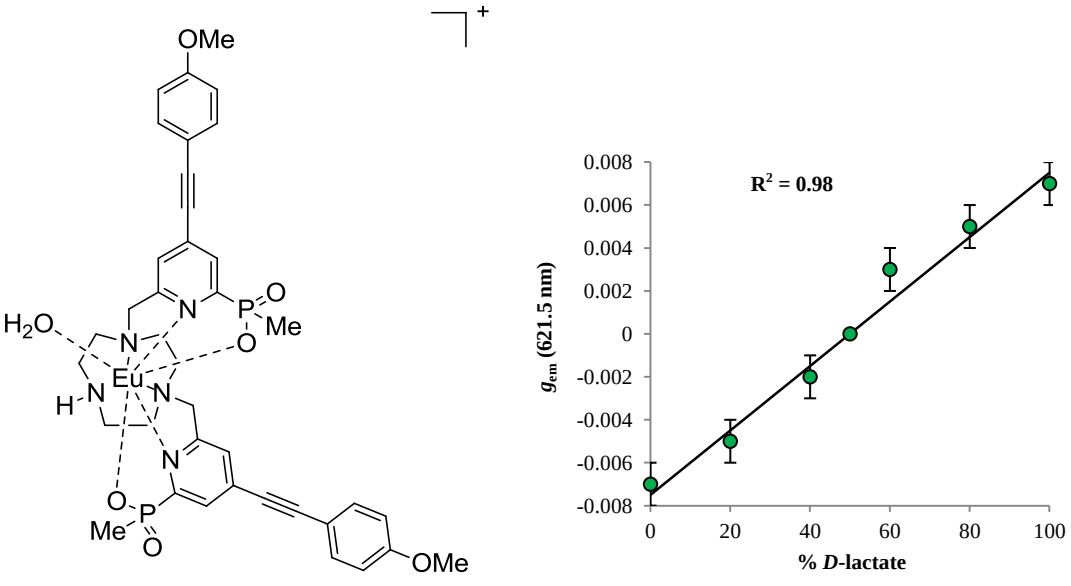

Figure 3.16: The structure of [Eu.$\mathbf{L}^{\mathbf{28}}$$(OH_2)]^+$ is shown alongside a plot displaying the variation of g_{em} at 621.5 nm with enantiomeric composition of *D*-lactate.[173]

CHAPTER FOUR

INVESTIGATIONS INTO ENANTIOSELECTIVE EXCITED STATE QUENCHING

4.1 Introduction

The work outlined in Chapter 3 demonstrated the utility of constitutionally mobile racemic lanthanide complexes in chiral detection. The inspiration for this study came from a consideration of the results obtained in previous investigations of induced CPL effects from racemic lanthanide complexes. Prior to undertaking the work detailed in Chapter 2 and 3 of this thesis, two mechanisms had been identified by which the presence of a chiral additive could lead to the induction of circular polarization in the emission output of a racemic lanthanide complex (see Section 1.5.2 of Chapter 1). One of these mechanisms is enantioselective excited state quenching.

Enantioselective excited state quenching is a phenomenon which can lead to the generation of an enantiomeric excess over time in the excited state of a racemic lanthanide complex. Provided that the rate of racemisation is slower than the rate of radiative decay, such an effect will yield the induction of circular polarization in the emission output of the complex. As outlined in Chapter 1, the observation of induced CPL from $[Ln(DPA)_3]^{3-}$ systems as a result of such chiral discrimination in the excited state has been demonstrated with a wide variety of chiral additives.[111, 112, 114, 122, 124, 125] However, this phenomenon has yet to be exemplified for lanthanide complexes of other structural motifs. This chapter details work carried out in an attempt to demonstrate enantioselective quenching of luminescence for a number of lanthanide complexes derived from macrocyclic ligands.

4.2 Experimental methodology

As mentioned in Section 1.5.2.2 of Chapter 1, the vast majority of enantioselective quenching effects reported to date have been identified and characterised by the measurement of time-resolved CPL spectral data. However, owing to lack of access to suitable instrumentation, it was necessary to employ alternative methods of investigation and analysis for the preliminary studies outlined in this chapter. Key to the choice of methods used was the hypothesis that enantioselective quenching phenomena may be exhibited in situations other than those involving chiral but racemic lanthanide complexes in the presence of small amounts of enantiomerically resolved chiral additives. Specifically, it was envisaged that examination of the quenching of an enantiopure lanthanide complex by enantiomerically pure samples of a given chiral species may reveal the occurrence of preferential quenching, through the use of Stern-

Volmer analysis. It should be noted that, although uncommon, the investigation of enantioselective quenching phenomena through the use of Stern-Volmer analysis is not entirely without precedent; the utility of such analysis in the identification and characterisation of enantioselective quenching phenomena was highlighted in a 2002 publication.[174]

4.2.1 Stern-Volmer analysis

Broadly speaking, quenching mechanisms can be classified into two categories.[175] Static quenching involves formation of a non-fluorescent complex between the quencher and the ground state emissive species. Meanwhile, dynamic (or collisional) quenching is effected through a diffusive encounter with the quenching species during the excited state lifetime of the emissive species. Quenching mechanisms belonging to the latter of these categories can be described by the Stern-Volmer equation, which relates the ratio of the emission intensity in the absence and presence of quencher, $\frac{F_0}{F}$, to the rate constant for the bimolecular quenching process, k_q, and the excited state lifetime in the absence of quencher, τ_0, as well as the concentration of quencher present in solution, $[Q]$.

$$\frac{F_0}{F} = 1 + k_q\tau_0[Q] = 1 + K_{SV}[Q] \qquad \text{(eqn. 14)}$$

Data gathered through steady-state luminescence measurements of dynamic quenching processes is frequently used in the calculation of Stern-Volmer quenching constants, ${K_{SV}}^{-1}$, which signify the concentration of quencher required to reduced the emission intensity to 50% of its original value. As is apparent from equation 14, for a dynamic quenching process occurring via a single mechanism, a plot of $\frac{F_0}{F}$ or $\frac{\tau_0}{\tau}$ will give a straight line with gradient K_{SV}.

As outlined in Section 1.3.4 of Chapter 1, quenching of the lanthanide-based emission from a sensitised lanthanide complex can occur via a number of different mechanisms, each of which is dynamic in nature. In light of this fact, it was anticipated that the characterisation of any chiral discriminatory effect occurring in the quenching of the luminescence from an enantiopure lanthanide complex by enantiomerically pure samples of a given chiral species would be possible by the calculation and comparison of Stern-Volmer quenching constants. It was hypothesised that for a given lanthanide complex these constants would differ in magnitude for each donor-acceptor pair, if an

enantioselective quenching effect was present. If successful, such an analysis would therefore facilitate the identification of quenchers suitable for use in subsequent CPL studies with structurally related racemic lanthanide complexes.

4.3 Examining quenching of lanthanide emission for a cyclen-based system

An enantiopure complex suitable for use in initial studies aimed at demonstrating chiral discrimination in the quenching of luminescence from lanthanide complexes based on macrocyclic frameworks was selected following an initial consideration of the various mechanisms by which the quenching of lanthanide-based emission from a sensitised complex is known to occur. To date, enantioselective quenching studies with $[Ln(DPA)_3]^{3-}$ complexes have typically been carried out with systems where quenching is assumed to occur via a short range electronic energy transfer process. On the basis of this, it was thought that it may prove worthwhile to explore systems in which quenching is known to occur via other mechanisms involving short range interactions.

As discussed in Section 1.3.4.2 of Chapter 1, one mechanism by which charge-transfer quenching of emission from sensitised lanthanide complexes incorporating electron-poor chromophores may occur involves the formation of an exciplex between the triplet excited state of the chromophore and the quenching molecule.[45, 46] It was hypothesised that if a system could be identified in which quenching occurs via this mechanism, where the structure of the lanthanide complex was such that the approach of the quenching molecule could only occur selectively to one face of the chromophore, then the prospects of chiral discrimination in any observed quenching effect would be enhanced. On the basis of this hypothesis, the cyclen-based terbium complex (*SSS*)-Δ-[Tb.$\mathbf{L}^{\mathbf{20b}}$]$^{3+}$ was selected for use in the preliminary experiments detailed in this section. The unusual serum albumin binding properties of this complex and its europium analogue (see Section 1.5.3.2, Chapter 1) had previously prompted a variety of NMR studies to be carried out using its yttrium analogue, (*SSS*)-Δ-[Y.$\mathbf{L}^{\mathbf{20b}}$]$^{3+}$.[134] Proton NMR spectra obtained for this complex in the absence of protein revealed that one face of the tetra-azatriphenylene moiety is blocked by a phenyl ring of the proximate (*S*)-α-methylbenzylamide group. This was confirmed by an extended DFT structural calculation carried out by Dr. I. Kuprov (University of Southampton), which generated a structure showing intramolecular π-overlap between the sensitising chromophore and a phenyl ring (Figure 4.1).[136]

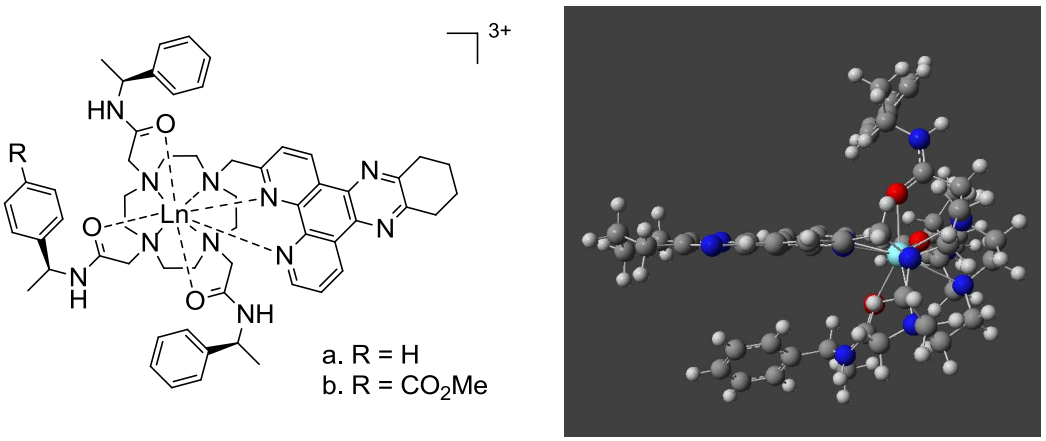

Figure 4.1: DFT calculated structure of (*SSS*)-Δ-[Y.**L**$^{\mathbf{20b}}$]$^{3+}$, the lower face of the sensitising moiety can be seen to be blocked by a proximate phenyl ring.[136]

4.3.1 Selecting the chiral quenchers

Two electron-rich aromatic reductants of differing conformational rigidity were selected for use in a series of initial experiments aimed at assessing the occurrence of chiral discriminatory phenomena in the quenching of the luminescence output of (*SSS*)-Δ-[Tb.**L**$^{\mathbf{20b}}$]$^{3+}$. The catechol derivative, DOPA, was one of the quenching species employed in the original mechanistic studies which led to the deduction that exciplex formation is implicated in deactivation of lanthanide luminescence, in certain instances of charge-transfer quenching.[45] Meanwhile, Trolox, a vitamin E analogue, is a well-known reductant which is known to quench triplet excited states by electron transfer.[176] It was hypothesised that quenching of the emission intensity from (*SSS*)-Δ-[Tb.**L**$^{\mathbf{20b}}$]$^{3+}$ in the presence of Trolox would also occur via a mechanism involving exciplex formation. It should be noted that the reduction potential of this latter species is known to be 0.48 V and is therefore comparable to that of catechol, which is 0.53 V.[177, 178]

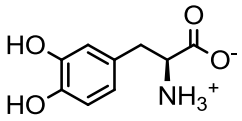

L-DOPA

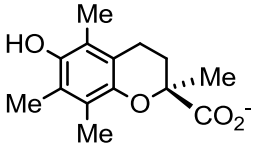

(*S*)-Trolox

Support for the hypothesis that quenching of the emission intensity from (*SSS*)-Δ-[Tb.**L**$^{\mathbf{20b}}$]$^{3+}$ in the presence of Trolox would occur via a mechanism involving exciplex formation was gained through an investigation carried out to assess the dependence of the quenching effect on solvent composition. Separate titrations were carried out in buffer solution and methanol and the modulation of the luminescence emission intensity from (*SSS*)-Δ-[Tb.**L**$^{\mathbf{20b}}$]$^{3+}$ was monitored as a function of (*S*)-Trolox concentration. As

can be seen from Figure 4.2, although a quenching effect was apparent in both methanol and buffer solution, a considerable solvent effect was observed.

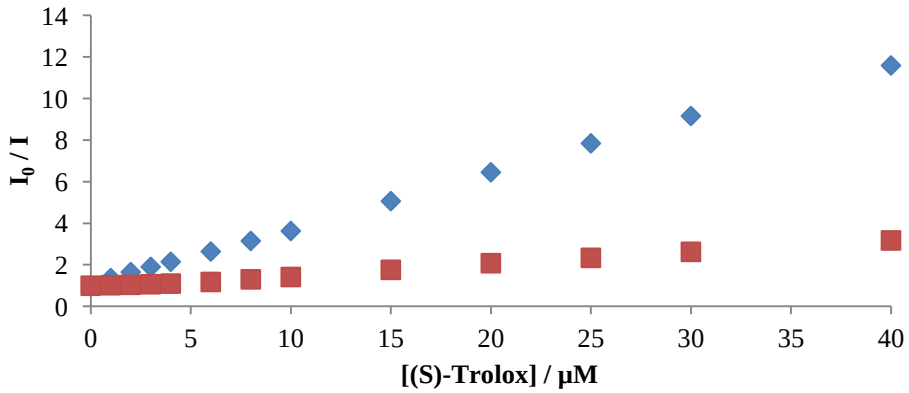

Figure 4.2: Comparison of the variation in emission intensity from (*SSS*)-Δ-[Tb.$\mathbf{L}^{\mathbf{20b}}$]$^{3+}$ as a function of [(*S*)-Trolox] in both MeOH (red squares; 295 K, 20 µM complex) and buffer solution (blue diamonds; 295 K, pH 7.4, 0.1 M HEPES, 0.1 M NaCl, 20 µM complex).

The observation that quenching was much less efficient in methanol than in the buffer solution supports the theory that quenching is occurring by a mechanism involving exciplex formation. Such behaviour suggests that a hydrophobic effect plays a role in the quenching process i.e. exclusion of high energy water from the surface of the π-moieties upon exciplex formation, which returns to the bulk where hydrogen bonding is facilitated.

4.3.2 Investigations into enantioselective quenching

To assess the occurrence of chiral discrimination in the quenching of the emission of (*SSS*)-Δ-[Tb.$\mathbf{L}^{\mathbf{20b}}$]$^{3+}$ in the presence of DOPA and Trolox, titrations were carried out in which the modulation of the luminescence emission intensity and lifetime of the complex was monitored as a function of quencher concentration, Q. Incremental additions of each enantiomer of both quenchers were made to 2 mL samples of (*SSS*)-Δ-[Tb.$\mathbf{L}^{\mathbf{20b}}$]$^{3+}$ which had been dissolved in 0.1 M HEPES containing 0.1 M NaCl at pH 7.4, to give solutions where the concentration of complex was 20 µM. The variation in I_0/I as a function of [Q] is shown in Figure 4.3; plots of τ_0/τ versus [Q] were similar in form in every case.

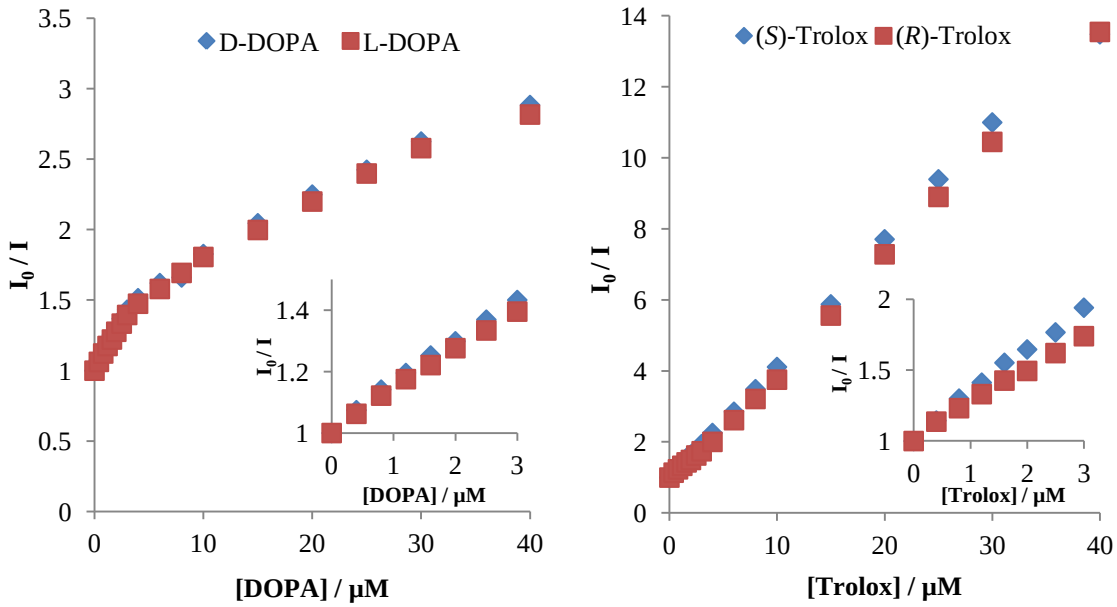

Figure 4.3: Comparison of the variation in emission intensity as a function of [DOPA] (left) and [Trolox] (right) for (*SSS*)-Δ-[Tb.**L**$^{\mathbf{20b}}$]$^{3+}$ (295 K, pH 7.4, 0.1 M HEPES, 0.1 M NaCl, 20 µM complex).

As is apparent from the Stern-Volmer plots presented in Figure 4.3, the emission intensity was found to decrease upon addition of each of the quenchers to solution samples of (*SSS*)-Δ-[Tb.**L**$^{\mathbf{20b}}$]$^{3+}$. Whilst an approximately linear plot of I_0/I *versus* [Q] was generated by analysis of titration data in the case of Trolox, the same could not be said for DOPA. The nature of the curvature observed in the plot of I_0/I *versus* [Q] for this latter species was reminiscent of observations outlined in previous publications detailing charge transfer quenching by electron rich species involving exciplex formation.[45]

The data gathered from both the lifetime and intensity measurements performed over the course of the titrations were used in the calculation of Stern-Volmer quenching constants (Table 4.1). In the case of Trolox, these values were calculated on the basis of analysis of data gathered over the full concentration range of each titration, 0 - 40 µM. Meanwhile, for DOPA, only the eight initial data points were used, which spanned the concentration range 0 - 3 µM. For a given quencher, agreement between the Stern-Volmer constants calculated on the basis of intensity and lifetime data was good, suggesting that it is reasonable to attribute the reduction of emission intensity and lifetime from (*SSS*)-Δ-[Tb.**L**$^{\mathbf{20b}}$]$^{3+}$ to the occurrence of a single dynamic mechanism.

Table 4.1: Stern-Volmer quenching constants for the dynamic quenching of emission from (*SSS*)-Δ-[Tb.$\mathbf{L}^{\mathbf{20b}}$]$^{3+}$ (295 K, pH 7.4, 0.1 M HEPES, 0.1 M NaCl, 20 μM complex).

Complex	Quencher	K_{SV}^{-1} / μM	
		Intensity data	Lifetime data
(*SSS*)-Δ-[Tb.$\mathbf{L}^{\mathbf{20b}}$]$^{3+}$	*L*-DOPA	7.7	7.5
	D-DOPA	7.0	6.7
	(*S*)-Trolox	3.1	3.8
	(*R*)-Trolox	3.1	3.6

As is clear from the Stern-Volmer quenching constants shown in Table 4.1, charge-transfer quenching was found to occur more efficiently in the presence of Trolox than in the presence of DOPA, notwithstanding their similar reducing power. This may in part be a reflection of the differing overall charge of the two quencher species when in buffer solution at pH 7.4. For Trolox, the overall charge is negative owing to the presence of the ionised carboxylate group, meaning that an attractive electrostatic interaction will exist with the positively charged terbium complex. Meanwhile, DOPA is zwitterionic and therefore no such electrostatic interaction is present.

Unfortunately, the results presented in Table 4.1 did not provide strong evidence to suggest any involvement of chiral discrimination in the charge transfer quenching processes for either Trolox or DOPA, with results obtained with enantiomeric species giving almost identical Stern-Volmer quenching constants in each case. This result was not entirely unexpected in the case of DOPA, where it was anticipated that the conformational flexibility of the quencher may negate the possibility of an enantiodifferential effect. Meanwhile, in light of these disappointing results, a series of computational studies examining the interaction between (*SSS*)-Δ-[Tb.$\mathbf{L}^{\mathbf{20a}}$]$^{3+}$ and the two Trolox enantiomers was conducted by Dr. I. Kuprov (University of Southampton). Initially, representative minimum energy structures for the diastereomeric exciplex species were generated using DFT (Figure 4.4). Examination of these structures revealed some difference in the orientation of the Trolox enantiomers relative to the tetraazatriphenylene moiety of the lanthanide complex, with a greater amount of aromatic overlap apparent in the case of (*S*)-Trolox. However, the energy difference between the diastereomeric exciplexes was found to be small (6 kJ mol^{-1}), suggesting that little enantioselectivity is likely to be apparent in the quenching interactions of these species. It should be noted that, although these initial calculations were carried out in the gas phase, subsequent calculations using implicit solvent also revealed little

energy difference. Such data therefore agrees with the experimental observations outlined above.

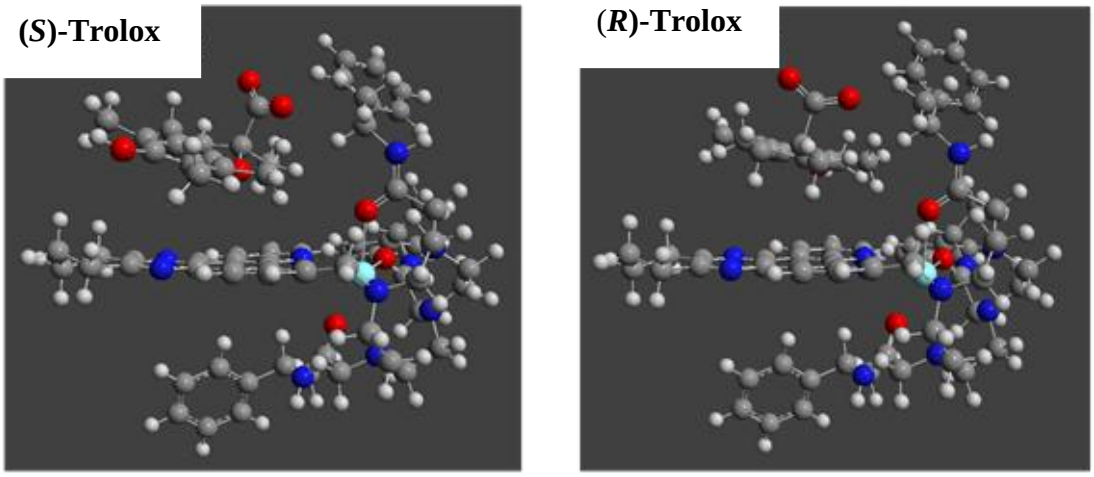

Figure 4.4: Minimum energy structures for the interaction of (*SSS*)-Δ-[Tb.$\mathbf{L}^{\mathbf{20a}}$]$^{3+}$ with (*S*)-Trolox (left) and (*R*)-Trolox (right) calculated using DFT structural calculations.

In spite of these results, it was hypothesised that a difference between the quenching effect of the two enantiomers may yet be seen for Trolox, if the electrostatic interaction between the lanthanide complex and the quencher species could be removed. This electrostatic interaction is non-directional so will not favour the formation of one diastereomeric exciplex over another. In order to generate a system in which this electrostatic interaction would not be significant, the methyl ester analogues of Trolox were synthesised, using a straightforward acid-catalysed esterification reaction. Subsequent titrations were carried out using these ester species under the conditions previously outlined. However, it was found that it was necessary to use a trace of methanol (< 1 % by volume) in order to ensure that the quenching species were fully dissolved. Figure 4.5 shows the variation in I_0/I as a function of quencher concentration for the (*R*)- and (*S*)- enantiomers of Trolox methyl ester, derived using data gathered in initial titrations.

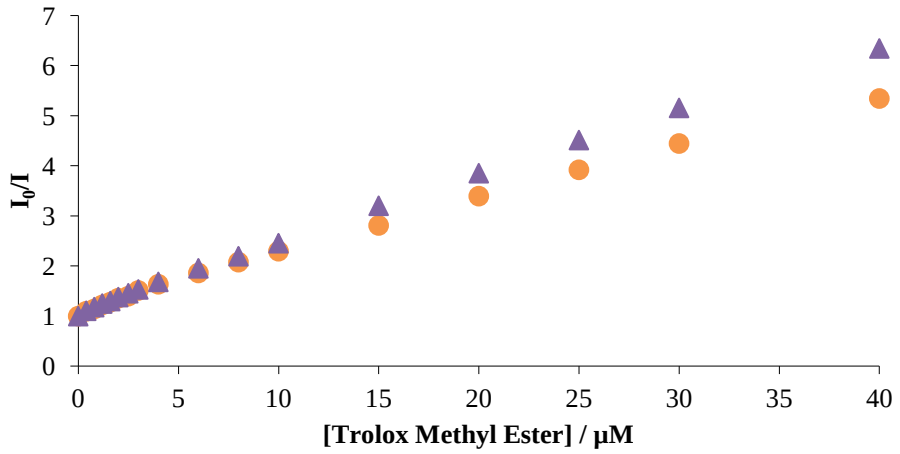

Figure 4.5: Stern-Volmer plots derived from titrations measuring the modulation of the emission intensity of (*SSS*)-Δ-[Tb.$\mathbf{L}^{\mathbf{20b}}$]$^{3+}$ in the presence of (*R*)- (purple triangles) and (*S*)- (orange circles) Trolox (295 K, pH 7.4, 0.1 M HEPES, 0.1 M NaCl, trace MeOH, 20 µM complex).

As can be seen from Figure 4.5, an approximately linear plot of I_0/I *versus* [Q] was generated by analysis of the initial titration data, with the extent of quenching seemingly less than had been observed with the parent acids. Stern-Volmer quenching constants were calculated by analysis of the data obtained over the full concentration range of each titration. In the case of the (*R*) enantiomer, a value of 7.5 µM was obtained by this analysis. Meanwhile, for the (*S*) enantiomer a slightly higher value of 9.2 µM was determined, indicating that quenching was slightly less efficient for (*S*)-Trolox methyl ester than its enantiomer. It should be noted that subsequent attempts to reproduce these results were not entirely successful. Although a difference in quenching efficiency of this sense was consistently observed for the two enantiomers, the same could not be said regarding the magnitude of the enantioselectivity. As was discussed in Section 1.5.2.2 of Chapter 1, the dependence of enantioselective quenching phenomena on sample conditions is a well-researched topic, with several studies having been carried out to assess the effect of variables such as ionic strength and solvent on the degree of enantioselectivity observed for a given system. In light of this and of the fact that the quenching interaction with Trolox had been found to shown significant solvent dependence (see Figure 4.2), a set of titrations was carried out in which the quenching of (*SSS*)-Δ-[Tb.$\mathbf{L}^{\mathbf{20b}}$]$^{3+}$ by (*R*)-Trolox methyl ester was monitored for solutions containing various trace amounts of methanol. However, no clear correlation was found to exist between the percentage of methanol present and the resulting Stern-Volmer quenching constants, suggesting that fluctuations in other sample conditions such as temperature may also play a role in the exact results obtained.

Despite the lack of reproducible results obtained in the experiments described above, a series of CPL studies was carried out to determine if the methyl ester derivative of Trolox could perturb the excited state racemic equilibrium of the neutral complex [Tb.**L**^{29}]. This racemic complex was selected due to its structural similarity with [Ln.**L**^{20}]$^{3+}$, in terms of the common presence of the tetra-azatriphenylene chromophore structure. CPL spectra were obtained for the complex in the presence of each enantiomer of the quenching species. Unfortunately, no evidence was found for the generation of circularly polarized emission in either system.

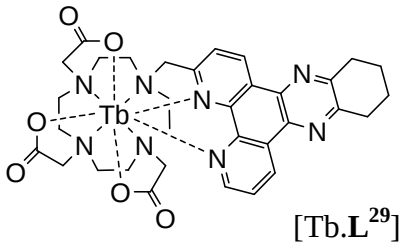

[Tb.**L**^{29}]

4.4 Examining quenching of lanthanide emission for complexes based on 1,4,7-triazacyclononane

Notwithstanding the apparent lack of promise shown by the results outlined in the previous section, it was decided that efforts should be made to study the possibility of enantioselective quenching phenomena using lanthanide complexes derived from ligands based on a structurally related macrocyclic framework, 1,4,7-triazacyclononane. Scheme 4.1 shows representative structures of a selection of ligands derived from this framework, each of which incorporates sensitising chromophores and has been utilised in the synthesis of racemic emissive 9-coordinate lanthanide complexes with *pseudo* C_3 symmetry. In complexes of **L**^{2}, **L**^{30} and **L**^{31}, the lanthanide centre is coordinated by the three nitrogen atoms of the 1,4,7-triazacyclononane core, along with the three pyridyl nitrogen donors and three carboxylate or phosphinate oxygen donors.[32, 179-181] In contrast, for complexes of **L**^{32}, the coordination requirements of the metal centre are satisfied solely by the tridentate chelating units incorporated into the pendant arms of the ligand structure.[182]

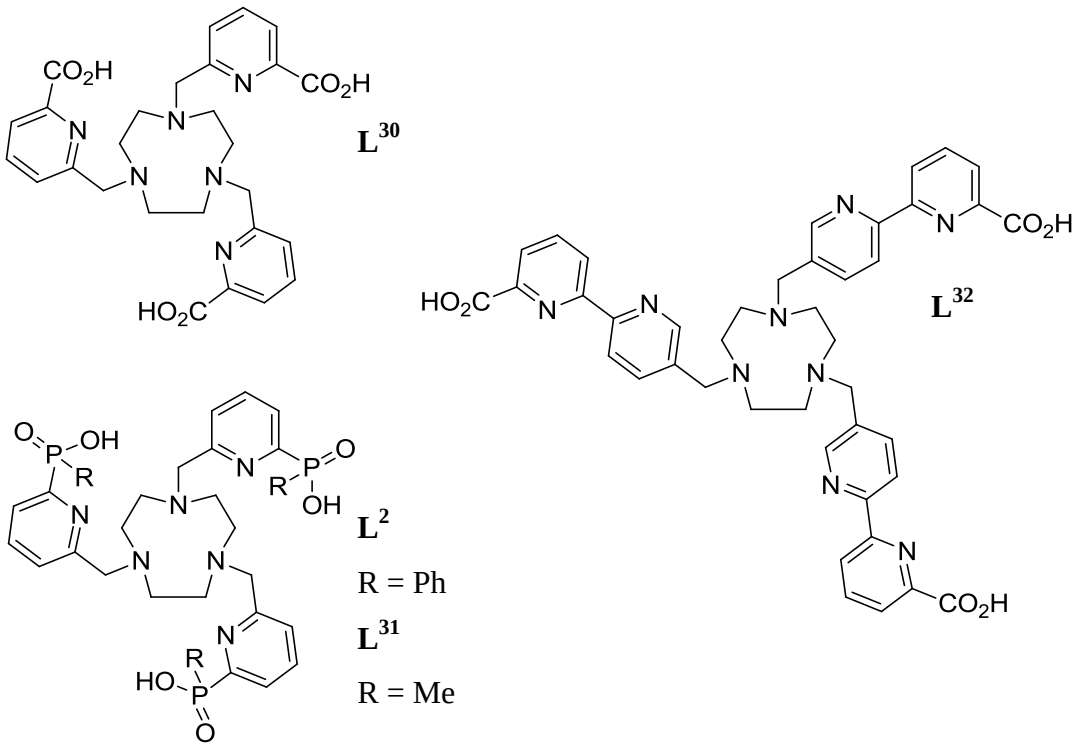

Scheme 4.1: Representative structures of nonadentate ligands based on a 1,4,7-triazacyclononane core.

As for complexes derived from DOTA (see Section 1.4.2, Chapter 1), the chirality of lanthanide systems derived from **L**^{30} can be described in terms of two torsion angles, the N-C-C-N angle of the macrocyclic ring, which can be +60^{o} or -60^{o} (δ and λ respectively), and the N-C-C-N_{py} angle of the pendant arms. If this latter angle is positive a Δ helicity results, if it is negative then a Λ helicity is defined. The existence of four stereoisomeric species, related as two pairs of enantiomers, is therefore predicted (Figure 4.6). However, to date structural studies of lanthanide complexes of **L**^{30} in both the solid state and solution have consistently revealed the existence of a single enantiomeric pair of complexes as a racemic mixture, which have been determined to have $\Delta(\lambda\lambda\lambda)$ and $\Lambda(\delta\delta\delta)$ helicity.[179] Meanwhile, variable temperature ^{1}H NMR spectroscopy experiments conducted using [Ln.**L**^{30}] (Ln = Eu^{3+}, Tb^{3+}, Gd^{3+}) have shown no evidence for the occurrence of dynamic processes, such as ring inversion and concerted arm rotation, suggesting high energy barriers for these processes.

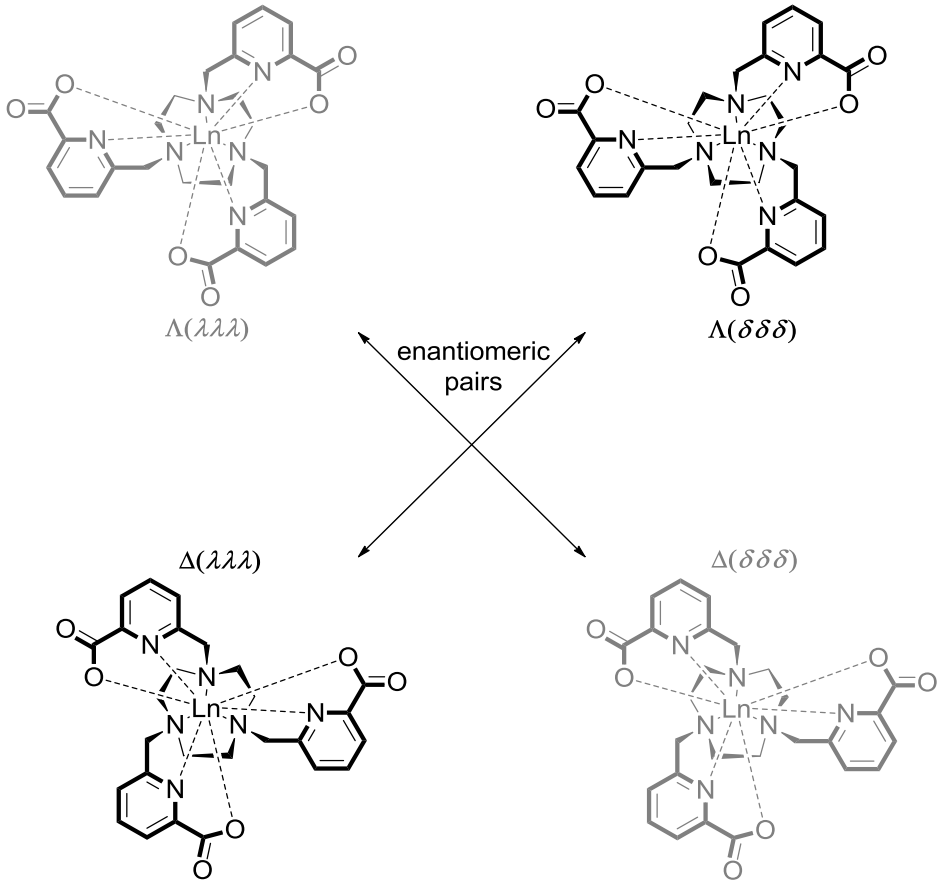

Figure 4.6: Schematic representative of the four stereoisomers of [Ln.**L**^{30}].

The chirality of lanthanide systems derived from **L**^{2} and **L**^{31} can be described in a similar manner to that outlined above. However, there is an extra element of chirality to consider for complexes of these ligands, owing to the fact that upon complexation a stereogenic centre is formed at phosphorus. In theory, cooperative binding of the three phosphinate moieties incorporated in the pendant arms of these ligands to a lanthanide centre could give rise to a mixture of diastereomeric species, where the configuration at phosphorus is (*SSS*)/(*RRR*) or (*SRS*)/(*RSR*). However, in the case of [Ln.**L**^{2}] and [Ln.**L**^{31}] the observation of a single phosphorus resonance in the ^{31}P NMR spectra of both systems suggested that the formation of complexes with an (*RSR*)/(*SRS*) configuration at phosphorus does not occur.[32, 181] In the case of [Ln.**L**^{2}], this hypothesis was supported by solid state crystallographic analysis. Indeed, structural analysis of [Ln.**L**^{2}] and [Ln.**L**^{31}] complexes using the analytical techniques already mentioned, along with others such as ^{1}H NMR spectroscopy, revealed the presence of a single enantiomeric pair of complexes as a racemic mixture, with (*RRR*)-Λ(*δδδ*) and (*SSS*)-Δ(*λλλ*) configuration. As for [Ln.**L**^{30}], no evidence for the occurrence of dynamic processes, such as ring inversion and concerted arm rotation, was obtained via variable

temperature ^{1}H NMR spectroscopy. Separation of the enantiomeric (*RRR*)-Λ(*δδδ*) and (*SSS*)-Δ(*λλλ*) species was achieved for [Ln.**L**^{2}] (Ln = Eu^{3+}, Tb^{3+}) using chiral HPLC. CPL spectra were subsequently recorded for the resolved complexes and were found to demonstrate high emission dissymmetry factors (see Figure 1.8, Chapter 1).

4.4.1 Synthesis and characterisation of a series of enantiopure lanthanide complexes based on 1,4,7-triazacyclononane

Before the methodology outlined in Section 4.2 of this chapter could be utilised for the study of enantioselective quenching phenomena for lanthanide complexes derived from ligands based on 1,4,7-triazacyclononane, it was first necessary to devise a means by which direct access to single enantiomeric species could be achieved. As discussed and exemplified in Section 1.4 of Chapter 1, the synthesis of enantiopure lanthanide complexes is typically achieved by the inclusion of asymmetric centres in the ligand. For ligands derived from macrocylic frameworks, asymmetry may be incorporated either directly onto the macrocycle or, alternatively, into the pendant arms. Although there are many examples of enantiopure lanthanide complexes synthesised using chiral DOTA-based ligands in accordance with this methodology, the same cannot be said for lanthanide complexes formed using ligands derived from the 1,4,7-triazacyclononane framework. The use of ligands derived from this framework is however much more widespread in transition metal coordination chemistry. Results of a recent study examining the synthesis and characterisation of a hexadentate copper complex, using the commercially available chiral ligand **L**^{33}, provided evidence to suggest that it is possible to achieve the control of configuration for complexes derived from 1,4,7-triazacyclononane by the use of similar methodology.[183]

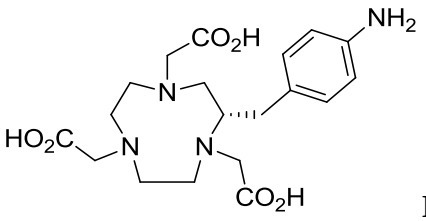

L^{33}

In light of the results outlined above, it was hypothesised that adaptation of the ligand framework for **L**^{2} or **L**^{31} to include a single C-substitution in the macrocylic framework may lead to the preferential formation of one enantiomerically pure complex stereoisomer in solution. Owing to the fact that the pyridyl methylphosphinate ligand

L[31] had been found to form complexes offering better water solubility, the complexes (*R*)- and (*S*)-[Ln.**L**[34]] (Ln = Eu^{3+}, Tb^{3+}) were chosen as the synthetic targets.

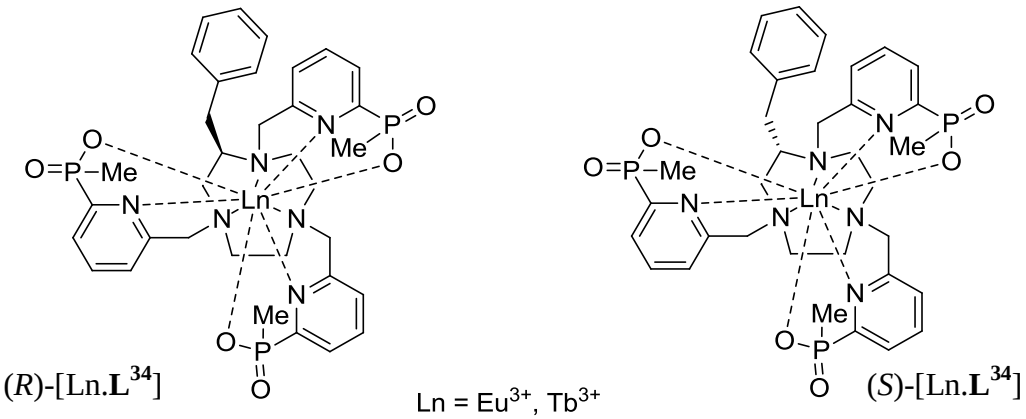

4.4.1.1 Synthetic aspects

Previously described methods were employed in the synthesis of the substituted complexes.[181, 184, 185] The synthetic pathway for the preparation of the enantiomeric substituted macrocycles is shown in Scheme 4.2.

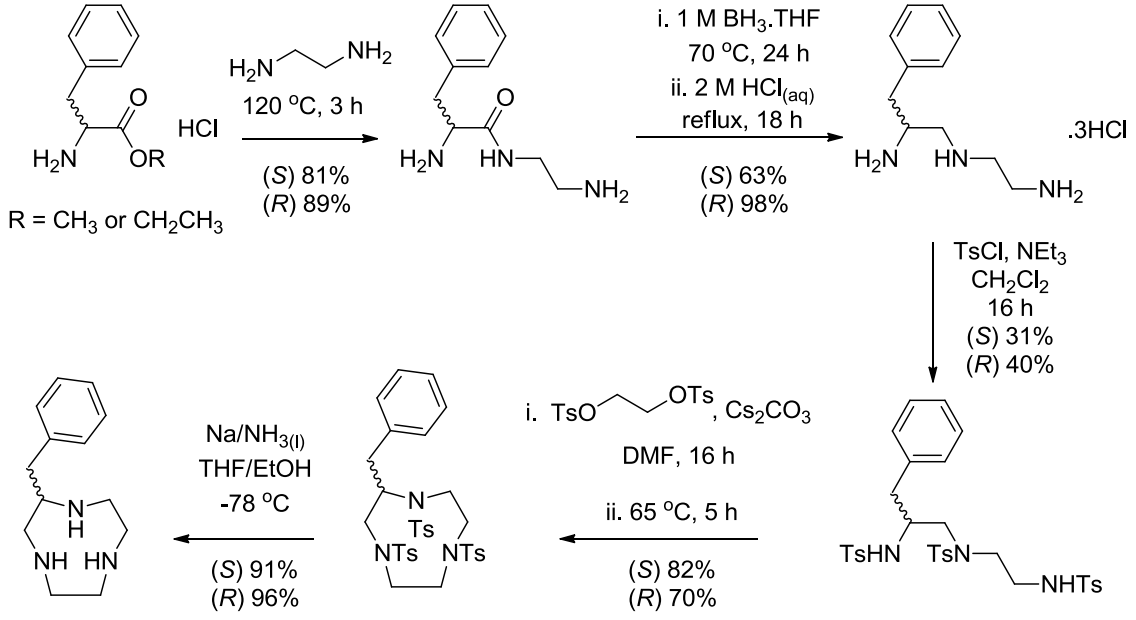

Scheme 4.2: Synthetic pathway for the preparation of chiral 2-benzyl-1,4,7-triazacyclononane derivatives.

With the exception of the tosylation reaction in step 3, where the occurrence of significant over-alkylation was found to limit the amount of desired product formed, yields greater than 70% were typically achieved in every stage of the synthesis. As expected, the yield of product in a given step was generally found to be similar,

regardless of which enantiomeric starting material was used. The detosylation of the ring nitrogens in the final stage of the synthesis was effected through the use of liquid ammonia and sodium, as opposed to lithium. Analysis of the product using ^{1}H NMR spectroscopy typically revealed the presence of trace amounts of contaminating material, with the presence of alkene CH resonances at 5.5 and 5.7 ppm suggesting that, although largely avoided, partial reduction of the aromatic ring in the benzyl substituent had occurred to a small extent. Following characterisation, the product was used immediately for N-alkylation without further purification (see Scheme 4.5).

The pyridyl methylphosphinate chromophore was prepared in parallel to the enantiomeric substituted macrocycles, in accordance with the synthetic pathway shown in Scheme 4.3.

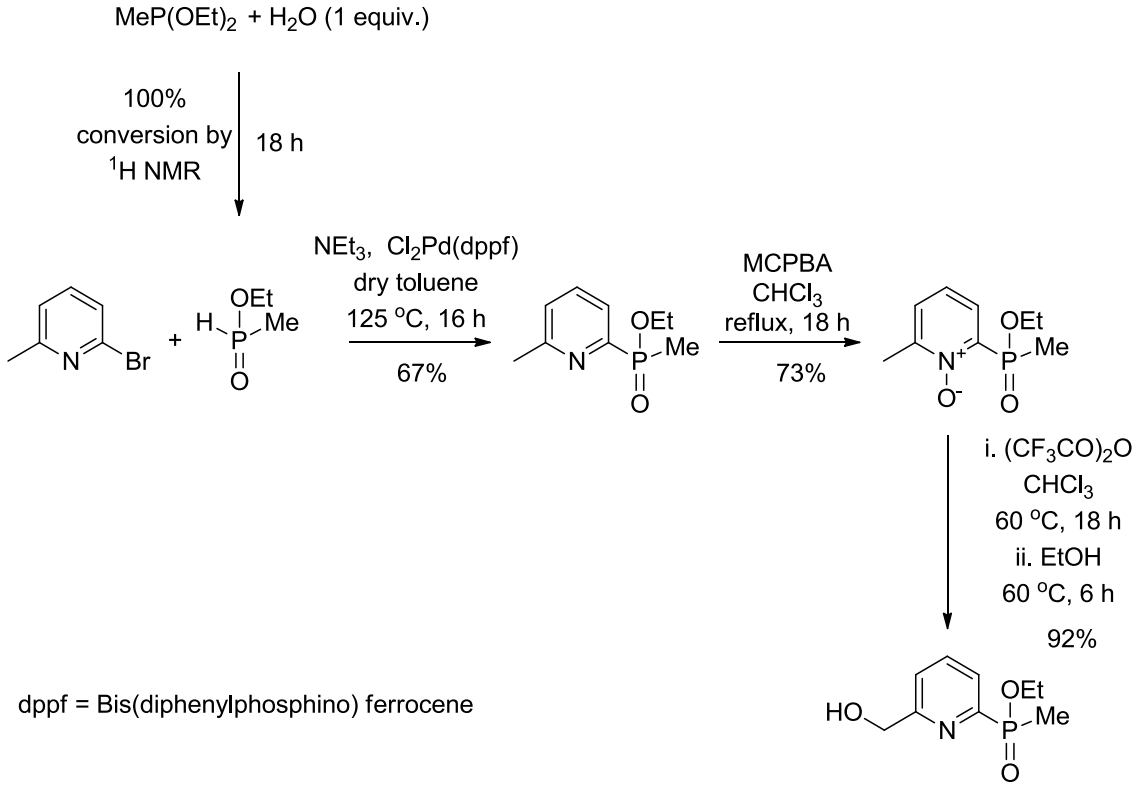

Scheme 4.3: Chromophore synthesis.

As can be seen from Scheme 4.3, reactions were again found to be high yielding. The catalyst [1,1'-bis(diphenylphosphino)ferrocene]dichloropalladium(II) was employed in the coupling reaction between 2-bromo-6-methylpyridine and ethyl methylphosphonite, which was found to afford a similar yield to that previously achieved in an analogous reaction using tetrakis(triphenylphosphine)palladium(0).[181] Formation of the pyridyl N-oxide was effected using MCPBA. Subsequent purification by column chromatography

on silica gel facilitated the removal of the benzoic acid side product. Conversion of this species to the final product shown in Scheme 4.3 was achieved in two stages. First, treatment with trifluoroacetic anhydride yielded a labile ester via a Boekelheide rearrangement, which was characterised by the presence of a singlet at ~ 5.5 ppm in its ^{1}H NMR spectrum, corresponding to the methylene group protons. Subsequent hydrolysis in aqueous ethanol gave the final product, with ^{1}H NMR spectroscopy revealing a shift in the methylene group protons to ~ 4.8 ppm (Figure 4.7).

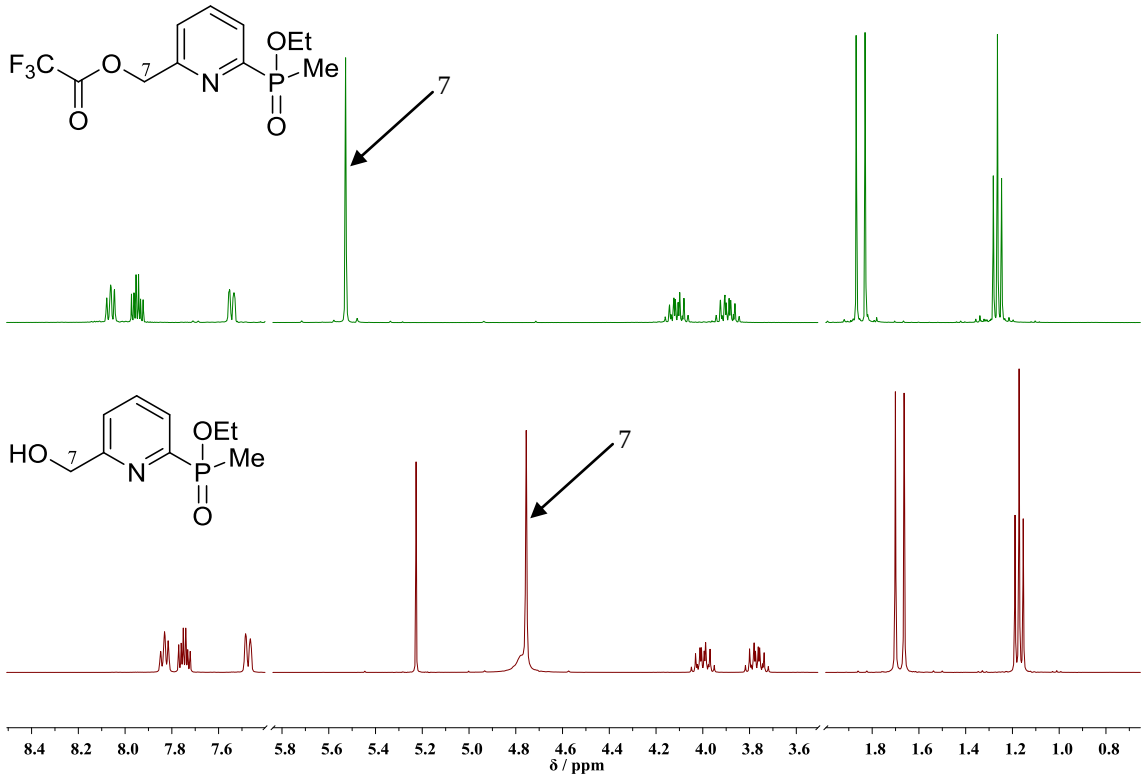

Figure 4.7: Comparison of ^{1}H NMR spectra for ethyl[6-hydroxymethyl]pyridine-2-yl](methyl)phosphinate and its ester precursor ($CDCl_3$, 295 K, 400 MHz).

In order to achieve ligand synthesis by alkylation of the previously described 1,4,7-triazacyclononane derivatives, it was necessary to first convert the pyridyl methylphosphinate alcohol species to its mesylate ester. Mesylation was carried out using methanesulfonyl chloride and triethylamine in THF at 5 ^{o}C (Scheme 4.4). This reaction was carried out multiple times, owing to the fact that it was necessary to prepare fresh samples of the mesylate for each alkylation reaction that was carried out. Each time, the reaction was monitored by TLC and typically found to be completed within 10 minutes.

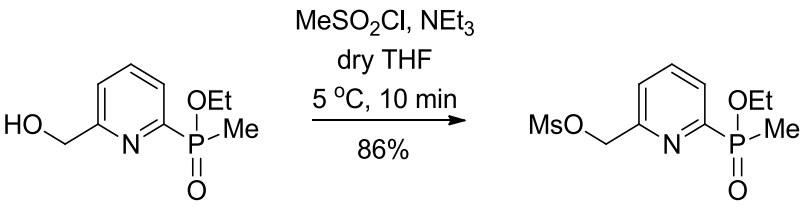

Scheme 4.4: Mesylation of ethyl[6-(hydroxymethyl)pyridine-2-yl](methyl)phosphinate.

Characterisation of the mesylate species was carried out using mass spectrometry and NMR spectroscopy. In most cases, some formation of an additional product was noted alongside the desired compound, which was identified as the chloromethyl species by analysis of the gathered spectroscopic data. The product was used for ligand synthesis without further purification, with alkylation of the previously described 1,4,7-triazacyclononane derivatives being carried out under standard conditions (K_2CO_3, CH_3CN) as shown in Scheme 4.5. Reactions were halted when complete consumption of the mesylated and chlorinated starting materials was apparent by TLC. The addition of a catalytic amount of potassium iodide was found to facilitate reaction of the latter species.

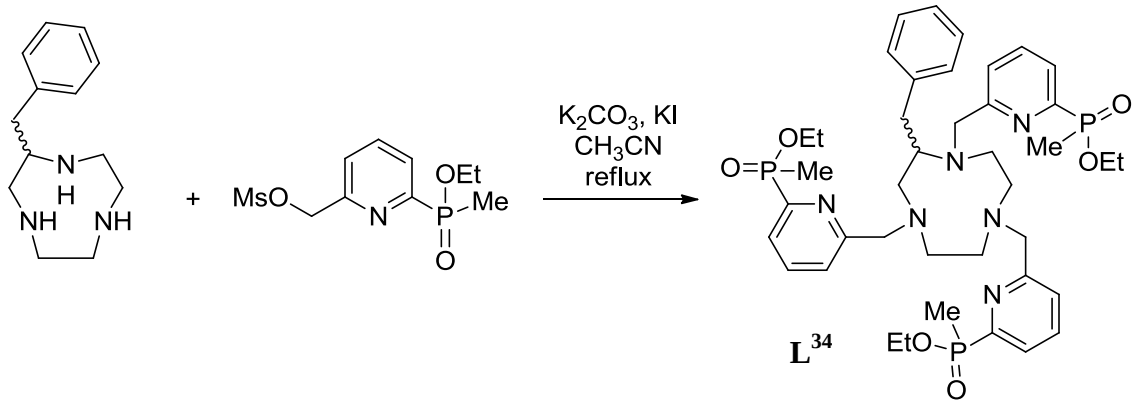

Scheme 4.5: Synthesis of $\mathbf{L}^{34}$.

As anticipated, the alkylation reaction depicted in Scheme 4.5 resulted in a mixture of products when either the (*R*) or (*S*) enantiomer of the macrocyclic starting material was used. Separation of these products was possible by column chromatography, facilitating the isolation of the desired triethyl ester protected ligands, (*R*)- and (*S*)-$\mathbf{L}^{34}$. Samples of the di-substituted ligand analogue, $\mathbf{L}^{35}$, were also isolated for both enantiomers. ^{1}H NMR spectra obtained for the enantiomers of this latter species were consistent with the presence of a single regioisomer in solution, presumably that in which the ring nitrogen located in closest proximity to the C-substitution is not alkylated. Unfortunately, the amount of material available was not sufficient to carry out detailed NMR studies needed in order to verify this hypothesis.

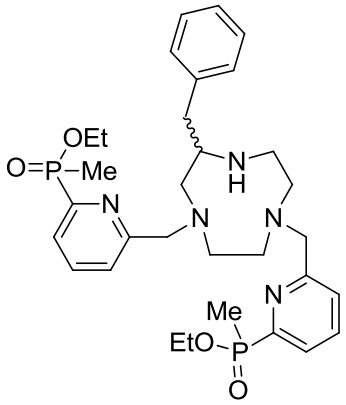

L[35]

The formation of lanthanide complexes using (*R*)- and (*S*)-**L**[34] was achieved in two further steps, shown in Scheme 4.6. Hydrolysis of the ethyl esters was confirmed by ESMS or ^{31}P NMR spectroscopy before proceeding to the second stage of the reaction scheme. Metal complexation was confirmed prior to isolation of each of the complexes by removing a sample of the reaction mixture and obtaining its emission spectrum in water. In each case, the characteristic emission spectra expected for europium and terbium were visible, following excitation of the phosphinate chromophore at 268 nm. Once the complexes had been isolated, purification was carried out by short-path column chromatography on silica. The purity of each complex was verified using HRMS and reverse phase HPLC.

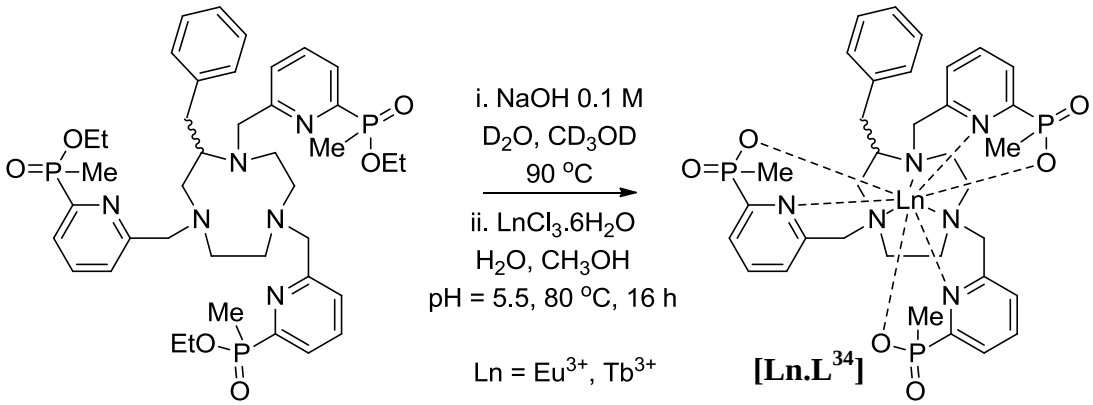

Scheme 4.6: Preparation of [Ln.**L**[34]].

It should be noted that the preparation of terbium complexes of the heptadentate ligands (*R*)- and (*S*)-**L**[35] was also achieved using similar methods to those shown in Scheme 4.6. However, owing to the charged nature of these di-substituted complexes, it was not possible to carry out purification via short-path column chromatography on silica. Analytical HPLC traces obtained for crude samples of both (*R*)- and (*S*)-[Tb.**L**[35]]$^{+}$ appeared to show the presence of two major species, with similar retention times.

Further analysis of both samples using LCMS revealed that for each complex the two major species present were of the same mass, which corresponded to the expected mass of [Tb.$\mathbf{L}^{35}$]$^{+}$. The removal of trace impurities from these complexes was subsequently achieved using preparative HPLC, though the method used did not allow isolation of separate samples of the isomeric species. Unfortunately, the amount of complex isolated was not sufficient to facilitate a structural analysis of the complexes formed.

4.4.1.2 Photophysical characterisation of (*R*)- and (*S*)-[Ln.$\mathbf{L}^{34}$]

Insight into the lanthanide ion environment in the purified europium and terbium complexes of the tri-substituted ligands (*R*)- and (*S*)-$\mathbf{L}^{34}$ was gained using a number of photophysical techniques. Characterisation was carried out with reference to results previously reported for the europium and terbium complexes of the achiral parent ligand $\mathbf{L}^{31}$.

The hydration state of the newly synthesised complexes was determined using the methodology outlined in Section 2.3.1 of Chapter 2. Experimentally determined radiative rate constants for the deactivation of the lanthanide excited state were found to be independent of the configuration at the substituted carbon centre in the macrocylic ring. Rates were determined in both H_2O and D_2O, therefore allowing the derivation of the hydration state, q', of each complex. Table 4.2 shows the experimentally determined data along with comparable data taken from the literature for [Ln.$\mathbf{L}^{31}$] (Ln = Eu^{3+}, Tb^{3+}).[181]

Table 4.2: Experimentally determined radiative rate constants and derived values of q' (± 20%) for europium and terbium complexes of (*R*)- and (*S*)-$\mathbf{L}^{34}$ as well as literature data for the europium and terbium complexes of $\mathbf{L}^{31}$ (295 K, pH 5.5).[181]

Complex	k_{H_2O} / ms^{-1}	k_{D_2O} / ms^{-1}	q'
[Eu.$\mathbf{L}^{31}$]	0.64	0.63	0.0
(*R*)- or (*S*)-[Eu.$\mathbf{L}^{34}$]	0.75	0.63	0.0
[Tb.$\mathbf{L}^{31}$]	0.39	0.34	0.0
(*R*)- or (*S*)-[Tb.$\mathbf{L}^{34}$]	0.38	0.37	0.0

As can be seen from Table 4.2, the values obtained in the investigations outlined above were extremely similar to those previously recorded for the europium and terbium complexes of $\mathbf{L}^{31}$, indicating that the lanthanide ions are in similar environments in complexes of these ligands. Comparison of the form of the emission spectral fingerprint

for the europium and terbium complexes of these ligands provided further evidence in support of this. As can be seen from Figure 4.8, not only was the form of the emission spectrum found to be identical for complexes of (*R*)- and (*S*)-**L**^{34}, but an extremely high degree of similarity was seen in comparison with spectra previously reported in the literature for lanthanide complexes formed using **L**^{31}.

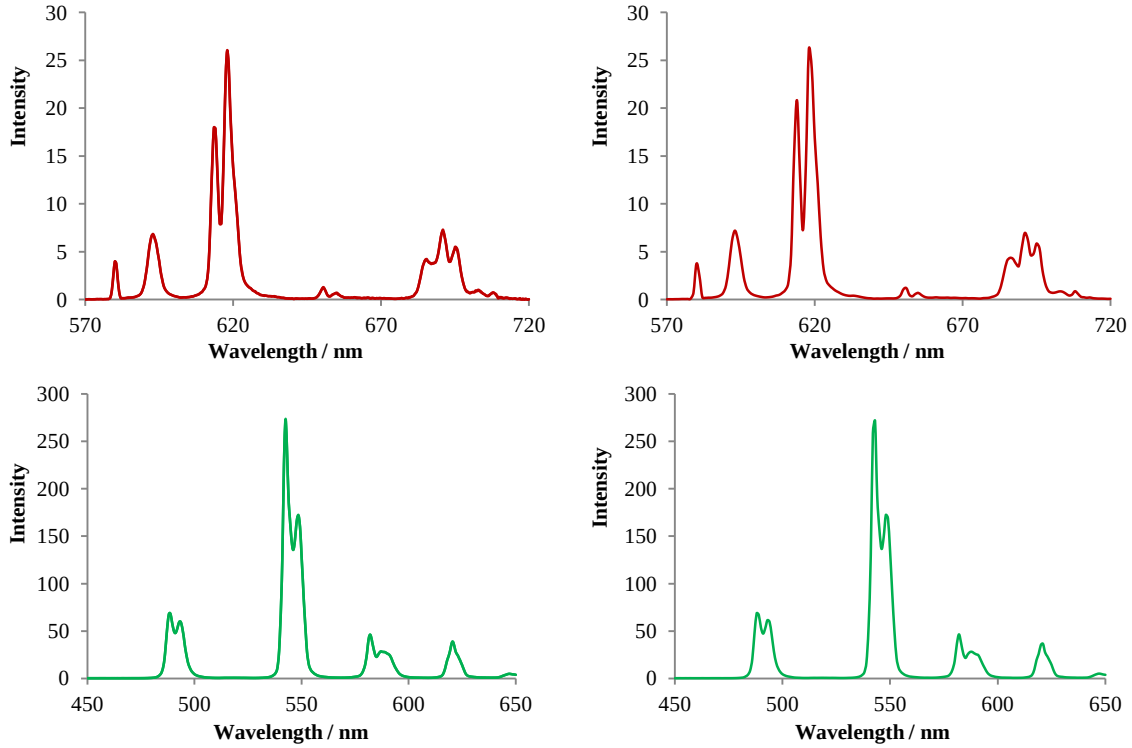

Figure 4.8: Emission spectra of the europium (top) and terbium (bottom) complexes of **L**^{34} (left) and **L**^{31} (right) in water, after excitation at 268 nm (295 K, pH 7.4, 0.1 M NaCl, 0.1 M HEPES).

4.4.1.3 Chiral analysis

As stated above, initial photophysical characterisation of the [Ln.**L**^{34}] complexes provided evidence to suggest a broad similarity between the immediate lanthanide ion coordination environment in comparison to analogous complexes of **L**^{31}. However, significant differences between the overall symmetry and chirality of the complex structures were revealed by the use of additional characterisation methods. Further analysis of the solution structure of the [Ln.**L**^{34}] complexes was carried out using NMR spectroscopic techniques. These methods not only allowed insight to be gained into the overall symmetry of the complexes, but also facilitated a more detailed examination of the nature of the relationship between the structure of complexes derived using (*R*)- and (*S*)-**L**^{34} for a given lanthanide ion.

As was mentioned in Section 4.4, ^{31}P NMR spectra obtained for the europium and terbium complexes of the achiral ligand $\mathbf{L^{31}}$ showed a single phosphorus resonance, suggesting that the arrangement of the ligand around the lanthanide ion gave rise to a structure with *pseudo* C_3 symmetry, in which the phosphorus centres adopt an (*SSS*)/(*RRR*) configuration. The disruption of this symmetry in europium and terbium complexes derived using the substituted ligand enantiomers (*R*)- and (*S*)-$\mathbf{L^{34}}$ was immediately apparent from ^{31}P NMR spectra obtained, which were each characterised by the presence of three peaks of equal intensity, consistent with the non-equivalence of the P atoms of the phosphinate moieties. The absence of rotational symmetry in the europium and terbium complexes of $\mathbf{L^{31}}$ was also apparent from their ^{1}H NMR spectra. Representative spectra are shown in Figure 4.9, which compares the ^{31}P and ^{1}H NMR spectra recorded for (*S*)-[Eu.$\mathbf{L^{34}}$] to those previously reported for [Eu.$\mathbf{L^{31}}$].

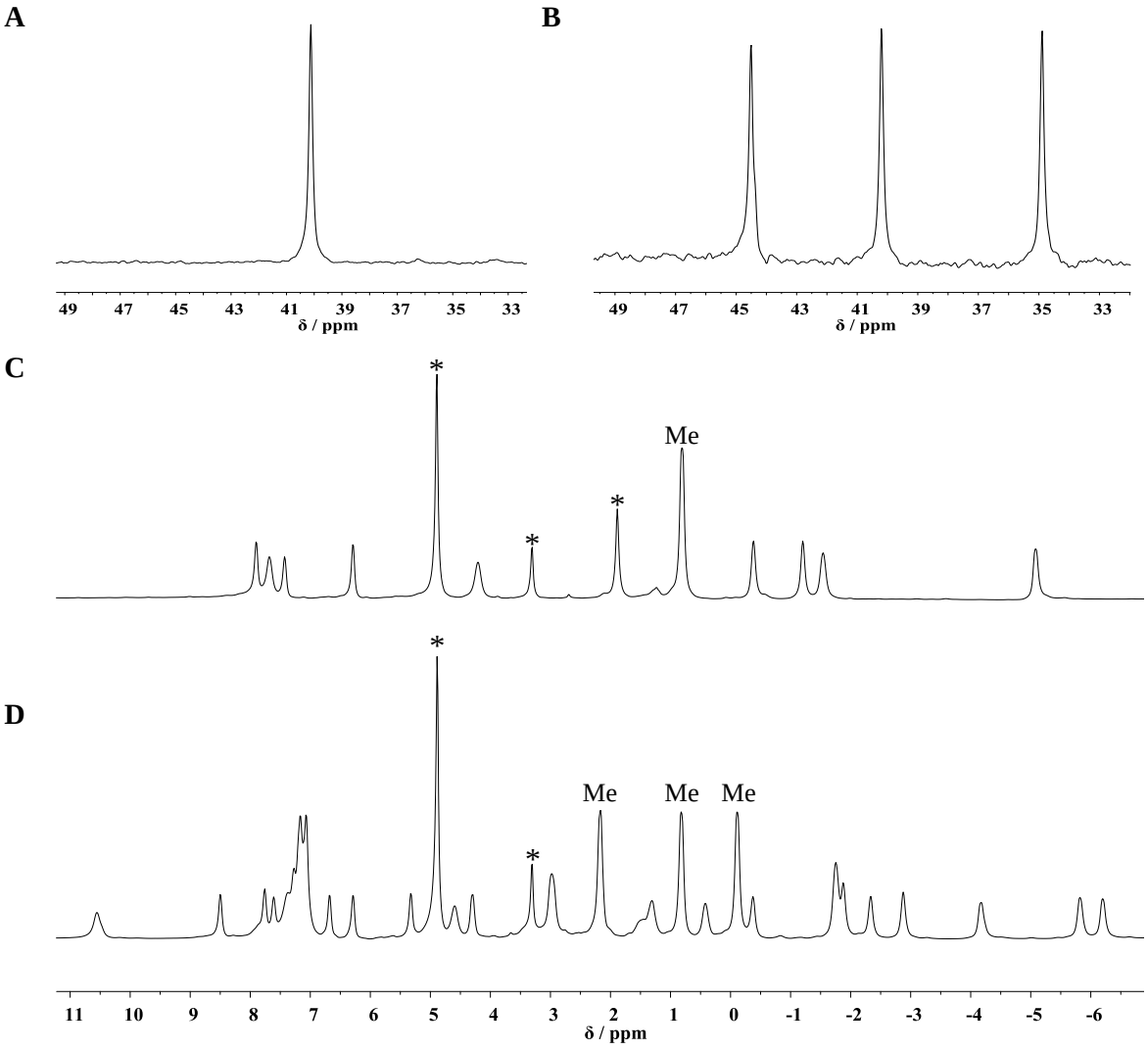

Figure 4.9: ^{31}P and ^{1}H NMR spectra obtained for (*S*)-[Eu.$\mathbf{L^{34}}$] (**B** and **D** respectively) in comparison to those previously reported for [Eu.$\mathbf{L^{31}}$] (**A** and **C**) * indicates solvent resonances (CD_3OD, 400 MHz).

As can be seen from Figure 4.9, the appearance of the ^{1}H and ^{31}P NMR spectra obtained for (*S*)-[Eu.**L**^{34}] were consistent with the presence of only one species in solution, with less than 4% of any minor species. This was also found to be the case for the terbium analogue of this complex. For a given lanthanide ion, the NMR spectra recorded for the complexes derived using (*R*)- and (*S*)-**L**^{34} were found to be almost identical in form, implying that the complexes formed using these ligands were enantiomeric in nature. Figure 4.10 shows a comparison of ^{1}H NMR spectra recorded for (*R*)- and (*S*)-[Tb.**L**^{34}] in MeOD at room temperature. The broader linewidth apparent in these spectra in comparison to the ^{1}H NMR spectra shown in Figure 4.9 is due to faster transverse relaxation rates, which arise due to the high magnetic susceptibility of the terbium ion.

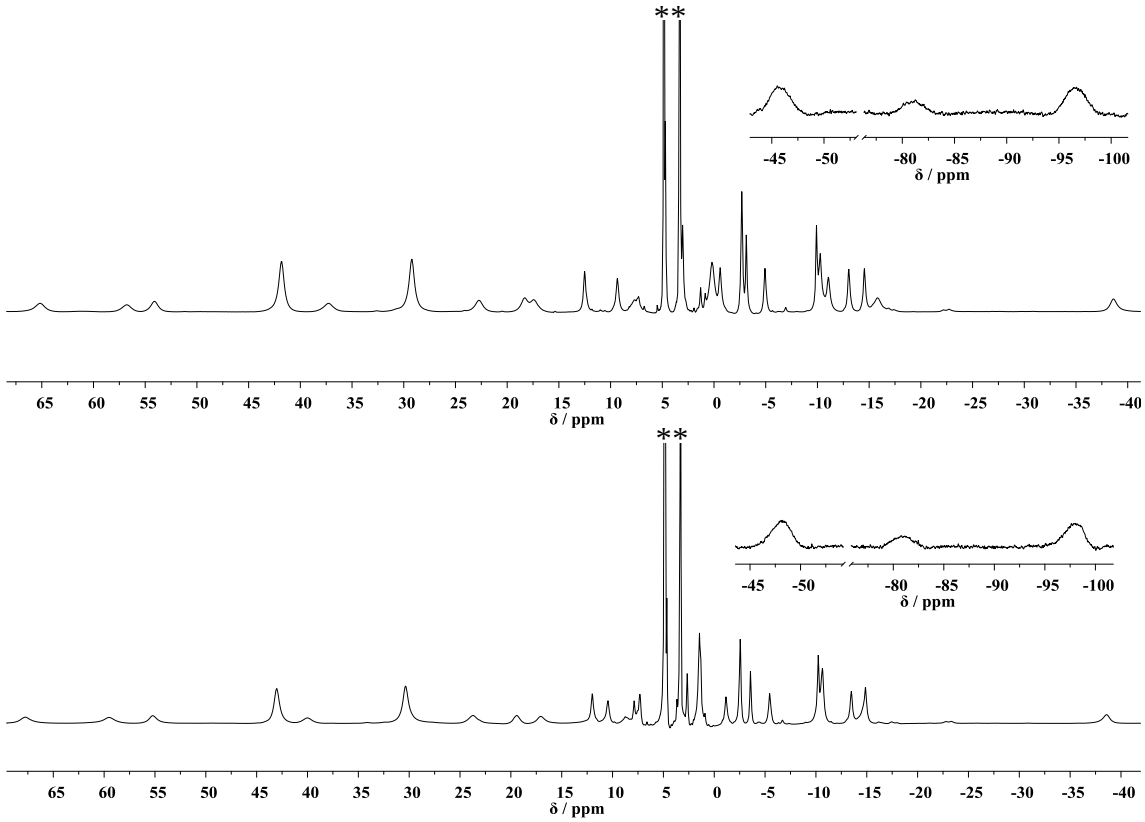

Figure 4.10: Comparison of ^{1}H NMR spectra recorded for samples of (*R*)- (top) and (*S*)- (bottom) [Tb.**L**^{34}] * indicates solvent resonances (CD_3OD, 400 MHz).

Based on the assumption that racemisation of the chiral centre in the ligand framework did not occur during the synthesis of these complexes, the results outlined above provided clear evidence to suggest that the incorporation of the ring substitution was successful in favouring the formation of a single enantiopure species in solution. In order to further substantiate this hypothesis, the enantiopurity of the complexes was probed using chiral HPLC. HPLC traces were obtained for samples of (*R*)- and (*S*)-

[Eu.**L**^{34}] using a CHIRALPAK-ID column with an isocratic elution of methanol (Figure 4.11).

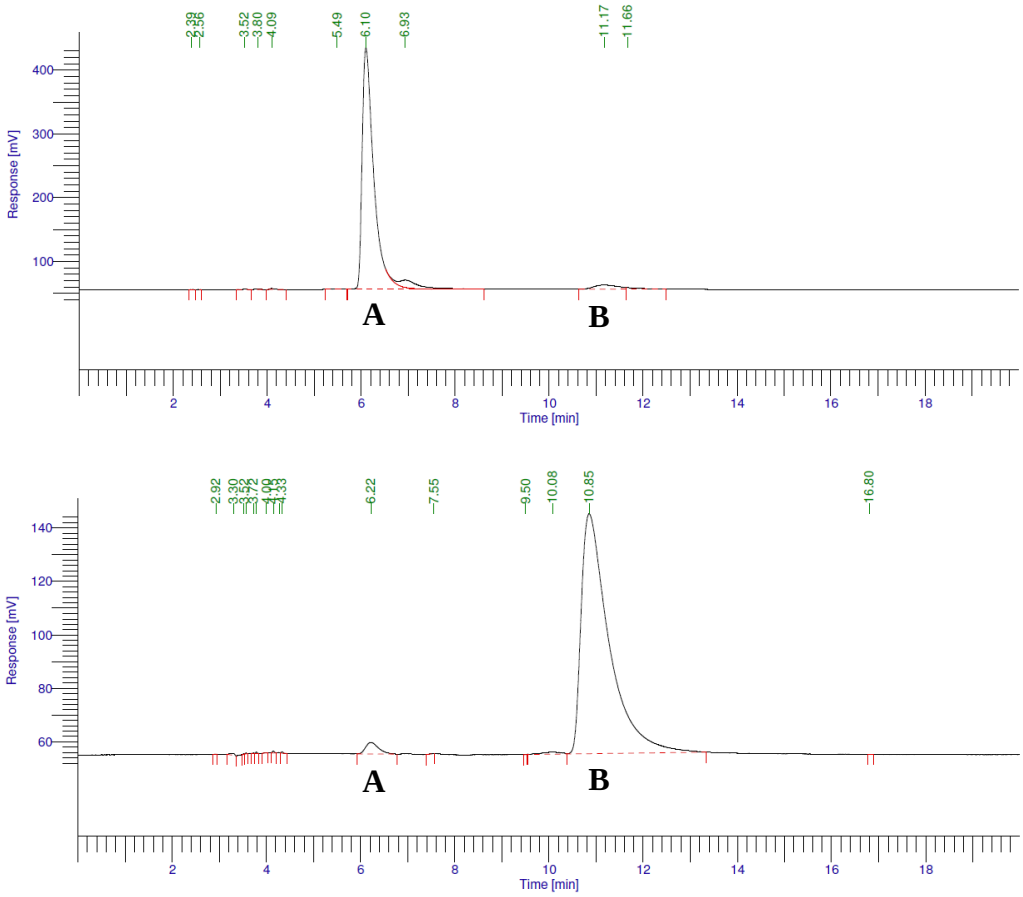

Figure 4.11: Chiral HPLC traces of (*R*)- and (*S*)-[Eu.**L**^{34}] (bottom and top respectively) run on a CHIRALPAK-ID column (MeOH, 1 mL min^{-1}, λ = 268 nm, 290 K).

As can be seen from Figure 4.11, the HPLC traces obtained using (*R*)- and (*S*)-[Eu.**L**^{34}] confirmed the presence of one major species in solution for both complexes; the amount of minor species present was found to be less than 5%. The differing retention times of the major species provided evidence to suggest opposing chirality. CPL spectra subsequently recorded in Durham for samples of (*R*)- and (*S*)-[Ln.**L**^{34}] in D_2O showed a mirror image relationship in the case of both the terbium and europium complexes, providing confirmation of the hypothesis that an enantiomeric relationship exists between the complexes (Figure 4.12).

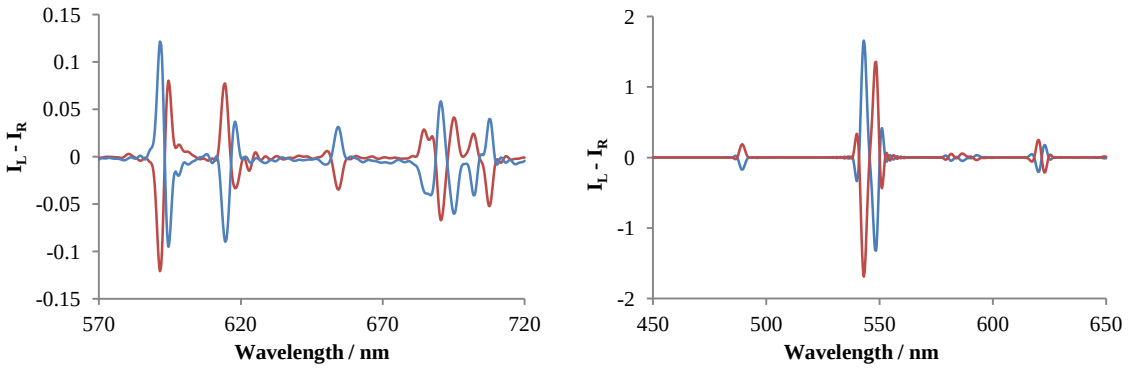

Figure 4.12: Circularly polarized emission spectra for (*R*)- (red) and (*S*)- (blue) [Ln.**L**^{34}] (Ln = Eu^{3+}, left and Tb^{3+}, right).

Emission dissymmetry factors were calculated for the enantiomeric complexes (Table 4.3). As expected from the appearance of the CPL spectra, the values of g_{em} at a chosen wavelength were found to be approximately equal and opposite for complexes of a given lanthanide ion derived from (*R*)- and (*S*)-**L**^{34}. The magnitude of the calculated g_{em} values was comparable to results previously found for enantiopure samples of the structurally related phenylphosphinate complex [Ln.**L**^{2}], which had been obtained following resolution of the complex by chiral HPLC (see Section 4.4).[32]

Table 4.3: Selected emission dissymmetry factors calculated using the data displayed in Figure 4.12.

	g_{em}					
Complex	$\Delta J = 1$		$\Delta J = 2$	$\Delta J = 3$	$\Delta J = 4$	
	(591.5 nm)	(595 nm)	(615 nm)	(654 nm)	(701.5 nm)	(708 nm)
(*S*)-[Eu.**L**^{34}]	+0.08	-0.09	-0.03	+0.19	-0.19	+0.39
(*R*)-[Eu.**L**^{34}]	-0.08	+0.09	+0.03	-0.22	+0.17	-0.38
	$\Delta J = 2$	$\Delta J = 1$		$\Delta J = 0$	$\Delta J = -1$	
	(489.5 nm)	(544 nm)	(548.5 nm)	(587 nm)	(620 nm)	(623 nm)
(*S*)-[Tb.**L**^{34}]	-0.07	+0.17	-0.19	-0.06	-0.15	+0.23
(*R*)-[Tb.**L**^{34}]	+0.07	-0.18	+0.20	+0.05	+0.17	-0.26

Comparison of the data displayed in Figure 4.12 and Table 4.3 to CPL spectral data previously reported for complexes of **L**^{2} allowed the helicity of the (*R*)- and (*S*)-[Ln.**L**^{34}] complexes to be assigned. In terms of the sign and sequence of the observed transitions, it was found that the CPL spectral signature of the europium and terbium complexes derived using (*R*)-**L**^{34} showed a distinct similarity to the CPL spectra of the (*SSS*)-Δ-($\lambda\lambda\lambda$) enantiomers of [Ln.**L**^{2}] (Ln = Eu^{3+}, Tb^{3+}). Meanwhile, a marked resemblance was also observed between the CPL spectral signature of the europium and terbium complexes derived using (*S*)-**L**^{34} and the CPL spectra of the (*RRR*)-Λ-($\delta\delta\delta$) enantiomers

of [Ln.$\mathbf{L}^{2}$] (Ln = Eu^{3+}, Tb^{3+}). Rationalisation of this observed stereoselectivity in complex formation was achieved through examination of the X-ray crystal structures obtained for the (*SSS*)-Δ-(*λλλ*) and (*RRR*)-Λ-(*δδδ*) enantiomers of another structurally related methylphosphinate complex, [Eu.$\mathbf{L}^{36}$], synthesised by Dr Nicholas Evans. The structure of this complex is shown in Figure 4.13, alongside the X-ray crystal structure of its (*SSS*)-Δ-(*λλλ*) enantiomer.[186]

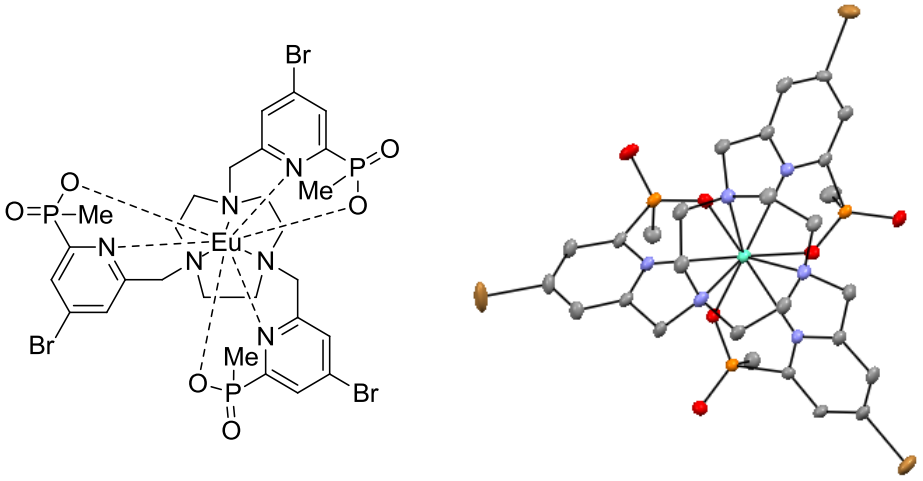

Figure 4.13: Structure of [Eu.$\mathbf{L}^{36}$] shown alongside the X-ray crystal structure of its (*SSS*)-Δ-(*λλλ*) enantiomer.[186]

A detailed consideration of the crystal structure shown in Figure 4.13 revealed that for this enantiomer substitution of either of the pseudo-equatorial ring hydrogen atoms would give an (*R*) configuration, whereas an (*S*) configuration would result from substitution of either of the pseudo-axial ring hydrogens (Figure 4.14[a]). The observation that complexes derived using (*R*)-$\mathbf{L}^{34}$ adopt an (*SSS*)-Δ-(*λλλ*) configuration in solution may therefore be attributed to the fact that the ring substituent will preferentially occupy an equatorial position. The same logic applies for rationalisation of the fact that complexes derived using (*S*)-$\mathbf{L}^{34}$ adopt an (*RRR*)-Λ-*(δδδ*) configuration.

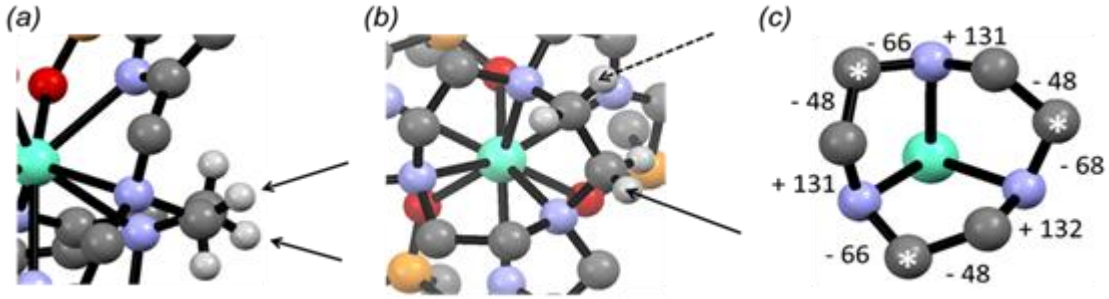

Figure 4.14: Views of the crystal structure of the (*SSS*)-Δ-(*λλλ*) enantiomer of [Eu.**L**[36]] illustrating (a) the pseudo-equatorial positions of the pro-(*R*) hydrogens on the ring, (b) the corner (filled arrow) versus side (dashed arrow) positions of the pro-(*R*) hydrogens and (c) the ring torsional angles; 'corner' carbons – those that fall between two gauche bonds – are marked with asterisks.[186]

Further examination of the crystal structure allows an additional conclusion to be drawn regarding the likelihood of substitution at each possible ring carbon location. Figure 4.14[b] serves to illustrate the pseudo-equatorial positions of the pro-(*R*) hydrogens on both corner and side carbon atoms within the 1,4,7-triazacyclononane ring, which are distinguishable on the basis of the ring torsional angles (Figure 4.14[c]).[187] As is apparent from Figure 4.14[b], substitution in an equatorial position at a side carbon atom will generate a complex in which the ring substituent is directed towards the three pyridyl arms, therefore leading to a greater steric demand than if the substituent is located in an equatorial position at a corner carbon atom, directed away from the pyridyl arms. One may therefore anticipate that for the lanthanide complexes of (*R*)- and (*S*)-**L**[34], the benzyl substituent will be located at a corner carbon position. Unfortunately, it did not prove possible to grow crystals of the [Ln.**L**[34]] complexes in order to confirm this hypothesis.

Before moving on, it is important to highlight that, although the results outlined above were consistent with the absence of racemisation during complex synthesis, chiral analysis of europium complexes derived from ligand frameworks synthesised in analogous work carried out by Dr Nicholas Evans did not yield such favourable results.[186] In the case of complexes derived using (*S*)-alanine and (*S*)-valine precursors, chiral HPLC analysis revealed the formation of complex enantiomers in a ratio between 2:1 and 9:1. Subsequent NMR spectroscopic analysis of the amide species formed in the first stage of macrocycle synthesis (Scheme 4.2) revealed that racemisation is able to occur during the reaction of the ester starting material with ethylenediamine, if the temperature is too high.

4.4.2 Synthesis and characterisation of a transition metal based chiral quencher

Having successfully achieved the synthesis of a set of enantiopure lanthanide complexes based on the 1,4,7-triazacyclononane macrocyclic framework, attention was turned to the identification of chiral quencher species suitable for use in preliminary studies of enantioselective quenching. Prior studies carried out in Durham by James Walton had revealed that a reduction in the signal intensity and lifetime of emission from the structurally related racemic complexes [Ln.**L**^{2}] and [Ln.**L**^{31}] (Ln = Eu^{3+}, Tb^{3+}) was observed in the presence of copper and manganese aqua ions, with preliminary investigations leading to the identification of energy transfer as the most likely quenching mechanism.[188] It was therefore decided that efforts should be directed towards the identification of suitable transition metal-based chiral quenchers.

As was mentioned in Section 1.5.2.2 of Chapter 1, the majority of studies of enantioselective quenching carried out to date have employed transition metal based complexes in the role of the chiral quencher. Although cobalt and ruthenium tris chelates have typically been the systems of choice in these studies, it was decided that the macrocyclic chiral cobalt complex [Co.**L**^{37}] may provide a suitable alternative. The synthesis and characterisation of a structurally related system, [Co.**L**^{38}], had previously been described in the literature and it was anticipated that the photophysical properties of [Co.**L**^{37}] would closely resemble those of this species.[189] Meanwhile, it was hoped that the introduction of a chiral substituent into the ligand framework for [Co.**L**^{37}] would lead to the formation of a single complex isomer in solution, as had been found to occur for the structurally related hexadentate copper complex, discussed in Section 4.4.1.

[Co.**L**^{37}]

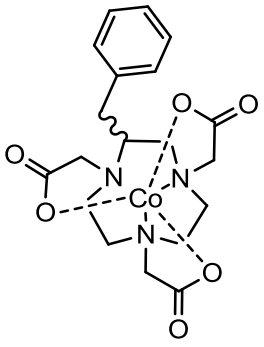

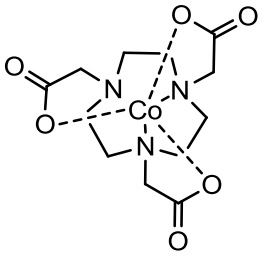

[Co.**L**^{38}]

4.4.2.1 Synthetic aspects

The synthesis of (*R*)-**L**^{37} was achieved by alkylation of a sample of (*R*)-2-benzyl-1,4,7-triazacyclononane, which had been prepared in accordance with Scheme 4.2, using *tert*-

butyl bromoacetate under standard conditions (K_2CO_3, CH_3CN). The progress of the reaction was monitored using LCMS. Metal complexation was subsequently carried out in two steps using previously described methodology (Scheme 4.7).[189]

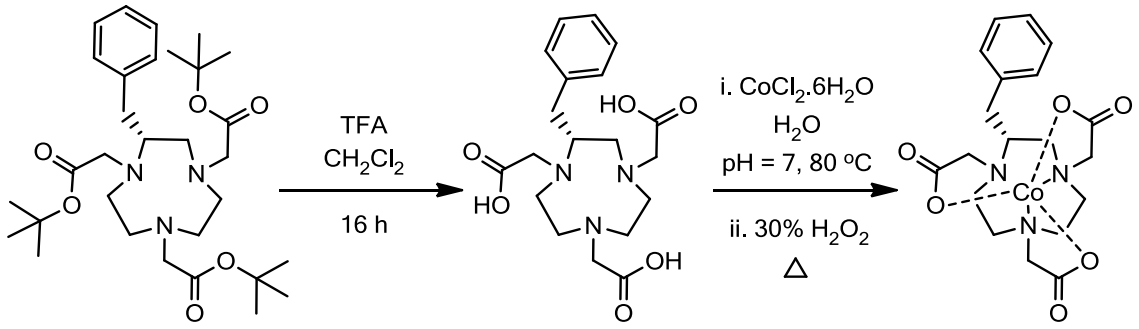

Scheme 4.7: Synthetic pathway for the preparation of (*R*)-[Co.**L**^{37}]. The overall yield of complex was 16%.

In light of the fact that samples of enantiomeric lanthanide complexes had already been prepared, it was proposed that the occurrence of enantioselective quenching phenomena should be assessed using a slightly different methodology to that outlined in Section 4.2. Specifically, it was suggested that examination of the quenching of emission from an enantiomeric pair of lanthanide complexes by a single stereoisomer of a chiral quencher may allow identification of enantioselective quenching effects. Hence, the synthesis of (*S*)-[Co.**L**^{37}] was not carried out. However, a sample of the achiral complex [Co.**L**^{38}] was prepared for use in control experiments. To achieve this, the commercially available ligand 1,4,7-triazacyclononane-1,4,7-triacetic acid was used in a metal complexation reaction carried out in accordance with the methodology outlined in the second stage of Scheme 4.7. The identity of the complexes was verified following their isolation by use of high resolution mass spectrometry.

4.4.2.2 Absorption properties

Following their isolation, absorption spectra were recorded for samples of (*R*)-[Co.**L**^{37}] and [Co.**L**^{38}] in aqueous solution. As anticipated, the observed spectral profiles were found to bear close resemblance to each other. In each case, the longest wavelength absorption band was found to be centred at 512 nm and was assigned to a spin-allowed d-d transition. An additional absorption maximum was observed at 372 nm, along with significant absorption below 320 nm, attributed to a LMCT band. Such behaviour is in close agreement with data reported for [Co.**L**^{38}] in the literature.[189] For each complex the absorption spectrum was run at a variety of concentrations and a plot of absorbance,

A, against complex concentration, *c*, facilitated the determination of molar extinction coefficients, ε, at chosen wavelengths in accordance with the Beer-Lambert law (equation 15).[22]

$$A = \varepsilon c l \qquad \text{(eqn. 15)}$$

Using the data gathered, an extinction coefficient of 348 $dm^3mol^{-1}cm^{-1}$ was calculated for (*R*)-[Co.**L**^{37}] at 512 nm (Figure 4.15). Meanwhile, a slightly lower value of 340 $dm^3mol^{-1}cm^{-1}$ was calculated for [Co.**L**^{38}], in reasonable agreement with the literature value of 330 $dm^3mol^{-1}cm^{-1}$.[189]

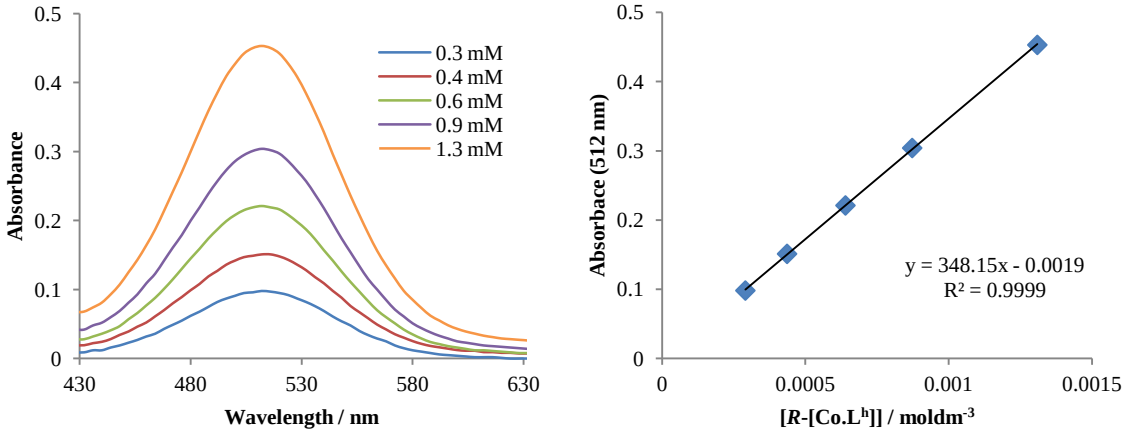

Figure 4.15: Absorption spectra recorded for five aqueous solutions of (*R*)-[Co.**L**^{37}] at differing concentrations (left) shown alongside a plot of the absorbance at 512 nm versus complex concentration.

4.4.2.3 Chiral analysis

Insight was gained into the structure adopted by (*R*)-[Co.**L**^{37}] through the use of X-ray diffraction techniques. A preliminary search of the Cambridge Structural Database carried out by Dr Dmitry S. Yufit in April 2013 revealed no examples of crystal structures for triacetate derivatives of 1,4,7-triazacyclononane incorporating asymmetric centres into the ring framework. Hence, crystals of (*R*)-[Co.**L**^{37}] suitable for analysis were isolated from aqueous solution, following recrystallisation of a sample of the originally isolated complex. Data collection and analysis was carried out by Dr Dmitry S. Yufit. Owing to the fact that [Co.**L**^{38}] had previously been reported to crystallise isotypically with its chromium analogue, the structure of which could be accessed using the CSD, solid state structural analysis was not carried out for this second complex.[189]

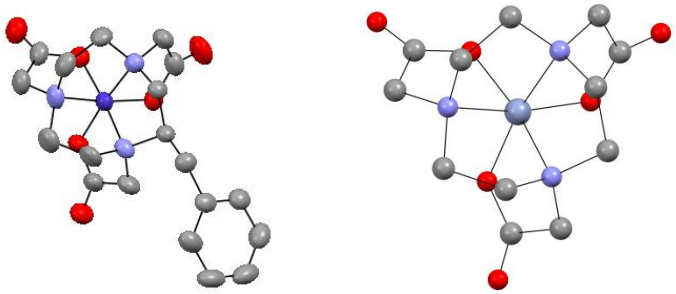

Figure 4.16: Crystal structure of (*R*)-[Co.**L**^{37}] (left) shown alongside the crystal structure of Δ-[Cr.**L**^{38}] (right). The atoms shown are: C (grey), N (lilac), O (red), Co (dark blue) and Cr (light blue).

As expected on the basis of the previously reported solid state structure of [Cr.**L**^{38}], the structure of (*R*)-[Co.**L**^{37}] was found to consist of monomeric, neutral molecules. Each cobalt ion was found to be coordinated by six donor atoms; the three ring nitrogens and three carboxylate oxygens (Figure 4.16). The complex crystallised in the space group $P2_1$, with four complexes in each monoclinic unit cell. Importantly, the solid state structural analysis revealed the presence of only one complex stereoisomer. This was in contrast to the solid state crystal structure of [Cr.**L**^{38}] reported in the literature, where both Δ and Λ complex stereoisomers were seen. Examination of the N-C-C-N torsion angles within the ring structure revealed an average angle of -45^{o}, consistent with a ($\lambda\lambda\lambda$) helicity. Meanwhile, the average N-C-C-O torsion angle for the acetate arms was found to be +18^{o}, consistent with a Δ helicity. This result was therefore in line with prior observations made in Section 4.4.1.3, pertaining to the [Ln.**L**^{34}] systems. Further evaluation of the ring torsional angles allowed corner and side carbon atoms within the 1,4,7-triazacyclononane ring to be distinguished and therefore facilitated verification of the hypothesis outlined in Section 4.4.1.3, which proposed that for the [Ln.**L**^{34}] systems the ring substituent was more likely to be located at a corner carbon position, and therefore directed away from the coordinating arms of the complex (Figure 4.17).

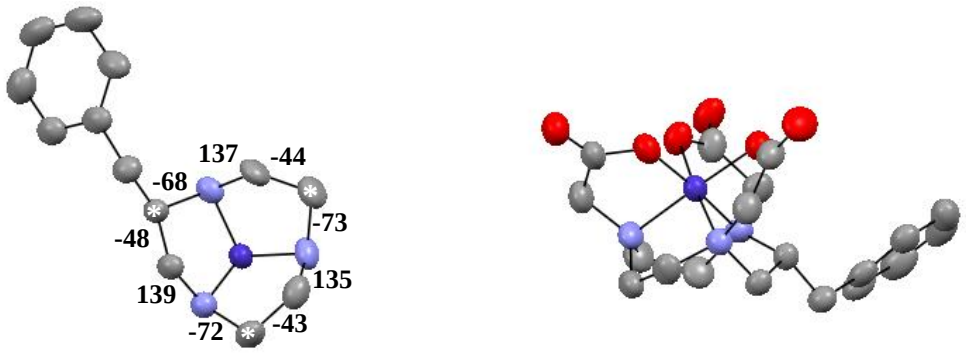

Figure 4.17: Views of the crystal structure of (*R*)-[Co.**L**^{37}] illustrating the ring torsional angles (as for Figure 4.14, 'corner' carbons are marked with asterisks) and the relative orientation of the ring substituent with respect to the coordinating arms of the complex.

Having achieved an analysis of the structure of (*R*)-[Co.**L**^{37}] in the solid state, attempts were made to probe the solution state structure of the complexes using circular dichroism spectroscopy. In light of results already outlined in this chapter, it was assumed that the number of isomers present for each complex in the solution state would mimic that found in the solid state. In accordance with this, it was predicted that a CD signal should only be observable for (*R*)-[Co.**L**^{37}]. As can be seen from Figure 4.18, this was indeed found to be the case.

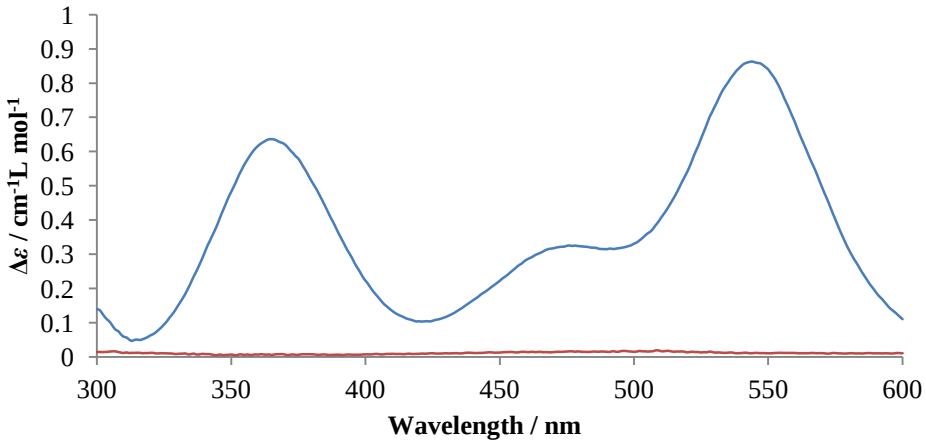

Figure 4.18: Electronic circular dichroism spectrum of (*R*)-[Co.**L**^{37}] (blue) and [Co.**L**^{38}] (red) in aqueous solution (295 K, pH 7.4).

4.4.3 Preliminary investigations into enantioselective quenching

A series of titrations was carried out to assess the quenching of the emission from (*R*)- and (*S*)-[Ln.**L**^{34}] (Ln = Eu^{3+}, Tb^{3+}) in the presence of these complexes. Incremental additions of each cobalt complex were made from concentrated stock solutions to 1 mL samples of (*R*)- and (*S*)-[Ln.**L**^{34}] (Ln = Eu^{3+}, Tb^{3+}), which had been dissolved in 0.1 M HEPES containing 0.1 M NaCl at pH 7.4, to give solutions where the concentration of

lanthanide complex was 20 μM. Owing to the fact that indirect excitation of the lanthanide complexes could only be achieved by irradiation at 268 nm and both the cobalt complexes had been found to exhibit significant absorption at this wavelength, lifetime measurements were used in place of emission intensity measurements to monitor the modulation of the luminescence output of each lanthanide complex over the course of the titrations. The variation in τ_0/τ as a function of [Q] is shown for each enantiomeric pair of lanthanide complexes in Figure 4.19.

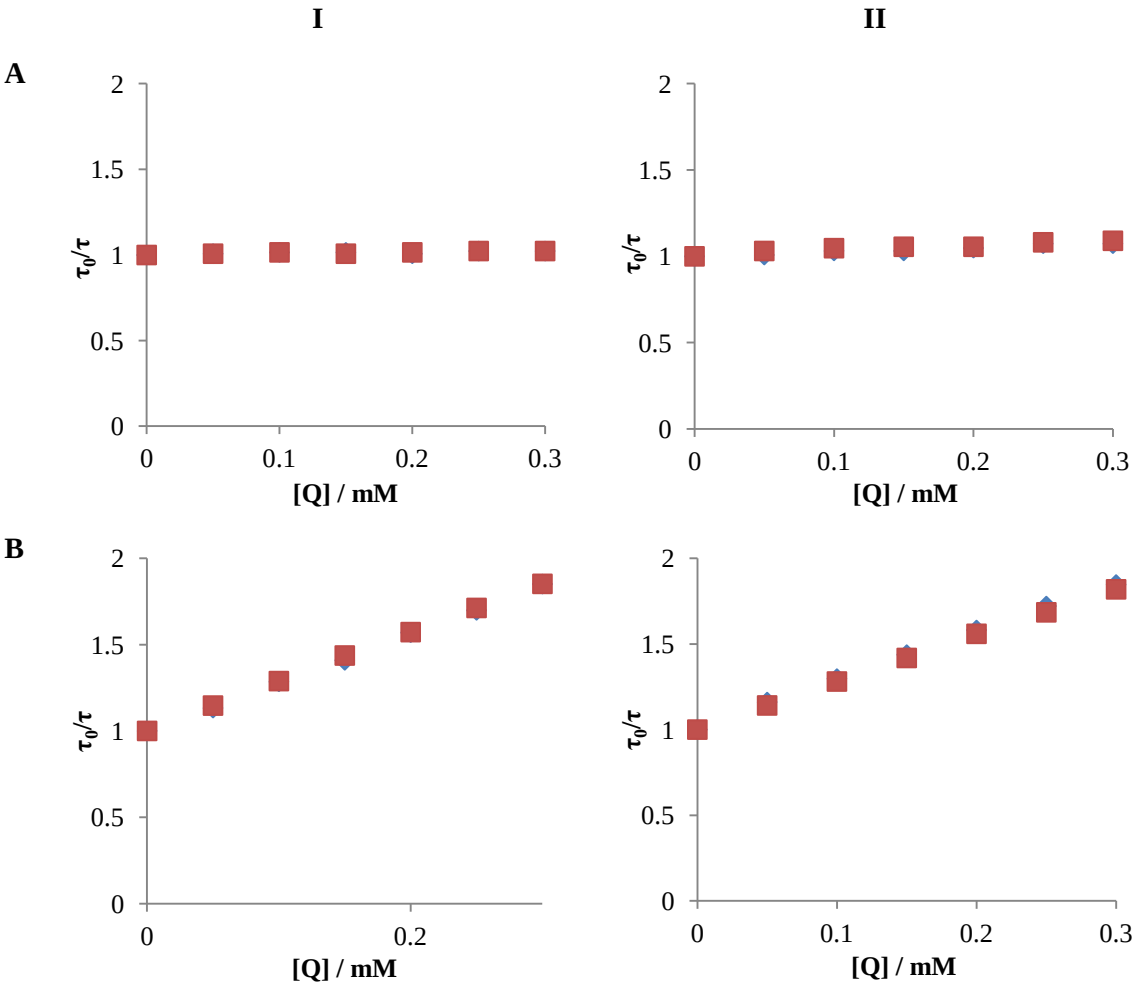

Figure 4.19: Comparison of the variation in emission lifetime as a function of [[Co.**L**^{38}]] (**I**) and [(*R*)-[Co.**L**^{37}]] (**II**) for (*R*)- (red) and (*S*)- (blue) [Ln.**L**^{34}] (**A** = Eu^{3+}; **B** = Tb^{3+}) (295 K, pH 7.4, 0.1 M HEPES, 0.1 M NaCl, 20 μM complex).

As is apparent from the plots presented in Figure 4.19, the lifetime data gathered in the titrations outlined above did not appear to provide any evidence to suggest the occurrence of enantioselective quenching phenomena. Whilst this result was in line with expectation in the case of experiments utilising [Co.**L**^{38}] as the quenching species, the lack of chiral discrimination observed in experiments carried out with (*R*)-[Co.**L**^{37}] was somewhat surprising. In the case of (*R*)- and (*S*)-[Tb.**L**^{34}], the data presented in Figure

4.19 was used in the calculation of Stern-Volmer quenching constants (Table 4.4). Whilst a slight difference was apparent in the values associated with the quenching interactions of (*R*)- and (*S*)-[Tb.**L**^{34}] with (*R*)-[Co.**L**^{37}], convincing evidence of an enantioselective effect was not obtained.

Table 4.4: Stern-Volmer quenching constants for the dynamic quenching of emission from (*R*)- and (*S*)-[Ln.**L**^{34}] by [Co.**L**^{38}] and (*R*)-[Co.**L**^{37}] (295 K, pH 7.4, 0.1 M HEPES, 0.1 M NaCl, 20 μM complex).

Complex	Quencher	K_{SV}^{-1} / μM
(*R*)-[Tb.**L**^{34}]	[Co.**L**^{38}]	353
(*S*)-[Tb.**L**^{34}]		353
(*R*)-[Tb.**L**^{34}]	(*R*)-[Co.**L**^{37}]	366
(*S*)-[Tb.**L**^{34}]		355

In an effort to gain insight into the results outlined above, a consideration of the mechanism by which the quenching of the luminescence output occurred was undertaken. As was mentioned in Section 1.5.2.2 of Chapter 1, previous studies detailing chiral discrimination in quenching of the luminescence output from $[Ln(DPA)_3]^{3-}$ (Ln = Eu^{3+}, Tb^{3+}) by chiral quenchers had typically attributed quenching to energy transfer mechanisms, which generally require spectral overlap between the emission spectrum of the donor and the absorption spectrum of the acceptor. The occurrence of enantioselectivity in the quenching interactions studied was ascribed to differences in energy transfer efficiencies in homochiral versus heterochiral Ln^{*}- Q collisional complexes, thought to arise in part due to structural differences between these diastereomeric encounter complexes. Figure 4.20 shows an overlay of the absorption spectrum recorded for (*R*)-[Co.**L**^{37}] in aqueous solution with representative emission spectra for [Ln.**L**^{34}] (Ln = Eu^{3+}, Tb^{3+}).

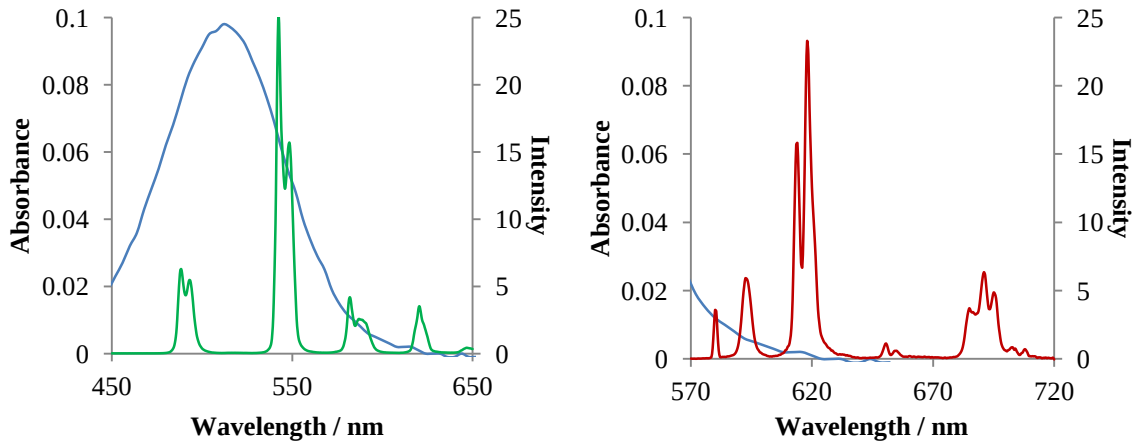

Figure 4.20: Absorption spectrum of (*R*)-[Co.**L**^{37}] (blue) as a function of wavelength (H_2O, 295 K) overlaid with representative emission spectra for [Ln.**L**^{34}] (Ln = Eu^{3+}, right and Tb^{3+} left).

In light of the differing degree of overlap between the absorption band of [Co.**L**^{38}] or (*R*)-[Co.**L**^{37}] at 511 nm and the europium and terbium emission bands of (*R*)- and (*S*)-[Ln.**L**^{34}] as demonstrated in Figure 4.20, it can be concluded that the Stern-Volmer plots shown in Figure 4.19 provide evidence to suggest that quenching also occurs via an energy transfer mechanism for the systems under consideration in this study. However, the lack of enantioselectivity observed in the quenching of the luminescence output from (*R*)- and (*S*)-[Ln.**L**^{34}] by (*R*)-[Co.**L**^{37}] reflects a high degree of similarity in the efficiency of energy transfer, perhaps indicating that in this case the observed quenching may be attributed mainly to long range energy transfer mechanisms. As can be seen from Table 4.4, the Stern-Volmer quenching constants associated with the quenching of (*R*)- or (*S*)-[Tb.**L**^{34}] by [Co.**L**^{38}] and (*R*)-[Co.**L**^{37}] were relatively high, with values of approximately 350 µM being obtained in all cases. Although this may no doubt in part be attributed to the absence of electrostatic attraction between the lanthanide and cobalt complexes, which do not have any overall charge, it also suggests a lack of accessibility to the lanthanide centre. Indeed, analysis of data gathered in a titration performed using the cyclen-based system [Tb.**L**^{22}(OH_2)]$^+$, featured in previous chapters of this thesis, in which the lanthanide centre is likely to be less shielded by the ligand framework, yielded a significantly lower Stern-Volmer quenching constant, with a value of 172 µM.

4.5 Conclusions and future work

The aim of the work outlined in this chapter was to identify macrocylic lanthanide complexes with potential utility in chiral quenching studies. Preliminary experiments focussed on the use of an enantiomerically pure cyclen-derived complex selected from

the literature, (*SSS*)-Δ-[Tb.$\mathbf{L}^{\mathbf{20b}}$]$^{3+}$. Previous structural studies of the yttrium analogue of this complex had revealed that one face of the tetraazatriphenylene moiety is blocked when the complex is in solution.

The quenching of emission from (*SSS*)-Δ-[Tb.$\mathbf{L}^{\mathbf{20b}}$]$^{3+}$ was examined in the presence of two electron-rich chiral quenching species, Trolox and DOPA. The latter of these species had previously been shown to deactivate lanthanide luminescence by a mechanism involving formation of an exciplex with the triplet excited state of the chromophore. Support for the hypothesis that quenching of the emission intensity from (*SSS*)-Δ-[Tb.$\mathbf{L}^{\mathbf{20b}}$]$^{3+}$ in the presence of Trolox would also occur by such a mechanism was gained in a preliminary investigation comparing the efficiency of quenching in buffer solution to that in methanol. A much higher quenching efficiency was observed in buffer, suggesting the hydrophobic effect plays a role in the quenching process, by encouraging exciplex formation.

Attempts were made to gather evidence for the occurrence of enantioselective quenching phenomena for (*SSS*)-Δ-[Tb.$\mathbf{L}^{\mathbf{20b}}$]$^{3+}$ using steady-state measurement techniques, in the presence of Trolox and DOPA. The utility of Stern-Volmer analysis in the identification and characterisation of enantioselective quenching phenomena had previously been highlighted in a 2002 publication.[174] Unfortunately, only weak evidence of enantioselectivity was seen in the quenching interaction between (*SSS*)-Δ-[Tb.$\mathbf{L}^{\mathbf{20b}}$]$^{3+}$ and either Trolox or DOPA, with enantiomeric quenchers giving almost identical Stern-Volmer constants. It was concluded that the degree of conformational flexibility in DOPA may negate the possibility of an enantioselective effect. Meanwhile, in the case of Trolox, DFT calculations revealed very little energy difference between diastereomeric exciplexes, suggesting that the observation of enantioselectivity is unlikely.

In spite of the results outlined above, it was hypothesised that in the case of Trolox, a difference between the quenching effect of the two enantiomers may be seen by removing the non-directional electrostatic component of the interaction with the terbium complex. The synthesis of the methyl ester analogues of Trolox was therefore undertaken, and titrations carried out using these species. Stern-Volmer analysis of the data gathered in these titrations revealed some evidence to suggest enantioselectivity in the quenching interaction. However, the results were not found to be entirely reproducible, presumably due to a high degree of sensitivity to sample conditions. A

series of steady-state CPL studies subsequently carried out using a structurally related racemic terbium complex, [Tb.**L**[29]], revealed no evidence for the induction of circular polarization in the emission output of this complex when in the presence of an enantiomerically pure sample of Trolox methyl ester.

A second set of investigations was undertaken to study the possibility of enantioselective quenching phenomena using lanthanide complexes derived from ligands based on 1,4,7-triazacyclononane. Initially, the synthesis of a set of lanthanide complexes incorporating a chiral centre directly onto this macrocyclic framework, (*R*)- and (*S*)-[Ln.**L**[34]] (Ln = Eu^{3+}, Tb^{3+}), was undertaken. Chiral analysis of the complexes formed using techniques such as NMR spectroscopy, chiral HPLC and CPL suggested the presence of a single complex stereoisomer in each case, the overall helicity of which was found to be determined by the nature of the ring C substitution. Analysis of the X-ray crystal structure for a related complex, [Eu.**L**[36]], allowed the origin of this chiral discrimination in complex formation to be identified. A chiral hexadentate cobalt complex based on a similar ligand framework, (*R*)-[Co.**L**[37]], was subsequently synthesised for use in studies of enantioselective quenching phenomena with these lanthanide complexes. Structural analysis of this complex was achieved in the solid state using X-ray crystallography. Meanwhile, circular dichroism spectroscopy revealed a racemic composition of the structurally related complex [Co.**L**[38]] in solution.

Preliminary investigations into enantioselective quenching were carried out using (*R*)- and (*S*)-[Ln.**L**[34]] (Ln = Eu^{3+}, Tb^{3+}) and (*R*)-[Co.**L**[37]]. Unfortunately, no evidence for chiral discrimination was observed, despite the fact that quenching was found to occur via an energy transfer mechanism. It was hypothesised that long-range mechanisms may be responsible for the observed deactivation of the lanthanide luminescence, with the magnitude of Stern-Volmer quenching constants observed suggesting a high degree of shielding at the lanthanide centre. Although the exact origin of the enantioselective quenching phenomena previously detailed in the literature remains to some extent a curiosity, it is generally thought to be the case that the effect may in part be attributed to structural differences between short range encounter complexes. Hence, it may be concluded that future work in this area should be directed towards the design and synthesis of macrocylic lanthanide systems in which short range energy transfer mechanisms with chiral quencher species may be encouraged by virtue of directional interactions such as hydrogen bonding. It is hoped that the construction of a CPL

spectrometer with time-resolved measurement capability at Durham will facilitate studies of such systems, as well as allowing verification of the results outlined in this chapter.

Although the work detailed in this chapter did not lead to the successful identification of macrocylic lanthanide complexes with potential utility in chiral quenching studies, some noteworthy results were obtained. Particularly important was the demonstration that it is possible to achieve complete control of the stereochemistry of triazacyclononane-based lanthanide complexes by the inclusion of a single substitution on a ring carbon atom. Such methodology could prove to be of great utility in the synthesis of chiral probes for application in CPL spectroscopy and microscopy, particularly given that additional synthetic work carried out in parallel to the work detailed in this chapter showed that this chiral discrimination in complex formation is conserved when pyridyl bromine substituents are included in the ligand framework (see (*S*)-[Ln.**L**^{39}] Section 5.2.2, Chapter 5).[186] The inclusion of such substituents in the ligand framework leads to the generation of complexes that may be further derivatised by C-C or C-N functionalization, therefore facilitating access to enantiopure triazacyclononane based complexes where sensitised emission is possible through excitation at longer wavelengths.

CHAPTER FIVE

EXPERIMENTAL DETAILS

5.1 General experimental

5.1.1 Reagents and solvents

Unless otherwise mentioned, all reagents were used as received from commercial suppliers (Acros, Alfa Aesar, CheMatech, Fischer Scientific, Merck, Sigma Aldrich and Strem). Solvents used were laboratory grade and were dried over appropriate drying agents when necessary. Air and water sensitive reactions were carried out under an atmosphere of dry argon. Water and H_2O refer to high purity water obtained from the "Purite Neptune" purification system.

5.1.2 Chromatography

Thin layer chromatography was performed using neutral aluminium oxide plates (Merck Millipore 60 F_{254}, neutral) or silica plates (Merck Millipore 60 F_{254}) and visualised under irradiation at 254 nm or by staining with iodine or Dragendorff's reagent. Preparative column chromatography was carried out using silica (Fluorochem Silicagel LC60A, 40-63 micron) or neutral aluminium oxide (Merck Millipore Aluminium Oxide 90 active neutral, activity stage I, 70-230 mesh), which was soaked overnight in ethyl acetate prior to use.

5.1.3 Spectroscopy

NMR spectra (^{1}H, ^{13}C, ^{31}P) were recorded on a Varian Mercury-400 (^{1}H 399.95 Hz and ^{31}P 161.90 MHz), Bruker Avance-400 (^{1}H 400.07 MHz, ^{13}C 100.60 MHz and ^{31}P 161.95 MHz), Bruker Avance-400 (^{1}H 400.13 MHz and ^{13}C 100.61 MHz), Varian Inova-500 (^{1}H 499.71 MHz and ^{13}C 125.65 MHz), Varian VNMRS-600 (^{1}H 599.75 MHz, ^{13}C 150.82 MHz and ^{31}P 242.78 MHz) or Varian VNMRS-700 (^{1}H 699.73 MHz and ^{13}C 175.95 MHz) spectrometer. Spectra were recorded in commercially available deuterated solvents and internally referenced to residual solvent signals.

Electrospray mass spectra were obtained on a TQD mass spectrometer equipped with an Acquity UPLC, an electrospray ion source and an Acquity photodiode array detector (Waters Ltd, UK). Methanol was used as the carrier solvent. For LCMS analyses a 2.1 x 50 mm 1.7 micron Acquity UPLC BEH C18 column was used. The solvent system was H_2O + 0.1% formic acid / MeOH (gradient elution, see Table 5.1).

Table 5.1: LCMS conditions.

Step	Time / min	Flow / mL min^{-1}	% H_2O	% MeOH
0	0	0.6	95.0	5.0
1	0.2	0.6	95.0	5.0
2	4.0	0.6	5.0	95.0
3	4.5	0.6	5.0	95.0
4	5.0	0.6	95.0	5.0

Accurate masses were recorded on a LCT Premier XE mass spectrometer or a QTOF Premier mass spectrometer both equipped with an Acquity UPLC, a lock-mass electrospray ion source and an Acquity photodiode array detector (Waters Ltd, UK). Methanol was used as the carrier solvent.

5.1.4 Melting points

Melting points were determined using a Sanyo Gallenkamp Melting Point Apparatus and are uncorrected.

5.1.5 HPLC

HPLC analysis was performed at 295 K using a Waters Mass Directed Auto Preparation (MDAP) system. The system consisted of a Waters 575 pump, Waters "System Fluidics Organizer", Waters 2545 "Binary Gradient Module", Waters 2767 "Sample Manager", Waters Fraction Collector III, Waters 2998 Photodiode Array Detector and Waters 3100 Mass Detector. An XBridge C18 OBD 4.6 x 100 mm, i.d. 5 µM column was used. The solvent system was H_2O +0.1% formic acid / MeOH +0.1% formic acid (gradient elution, see Table 5.2).

Table 5.2: HPLC conditions used for the analysis of complexes.

Step	Time / min	Flow / mL min^{-1}	% H_2O	% MeOH
0	0.0	1.0	90.0	10.0
1	10.0	1.0	5.0	95.0
2	13.0	1.0	5.0	95.0
3	13.5	1.0	90.0	10.0
4	16.5	1.0	90.0	10.0

Preparative HPLC for [Gd.$\mathbf{L}^{22}$(OH_2)]$^+$ and (*R*)-[Ln.$\mathbf{L}^{23}$(OH_2)]$^+$ was performed at 295 K using the same Waters MDAP system. An XBridge C18 OBD 19 x 100 mm, i.d. 5 µM column was used. The solvent system was H_2O +0.1% formic acid / MeOH +0.1% formic acid (gradient elution, see Table 5.3). Fraction collection was automatically triggered by mass detection.

Table 5.3: HPLC conditions used for the purification of [Gd.$\mathbf{L}^{22}$(OH_2)]$^+$ and (*R*)-[Ln.$\mathbf{L}^{23}$(OH_2)]$^+$.

Step	Time / min	Flow / mL min^{-1}	% H_2O	% MeOH
0	0	17.0	90.0	10.0
1	0.2	17.0	90.0	10.0
2	0.7	17.0	90.0	10.0
3	11	17.0	5.0	95.0
4	14	17.0	5.0	95.0
5	14.5	17.0	90.0	10.0
6	16.5	17.0	90.0	10.0

Preparative HPLC for (*S*)- and (*R*)-[Tb.$\mathbf{L}^{35}$] was performed at 295 K using a Shimadzu system consisting of a Degassing Unit (DGU-20A_{5R}), a Prominence Preparative Liquid Chromatograph (LC-20AP), a Prominence UV/Vis Detector (SPD-20A) and a Communications Bus Module (CBM-20A). An XBridge C18 OBD 19 x 100 mm, i.d. 5 µM column was used. The solvent system was H_2O +0.1% formic acid / MeOH +0.1% formic acid (gradient elution, see Table 5.4). The UV detector was set at 268 nm and fraction collection was performed manually.

Table 5.4: HPLC conditions used for the purification of (*S*)- and (*R*)-[Tb.$\mathbf{L}^{35}$].

Step	Time / min	Flow / mL min^{-1}	% H_2O	% MeOH
0	0	17.0	90.0	10.0
1	3.0	17.0	90.0	10.0
2	13.0	17.0	0.0	100.0
3	16.0	17.0	0.0	100.0
4	17.0	17.0	90.0	10.0

Chiral HPLC was performed at 290 K on a Perkin Elmer system consisting of a Perkin Elmer Series 200 pump, Perkin Elmer Series 200 auto-sampler and Perkin Elmer Series 200 UV/Vis detector. A CHIRALPAK-ID 250 x 4.6 mm 5 µM column was used, with a

flow rate of 1.0 mL min^{-1} and a solvent system of MeOH (isocratic elution). The UV detector was set at an appropriate wavelength according to the species being analysed.

5.1.6 Optical spectroscopy

Unless otherwise specified, quartz cuvettes with a pathlength of 1 cm or disposable UV-grade methacrylate cuvettes were used to contain all samples.

UV/Vis absorbance spectra were measured on an ATI Unicam UV/Vis spectrometer (Model UV2) using Vision version 3.33 software. Molar extinction coefficients were determined by first dissolving a known amount of solid in a known amount of solvent to give a bulk solution. Five solutions of known concentration, with absorbances ranging between 0.05 and 0.5, were made up by dilution of the bulk solution. Molar extinction coefficients, ε, were calculated in accordance with the Beer-Lambert law (equation 15),[22] by plotting absorbance, A, against complex concentration, c.

$$A = \varepsilon c l \qquad \text{(eqn. 15)}$$

Absorbance measurements of 96-well plates were made on an Analytik Jena FLASHScan 530 using WinFLASH version 1.5 software.

Emission spectra were recorded on an ISA Jobin-Yvon Spex Fluorolog-3 luminescence spectrometer using DataMax version 2.2.10 software. Unless otherwise stated, an integration time of 0.5 seconds, increment of 0.5 nm and excitation and emission slits of 2.5 and 1.5 nm respectively were used.

Quantum yields were determined by Dr L-O. Palsson at Durham University using a HORIBA Jobin-Yvon Fluorolog 3-22 Tau-3 fluorimeter with a Labsphere Optical Spectralon integrating sphere (diameter 100 mm, reflectance > 99% over 400 – 1500 nm range) and a method developed by Porrés *et al.*[190] Measurements were performed at 295 K using solutions with absorbances of 0.15 at λ_{max}, contained in a cylindrical quartz cuvette (8 mm diameter) fitted with a Teflon stopper.

All of the CPL spectra shown in Chapter 2 were measured with the assistance of Dr R. D. Peacock, using a custom built (Glasgow University, UK) CPL spectrometer based on a Spex-Fluoromax-2-spectrofluorimeter. In all other cases, a custom built in-house CPL spectrometer was used. This consisted of a laser driven light source (Energetiq EQ-99 LDLS, spectral range 170 to 2100 nm) coupled to an Acton SP2150 monochromator

(600 g/nm, 300 nm Blaze), allowing excitation wavelengths to be selected with a 6 nm FWHM band-pass. The collection of the emitted light (90 º angle set up) was facilitated by a Lock-In Amplifier (Hinds Instruments Signaloc 2100) and Photoelastic Modulator (Hinds Instruments PEM-90). The differentiated light was focused onto an Acton SP2150 monochromator (1200 g/nm, 500 nm Blaze) equipped with a high sensitivity cooled Photo Multiplier Tube (Hamamatsu 7155-01 red corrected). Spectra were recorded using a 5 spectral average sequence with 0.5 nm spectral intervals and 500 μs integration time. The recorded CPL spectra then underwent a 25% Fourier transformation smoothening protocol using Origin 8.0 Software (Origin Labs) to enhance visual appearance (all calculations were carried out using raw spectral data). In both cases samples were run at room temperature and indirect excitation at an appropriate wavelength was used. A schematic of the Durham CPL instrumentation is shown in Figure 5.1.

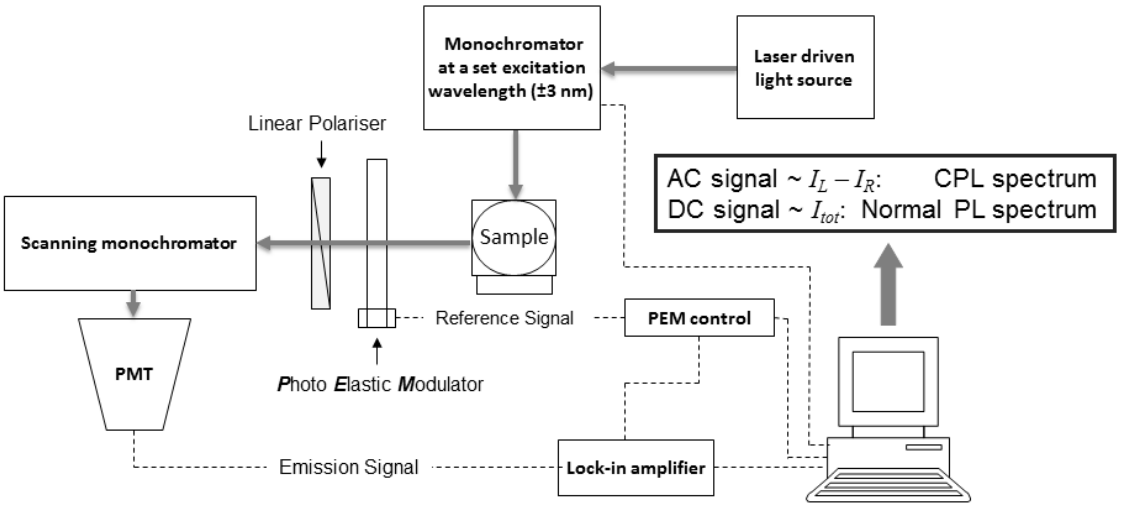

Figure 5.1: Schematic diagram of Durham CPL instrumentation.

Absorption and ECD spectra collected by Dr L. Di Bari at Pisa were acquired on a JASCO V650 spectrophotometer and a JASCO J715 spectropolarimeter respectively. Samples were run in cylindrical quartz cells at room temperature. The band width was set to 2.0 nm, response to 1 sec and scan speed to 50 nm/min. Up to 4 accumulations were averaged to improve S/N. In all cases the absorbance and dichroism data were scaled for the total concentration of complex to yield ε and Δε' (the prime indicates that the real concentration of the ECD-active species is uncertain).

ECD spectra for (*R*)-[Co.**L**[37]] and [Co.**L**[38]] were measured with the assistance of Lara Small on a JASCO J-810 CD Spectropolarimeter using Jasco's Spectra Manager™

software. The band width was set to 1.0 nm, response to 2 sec and scan speed to 50 nm/min.

5.1.7 Lifetime measurements

A Perkin Elmer LS55 luminescence spectrometer with FL Winlab Molecular Spectroscopy version 4.00.02 software was used to obtain lifetime measurements. Lifetime measurements were typically obtained by indirect excitation of the lanthanide (III) ion *via* the chromophore using a short pulse of light (at λ_{max}) followed by monitoring the integrated intensity of the light emitted at a chosen wavelength (612-620 nm for europium and 540-550 nm for terbium depending on the measured species) during a fixed gate time, t_g, after a delay time, t_d. Measurements were made for a minimum of 20 delay times, covering 3 or more lifetimes. A gate time of 0.1 ms was used, and the excitation and emission slits were set to 10 and 5 nm respectively. The obtained decay curves were plotted in Microsoft Excel and fitted to equation 16.

$$I = A_0 + A_1 e^{-kt} \qquad \text{(eqn. 16)}$$

I: intensity at time t following excitation

A_0: intensity when decay has ceased

A_1: pre-exponential factor

k: rate constant for the depopulation of the excited state

The excited state lifetime, τ, is the inverse of the radiative rate constant, k.

5.1.8 Determination of inner sphere hydration number (q')[55]

The rate constant for the depopulation of a lanthanide excited state in water can be represented as a sum of three rate constants, denoting radiative decay (k_r), non-radiative decay by energy transfer to XH oscillators ($\Sigma\, k_{XH}$) and all other non-radiative decay (k_{nr}).

$$k_{H_2O} = k_r + k_{nr} + \Sigma k_{XH} \qquad \text{(eqn. 17)}$$

Following D_2O exchange, it is assumed that the exchangeable XH oscillators no longer contribute to the quenching. Hence, the expression can be simplified to contain only the first two terms.

$$k_{D_2O} = k_r + k_{nr} \qquad \text{(eqn. 18)}$$

It follows that the difference between the rate constants in H_2O and D_2O can be expressed as being equal to the sum of all rate constants for non-radiative decay by energy transfer to XH oscillators.

$$\Delta k = k_{H_2O} - k_{D_2O} = \Sigma k_{XH} \qquad \text{(eqn. 19)}$$

If it is assumed that OH oscillators are the major contributor to the Σk_{XH} term, then the total number of water molecules located in the inner coordination sphere can be calculated using equation 20.

$$q' = A\,(\Delta k - x - y) \qquad \text{(eqn. 20)}$$

Where *A* is a proportionality constant, defining the sensitivity of the lanthanide ion to vibronic quenching by OH oscillators. This takes a value of 1.2 ms for europium complexes and 5 ms for terbium complexes. Meanwhile, *x* is a correction factor, which allows for the effect of closely diffusing OH oscillators, taking a value of 0.25 ms^{-1} for europium complexes and 0.06 ms^{-1} for terbium complexes. For europium complexes it is also necessary to take into account proximal amide NH oscillators, with *y* taking a value of $0.075n$ ms^{-1} where *n* is the number of proximate carbonyl-bound amide groups.

5.1.9 pH Measurements

Adjustment of pH was performed using conc. $NaOH_{(aq)}$ and conc. $HCl_{(aq)}$ to prevent any considerable increase in sample volume. Measurements of pH were carried out using a Jenway 3510 pH meter with a Jenway combination electrode or a Jenway 3020 pH meter with an Aldrich glass combination pH electrode, both calibrated using buffer solutions of pH 4.00 ± 0.01, 7.00 ± 0.01 and 10.00 ± 0.01 (Sigma Aldrich).

5.1.10 Luminescence titrations

Luminescence titrations were carried out at pH 7.4 using solutions containing 0.1 M NaCl in order to maintain a constant ionic background. In most cases, volumetric addition of stock solutions was carried out, such that the increase in sample volume was kept to a minimum (<5%). In the case of HSA and γ-Ig-G, the protein was added directly to the solution as a lyophilised solid. For protein titrations, the pH was adjusted as necessary after each addition using conc. $HCl_{(aq)}$ and conc. $NaOH_{(aq)}$. All proteins and other analytes used were purchased from Sigma Aldrich.

5.1.11 Binding constant determination

Apparent binding constants were calculated by fitting equation 21 to emission or lifetime data, using a non-linear least squares fitting algorithm in Microsoft Excel 2010, with the solver add-in.

$$[X] = \frac{f/K + [LnL]^* f - [LnL]^* f^2}{1-f} \quad \text{where} \quad f = \frac{F - F_0}{F_1 - F_0} \qquad \text{(eqn. 21)}$$

[*X*]: Total concentration of the selected analyte in solution

[*LnL*]: Total concentration of the complex

K: Binding constant

F: Either intensity ratio of selected peaks or lifetime ratio

F_0: Initial ratio

F_1: Final ratio

5.1.12 Relaxivity studies

Relaxivity measurements for [Gd.**L**^{22}(OH$_2$)]$^+$ were made in water at 37 ^{o}C and 60 MHz on a Bruker Minispec mq60 instrument. The mean value of three separate measurements was recorded, and values stated were corrected for the diamagnetic contribution of water (R_{1d} = 0.25 at 60 MHz, 310 K).

5.1.13 Single crystal X-Ray diffraction

Data for the crystal of (*R*)-[Co.**L**^{37}] were collected and processed by Dr D. S. Yufit. Data were recorded at 120 K on a Rigaku Saturn 724+ diffractometer at station ***I19*** of the Diamond Light Source synchrotron (undulator, λ = 0.6889 Å, ω-scan, 1.0°/frame) and processed using Bruker APEXII software. The temperature of the sample was maintained at 120 K by a Cryostream (Oxford Cryosystems) open-flow nitrogen cryostat. 6473 reflections were collected yielding 3721 unique data (R_{int} = 0.0541). The structure was solved by direct method and refined by full-matrix least squares on F^2 for all data using SHELXTL[191] and OLEX2[192] software. All non-hydrogen atoms were refined with anisotropic displacement parameters, H-atoms were placed in calculated positions and refined in riding mode with U_{iso}(H) = 1.2 U_{iso} of corresponding parent atom. The absolute configuration of the compound has been established by measurements of anomalous dispersion effects (Flack parameter 0.06(4),[193] Hooft parameter 0.07(2)[194]). The crystal data and further details of the refinement are listed later in Section 5.2.3 and in Appendix 1.

5.2 Synthetic experimental detail

Ethyl [4-bromo-6-(hydroxymethyl)pyridin-2-yl](methyl)phosphinate was made by Nicholas Evans.[195] $[Ln.\mathbf{L}^{22}(OH_2)]^+$ (Ln = Eu^{3+}, Tb^{3+}) was synthesised by Ga-Lai Law,[137] $[Eu.\mathbf{L}^{27}(OH_2)]^+$ was prepared by James Walton[152, 188] and (*SSS*)-Δ-$[Tb.\mathbf{L}^{20b}]^{3+}$ was made by Craig Montgomery.[139]

5.2.1 Cyclen-based complexes and precursors

6-Methyl-2-phenoxynicotinic acid[138, 196]

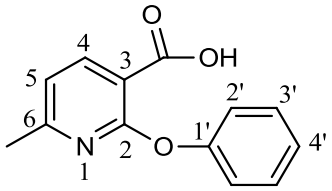

A solution of NaOMe was prepared by dissolving sodium (840 mg, 36.5 mmol) in anhydrous methanol (20 mL). 2-Chloro-6-methylnicotinic acid (3 g, 17.5 mmol) and phenol (7.8 g, 83.2 mmol) were added to the NaOMe solution and the reaction mixture was stirred under an argon atmosphere for 15 min. The solvent was removed under reduced pressure yielding a yellow oil, which was heated to 180 ^oC for 3.5 h and subsequently allowed to cool to room temperature. The reaction mixture was dissolved in water (30 mL) and washed with ether (3 x 20 mL). The pH of the aqueous phase was adjusted to 4 by the addition of acetic acid, causing the product to precipitate as an off-white solid that was collected by filtration and dried under high vacuum (2.58 g, 11.26 mmol, 64%). m.p. 156-157 ^oC (lit.[196] 155-156 ^oC); δ_H (400 MHz, $CDCl_3$) 2.40 (3H, s, CH_3), 7.03 (1H, d, J = 8.0 Hz, H^5), 7.18 (2H, d, J = 7.5 Hz, $H^{2'}$), 7.29 (1H, t, J = 7.5 Hz, $H^{4'}$), 7.44 (2H, t, J = 7.5 Hz, $H^{3'}$), 8.41 (1H, d, J = 8.0 Hz, H^4); δ_C (100 MHz, $CDCl_3$) 24.5 (1C, CH_3), 110.5 (1C, C^3), 119.3 (1C, C^5), 121.8 (2C, $C^{2'}$), 125.7 (1C, $C^{4'}$), 129.7 (2C, $C^{3'}$), 143.6 (1C, C^4), 152.6 (1C, $C^{1'}$), 160.6 (1C, C^2), 163.2 (1C, C^6), 165.5 (1C, COOH); *m/z* ($HRMS^+$) 230.0828 $[M + H]^+$ ($C_{13}H_{12}NO_3$ requires 230.0817).

2-Methyl-1-azaxanthone[138, 197]

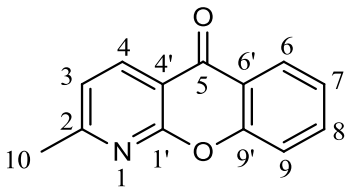

Polyphosphoric acid (80 g) was added to 6-methyl-2-phenoxynicotinic acid (1.72 g, 7.50 mmol) and the reaction mixture was heated at 120 ^{o}C for 20 h under argon with stirring. The light-brown liquid was allowed to cool to room temperature before pouring onto ice-water (250 mL) with stirring until a homogenous solution formed. The pH of the resulting solution was adjusted to 12 by the addition of KOH pellets and the aqueous solution was then extracted with dichloromethane (3 x 100 mL). The organic extracts were combined, dried over magnesium sulfate and filtered. Removal of the solvent under reduced pressure yielded the title compound as an off-white solid (1.26 g, 5.97 mmol, 80%). m.p. 134–139 ^{o}C (lit.[197] 136-138 ^{o}C); δ_H (700 MHz, $CDCl_3$) 2.61 (3H, s, H^{10}), 7.20 (1H, d, *J* = 8.0 Hz, H^3), 7.32 (1H, ddd, *J* = 8.0, 7.0, 1.0 Hz, H^7), 7.49 (1H, dd, *J* = 9.0, 1.0 Hz, H^9), 7.67 (1H, ddd, *J* = 9.0, 7.0, 1.5 Hz, H^8), 8.19 (1H, dd, *J* = 8.0, 1.5 Hz, H^6), 8.47 (1H, d, *J* = 8.0 Hz, H^4); δ_C (100 MHz, $CDCl_3$) 25.1 (1C, C^{10}), 114.3 (1C, $C^{4'}$), 118.5 (1C, C^9), 121.2 (1C, C^3), 121.7 (1C, $C^{6'}$) , 124.6 (1C, C^7), 126.7 (1C, C^6), 135.4 (1C, C^8), 137.3 (1C, C^4), 155.7 (1C, $C^{9'}$), 160.0 (1C, $C^{1'}$), 165.1 (1C, C^2), 177.4 (1C, C^5); *m/z* (HRMS$^+$) 212.0721 $[M+H]^+$ ($C_{13}H_{10}NO_2$ requires 212.0712).

2-Bromomethyl-1-azaxanthone[138]

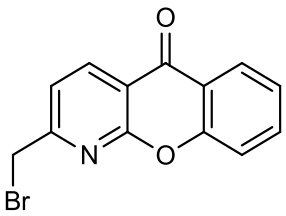

2-Methyl-1-azaxanthone (1.85 g, 8.73 mmol) was dissolved in carbon tetrachloride (25 mL). A tungsten lamp was used to heat the reaction mixture prior to the addition of N-bromosuccinimide (1.56 g, 8.73 mmol) and dibenzoyl peroxide (10 mg, 0.04 mmol), it was then left to stir under argon using the lamp for activation. The reaction was monitored by ^{1}H NMR spectroscopy and TLC (SiO_2, toluene-CH_2Cl_2-CH_3OH, 49.5 : 49.5 : 1) and stopped after 18 h. After cooling to room temperature, the mixture was filtered and the solvent was subsequently removed under reduced pressure. Purification

by column chromatography on silica gel (toluene-CH_2Cl_2, 1 : 1) gave the title compound as a white crystalline solid (301 mg, 1.04 mmol, 12%). m.p. 201-203 ^oC (lit.[138] 169-171 ^oC); R_f (SiO_2, toluene-CH_2Cl_2-CH_3OH, 49.5 : 49.5 : 1) : 0.28; δ_H (400 MHz, $CDCl_3$) 4.60 (2H, s, H^{10}), 7.44 (1H, ddd, J = 8.0, 7.0, 1.0 Hz, H^7), 7.56 (1H, d, J = 8.0 Hz, H^3), 7.61 (1H, dd, J = 8.5, 1.0 Hz, H^9), 7.78 (1H, ddd, J = 8.5, 7.0, 1.5 Hz, H^8), 8.29 (1H, dd, J = 8.0, 1.5 Hz, H^6), 8.70 (1H, d, J = 8.0 Hz, H^4); δ_C (100 MHz, $CDCl_3$) 32.0 (1C, C^{10}), 115.8 (1C, $C^{4'}$), 118.3 (1C, C^9), 120.6 (1C, C^3), 121.5 (1C, $C^{6'}$), 124.7 (1C, C^7), 126.6 (1C, C^6), 135.6 (1C, C^8), 138.5 (1C, C^4), 155.5 (1C, $C^{9'}$), 159.6 (1C, $C^{1'}$), 161.8 (1C, C^2), 176.8 (1C, C^5); *m/z* (HRMS$^+$) 289.9807 $[M + H]^+$ ($C_{13}H_9{}^{79}BrNO_2$ requires 289.9817).

1,4,7,10-Tetraaza-cyclododecane-1,7-dicarboxylic acid dibenzyl ester[141]

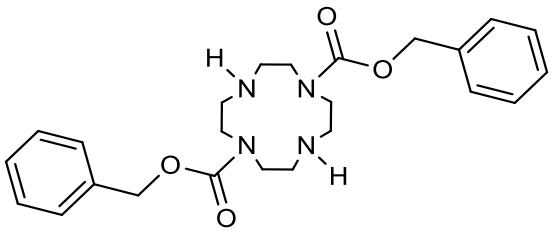

Disodium hydrogen phosphate (14 g, 98.62 mmol) was added to a solution of cyclen (5 g, 29.02 mmol) in water:dioxane (50:20, 70 mL). The pH was then adjusted to between 2.5 and 3 using conc. $HCl_{(aq)}$. Benzyl chloroformate (10.0 mL, 70.05 mmol) in dioxane (20 mL) was added dropwise to the reaction mixture over 2.5 h at room temperature and it was stirred for 18 h to yield a colourless solution containing a white precipitate. The solvent was removed from the crude mixture under reduced pressure to yield a viscous white gum, which was dissolved in water (100 mL). The pH of the resulting solution was then adjusted to 7 by the addition of conc. $KOH_{(aq)}$. The aqueous solution was washed with diethyl ether (3 x 50 mL) to facilitate the removal of reaction side products. This was followed by extraction of the product from the aqueous phase using dichloromethane (3 x 50 mL). The organic phase was then dried under reduced pressure to yield the product as a colourless viscous oil, which was redissolved in dichloromethane (5 mL). The addition of cold ether (60 mL) to the dichloromethane solution caused the product to precipitate, yielding a coarse white powder that was collected by centrifugation (8.03 g, 18.24 mmol, 63%). m.p. 121–124 ^oC (lit.[198] 113-116 ^oC); δ_H (400 MHz, $CDCl_3$) 2.26 (2H, s br, 2 x NH), 2.83 – 3.09 (8H, m br, cyclen CH_2), 3.50 – 3.84 (8H, m br, cyclen CH_2), 5.15 (4H, s, CH_2Ph), 7.31 – 7.41 (10H, m, Ar); δ_C

(100 MHz, $CDCl_3$) 49.0, 49.3, 49.6, 50.0, 50.1, 50.2, 50.6 (8C, cyclen CH_2), 67.7, 67.8 (2C, CH_2Ph), 127.9, 128.0, 128.3, 128.4, 128.6, 128.7 (10C, Ar), 135.8, 135.9 (2C, $Ar_{(q)}$), 156.0, 156.1 (2C, C=O); *m/z* ($HRMS^+$) 441.2509 $[M + H]^+$ ($C_{24}H_{33}N_4O_4$ requires 441.2502).

4,10-Bis-(*tert*-butoxycarbonylmethyl)-1,4,7,10-tetraazacyclododecane-1,7-dicarboxylic acid dibenzyl ester[139]

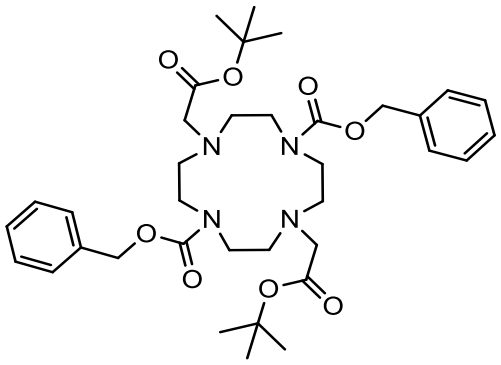

Caesium carbonate (2.2 g, 6.81 mmol) and *tert*-butyl bromoacetate (970 mg, 4.97 mmol) were added to a solution of 1,4,7,10-tetraazacyclododecane-1,7-dicarboxylic acid dibenzyl ester (1 g, 2.27 mmol) in anhydrous acetonitrile (10 mL). The reaction mixture was stirred at reflux for 18 h under argon. After this time the reaction mixture was allowed to cool to room temperature and the solvent was removed under reduced pressure. The resulting residue was dissolved in dichloromethane (15 mL) and the organic solution was washed with water (3 x 10 mL), to facilitate the removal of caesium salts, before being dried over magnesium sulfate and filtered. Removal of the solvent under reduced pressure yielded the crude product, which was purified by column chromatography on silica gel (gradient elution: CH_2Cl_2 to 1% CH_3OH-CH_2Cl_2) to give the title compound as a yellow oil (674 mg, 1.01 mmol, 44%). *R*f (SiO_2, CH_2Cl_2-CH_3OH, 95 : 5) : 0.59; δ_H (400 MHz, $CDCl_3$) 1.41 (18H, s, ^{t}Boc CH_3), 2.87 (8H, br s, cyclen CH_2), 3.11 – 3.50 (12H, m, cyclen CH_2; CH_2CO), 5.10 (4H, s, CH_2Ph), 7.19 – 7.39 (10H, m, Ar); δ_C (100 MHz, $CDCl_3$) 28.1 (6C, ^{t}Boc CH_3), 46.6, 46.9, 54.0, 54.3 (8C, cyclen CH_2), 55.9 (2C, CH_2CO), 66.8 (2C, CH_2Ph), 80.8 (2C, ^{t}Boc$_{(q)}$), 127.8, 128.4 (10C, Ar), 136.8 (2C, $Ar_{(q)}$), 156.4 (2C,Cbz C=O), 170.4 (2C, ^{t}Boc C=O); *m/z* (HRMS+) 669.3879 [M + H]+ ($C_{36}H_{53}N_4O_8$ requires 669.3863).

1,7-Bis-(*tert*-butoxycarbonylmethyl)-1,4,7,10-tetraazacyclododecane[199]

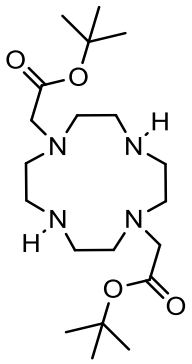

4,10-Bis-(*tert*-butoxycarbonylmethyl)-1,4,7,10-tetraazacyclododecane-1,7-dicarboxylic acid dibenzyl ester (674 mg, 1.01 mmol) in EtOH (10 mL) was shaken in a Parr hydrogenation flask at 40 psi over $Pd(OH)_2/C$ (150 mg) for 18 h. The resulting mixture was filtered through celite to give a colourless solution. The solvent was removed under reduced pressure, yielding the desired product as a yellow oil (346 mg, 0.85 mmol, 86%); δ_H (400 MHz, $CDCl_3$) 1.32 (18H, s, ^{t}Boc CH_3), 2.70 (8H, br s, cyclen CH_2), 2.84 (8H, br s, cyclen CH_2), 3.29 (4H, s, CH_2CO); δ_C (100 MHz, $CDCl_3$) 28.1 (6C, ^{t}Boc CH_3), 47.0, 51.4, 56.8, 57.8 (10C, cyclen CH_2, CH_2CO), 81.2 (2C, ^{t}Boc$_{(q)}$), 171.1 (2C, ^{t}Boc C=O); *m/z* (HRMS+) 401.3122 [M + H]+ ($C_{20}H_{41}N_4O_4$ requires 401.3128).

1,7-Bis-(*tert*-butoxycarbonylmethyl)-4,10-bis[2-methyl-1-azaxanthone]-1,4,7,10-tetraazacyclododecane[137]

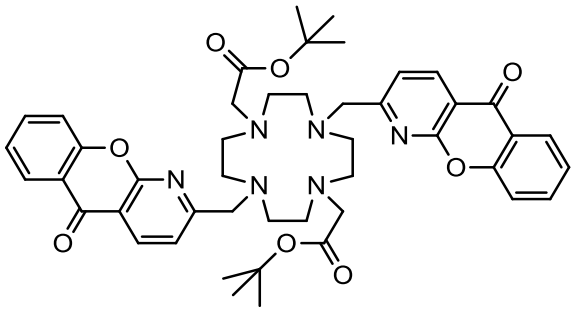

1,7-Bis-(*tert*-butoxycarbonylmethyl)-1,4,7,10-tetraazacyclododecane (187 mg, 0.47 mmol), 2-bromomethyl-1-azaxanthone (284 mg, 0.98 mmol) and caesium carbonate (305 mg, 0.94 mmol) were stirred in anhydrous acetonitrile (5 mL) at reflux under argon. The reaction was monitored by TLC to confirm that all the brominated starting material had been consumed. After 48 h the reaction mixture was allowed to cool to room temperature and the solvent was removed under reduced pressure. The resulting residue was dissolved in dichloromethane (10 mL) and the organic solution was washed

with water (3 x 10 mL), to facilitate the removal of caesium salts, before being dried over magnesium sulfate and filtered. Removal of the solvent under reduced pressure yielded the crude product, which was purified by column chromatography on silica gel (gradient elution: CH_2Cl_2 to 6% CH_3OH-CH_2Cl_2) to give the title compound as an orange oil (53 mg, 0.07 mmol, 14%). R_f (SiO_2, CH_2Cl_2-CH_3OH, 95 : 5) : 0.29; δ_H (700 MHz, $CDCl_3$) 1.11 (18H, s, ^{t}Boc CH_3), 2.45-3.05 (20H, br m, cyclen CH_2, CH_2CO), 3.98 (4H, br s, H^{10}), 6.97 (2H, d, J = 8.5 Hz, H^9), 7.25 (2H, m, H^7), 7.45 (2H, ddd, J = 8.5, 7.5, 1.5 Hz, H^8), 7.50 (2H, d, J = 8.0 Hz, H^3), 8.16 (2H, dd, J = 8.0, 1.5 Hz, H^6), 8.74 (2H, d, J = 8.0 Hz, H^4); δ_C (100 MHz, $CDCl_3$) 27.8 (6C, ^{t}Boc CH_3), 53.4, 58.0, 59.5 (12C, cyclen CH_2, CH_2CO, C^{10}), 82.1 (2C, ^{t}Boc$_{(q)}$), 115.6 (2C, $C^{4'}$), 117.9 (2C, C^9), 121.2, 121.4 (4C, C^3, $C^{6'}$), 124.8 (2C, C^7), 126.6 (2C, C^6), 135.4 (2C, C^8), 138.5 (2C, C^4), 155.2 (2C, $C^{9'}$), 160.4 (2C, $C^{1'}$), 165.2 (2C, C^2), 172.0 (2C, ^{t}Boc C=O), 176.9 (2C, C^5); *m/z* (HRMS+) 819.4099 $[M+H]^+$ ($C_{46}H_{55}N_6O_8$ requires 819.4081).

$[Gd.L^{22}(OH_2)]^+$

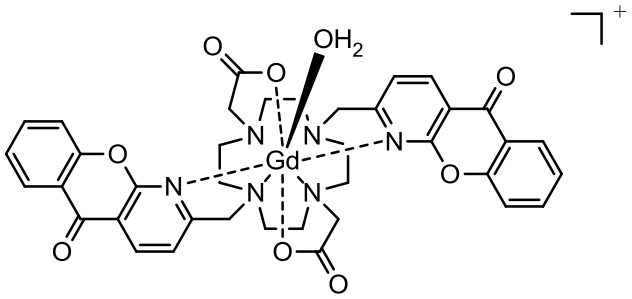

Trifluoroacetic acid (1 mL) was added to a solution of 1,7-bis-(tert-butoxycarbonylmethyl) - 4,10 - bis[2-methyl-1-azaxanthone] - 1,4,7,10 - tetraazacyclododecane (53 mg, 0.07 mmol) in dichloromethane (0.5 mL). The mixture was left stirring for 60 h at room temperature. The solvent was removed under reduced pressure and the resulting residue re-dissolved in dichloromethane three times to aid the removal of excess acid and *tert*-butyl alcohol. The product was checked by ESMS to confirm complete ester hydrolysis and was used immediately for complexation with gadolinium acetate.

The ligand was dissolved in a mixture of methanol and water (1 : 2, 3 mL) and sonicated. The pH of the solution was raised to 5.5 by the addition of aqueous ammonia solution. Gadolinium acetate (32.7 mg, 0.098 mmol) was added and the reaction mixture was heated at 90 ^{o}C overnight. The reaction mixture was allowed to cool to

room temperature. The pH of the mixture was raised to 10.0 using aqueous ammonia solution and the solution was stirred for 1 h at room temperature to precipitate excess Gd^{3+} as $Gd(OH)_3$. Syringe filtration was used to remove the resulting solid before restoring the pH of the mixture to 5.5 by the addition of glacial acetic acid. The sample was lyophilised to give a yellow oil, which was purified using preparative HPLC. The title complex was obtained as an off-white solid (3.4 mg, 0.004 mmol, 6%). *m/z* ($HRMS^+$) 858.1806 $[M]^+$ ($C_{38}H_{36}N_6O_8{}^{154}Gd$ requires 858.1803); (HPLC) t_R = 5.9 min; λ_{max} (H_2O) 336 nm.

(*S*)-2-Bromopentanedioic acid 5-benzyl ester 1-*tert*-butyl ester[139]

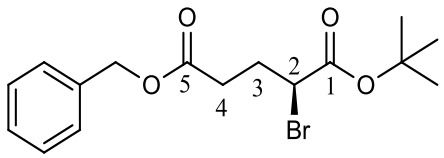

A solution of $NaNO_2$ (5.50 g, 80.1 mmol) in H_2O (50 mL) was added dropwise over 30 min to a stirred solution of (*S*)-glutamic acid 5-benzyl ester (10.0 g, 42.1 mmol) and NaBr (16.0 g, 156 mmol) in 1 M HBr (250 mL), cooled at -5 ^oC. After 16 h, conc. $H_2SO_{4(aq)}$ (5 mL) was slowly added to the reaction mixture, which was then extracted with diethyl ether (3 x 300 mL). The combined organic extracts were washed with brine (2 x 200 mL), dried over magnesium sulfate and filtered. Removal of the solvent under reduced pressure yielded a yellow oil, which was subsequently dissolved in a mixture of *tert*-butyl acetate (50 mL) and $HClO_4$ in H_2O (70%, 0.34 mmol). After the resulting solution had been stirred at room temperature for 16 h, H_2O (60 mL) was added. The organic phase was separated and washed with H_2O (60 mL), followed by 5% $Na_2CO_{3(aq)}$ (60 mL) before being dried over magnesium sulfate and filtered. Removal of the solvent under reduced pressure yielded the crude product, which was purified by column chromatography on silica gel (gradient elution: hexane to 10% EtOAc-hexane) to give the title compound as a yellow oil (1.90 g, 5.32 mmol, 13%). R_f (SiO_2, hexane-EtOAc, 95 : 5) : 0.17; δ_H (400 MHz, $CDCl_3$) 1.46 (9H, s, ^{t}Boc CH_3), 2.18 – 2.27 (1H, m, H^3), 2.30 – 2.39 (1H, m, H^3), 2.47 – 2.59 (2H, m, H^4), 4.24 (1H, dd, *J* = 8.0, 6.0 Hz, H^2), 5.09 (2H, s, CH_2Ph), 7.23 – 7.39 (5H, m, Ar); δ_C (100 MHz, $CDCl_3$) 27.7 (3C, ^{t}Boc CH_3), 29.8 (1C, C^3), 31.6 (1C, C^4), 46.6 (1C, C^2), 66.4 (1C, CH_2Ph), 82.4 (1C, ^{t}Boc$_{(q)}$), 128.2, 128.3, 128.6 (5C, Ar), 135.9 (1C, $Ar_{(q)}$), 168.1 (1C, ^{t}Boc C=O), 171.7 (1C, Cbz C=O); *m/z* ($HRMS^+$) 379.0516 $[M + Na]^+$ ($C_{16}H_{21}{}^{79}BrO_4Na$ requires 379.0521).

2-(1,4,7,10-Tetraaza-cyclododecane-1,7-dicarboxylic acid dibenzyl ester)-pentanedioic acid 5-benzyl ester 1-*tert*-butyl ester

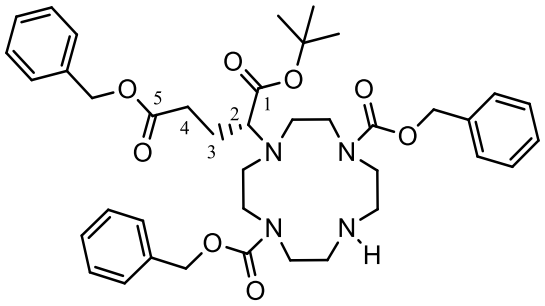

1,4,7,10-Tetraaza-cyclododecane-1,7-dicarboxylic acid dibenzyl ester (1.17 g, 2.66 mmol) was combined with (*S*)-2-bromopentanedioic acid 5-benzyl ester 1-*tert*-butyl ester (1.04 g, 2.92 mmol) and K_2CO_3 (368 mg, 2.66 mmol). The mixture was stirred in anhydrous acetonitrile (10 mL) at reflux for 36 h, under argon. After cooling to room temperature, the solvent was removed under reduced pressure. The resulting residue was dissolved in dichloromethane (20 mL) and the organic solution was then washed with water (3 x 10 mL), to facilitate the removal of KBr/K_2CO_3, before being dried over magnesium sulfate and filtered. Removal of the solvent under reduced pressure yielded the crude product, which was purified by column chromatography on silica gel (gradient elution: CH_2Cl_2 to 5% CH_3OH-CH_2Cl_2) to give the title compound as a yellow oil (740 mg, 1.02 mmol, 39%). R_f (SiO_2, CH_2Cl_2-CH_3OH, 95 : 5) : 0.19; δ_H (400 MHz, $CDCl_3$) 1.46 (9H, s, ^{t}Boc CH_3), 1.64 – 2.43 (5H, m, $H^{2,3,4}$), 2.53 – 2.96 (6H, m, cyclen CH_2), 3.21 – 3.83 (10H, m, cyclen CH_2), 5.09 (6H, s, CH_2Ph), 7.16 – 7.61 (15H, m, Ar); δ_C (100 MHz, $CDCl_3$) 24.7 (1C, C^3), 28.4 (3C, ^{t}Boc CH_3), 30.5 (1C, C^4), 47.7, 48.1, 49.3, 49.8, 50.4, 50.8, 51.6 (8C, cyclen CH_2), 60.1 (1C, C^2), 66.3, 67.4, 67.6 (3C, CH_2Ph), 81.4 (1C, ^{t}Boc$_{(q)}$), 128.1, 128.3, 128.4, 128.5, 128.6 (15C, Ar), 136.2, 136.5, 136.7 (3C, Ar$_{(q)}$), 156.8 (2C,Cbz C=O), 171.1 (1C, C^1), 172.9 (1C, C^5); *m/z* (HRMS$^+$) 717.3862 $[M + H]^+$ ($C_{40}H_{53}N_4O_8$ requires 717.3863).

2- (7 - *tert* - Butoxycarbonylmethyl- 1,4,7,10 - tetraaza - cyclododecane -4,10-dicarboxylic acid dibenzyl ester)-pentanedioic acid 5-benzyl ester 1-*tert*-butyl ester

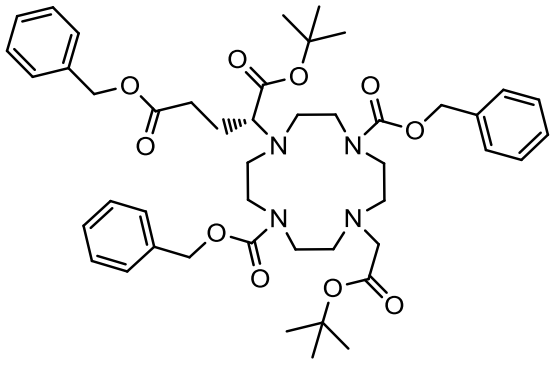

Caesium carbonate (526 mg, 1.61 mmol) and *tert*-butyl bromoacetate (252 mg, 1.29 mmol) were added to a solution of 2-(1,4,7,10-tetraaza-cyclododecane-1,7-dicarboxylic acid dibenzyl ester)-pentanedioic acid 5-benzyl ester 1-*tert*-butyl ester (771 mg, 1.08 mmol) in anhydrous acetonitrile (10 mL). The reaction mixture was stirred at reflux for 18 h under argon. After this time the reaction mixture was allowed to cool to room temperature and the solvent was removed under reduced pressure. The resulting residue was dissolved in dichloromethane (20 mL) and the organic solution was washed with water (3 x 10 mL), to facilitate the removal of caesium salts, before being dried over magnesium sulfate and filtered. Removal of the solvent under reduced pressure yielded the crude product, which was purified by column chromatography on silica gel (gradient elution: CH_2Cl_2 to 1.5% CH_3OH-CH_2Cl_2) to give the title compound as a yellow oil (590 mg, 0.71 mmol, 66%). R_f (SiO_2, CH_2Cl_2-CH_3OH, 95 : 5) : 0.59; δ_H (400 MHz, $CDCl_3$) 1.45 (18H, s, ^{t}Boc CH_3), 1.64 – 2.41 (5H, m, $H^{2,3,4}$), 2.63 – 2.98 (6H, m, cyclen CH_2), 2.99 – 3.68 (12H, m, cyclen CH_2; CH_2CO), 5.01 – 5.21 (6H, m, CH_2Ph), 7.20 – 7.46 (15H, m, Ar); δ_C (100 MHz, $CDCl_3$) 25.3 (1C, C^3), 28.2 (6C, ^{t}Boc CH_3), 30.8 (1C, C^4), 47.3, 48.2, 52.0 (8C, cyclen CH_2), 54.5 (1C, CH_2CO), 56.1 (1C, C^2), 66.2, 67.1, 68.6 (3C, CH_2Ph), 81.0, 81.2 (2C, ^{t}Boc$_{(q)}$), 128.0, 128.1, 128.2, 128.3, 128.5, 128.6 (15C, Ar), 136.2 (1C, Ar$_{(q)}$), 136.9 (2C, Ar$_{(q)}$), 156.6 (2C,Cbz C=O), 170.2 (1C, ^{t}Boc C=O), 172.0 (1C, ^{t}Boc C=O), 173.0 (1C, C^5); *m/z* (HRMS$^+$) 831.4559 $[M + H]^+$ ($C_{46}H_{63}N_4O_{10}$ requires 831.4544).

2-(7-*tert*-Butoxycarbonylmethyl-1,4,7,10-tetraaza-cyclododecane)-pentanedioic acid 1-*tert*-butyl ester

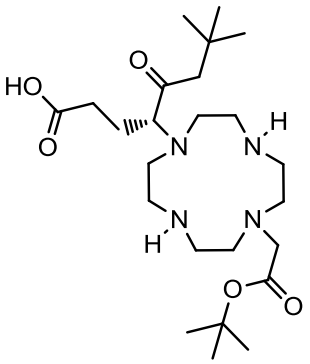

2- (4 - *tert* - Butoxycarbonylmethyl- 1,4,7,10 - tetraaza - cyclododecane -1,7-dicarboxylic acid dibenzyl ester)-pentanedioic acid 5-benzyl ester 1-*tert*-butyl ester (581 mg, 0.70 mmol) in EtOH (15 mL) was shaken in a Parr hydrogenation flask at 40 psi over $Pd(OH)_2/C$ (150 mg) for 24 h. The resulting mixture was filtered through celite to give a colourless solution. The solvent was removed under reduced pressure, yielding the desired product as a yellow oil (333 mg, 0.70 mmol, 100%); δ_H (700 MHz, $CDCl_3$) 1.39 (18H, s, ^{t}Boc CH_3), 1.90 – 1.96 (2H, br m, H^3), 2.29 (2H, d, J = 5.5 Hz, H^4), 2.69 – 2.99 (16H, m, cyclen CH_2), 3.18 (1H, d, J = 8.5 Hz, H^2), 3.30 (1H, d, J = 17.5 Hz, CH_2CO), 3.38 (1H, d, J = 17.5 Hz, CH_2CO), 7.80 (3H, br s, OH; 2 x NH); δ_C (176 MHz, $CDCl_3$) 25.9 (1C, C^3), 28.1 (6C, ^{t}Boc CH_3), 33.8 (1C, C^4), 46.6, 46.8, 51.3 (8C, cyclen CH_2), 56.8 (1C, CH_2CO), 65.2 (1C, C^2), 81.3, 81.8 (2C, ^{t}Boc$_{(q)}$), 170.9 (1C, CH_2CO), 171.8 (1C, C^1), 178.6 (1C, C^5); *m/z* ($HRMS^+$) 473.3316 $[M + H]^+$ ($C_{23}H_{45}N_4O_6$ requires 473.3339).

2-(7-*tert*-Butoxycarbonylmethyl-1,4,7,10-tetraaza-cyclododecane)-pentanedioic acid 5-methyl ester 1-*tert*-butyl ester

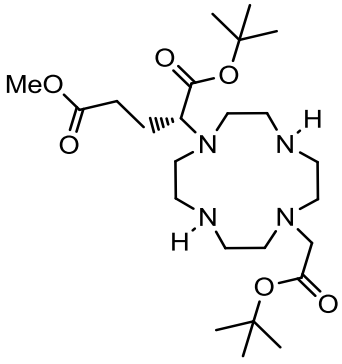

2-(4-*tert*-Butoxycarbonylmethyl-1,4,7,10-tetraaza-cyclododecane)-pentanedioic acid 1-*tert*-butyl ester (282 mg, 0.60 mmol) was dissolved in methanol (5 mL) and the pH of

the solution was adjusted to 0 by the addition of conc. $HCl_{(aq)}$. The reaction mixture was left to stir at room temperature for 1 h and the solvent was removed under reduced pressure. The resulting residue was dissolved in dichloromethane (5 mL) and washed with saturated $NaHCO_{3(aq)}$ solution (10 mL) before being dried over magnesium sulfate and filtered. Removal of the solvent under reduced pressure yielded the title compound as a yellow oil (137 mg, 0.28 mmol, 47%); δ_H (700 MHz, $CDCl_3$) 1.42 (18H, s, ^{t}Boc CH_3), 1.85 – 1.92 (1H, m, H^3), 1.99 – 2.06 (1H, m, H^3), 2.38 - 2.54 (6H, m, H^4; cyclen CH_2), 2.62 – 2.88 (12H, m, cyclen CH_2), 3.22 - 3.34 (3H, m, H^2; CH_2CO), 3.63 (3H, s, CO_2Me); δ_C (176 MHz, $CDCl_3$) 24.8 (1C, C^3), 28.0 (6C, ^{t}Boc CH_3), 30.7 (1C, C^4), 46.1, 46.2, 49.5, 52.1 (8C, cyclen CH_2), 51.5 (1C, CO_2Me), 57.0 (1C, **C**H_2CO), 63.4 (1C, C^2), 80.8, 81.1 (2C, ^{t}Boc$_{(q)}$), 170.8 (1C, CH_2**C**O), 171.6 (1C, C^1), 173.5 (1C, C^5); *m/z* ($HRMS^+$) 487.3503 $[M + H]^+$ ($C_{24}H_{47}N_4O_6$ requires 487.3496).

2-(4,10-[2-Methyl-1-azaxanthone]-7-*tert*-butoxycarbonylmethyl-1,4,7,10-tetraaza-cyclododecane)-pentanedioic acid 5- methyl ester 1-*tert*-butyl ester

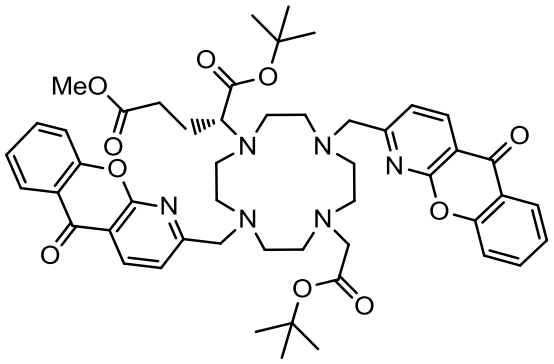

Caesium carbonate (184 mg, 0.56 mmol) and 2-methyl-1-azaxanthone (171 mg, 0.59 mmol) were added to a solution of 2-(7-*tert*-butoxycarbonylmethyl-1,4,7,10-tetraaza-cyclododecane)-pentanedioic acid 5-methyl ester 1-*tert*-butyl ester (137 mg, 0.28 mmol) in anhydrous acetonitrile (5 mL). The reaction mixture was stirred at reflux for 18 h under argon. After this time the reaction mixture was allowed to cool to room temperature and filtered to facilitate the removal of caesium salts. Removal of the solvent under reduced pressure yielded the crude product. Column chromatography on silica gel (gradient elution: CH_2Cl_2 to 5% CH_3OH-CH_2Cl_2) allowed isolation of a yellow oil containing the title compound (107.9 mg, 0.12 mmol, 20%). R_f (SiO_2, CH_2Cl_2-CH_3OH, 95 : 5) : 0.05; *m/z* ($HRMS^+$) 905.4443 $[M + H]^+$ ($C_{50}H_{61}N_6O_{10}$ requires 905.4449). This compound was used directly in the following complexation reaction, without further purification.

(*R*)-[Eu.L^{23}(OH$_2$)]$^+$

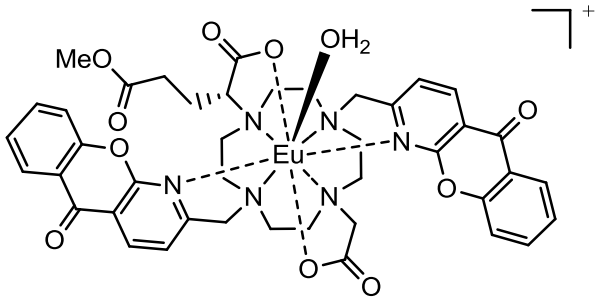

Trifluoroacetic acid (1 mL) was added to a solution of crude 2-(4,10-[2-methyl-1-azaxanthone] - 7 - *tert* - butoxycarbonylmethyl - 1,4,7,10 - tetraaza - cyclododecane) - pentanedioic acid 5-methyl ester 1-*tert*-butyl ester (21.4 mg, 0.024 mmol) in dichloromethane (0.5 mL). The mixture was left for 48 h at room temperature. The solvent was removed under reduced pressure and the resulting residue re-dissolved in dichloromethane three times to aid the removal of excess acid and *tert*-butyl alcohol. The product was checked by LCMS after 18 h and 36 h to confirm complete ester hydrolysis, after 48 h the signal relating to the unhydrolysed ligand (t_R = 2.64 min) had disappeared completely from the LCMS trace and a new signal had appeared relating to the hydrolysed ligand (t_R = 2.13 min). The product was used immediately for complexation with europium chloride.

The ligand was dissolved in a mixture of methanol and water (1 : 2, 3 mL) and sonicated. The pH of the solution was raised to 5.5 by the addition of a 1 M solution of $KOH_{(aq)}$. $EuCl_3.6H_2O$ (8.67 mg, 0.024 mmol) was added and the reaction mixture was heated at 90 ^oC overnight. Emission spectroscopy was used to ascertain whether complexation was complete before allowing the reaction mixture to cool to room temperature. The pH of the mixture was raised to 10.0 using dilute $KOH_{(aq)}$ and the solution was stirred for 1 h at room temperature to precipitate excess Eu^{3+} as $Eu(OH)_3$. Centrifugation was used to remove the resulting solid before restoring the pH of the mixture to 5.5 by the addition of dilute $HCl_{(aq)}$. Removal of the solvent under reduced pressure gave a yellow solid which was lyophilised to give a crude mixture. The crude mixture was purified using preparative HPLC, yielding the title complex as an off-white solid (2.0 mg, 0.002 mmol, 9%). *m/z* (HRMS$^+$) 941.2178 $[M + H]^+$ ($C_{42}H_{42}N_6O_{10}Eu$ requires 941.2161); (HPLC) t_R = 10.9 min; λ_{max} (H_2O) 336 nm; $\tau(H_2O)$ = 0.47 ms; $\tau(D_2O)$ = 1.42 ms.

(*R*)-[Tb.L^{23}(OH$_2$)]$^+$

An analogous procedure to that described for the synthesis of (*R*)-[Eu.**L**^{23}(OH$_2$)]$^+$ was followed, using $TbCl_3.6H_2O$ (8.83 mg. 0.024 mmol) in place of $EuCl_3.6H_2O$. The title complex was isolated as an off-white solid, following preparative HPLC (2.0 mg, 0.002 mmol, 9%). *m/z* (HRMS$^+$) 949.2249 $[M + H]^+$ ($C_{42}H_{42}N_6O_{10}Tb$ requires 949.2216); (HPLC) t_R = 11.1 min; λ_{max} (H_2O) 336 nm; $\tau(H_2O)$ = 1.82 ms; $\tau(D_2O)$ = 3.17 ms.

5.2.2 Triazacyclononane-based complexes and precursors

***N'*-(2-Aminoethyl)-*L*-phenylalaninamide**[200, 201]

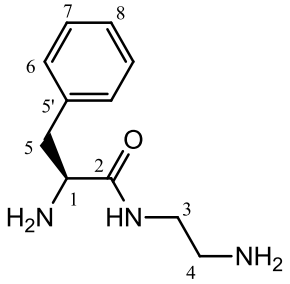

L-Phenylalanine ethyl ester hydrochloride (3.30 g, 14.4 mmol) was added in small portions over 1 h to stirred ethylenediamine (30 mL) at 90 ^oC under an atmosphere of argon. The reaction mixture was heated at 120 ^oC for 3 h. Excess ethylenediamine was removed by distillation under reduced pressure, yielding an orange oil to which $NaOH_{(aq)}$ (4 M, 6 mL) was added. The solvent was removed under reduced pressure and the resulting residue dissolved in methanol (15 mL) before being filtered under vacuum. Dichloromethane (15 mL) was added to the resulting filtrate, which was subsequently filtered through celite. Removal of the solvent under reduced pressure yielded a gritty yellow oil, which was redissolved in dichloromethane (30 mL) and filtered through celite for a second time. This process was repeated once more, giving the title compound as a 'grit-free' yellow oil (2.42 g, 11.7 mmol, 81%). ν_{max} / cm^{-1} 3287 (amide N-H stretch), 2924 (C-H stretch), 1648 (C=O stretch); δ_H (600 MHz, $CDCl_3$) 1.59 (4H, br s, 2 x NH_2), 2.74 (1H, dd, *J* = 13.5, 9.0 Hz, H^5), 2.79 (2H, t, *J* = 6.0 Hz, H^4), 3.23 (1H, dd, *J* = 13.5, 4.5 Hz, H^5), 3.25 – 3.33 (2H, m, H^3), 3.61 (1H, dd, *J* = 9.0, 4.5 Hz, H^1), 7.17 – 7.34 (5H, m, Ar), 7.47 (1H, br s, NH); δ_C (151 MHz, $CDCl_3$); 41.1 (1C, C^5), 41.4 (1C, C^4), 41.8 (1C, C^3), 56.5 (1C, C^1), 126.7 (1C, C^8), 128.6 (2C, C^7), 129.2 (2C, C^6), 137.8 (1C, C$^{5'}$), 174.5 (1C, C=O); *m/z* (HRMS$^+$) 208.1442 $[M + H]^+$ ($C_{11}H_{18}N_3O$ requires 208.1450).

N'-(2-Aminoethyl)-*D*-phenylalaninamide[200, 201]

The title compound was prepared using an analogous procedure to that described for *N'*-(2-aminoethyl)-*L*-phenylalaninamide. The starting material, *L*-phenylalanine ethyl ester hydrochloride, was replaced by *D*-phenylalanine methyl ester hydrochloride (4.10 g, 19.0 mmol). The title compound was isolated as a yellow oil (3.52 g, 16.9 mmol, 89%). Spectroscopic characteristics were identical to those observed for the *L* isomer.

(*S*)-*N'*-(2-Aminoethyl)-1-benzylethane-1,2-diamine[201]

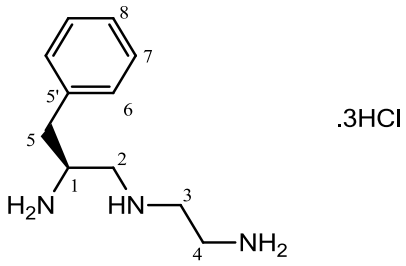

A solution of BH_3.THF in THF (1M, 100 mL) was added to *N'*-(2-aminoethyl)-*L*-phenylalaninamide (2.40 g, 11.6 mmol) in a flask at 0 ^oC under a flowing stream of argon. The resulting reaction mixture was allowed to warm to room temperature then stirred under argon at 70 ^oC for 24 h. After this time, a small sample of the reaction mixture was taken and IR spectroscopy used to confirm that the reaction had reached completion. The remainder of the reaction mixture was quenched by addition of methanol (15 mL) at 0 ^oC. Removal of the solvent under reduced pressure yielded a white residue, which was stirred at reflux in $HCl_{(aq)}$ (2 M, 75 mL) for 18 h. The reaction mixture was allowed to cool to room temperature and the solvent was removed by co-evaporation with methanol, giving the title compound as a highly hygroscopic, white solid (2.20 g, 7.3 mmol, 63%). ν_{max}/cm^{-1} 2927 (C-H stretch); δ_H (600 MHz, D_2O) 2.92 (1H, dd, *J* = 14.0, 8.5 Hz, H^5), 3.09 (1H, dd, *J* = 14.0, 6.0 Hz, H^5), 3.25 – 3.47 (6H, m, $H^{2,3,4}$), 3.85 – 3.90 (1H, m, H^1), 7.23 – 7.24 (2H, m, H^6), 7.27 – 7.29 (1H, m, H^8), 7.32 – 7.34 (2H, m, H^7); δ_C (151 MHz, D_2O) 35.3 (1C, C^4), 36.3 (1C, C^5), 45.0 (1C, C^3), 49.0 (1C, C^2), 49.8 (1C, C^1), 128.2 (1C, C^8), 129.4 (4C, $C^{6,7}$), 133.6 (1C, $C^{5'}$); *m/z* ($HRMS^+$) 194.1651 $[M + H]^+$ ($C_{11}H_{20}N_3$ requires 194.1657).

(*R*)-*N'*-(2-Aminoethyl)-1-benzylethane-1,2-diamine[201]

The title compound was prepared using an analogous procedure to that described for (*S*)-*N'*-(2-Aminoethyl)-1-benzylethane-1,2-diamine. The starting material, *N'*-(2-aminoethyl)-*L*-phenylalaninamide, was replaced by *N'*-(2-aminoethyl)-*D*-

phenylalaninamide (2.26 g, 10.9 mmol). The title compound was isolated as a yellow oil (3.22 g, 10.7 mmol, 98%). Spectroscopic characteristics were identical to those observed for the *L* isomer.

(*S*)-1-*N'*-1-Benzyl - 1, 5 - bistoluene - *p* - sulfonamido - 3 - toluene - *p* - sulphonyl - 3 - azapentane

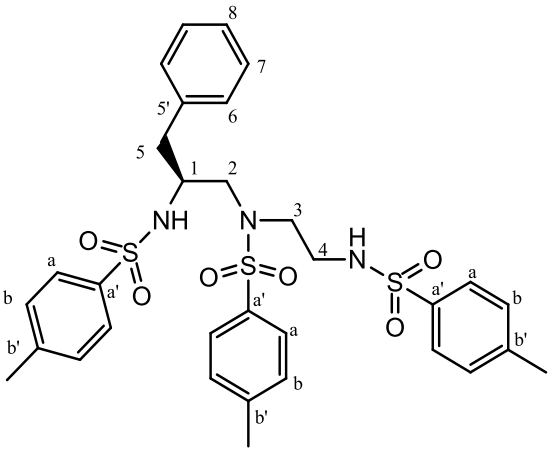

A solution of *p*-toluenesulfonyl chloride (2.52 g, 13.2 mmol) in dry dichloromethane (50 mL) was added dropwise to a solution of (*S*)-*N'*-(2-aminoethyl)-1-benzylethane-1,2-diamine (1.14 g, 3.8 mmol) and triethylamine (3.43 g, 4.8 mL, 34.0 mmol) in dry dichloromethane (75 mL) over 1 h under an atmosphere of argon. The reaction mixture was stirred under argon for 16 h. The resulting organic phase was washed with H_2O (3 x 90 mL) and the solvent removed under reduced pressure, yielding the crude product as a brown oil. The crude product was subsequently purified by column chromatography on silica gel (gradient elution: CH_2Cl_2 to 5% EtOAc-CH_2Cl_2) to give the title compound as a white solid (0.78 g, 1.2 mmol, 31%). m.p. 100.5-101 ^oC; R_f (SiO_2, CH_2Cl_2-EtOAc, 95 : 5) : 0.42; δ_H (700 MHz, $CDCl_3$) 2.33 - 2.36 (9H, m, 3 x CH_3), 2.52 (1H, dd, *J* = 14.0, 8.0 Hz, H^5), 2.79 (1H, dd, *J* = 14.0, 6.0 Hz, H^5), 2.97 – 3.08 (4H, m, $H^{2,3,4}$), 3.12 (1H, dd, *J* = 13.5, 6.5 Hz, H^3), 3.22 (1H, dd, *J* = 14.5, 6.5 Hz, H^2), 3.59 – 3.64 (1H, m, H^1), 5.33 (1H, d, *J* = 6.5 Hz, NH), 5.58 (1H, t, *J* = 6.0 Hz, CH_2*NH*), 6.88 (2H, d, *J* = 7.0 Hz, H^6), 7.05 – 7.10 (5H, m, $H^{7, 8, b}$), 7.21 – 7.25 (4H, m, H^b), 7.52 (4H, d, *J* = 8.0 Hz, H^a), 7.71 (2H, d, *J* = 8.0 Hz, H^a); δ_C (176 MHz, $CDCl_3$) 21.5 (3C, 3 x CH_3), 38.7 (1C, C^5), 42.3 (1C, C^4), 50.9 (1C, C^3), 54.6 (2C, $C^{1, 2}$), 126.5 (1C, C^8), 127.0, 127.1, 127.4 (6C, C^a), 128.5 (2C, C^7), 129.1 (2C, C^6), 129.7, 129.8, 129.9 (6C, C^b), 134.4 (1C, $C^{a'}$), 136.5 (2C, $C^{a',5'}$), 136.8 (1C, $C^{a'}$), 143.2, 143.4, 144.0 (3C, $C^{b'}$); *m/z* ($HRMS^+$) 678.1744 $[M + Na]^+$ ($C_{32}H_{37}N_3O_6S_3Na$ requires 678.1742).

(*R*)-1-*N'*-1-Benzyl - 1, 5 - bistoluene - *p* - sulfonamido - 3 - toluene - *p* - sulphonyl - 3 - azapentane

The title compound was prepared using an analogous procedure to that described for (*S*)-1-*N'*-1-benzyl-1,5-bistoluene-*p*-sulfonamido-3-toluene-*p*-sulphonyl-3-azapentane. The starting material, (*S*)-*N'*-(2-aminoethyl)-1-benzylethane-1,2-diamine, was replaced by (*R*)-*N'*-(2-aminoethyl)-1-benzylethane-1,2-diamine (1.44 g, 4.8 mmol). The title compound was isolated as a white solid (1.24 g, 1.9 mmol, 40%). Spectroscopic characteristics were identical to those observed for the (*S*) isomer.

(*S*)-2-Benzyl-1,4,7-tris(toluene-*p*-sulphonyl)-1,4,7-triazacyclononane

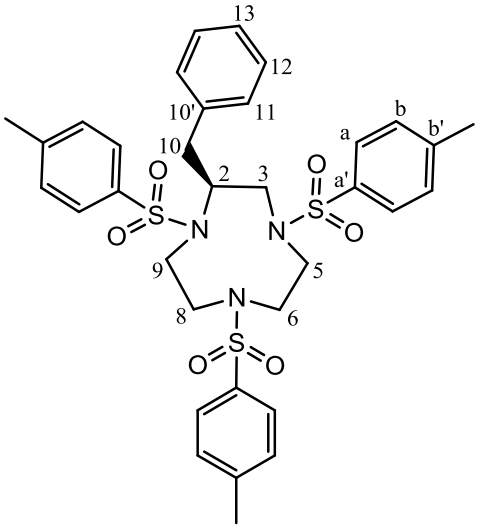

A solution of ethylene glycol bis(toluene-*p*-sulphonate) (235 mg, 0.63 mmol) in anhydrous DMF (14 mL) was added dropwise over 1 h to a stirred solution of (*S*)-1-*N'*-1-benzyl-1, 5-bistoluene-*p*-sulfonamido-3-toluene-*p*-sulphonyl-3-azapentane (396 mg, 0.60 mmol) and caesium carbonate (591 mg, 1.81 mmol) in anhydrous DMF (27 mL), at room temperature. After 16 h, the temperature was increased to 65 ^{o}C and the reaction mixture was heated at this temperature for 5 h before being allowed to cool to room temperature. Removal of the solvent under reduced pressure yielded a yellow residue, which was redissolved in chloroform (40 mL) and washed with H_2O (2 x 30 mL), before being dried over magnesium sulfate and filtered. Removal of the solvent under reduced pressure yielded the crude product, which was purified by column chromatography on silica gel (gradient elution: CH_2Cl_2 to 2% EtOAc-CH_2Cl_2) to give the title compound as a white solid (0.34 g, 0.50 mmol, 82%). m.p. 116.5-119 ^{o}C; R_f (SiO_2, CH_2Cl_2) : 0.13; δ_H (700 MHz, $CDCl_3$) 2.35 (3H, s, CH_3), 2.38 (3H, s, CH_3), 2.41 (3H, s, CH_3), 2.54 (1H, br s, H^{10}), (second H^{10} proton is obscured under CH_3 singlets), 2.88 – 3.32 (6H, m, ring CH_2's), 3.56 – 3.84 (4H, m, ring CH_2's), 4.73 (1H, br s, H^2),

7.04 – 7.13 (4H, m, $H^{a, b}$) 7.15 (2H, d, *J* = 7.5 Hz, H^{11}), 7.29 – 7.33 (5H, m, $H^{b, 13}$), 7.34 (2H, t, *J* = 7.5 Hz, H^{12}), 7.62 (2H, d, *J* = 8.0 Hz, H^{a}), 7.84 (2H, d, *J* = 8.0 Hz, H^{a}); δ_C (176 MHz, $CDCl_3$) 21.4, 21.5 (3C, 3 x CH_3), 36.4 (1C, C^{10}), 46.1, 50.9, 53.5, 53.6 (4C, $C^{5, 6, 8, 9}$), 54.7 (1C, C^{3}), 60.2 (1C, C^{2}), 126.7 (1C, C^{13}), 127.3, 127.5 (3C, C^{a}), 128.7 (2C, C^{12}), 129.3 (2C, C^{11}), 129.6, 129.9, 130.0 (3C, C^{b}), 133.6, 134.2, 137.0, 137.1 (4C, $C^{a', 10'}$), 143.4, 143.8, 144.2 (3C, $C^{b'}$); *m/z* ($HRMS^+$) 682.2087 $[M + H]^+$ ($C_{34}H_{40}N_3O_6S_3$ requires 682.2079).

(*R*)-2-Benzyl-1,4,7-tris(toluene-*p*-sulphonyl)-1,4,7-triazacyclononane

The title compound was prepared using an analogous procedure to that described for (*S*)-2-benzyl-1,4,7-tris(toluene-*p*-sulphonyl)-1,4,7-triazacyclononane. The starting material, (*S*)-1-*N'*-1-benzyl-1, 5-bistoluene-*p*-sulfonamido-3-toluene-*p*-sulphonyl-3-azapentane, was replaced by (*R*)-1-*N'*-1-benzyl-1, 5-bistoluene-*p*-sulfonamido-3-toluene-*p*-sulphonyl-3-azapentane (0.93 g, 1.4 mmol). The title compound was isolated as a white solid (0.65 g, 1.0 mmol, 70%). Spectroscopic characteristics were identical to those observed for the (*S*) isomer.

(*S*)-2-Benzyl-1,4,7-triazacyclononane

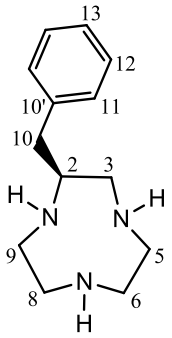

Ammonia (30 mL) was condensed into a solution of (*S*)-2-benzyl-1,4,7-tris(toluene-*p*-sulphonyl)-1,4,7-triazacyclononane (350 mg, 0.51 mmol) in a mixture of anhydrous THF (15 mL) and anhydrous ethanol (1 mL) whilst stirring under argon at -78 ^{o}C. Sodium (580 mg, excess) was added in small portions to the solution and a strong blue colour developed. The solution was slowly warmed to RT overnight; during this period the solution evaporated to leave a white solid. The white solid was dissolved in ethanol (10 mL) and water (15 mL) and the solvent removed under reduced pressure. The resulting residue was dissolved in $HCl_{(aq)}$ (2 M, 15 mL) and washed with diethyl ether (2 x 15 mL). The aqueous layer was concentrated, and the resulting off-white solid was dissolved in KOH solution (6 M, 15 mL) and extracted with dichloromethane (3 x 15

mL). The organic layer was concentrated to give a colourless oil containing the title compound (102 mg, 0.46 mmol, 91%). δ_H (400 MHz, $CDCl_3$) 1.75 (3H, br s, 3 x NH), 2.37 – 2.47 (2H, m, H^{10}), 2.50 – 2.81 (10 H, br m, ring CH_2's), 2.86 – 2.96 (1H, m, H^2), 7.09 – 7.25 (5H, m, Ar); δ_C (101 MHz, $CDCl_3$) 40.7 (1C, C^{10}), 43.7, 45.4, 46.6, 47.3, 49.9 (5C, $C^{3, 5, 6, 8, 9}$), 57.6 (1C, C^2), 126.3 (1C, C^{13}), 128.5 (2C, C^{12}), 129.1 (2C, C^{11}), 139.0 (1C, $C^{10'}$); *m/z* ($HRMS^+$) 220.1815 $[M + H]^+$ ($C_{13}H_{22}N_3$ requires 220.1814). This compound was used directly in the subsequent reaction, without further purification.

(*R*)-2-Benzyl-1,4,7-triazacyclononane

The title compound was prepared using an analogous procedure to that described for (*S*)-2-Benzyl-1,4,7-triazacyclononane. The starting material, (*S*)-2-benzyl-1,4,7-tris(toluene-*p*-sulphonyl)-1,4,7-triazacyclononane, was replaced by (*R*)-2-benzyl-1,4,7-tris(toluene-*p*-sulphonyl)-1,4,7-triazacyclononane (0.66 g, 1.0 mmol). The title compound was isolated as a yellow oil (0.20 g, 0.93 mmol, 96%). Spectroscopic characteristics were identical to those observed for the (*S*) isomer.

Ethyl methylphosphinate[181]

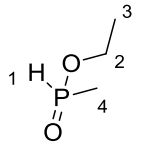

Neat diethyl methylphosphonite (2 g, 14.7 mmol) was stirred under argon at RT and H_2O (264 μL, 14.7 mmol) was added. The mixture was stirred at RT for 18 h. ^{1}H- and ^{31}P-NMR spectroscopy were used to confirm the formation of the title compound, which was subsequently used *in situ* without further purification. The reaction mixture also contained one equivalent of ethanol as a by-product (100% conversion by ^{1}H-NMR spectroscopy). δ_H (400 MHz, $CDCl_3$) 1.37 (3H, t, $^3J_{H\text{-}H}$ = 7.0 Hz, H^3), 1.54 (3H, dd, $^2J_{H\text{-}P}$ = 15.0 Hz $^3J_{H\text{-}H}$ = 2.0 Hz, H^4), 4.01 – 4.24 (2H, m, H^2), 7.22 (1H, dq, $^1J_{H\text{-}P}$ = 537 Hz, $^3J_{H\text{-}H}$ = 2.0 Hz); δ_P (162 MHz, $CDCl_3$) +32.5; *m/z* ($HRMS^+$) 131.0246 $[M + Na]^+$ ($C_3H_9O_2PNa$ requires 131.0238).

Ethyl (6-methylpyridin-2-yl)(methyl)phosphinate[181]

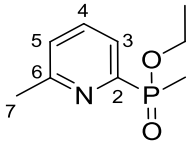

Toluene (20 mL), 2-bromo-6-methylpyridine (2.10 g, 12.3 mmol) and triethylamine (4.35 g, 43 mmol) were added to neat ethyl methylphosphinate (1.59 g, 14.7 mmol), containing one equivalent of ethanol. Argon was bubbled through the solution for 30 min prior to the addition of $PdCl_2(dppf)\cdot CH_2Cl_2$ (0.22 g, 0.27 mmol). The reaction mixture was stirred at 125 ^oC for 16 h under argon. Once cooled to room temperature, the solvent was removed under reduced pressure. The crude product was purified by column chromatography on silica gel (gradient elution: EtOAc-Hexane, 50 : 50, to EtOAc-Hexane, 80 : 20) to give the title compound as a brown oil (1.63 g, 8.21 mmol, 67%). R_f (SiO_2, EtOAc-Hexane, 75 : 25) : 0.10; δ_H (700 MHz, $CDCl_3$) 1.06 (3H, t, $^3J_{H\text{-}H}$ = 7.0 Hz, $OCH_2\mathit{CH_3}$), 1.57 (3H, d, $^2J_{H\text{-}P}$ = 15.0 Hz, $P\mathit{CH_3}$), 2.41 (3H, s, H^7), 3.60 – 3.97 (2H, m, $O\mathit{CH_2}CH_3$), 7.09 (1H, d, $^3J_{H\text{-}H}$ = 8.0 Hz, H^5), 7.51 (1H, td, $^3J_{H\text{-}H}$ = 8.0 Hz $^4J_{H\text{-}P}$ = 4.5 Hz, H^4), 7.67 (1H, t, $^3J_{H\text{-}H}$ = 8.0 Hz, H^3); δ_C (100 MHz, $CDCl_3$) 13.0 (1C, d, $^1J_{C\text{-}P}$ = 103.5 Hz, $P\mathit{CH_3}$), 16.0 (1C, d, $^3J_{C\text{-}P}$ = 6.5 Hz, $OCH_2\mathit{CH_3}$), 24.1 (1C, s, C^7), 60.4 (1C, d, $^2J_{C\text{-}P}$ = 6.0 Hz, $O\mathit{CH_2}CH_3$), 124.2 (1C, d, $^2J_{C\text{-}P}$ = 21.5 Hz, C^3), 125.3 (1C, d, $^4J_{C\text{-}P}$ = 3.0 Hz, C^5), 135.7 (1C, d, $^3J_{C\text{-}P}$ = 10.0 Hz, C^4), 153.3 (1C, d, $^1J_{C\text{-}P}$ = 158.5 Hz, C^2), 159.0 (1C, d, $^3J_{C\text{-}P}$ = 20.0 Hz, C^6); δ_P (162 MHz, $CDCl_3$) +39.0; *m/z* ($HRMS^+$) 200.0824 $[M + H]^+$ ($C_9H_{15}NO_2P$ requires 200.0840).

Ethyl (6-methyl-1-oxo-pyridin-2-yl)(methyl)phosphinate[181]

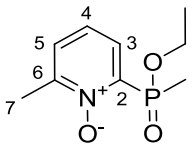

3-Chloroperbenzoic acid (3.21 g, 18.6 mmol) was added to a solution of ethyl (6-methylpyridin-2-yl)(methyl)phosphinate (1.85 g, 9.3 mmol) in anhydrous chloroform (40 mL). The reaction mixture was stirred at reflux for 18 h under argon. After this time the reaction mixture was allowed to cool to room temperature and the solvent was removed under reduced pressure. The resulting residue was dissolved in dichloromethane (50 mL) and the organic solution was washed with 0.5 M $NaHCO_3$ (30 mL) and then extracted with dichloromethane (50 mL). The organic extracts were subsequently combined with the original organic solution, dried over magnesium sulfate

and filtered. Removal of the solvent under reduced pressure yielded the crude product, which was purified by column chromatography on silica gel (gradient elution: CH_2Cl_2 to 2% CH_3OH-CH_2Cl_2) to give the title compound as a yellow oil (1.46 g, 6.8 mmol, 73%). R_f (SiO_2, CH_2Cl_2-CH_3OH, 95 : 5) : 0.23; δ_H (400 MHz, $CDCl_3$) 1.16 (3H, t, $^3J_{H\text{-}H}$ = 7.0 Hz, $OCH_2\mathit{CH_3}$), 1.84 (3H, d, $^2J_{H\text{-}P}$ = 16.5 Hz, $P\mathit{CH_3}$), 2.37 (3H, s, H^7), 3.73 – 4.09 (2H, m, $O\mathit{CH_2}CH_3$), 7.15 (1H, td, $^3J_{H\text{-}H}$ = 8.0 Hz, $^4J_{H\text{-}P}$ = 2.0 Hz, H^4), 7.29 – 7.35 (1H, m, H^5), 7.77 (1H, td, $^3J_{H\text{-}H}$ = 8.0 Hz, $^3J_{H\text{-}P}$ = 2.0 Hz, H^3); δ_C (101 MHz, $CDCl_3$) 14.1 (1C, d, $^1J_{C\text{-}P}$ = 111.0 Hz, $P\mathit{CH_3}$), 16.0 (1C, d, $^3J_{C\text{-}P}$ = 6.0 Hz, $OCH_2\mathit{CH_3}$), 17.0 (1C, s, C^7), 61.2 (1C, d, $^2J_{C\text{-}P}$ = 7.0 Hz, $O\mathit{CH_2}CH_3$), 123.9 (1C, d, $^3J_{C\text{-}P}$ = 9.5 Hz, C^4), 129.0 (1C, d, $^4J_{C\text{-}P}$ = 1.5 Hz, C^5), 129.9 (1C, d, $^2J_{C\text{-}P}$ = 10.5 Hz, C^3), 142.2 (1C, d, $^1J_{C\text{-}P}$ = 141.0 Hz, C^2), 149.2 (1C, d, $^3J_{C\text{-}P}$ = 3.5 Hz, C^6); δ_P (162 MHz, $CDCl_3$) +33.0; *m/z* ($HRMS^+$) 238.0608 $[M + Na]^+$ ($C_9H_{14}NO_3PNa$ requires 238.0609).

Ethyl [6-(hydroxymethyl)pyridin-2-yl](methyl)phosphinate[181]

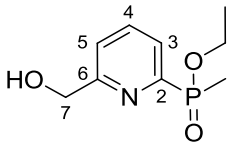

Trifluoroacetic anhydride (5 mL, 36.0 mmol) was added to a solution of ethyl (6-methyl-1-oxo-pyridin-2-yl)(methyl)phosphinate (1.46 g, 6.8 mmol) in anhydrous chloroform (40 mL). The reaction mixture was stirred at 60 °C for 18 h under argon and was subsequently allowed to cool to room temperature. The solvent was removed under reduced pressure and ^1H NMR spectroscopy used to confirm full conversion to the trifluoroacetate analogue of the title compound. The residue was dissolved in aqueous ethanol (50%, 35 mL) and stirred at 60 °C for 6 h. Removal of the solvent under reduced pressure yielded the crude product, which was purified by column chromatography on silica gel (gradient elution: CH_2Cl_2 to 4% CH_3OH-CH_2Cl_2) to give the title compound as a yellow oil (1.35 g, 6.3 mmol, 92%). R_f (SiO_2, CH_2Cl_2-CH_3OH, 95 : 5) : 0.31; δ_H (400 MHz, $CDCl_3$) 1.17 (3H, t, $^3J_{H\text{-}H}$ = 7.0 Hz, $OCH_2\mathit{CH_3}$), 1.68 (3H, d, $^2J_{H\text{-}P}$ = 15.0 Hz, $P\mathit{CH_3}$), 3.69 – 4.08 (2H, m, $O\mathit{CH_2}CH_3$), 4.76 (2H, s, $\mathit{CH_2}OH$), 7.47 (1H, d, $^3J_{H\text{-}H}$ = 8.0 Hz, H^5), 7.75 (1H, td, $^3J_{H\text{-}H}$ = 8.0 Hz, $^4J_{H\text{-}P}$ = 4.5 Hz, H^4), 7.83 (1H, t, $^3J_{H\text{-}H}$ = 8.0 Hz, H^3); δ_C (176 MHz, $CDCl_3$) 13.4 (1C, d, $^1J_{C\text{-}P}$ = 104.0 Hz, $P\mathit{CH_3}$), 16.3 (1C, d, $^3J_{C\text{-}P}$ = 6.5 Hz, $OCH_2\mathit{CH_3}$), 61.1 (1C, d, $^2J_{C\text{-}P}$ = 6.5 Hz, $O\mathit{CH_2}CH_3$), 64.4 (1C, s, $\mathit{CH_2}OH$), 123.0 (1C, d, $^4J_{C\text{-}P}$ = 3.0 Hz, C^5), 126.0 (1C, d, $^2J_{C\text{-}P}$ = 21.5 Hz, C^3), 136.7 (1C, d, $^3J_{C\text{-}P}$ = 10.0 Hz, C^4), 152.8 (1C, $^1J_{C\text{-}P}$ = 158.0 Hz, C^2), 161.4 (1C, d, $^3J_{C\text{-}P}$ = 18.5

Hz, C^6); δ_P (162 MHz, $CDCl_3$) +39.3; *m/z* (HRMS$^+$) 216.0778 $[M + H]^+$ ($C_9H_{15}NO_3P$ requires 216.0790).

(6-[Ethoxy(methyl)phosphoryl]pyridine-2-yl)methyl methanesulphonate[181]

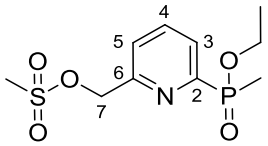

Triethylamine (0.70 mL, 5.01 mmol) was added to a solution of ethyl [6-(hydroxymethyl)pyridin-2-yl](methyl)phosphinate (359 mg, 1.67 mmol) in anhydrous THF (8 mL). The mixture was stirred at 5 ^oC and methanesulfonyl chloride (0.19 mL, 2.51 mmol) was added. The reaction was monitored by TLC (SiO_2, CH_2Cl_2-CH_3OH, 95 : 5, $R_{f(product)}$ = 0.33, $R_{f(reactant)}$ = 0.31) and stopped after 10 min. The solvent was removed under reduced pressure and the resulting residue dissolved in dichloromethane (20 mL) and washed with saturated sodium chloride solution (4 x 15 mL). Removal of the solvent from the organic layer, after it had been dried over magnesium sulfate and filtered, yielded the title compound as a yellow oil, which was used directly in the next step without further purification (421 mg, 1.44 mmol, 86%). R_f (SiO_2, CH_2Cl_2-CH_3OH, 95 : 5) : 0.33; δ_H (400 MHz, $CDCl_3$) 0.99 (3H, t, $^3J_{H-H}$ = 7.0 Hz, $OCH_2\mathit{CH_3}$), 1.49 (3H, d, $^2J_{H-P}$ = 15.0 Hz, $P\mathit{CH_3}$), 2.90 (3H, s, $SO_2\mathit{CH_3}$), 3.52 – 3.95 (2H, m, $O\mathit{CH_2}CH_3$), 5.13 (2H, s, H^7), 7.39 (1H, d, $^3J_{H-H}$ = 8.0 Hz, H^5), 7.60 – 7.83 (2H, m, $H^{3, 4}$); δ_P (162 MHz, $CDCl_3$) +38.2; *m/z* (HRMS$^+$) 294.0560 $[M + H]^+$ ($C_{10}H_{17}NO_5PS$ requires 294.0565).

It should be noted that in some instances this reaction was found to yield the formation of an additional product alongside the title compound. This was identified as ethyl [6-(chloromethyl)pyridin-2-yl](methyl)phosphinate. In instances where the formation of this by-product occurred, its presence was signalled by the occurrence of an additional signal at 4.56 ppm in the ^1H NMR spectrum, corresponding to H^7. It was still possible to use the product directly in the subsequent alkylation step without further purification. However, it was necessary to add a catalytic amount of potassium iodide to the reaction mixture in order for the alkylation to proceed. R_f (SiO_2, CH_2Cl_2-CH_3OH, 95 : 5) : 0.38; δ_P (162 MHz, $CDCl_3$) +38.5; *m/z* (HRMS$^+$) 234.0446 $[M + H]^+$ ($C_9H_{14}NO_2PCl$ requires 234.0451).

Triethyl 6, 6', 6'' - ((*S*) - 2 - benzyl - 1, 4, 7 - triazacyclononane - 1, 4, 7 - triyl) tris (methylene) tris (pyridine - 6, 2 - diyl) tris (methylphosphinate) and **diethyl 6,6'-((*S*) - 2 - benzyl - 1, 4, 7 - triazacyclononane - 1, 4 - diyl) bis (methylene) bis (pyridine - 6, 2 - diyl) bis (methylphosphinate)**

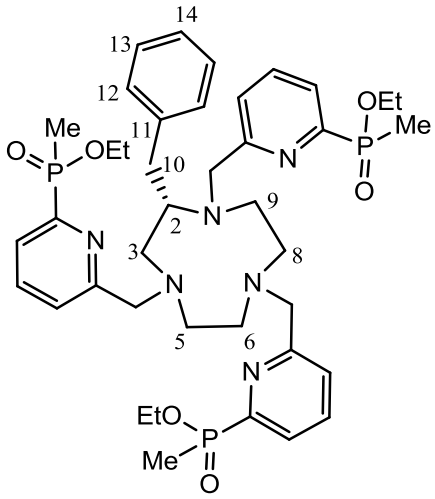

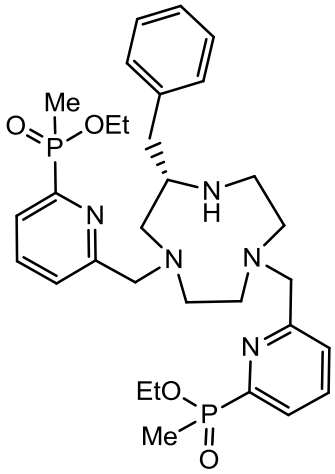

(*S*)-2-Benzyl-1,4,7-triazacyclononane (50 mg, 0.23 mmol), (6-[ethoxy(methyl)phosphoryl] pyridine-2-yl)methyl methanesulphonate/ ethyl [6-(chloromethyl)pyridin-2-yl](methyl)phosphinate (182 mg, 3:2, '0.68' mmol), potassium carbonate (94 mg, 0.68 mmol) and potassium iodide (90 mg, 0.54 mmol) were stirred in anhydrous acetonitrile (5 mL) at reflux under argon. The reaction was monitored by TLC to confirm that all the mesylated and chlorinated starting material had been consumed. After 2 h the reaction mixture was allowed to cool to room temperature and filtered to facilitate the removal of potassium salts. Removal of the solvent under reduced pressure yielded the crude products, which were separated and purified by column chromatography on silica gel (gradient elution: CH_2Cl_2 to 9% CH_3OH-CH_2Cl_2), giving triethyl 6, 6', 6'' - ((*S*) - 2 - benzyl - 1, 4, 7 - triazacyclononane - 1, 4, 7 - triyl) tris (methylene) tris (pyridine - 6, 2 - diyl) tris (methylphosphinate) (66 mg, 0.08 mmol, 35%) and diethyl 6, 6' - ((*S*) - 2 - benzyl - 1, 4, 7 - triazacyclononane - 1, 4 - diyl) bis (methylene) bis (pyridine - 6, 2 - diyl) bis (methylphosphinate) (26 mg, 0.04 mmol, 18%) as yellow oils.

Triethyl 6, 6', 6'' - ((*S*) - 2 - benzyl - 1, 4, 7 - triazacyclononane - 1, 4, 7 - triyl) tris (methylene) tris (pyridine - 6, 2 - diyl) tris (methylphosphinate). R_f (SiO_2, CH_2Cl_2-CH_3OH, 90 : 10) : 0.25; δ_H (400 MHz, $CDCl_3$) 0.97 – 1.35 (9H, br m, 3 x $OCH_2\mathit{CH_3}$), 1.50 – 1.94 (9H, br m, 3 x $P\mathit{CH_3}$), 2.45 – 4.69 (25 H, br m, ring CH_2's, 3 x OCH_2, 3 x

NCH_2, $H^{2, 10}$), 6.97 – 8.07 (14H, br m, Ar); δ_P (162 MHz, $CDCl_3$) +39.0; *m/z* ($HRMS^+$) 811.3654 $[M + H]^+$ ($C_{40}H_{58}N_6O_6P_3$ requires 811.3631).

Diethyl 6, 6' - ((*S*) - 2 - benzyl - 1, 4, 7 - triazacyclononane - 1, 4 - diyl) bis (methylene) bis (pyridine - 6, 2 - diyl) bis (methylphosphinate). R_f (SiO_2, CH_2Cl_2-CH_3OH, 90 : 10) : 0.42; δ_H (400 MHz, $CDCl_3$) 1.16 – 1.41 (6H, m, 2 x OCH_2CH_3), 1.63 – 1.85 (6H, m, 2 x PCH_3), 2.37 – 3.47 (12H, m, ring CH_2's, H^{10}), 3.62 – 4.16 (8H, br m, 2 x OCH_2, 2 x NCH_2), 4.14 – 4.24 (1H, m, H^2), 7.20 – 7.90 (11H, br m, Ar); δ_P (162 MHz, $CDCl_3$) +39.0; *m/z* ($HRMS^+$) 614.3018 $[M + H]^+$ ($C_{31}H_{46}N_5O_4P_2$ requires 614.3025)

Triethyl 6, 6', 6'' - ((*R*) - 2 - benzyl - 1, 4, 7 - triazacyclononane - 1, 4, 7 - triyl) tris (methylene) tris (pyridine - 6, 2 - diyl) tris (methylphosphinate)

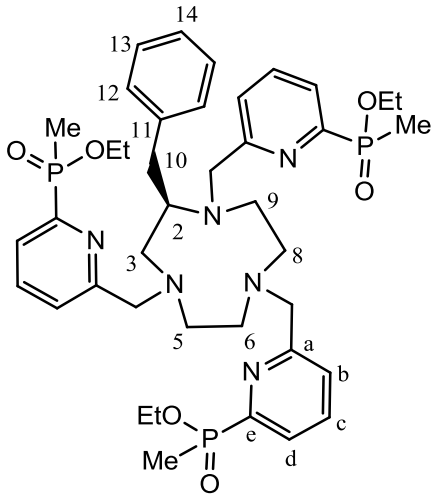

(*R*)-2-Benzyl-1,4,7-triazacyclononane (102 mg, 0.47 mmol), (6-[ethoxy(methyl)phosphoryl] pyridine-2-yl)methyl methanesulphonate (420 mg, 1.43 mmol) and potassium carbonate (193 mg, 1.39 mmol) were stirred in anhydrous acetonitrile (5 mL) at reflux under argon. The reaction was monitored by TLC to confirm that all the mesylated starting material had been consumed. After 3 h the reaction mixture was allowed to cool to room temperature and filtered to facilitate the removal of potassium salts. Removal of the solvent under reduced pressure yielded the crude product, which was purified by column chromatography on silica gel (gradient elution: CH_2Cl_2 to 25% CH_3OH-CH_2Cl_2) to give the title compound as a yellow oil (91 mg, 0.11 mmol, 24%). R_f (SiO_2, CH_2Cl_2-CH_3OH, 90 : 10) : 0.25; δ_H (700 MHz, $CDCl_3$) 1.14 – 1.21 (9H, br m, 3 x OCH_2CH_3), 1.63 – 1.74 (9H, br m, 3 x PCH_3), 2.39 – 3.34 (13H, br m, ring CH_2's, H^2, H ^{10}), 3.51 –4.11 (12H, br m, 3 x OCH_2 and 3 x NCH_2),

7.00 – 7.06 (2H, m, H^{12}), 7.07 - 7.12 (1H, m, H^{14}), 7.12 - 7.16 (2H, m, H^{13}), 7.33 – 7.49 (3H, m, H^{b}), 7.59 – 7.72 (3H, m, H^{c}), 7.81 – 7.87 (3H, m, H^{d}); δ_P (162 MHz, $CDCl_3$) +39.3; δ_C (176 MHz, $CDCl_3$) 13.0 - 13.6 (3C, m, P*CH*$_3$), 16.3 - 16.4 (3C, m, OCH_2*CH*$_3$), 35.6 (br s, 1C, C^{10}), 51.5 (br s, 1C, C^{9}), 55.7, 56.2, 56.7 (3C, $C^{5, 6, 8}$), 58.0 (1C, C^{3}), 60.8 (3C, m, O*CH*$_2$$CH_3$), 62.7 (1C, C^{2}), 64.2, 64.6 (3C, N*CH*$_2$), 125.0, 125.3, 125.4 (3C, C^{b}), 125.6, 125.7 (3C, C^{d}), 125.8 (1C, C^{14}), 128.2 (2C, C^{12}), 129.0 (2C, C^{13}), 136.1 (3C, C^{c}), 140.4 (1C, C^{11}), 153.0 - 154.2 (3C, m, C^{e}), 161.2, 162.1 (3C, C^{a}); *m/z* (HRMS$^+$) 811.3638 $[M + H]^+$ ($C_{40}H_{58}N_6O_6P_3$ requires 811.3631).

Diethyl 6, 6' - ((*R*) - 2 - benzyl - 1, 4, 7 - triazacyclononane - 1, 4 - diyl) bis (methylene) bis (pyridine - 6, 2 - diyl) bis (methylphosphinate)

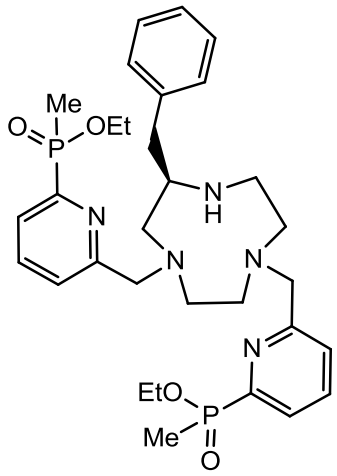

(*R*)-2-Benzyl-1,4,7-triazacyclononane (128 mg, 0.58 mmol), (6-[ethoxy(methyl)phosphoryl] pyridine-2-yl)methyl methanesulphonate (341 mg, 1.16 mmol) and potassium carbonate (242 mg, 1.75 mmol) were stirred in anhydrous acetonitrile (5 mL) at reflux under argon. The reaction was monitored by TLC to confirm that all the mesylated starting material had been consumed. After 4 h the reaction mixture was allowed to cool to room temperature and filtered to facilitate the removal of potassium salts. Removal of the solvent under reduced pressure yielded the crude product, which was purified by column chromatography on silica gel (gradient elution: CH_2Cl_2 to 6% CH_3OH-CH_2Cl_2) to give the title compound as a yellow oil (54 mg, 0.09 mmol, 15%). R_f (SiO_2, CH_2Cl_2-CH_3OH, 90 : 10) : 0.39; δ_H (700 MHz, $CDCl_3$) 1.14 – 1.24 (6H, br m, 3 x OCH_2*CH*$_3$), 1.62 – 1.73 (6H, br m, 3 x P*CH*$_3$), 2.60 – 3.28 (15 H, br m, ring CH_2's, H^{10}), 3.75 – 4.06 (9H, br m, H^2, OCH_2 x 2, NCH_2 x 2), 7.17 – 7.22 (2H, m, H^{14} and 1 x H^{b}), 7.24 – 7.29 (2H, m, H^{13}), 7.29 – 7.33 (1H, m, 1 x H^{b}), 7.37 - 7.43 (2H, m, $H^{c\ or\ d}$), 7.51 (2H, br s, H^{12}), 7.67 – 7.76 (2H, m, $H^{c\ or\ d}$); δ_P (162

MHz, $CDCl_3$) +39.5; δ_C (176 MHz, $CDCl_3$) 13.4 - 15.1 (2C, m, $OCH_2\mathit{CH_3}$), 16.4 - 16.5 (2C, m, PCH_3), 37.4, 45.8, 49.9, 50.6 (6C, ring CH_2's, C^{10}), 57.1 (1C, C^2), 61.1 - 61.8 (4C, m, 2 x NCH_2, 2 x $O\mathit{CH_2}CH_3$), 124.7, 124.9 (2C, C^b), 125.3 - 125.7 (4C, m, $C^{c,\ d}$), 127.3 (1C, C^{14}), 129.0 (1C, C^{13}), 129.5 (1C, C^{12}), 135.7 (1C, C^{11}), 152.8 - 154.4 (2C, m, C^e), 159.3 - 159.8 (2C, m, C^a); *m/z* ($HRMS^+$) 614.3032 $[M + H]^+$ ($C_{31}H_{46}N_5O_4P_2$ requires 614.3025).

(*S*)-[Eu.L^{34}]

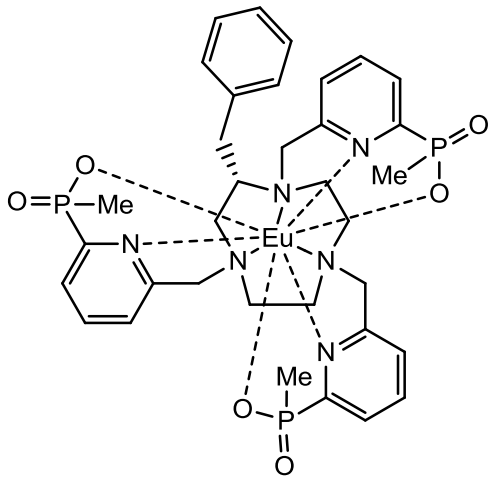

Triethyl 6, 6', 6'' - ((*S*) - 2 - benzyl - 1, 4, 7 - triazacyclononane - 1, 4, 7 - triyl) tris (methylene) tris (pyridine - 6, 2 - diyl) tris (methylphosphinate) (32 mg, 0.04 mmol) was dissolved in CD_3OD (3.5 mL) and a solution of 0.1 M NaOH in D_2O (3.5 mL) was added. The reaction mixture was heated for 16 h at 90 ^oC with stirring. Subsequent removal of the solvent under reduced pressure yielded the deprotected ligand as a white solid. The product was checked by ESMS to confirm complete hydrolysis of the ester groups and was used immediately for complexation with europium chloride.

The ligand was dissolved in H_2O : CH_3OH (4 : 1, 2.5 mL) and the pH of the solution adjusted to 5.5 using dilute $HCl_{(aq)}$. $EuCl_3.6H_2O$ (15.9 mg, 0.04 mmol) was added and the reaction mixture was heated at 80 ^oC for 16 h. After allowing the reaction mixture to cool to room temperature, the pH was raised to 10.0 by the addition of dilute $NaOH_{(aq)}$. The resulting solution was stirred for 1 h causing excess Eu^{3+} to precipitate as $Eu(OH)_3$, which was removed by filtration. The pH of the resulting solution was restored to 5.5 by the addition of dilute $HCl_{(aq)}$ and the solvent lypohilised to give the crude product. The crude product was taken in to CH_2Cl_2 : CH_3OH (8 : 2, 2 mL) and the solution filtered to facilitate the removal of salts. Subsequent removal of solvent under reduced pressure yielded an off-white solid which was further purified by column chromatography on

silica gel (CH_2Cl_2 : CH_3OH : NH_3, 80 : 20 : 1) to give the title compound as an off-white solid (17 mg, 0.02 mmol, 50%). R_f (SiO_2, CH_2Cl_2-CH_3OH-NH_3, 80 : 20 : 1) : 0.16; δ_H (600 MHz, CD_3OD) -6.06 (1H), -5.69 (1H), -4.08 (1H), -2.76 (1H), -2.26 (1H), -1.80 (1H), -1.62 (2H), -0.34 (1H), -0.05 (3H), 0.52 (1H), 0.86 (3H), 1.36 (1H), 2.18 (3H), 2.93 (1H), 3.00 (1H), 3.35 (1H), 4.28 (1H), 4.57 (1H), 5.32 (1H), 6.27 (1H), 6.66 (1H), 7.06 - 7.74 (12H), 8.46 (1H), 10.39 (1H); δ_P (243 MHz, CD_3OD) 35.0, 40.3, 44.4; *m/z* ($HRMS^+$) 875.1659 $[M + H]^+$ ($^{151}EuC_{34}H_{43}N_6O_6P_3$ requires 875.1656); (HPLC) t_R = 5.96 min; λ_{max} (H_2O) 268 nm; $\tau(H_2O)$ = 1.34 ms; $\tau(D_2O)$ = 1.60 ms.

(*S*)-[Tb.L^{34}]

An analogous procedure to that described for the synthesis of (*S*)-Eu.**L**^{34}] was followed, using $TbCl_3.6H_2O$ (10.9 mg, 0.03 mmol) in the place of $EuCl_3.6H_2O$. Purification by silica gel chromatography (CH_2Cl_2 : CH_3OH : NH_3, 80 : 20 : 1) yielded the title complex as an off-white solid (22.4 mg, 0.025 mmol, 88%). R_f (SiO_2, CH_2Cl_2-CH_3OH-NH_3, 80 : 20 : 1) : 0.14; δ_H (600 MHz, CD_3OD) -92.9 (1H), -78.4 (1H), -43.0 (1H), -37.2 (H), -15.9 (1H), -13.7 (1H), -12.3 (1H), -10.8 -9.2 (5H), -4.4 (1H), -2.7 (1H), -2.4 (3H), -0.2, 1.3 (9H), 7.3 (1H), 8.8 (1H), 12.6 (1H), 17.2 (2H), 21.5 (1H), 27.9 (3H), 35.2 (1H), 40.2 (3H), 52.3 (1H), 54.2 (1H), 62.3 (1H); δ_P (243 MHz, CD_3OD) -32.7, 7.2, 51.1; *m/z* ($HRMS^+$) 883.1718 $[M + H]^+$ ($^{159}TbC_{34}H_{43}N_6O_6P_3$ requires 883.1710); (HPLC) t_R = 6.03 min; λ_{max} (H_2O) 268 nm; $\tau(H_2O)$ = 2.62 ms; $\tau(D_2O)$ = 2.71 ms.

(*R*)-[Eu.L^{34}]

Triethyl 6, 6', 6'' - ((*R*) - 2 - benzyl - 1, 4, 7 - triazacyclononane - 1, 4, 7 - triyl) tris (methylene) tris (pyridine - 6, 2 - diyl) tris (methylphosphinate) (34 mg, 0.04 mmol) was dissolved in CD_3OD (3.0 mL) and a solution of 0.1 M NaOH in D_2O (3.7 mL) was added. The reaction mixture was heated for 5 h at 90 ^oC with stirring. Subsequent removal of the solvent under reduced pressure yielded the deprotected ligand as a white solid. The product was checked by ESMS and ^{31}P NMR spectroscopy (δ_P (162 MHz, $CDCl_3$) +26.4, 26.9, 27.4) to confirm complete hydrolysis of the ester groups and was used immediately for complexation with europium chloride.

The ligand was reacted with europium chloride using an analogous procedure to that described for the synthesis of (*S*)-[Eu.**L**^{34}]. Purification by silica gel chromatography (CH_2Cl_2 : CH_3OH : NH_3, 80 : 20 : 1) yielded the title complex as an off-white solid (27

mg, 0.03 mmol, 73%). Spectroscopic characteristics were identical to those observed for the (*S*) enantiomer.

(*R*)-[Tb.L^{34}]

An analogous procedure to that described for the synthesis of (*R*)-[Eu.**L**^{34}] was followed, using $TbCl_3.6H_2O$ (13.5 mg, 0.04 mmol) in the place of $EuCl_3.6H_2O$. Purification by silica gel chromatography (CH_2Cl_2 : CH_3OH : NH_3, 80 : 20 : 1) yielded the title complex as an off-white solid (17.5 mg, 0.020 mmol, 55%). Spectroscopic characteristics were identical to those observed for the (*S*) enantiomer.

(*S*)-[Tb.L^{35}(OH$_2$)]$^+$

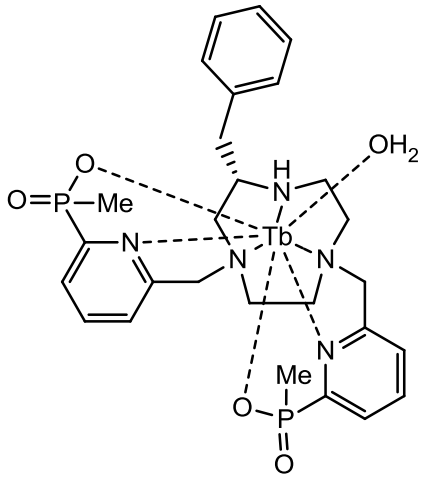

Diethyl 6, 6' - ((*S*) - 2 - benzyl - 1, 4, 7 - triazacyclononane - 1, 4 - diyl) bis (methylene) bis (pyridine - 6, 2 - diyl) bis (methylphosphinate) (11 mg, 0.02 mmol) was dissolved in CD_3OD (1.0 mL) and a solution of 0.1 M NaOH in D_2O (1.0 mL) was added. The reaction mixture was heated for 3 h at 90 ^oC with stirring. Subsequent removal of the solvent under reduced pressure yielded the deprotected ligand as a white solid. The product was checked by ^{31}P NMR spectroscopy (δ_P (162 MHz, $CDCl_3$) +27.3) to confirm complete hydrolysis of the ester groups and was used immediately for complexation with terbium chloride.

The ligand was dissolved in H_2O : CH_3OH (4 : 1, 3.0 mL) and the pH of the solution adjusted to 5.5 using dilute $HCl_{(aq)}$. $TbCl_3.6H_2O$ (7.5 mg, 0.02 mmol) was added and the reaction mixture was heated at 80 ^oC for 32 h. After allowing the reaction mixture to cool to room temperature, the pH was raised to 10.0 by the addition of dilute $NaOH_{(aq)}$. The resulting solution was stirred for 2 h causing excess Tb^{3+} to precipitate as $Tb(OH)_3$, which was removed by filtration. The pH of the resulting solution was restored to 5.5 by

the addition of dilute $HCl_{(aq)}$ and the solvent lypohilised to give the crude product. The crude product was taken in to CH_2Cl_2 : CH_3OH (8 : 2, 2 mL) and the solution filtered to facilitate the removal of salts. Subsequent removal of solvent under reduced pressure yielded an off-white solid which was further purified by preparative HPLC, giving the title compound as a white solid (1.8 mg, 0.003 mmol, 14%). *m/z* (HRMS$^+$) 714.1414 $[M + H]^+$ ($^{159}TbC_{27}H_{35}N_5O_4P_2$ requires 714.1418); (HPLC) t_R = 4.54 and 4.73 min; λ_{max} (H_2O) 268 nm; $\tau(H_2O)$ = 1.26 ms; $\tau(D_2O)$ = 2.20 ms.

(*R*)-[Tb.L^{35}(OH$_2$)]$^+$

An analogous procedure to that described for the synthesis of (*S*)-[Tb.**L**^{35}$(OH_2)]^+$ was followed, using $TbCl_3.6H_2O$ (23.0 mg, 0.06 mmol). Purification by preparative HPLC yielded the title complex as a white solid (14.6 mg, 0.02 mmol, 37%). Spectroscopic characteristics were identical to those observed for the (*S*) enantiomer.

(4-Bromo-6-(ethoxy(methyl)phosphoryl)pyridine-2-yl)methyl methanesulfonate

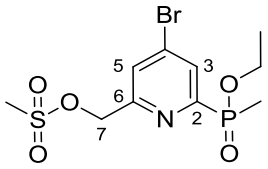

Triethylamine (0.26 mL, 1.85 mmol) was added to a solution of ethyl [4-bromo-6-(hydroxymethyl)pyridin-2-yl](methyl)phosphinate (181 mg, 0.61 mmol) in anhydrous THF (4 mL). The mixture was stirred at 5 ^oC and methanesulfonyl chloride (0.07 mL, 0.92 mmol) was added. The reaction was monitored by TLC (SiO_2, CH_2Cl_2-CH_3OH, 95 : 5, $R_{f(product)}$ = 0.38, $R_{f(reactant)}$ = 0.28) and stopped after 10 min. The solvent was removed under reduced pressure and the resulting residue dissolved in dichloromethane (20 mL) and washed with saturated sodium chloride solution (2 x 15 mL). Removal of the solvent from the organic layer yielded the title compound as a yellow oil, which was found to be contaminated with small amounts of ethyl [4-bromo-6-(chloromethyl)pyridin-2-yl](methyl)phosphinate (SiO_2, CH_2Cl_2-CH_3OH, 95 : 5, R_f = 0.45). The product was used directly in the subsequent alkylation step without further purification (171 mg, '0.46 mmol', '75%'). R_f (SiO_2, CH_2Cl_2-CH_3OH, 95 : 5) : 0.38; δ_H (400 MHz, $CDCl_3$) 1.19 (3H, t, $^3J_{H\text{-}H}$ = 7.0 Hz, $OCH_2\mathit{CH_3}$), 1.67 (3H, d, $^2J_{H\text{-}P}$ = 15.0 Hz, $P\mathit{CH_3}$), 3.07 (3H, s, $SO_2\mathit{CH_3}$), 3.73 – 4.11 (2H, m, $O\mathit{CH_2}CH_3$), 5.26 (2H, s, H^7), 7.70 (1H, s, H^5), 8.08 (1H, dd , $^3J_{H\text{-}P}$ = 6.0 Hz, $^4J_{H\text{-}H}$ = 2.0 Hz, H^3); δ_P (162 MHz, $CDCl_3$) +37.2; *m/z* (HRMS$^+$) 371.9666 $[M + H]^+$ ($C_{10}H_{16}NO_5PS^{79}Br$ requires 371.9670).

Triethyl 6, 6', 6'' - ((*S*) - 2 - benzyl - 1, 4, 7 - triazacyclononane - 1, 4, 7 - triyl) tris (methylene) tris (4 - bromopyridine - 6, 2 - diyl) tris (methylphosphinate)

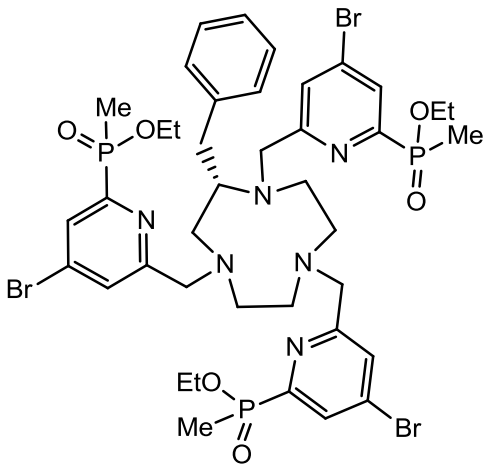

(*S*)-2-Benzyl-1,4,7-triazacyclononane (36 mg, 0.16 mmol), 4-bromo-6-(ethoxy(methyl)phosphoryl)pyridine-2-yl)methyl methanesulfonate (171 mg, '0.46 mmol'), potassium carbonate (68 mg, 0.49 mmol) and potassium iodide (33 mg, 0.20 mmol) were stirred in anhydrous acetonitrile (7 mL) at reflux under argon. The reaction was monitored by TLC to confirm that all the mesylated starting material had been consumed. After 4 h the reaction mixture was allowed to cool to room temperature and filtered to facilitate the removal of potassium salts. Removal of the solvent under reduced pressure yielded the crude product, which was purified by column chromatography on silica gel (gradient elution: CH_2Cl_2 to 7% CH_3OH-CH_2Cl_2) to give the title compound as a yellow oil (49 mg, 0.05 mmol, 29%). R_f (SiO_2, CH_2Cl_2-CH_3OH, 95 : 5) : 0.27; δ_H (400 MHz, $CDCl_3$) 1.12 – 1.43 (9H, br m, 3 x OCH_2CH_3), 1.54 – 1.93 (9H, br m, 3 x PCH_3), 2.36 – 4.89 (25 H, br m, ring CH_2's, 3 x OCH_2, $H^{2, 10, 14}$), 7.07 – 8.22 (11H, br m, Ar); δ_P (162 MHz, $CDCl_3$) + 36.1, +37.0, +37.2; *m/z* ($HRMS^+$) 1045.098 $[M + H]^+$ ($C_{40}H_{55}N_6O_6P_3{}^{79}Br_3$ requires 1045.095).

(*S*)-[Eu.L^{39}]

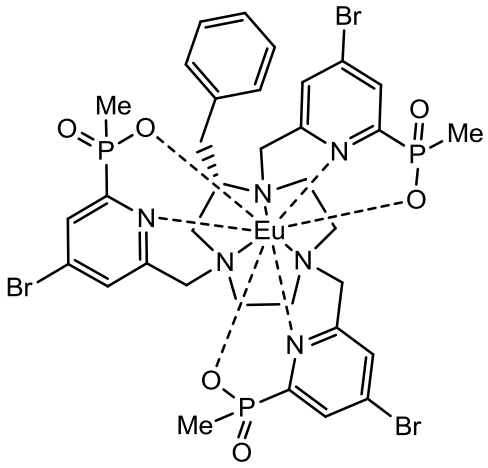

Triethyl 6, 6', 6" - ((*S*) - 2 - benzyl - 1, 4, 7 - triazacyclononane - 1, 4, 7 - triyl) tris (methylene) tris (4 - bromopyridine - 6, 2 - diyl) tris (methylphosphinate) (26 mg, 0.025 mmol) was dissolved in CD_3OD (2.4 mL) and a solution of 0.1 M NaOH in D_2O (2.2 mL) was added. The reaction mixture was heated for 5 h at 90 ^oC with stirring. Subsequent removal of the solvent under reduced pressure yielded the deprotected ligand as a white solid. The product was checked by ESMS and ^{31}P NMR spectroscopy (δ_P (162 MHz, $CDCl_3$) +25.9) to confirm complete hydrolysis of the ester groups and was used immediately for complexation with europium nitrate.

The ligand was dissolved in H_2O : CH_3OH (4 : 1, 1.5 mL) and the pH of the solution adjusted to 5.5 using dilute $HBr_{(aq)}$. $Eu(NO_3)_3.5H_2O$ (11.5 mg, 0.027 mmol) was added and the reaction mixture was heated at 80 ^oC for 16 h. After allowing the reaction mixture to cool to room temperature, the pH was raised to 10.0 by the addition of dilute $NaOH_{(aq)}$. The resulting solution was stirred for 1 h causing excess Eu^{3+} to precipitate as $Eu(OH)_3$, which was removed by filtration. The pH of the resulting solution was restored to 5.5 by the addition of dilute $HBr_{(aq)}$ and the solvent lypohilised to give the crude product. The crude product was taken in to CH_2Cl_2 : CH_3OH (8 : 2, 2 mL) and the solution filtered to facilitate the removal of salts. Subsequent removal of solvent under reduced pressure yielded an off-white solid which was further purified by column chromatography on silica gel (CH_2Cl_2 : CH_3OH : NH_3, 80 : 20 : 1) to give the title compound as an off-white solid (21 mg, 0.02 mmol, 76%). R_f (SiO_2, CH_2Cl_2-CH_3OH-NH_3, 80 : 20 : 1) : 0.56; δ_H (400 MHz, CD_3OD) -6.46 (1H), -6.03 (1H), -4.54 (1H), -3.12 (1H), -2.76 (1H), -2.49 (1H), -2.38 (1H), -2.23 (1H), -0.70 (1H), -0.34 (5H), 0.52 (3H), 1.30 - 1.48 (2H), 1.87 (3H), 2.52 (1H), 2.85 (1H), 4.24 (1H), 4.48 (1H), 6.16 (1H), 7.16 - 7.52 (7H), 7.89 (2H), 8.51 (1H), 9.23 (1H), 10.87 (1H); δ_P (162 MHz,

CD_3OD) 33.5, 40.2, 43.9; *m/z* ($HRMS^+$) 1109.904 $[M + H]^+$ ($^{151}EuC_{34}H_{40}N_6O_6P_3{}^{79}Br_3$ requires 1109.905); (HPLC) t_R = 8.21 min; λ_{max} (H_2O) 268 nm; $\tau(H_2O)$ = 1.25 ms; $\tau(D_2O)$ = 1.59 ms.

(*S*)-[Tb.L^{39}]

An analogous procedure to that described for the synthesis of (*S*)-[Eu.**L**^{39}] was followed, using $Tb(NO_3)_3.5H_2O$ (7.4 mg, 0.02 mmol) in the place of $Eu(NO_3)_3.5H_2O$. Purification by silica gel chromatography (CH_2Cl_2 : CH_3OH : NH_3, 80 : 20 : 1) yielded the title complex as an off-white solid (3.3 mg, 0.003 mmol, 18%). R_f (SiO_2, CH_2Cl_2-CH_3OH-NH_3, 80 : 20 : 1) : 0.53; δ_P (243 MHz, CD_3OD) -30.4, 5.6, 50.2; *m/z* ($HRMS^+$) 1116.905 $[M + H]^+$ ($^{159}TbC_{34}H_{40}N_6O_6P_3{}^{79}Br_3$ requires 1116.903); (HPLC) t_R = 11.24 min; λ_{max} (H_2O) 268 nm; $\tau(H_2O)$ = 2.32 ms; $\tau(D_2O)$ = 2.40 ms.

5.2.3 Chiral quenchers and precursors

(*S*)-6-Hydroxy-2,5,7,8-tetramethylchromane-2-carboxylic acid methyl ester

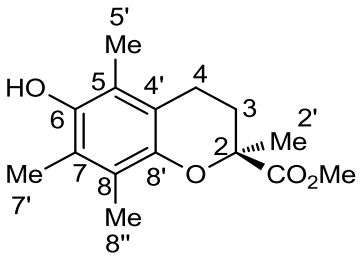

(*S*)-6-Hydroxy-2,5,7,8-tetramethylchromane-2-carboxylic acid (200 mg, 0.80 mmol) was dissolved in methanol (5 mL) and the solution was acidified using conc. $H_2SO_{4(aq)}$. The solution was heated at reflux for 4 h, allowed to cool to room temperature and then diluted with water (25 mL). The aqueous solution was extracted with ether (3 x 20 mL) and the organic extracts were combined and washed with saturated $NaHCO_{3(aq)}$ solution (2 x 30 mL) followed by water (2 x 30 mL) before being dried over magnesium sulfate and filtered. Removal of the solvent under reduced pressure yielded the title compound as a white crystalline solid (164 mg, 0.62 mmol, 78%). m.p. 137–140 ^oC (lit.[202] 134.5-136 ^oC); δ_H (500 MHz, $CDCl_3$) 1.62 (3H, s, $H^{2'}$), 1.85 – 1.91 (1H, m, H^3), 2.07 (3H, s, $H^{5'}$), 2.17 (3H, s, $H^{7'}$), 2.20 (3H, s, $H^{8''}$), 2.42 – 2.47 (1H, m, H^3), 2.48 – 2.57 (1H, m, H^4), 2.64 – 2.69 (1H, m, H^4), 3.69 (3H, s, OCH_3), 4.28 (1H, s, OH); δ_C (126 MHz, $CDCl_3$) 11.5 (1C, $C^{5'}$), 12.1 (1C, $C^{8''}$), 12.4 (1C, $C^{7'}$), 21.2 (1C, C^4), 25.7 (1C, $C^{2'}$), 30.9 (1C, C^3), 52.6 (1C, OCH_3), 79.8 (C^2), 117.1 (1C, $C^{4'}$), 118.6 (1C, C^5), 121.5 (1C, C^7),

122.8 (1C, C^8), 145.5 (1C, C^6), 145.7 (1C, $C^{8'}$), 174.1 (1C, C=O); *m/z* ($HRMS^+$) 287.1256 $[M + Na]^+$ ($C_{15}H_{20}O_4Na$ requires 287.1259).

(*R*)-6-Hydroxy-2,5,7,8-tetramethylchromane-2-carboxylic acid methyl ester

The title compound was prepared using an analogous procedure to that described for (*S*)-6-hydroxy-2,5,7,8-tetramethylchromane-2-carboxylic acid methyl ester. The starting material (*S*)-6-hydroxy-2,5,7,8-tetramethylchromane-2-carboxylic acid was replaced by (*R*)-6-hydroxy-2,5,7,8-tetramethylchromane-2-carboxylic acid (200 mg, 0.80 mmol). The title compound was isolated as a white crystalline solid (182 mg, 0.69 mmol, 86%). Spectroscopic characteristics were identical to those observed for the (*S*) isomer.

(*R*)-*Tert*-butyl 2,2',2''-(2-benzyl-1,4,7-triazacyclononane-1,4,7-triyl)triacetate

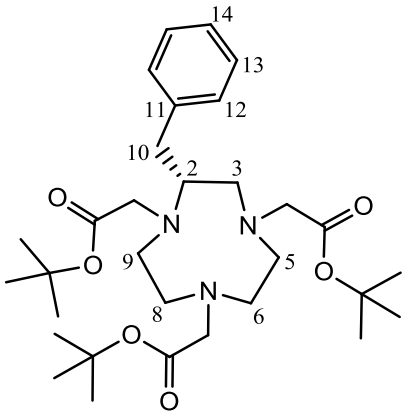

(*R*)-2-Benzyl-1,4,7-triazacyclononane (90 mg, 0.41 mmol), *tert*-butyl bromoacetate (200 mg, 1.02 mmol) and potassium carbonate (169 mg, 1.23 mmol) were stirred in anhydrous acetonitrile (5 mL) at 40 ^oC under argon. The reaction was monitored by LCMS to confirm that all the starting material had been consumed. After 30 min, the reaction mixture was allowed to cool to room temperature and filtered to facilitate the removal of potassium salts. Removal of the solvent under reduced pressure yielded the crude product, which was purified by column chromatography on silica gel (gradient elution: CH_2Cl_2 to 5% CH_3OH-CH_2Cl_2) to give the title compound as a colourless oil (49 mg, 0.09 mmol, 21%). R_f (SiO_2, CH_2Cl_2-CH_3OH, 95 : 5) : 0.46; δ_H (700 MHz, $CDCl_3$) 1.36 (9H, s, ^{t}Boc CH_3), 1.41 (9H, s, ^{t}Boc CH_3), 1.42 (9H, s, ^{t}Boc CH_3), 2.63 - 2.71 (2H, m, ring CH_2's), 2.77 (1H, dd, *J* = 14.0, 6.5 Hz, H^{10}), 2.84 (1H, dd, *J* = 14.0, 7.5 Hz, H^{10}), 3.08 (2H, d, *J* = 3.0 Hz, NCH_2), 3.17 - 3.54 (10H, br m, ring CH_2's, H^2, ½ x NCH_2), 3.70 (1H, d, *J* = 17.5 Hz, ½ x NCH_2), 3.81 (1H, d, *J* = 17.5 Hz, ½ x NCH_2), 4.22 (1H, d, *J* = 17.5 Hz, ½ x NCH_2), 7.18 - 7.22 (3H, m, $H^{12, 14}$), 7.24 - 7.30 (2H, m,

H^{13}); δ_C (176 MHz, $CDCl_3$) 27.9 (3C, ^{t}Boc CH_3), 28.0 (3C, ^{t}Boc CH_3), 28.1 (3C, ^{t}Boc CH_3), 34.8 (1C, C^{10}), 43.7, 46.0, 50.5, 51.4, 51.5 (5C, ring CH_2's, C^2), 53.9 (1C, NCH_2), 54.4 (1C, ring CH_2), 55.5 (1C, NCH_2), 56.3 (1C, NCH_2), 81.6, 82.0, 82.9 (3C, ^{t}Boc$_{(q)}$), 126.7 (1C, C^{14}), 128.8 (2C, C^{13}), 129.1 (2C, C^{12}), 137.8 (1C, C^{11}), 166.4, 168.8, 170.7 (3C, C=O); *m/z* (HRMS$^+$) 562.3851 $[M + H]^+$ ($C_{31}H_{52}N_3O_6$ requires 562.3856).

(*R*)-[Co.L^{37}]

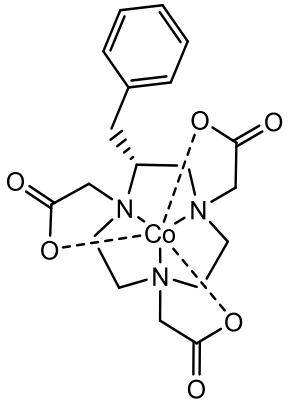

Trifluoroacetic acid (1 mL) was added to a solution of (*R*)-*tert*-butyl 2,2',2''-(2-benzyl-1,4,7-triazacyclononane-1,4,7-triyl)triacetate (142 mg, 0.24 mmol) in dichloromethane (0.5 mL). The mixture was left for 16 h at room temperature and was checked by LCMS to confirm complete ester hydrolysis. The solvent was removed under reduced pressure and the resulting residue re-dissolved in dichloromethane three times to aid the removal of excess acid and *tert*-butyl alcohol.

The ligand was dissolved in water (2 mL) and the pH adjusted to 7.0 by the addition of conc. $NaOH_{(aq)}$. The solution was heated to 80 ^{o}C and $CoCl_2.6H_2O$ (25 mg, 0.11 mmol) was added. Dropwise addition of 30% H_2O_2 solution (0.36 mL) led to the formation of a deep pink solution. The volume of the solution was reduced to approximately 1 mL by evaporation, it was then filtered and allowed to cool to room temperature. When the solution was left at 5 ^{o}C for 60 h, pink needle-like crystals precipitated, which were recrystallised from hot water (8.0 mg, 0.02 mmol, 16%). *m/z* (HRMS$^+$) 450.1078 $[M + H]^+$ ($^{59}CoC_{19}H_{25}N_3O_6$ requires 450.1075); λ_{max} (H_2O) 512 nm (ε = 330 M^{-1} cm^{-1}); Crystals of the complex were examined by X-Ray crystallography: $C_{19}H_{24}N_3O_6Co$, M_r = 449.34, monoclinic ($P2_1$); a = 8.9747(7) Å, b = 7.4776(6) Å, c = 15.0100(12) Å, V = 962.28(13) Å^3, Z = 2; μ = 0.864 mm^{-1}, D_{calc} = 1.551 $mg.mm^{-3}$, T = 120 K; 3721 independent reflections (R_{int} = 0.0541), R_1 = 0.0693, ωR_2 = 0.1772 ($I \geq 2\sigma(I)$).

[Co.L^{38}][189]

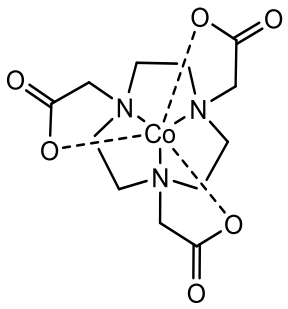

1,4,7-Triazacyclononane-1,4,7-triacetic acid (264 mg, 0.87 mmol) was dissolved in water (2 mL) and the pH adjusted to 7.0 by the addition of conc. $NaOH_{(aq)}$. The solution was heated to 80 ^{o}C and $CoCl_2.6H_2O$ (92 mg, 0.38 mmol) was added. Dropwise addition of 30% H_2O_2 solution (1.32 mL) led to the formation of a deep pink solution, which was allowed to cool to room temperature. Upon standing at room temperature for 16 h, pink needle-like crystals precipitated (93 mg, 0.25 mmol, 68%). *m/z* ($HRMS^+$) 360.0600 $[M + H]^+$ ($^{59}CoC_{12}H_{19}N_3O_6$ requires 360.0606); λ_{max} (H_2O) 512 nm (ε = 300 M^{-1} cm^{-1}).

REFERENCES

REFERENCES

1. B. Valeur and M. r. N. Berberan-Santos, *J. Chem. Educ.*, 2011, **88**, 731-738.
2. S. E. Braslavsky, *Pure Appl. Chem.*, 2007, **79**, 293-465.
3. V. Fernandez-Moreira, F. L. Thorp-Greenwood and M. P. Coogan, *Chem. Commun.*, 2010, **46**, 186-202.
4. D. Parker, *Aust. J. Chem.*, 2011, **64**, 239-243.
5. J. P. Riehl and F. S. Richardson, *Chem. Rev.*, 1986, **86**, 1-16.
6. I. Z. Steinberg and A. Gafni, *Rev. Sci. Instrum.*, 1972, **43**, 409-413.
7. J. P. Riehl and G. Muller, in *Comprehensive Chiroptical Spectroscopy: Instrumentation, Methodologies and Theoretical Simulations*, eds. N. Berova, P. L. Polavarapu, K. Nakanishi and R. W. Woody, John Wiley and Sons, Hobeken, NJ, USA, 2012, vol. 1, ch. 3, pp. 65 - 90.
8. R. A. Shatwell and A. J. McCaffery, *Journal of Physics E: Scientific Instruments*, 1974, **7**, 297.
9. G. L. Nilmes and J. P. Riehl, *J. Phys. Chem.*, 1983, **87**, 3300-3304.
10. D. H. Metcalf, S. W. Snyder, S. Wu, G. L. Hilmes, J. P. Riehl, J. N. Demas and F. S. Richardson, *J. Am. Chem. Soc.*, 1989, **111**, 3082-3083.
11. D. H. Metcalf, S. W. Snyder, J. N. Demas and F. S. Richardson, *J. Phys. Chem.*, 1990, **94**, 7143-7153.
12. D. H. Metcalf, S. W. Snyder, J. N. Demas and F. S. Richardson, *J. Am. Chem. Soc.*, 1990, **112**, 469-479.
13. F. S. Richardson and J. P. Riehl, *Chem. Rev.*, 1977, **77**, 773-792.
14. H. P. J. M. Dekkers, in *Circular Dichroism: Principles and Applications*, eds. N. Berova, K. Nakanishi and R. W. Woody, Wiley-VCH, New York, 2nd edn., 2000, ch. 7, pp. 185 - 215.
15. C. A. Emeis and L. J. Oosterhoff, *J. Chem. Phys.*, 1971, **54**, 4809-4819.
16. H. G. Brittain, *Chirality*, 1996, **8**, 357-363.
17. H. Maeda, Y. Bando, K. Shimomura, I. Yamada, M. Naito, K. Nobusawa, H. Tsumatori and T. Kawai, *J. Am. Chem. Soc.*, 2011, **133**, 9266-9269.
18. It should be noted that the value of the emission dissymmetry factor given here is twice the value reported in the literature. This is because, in their article, the authors wrongly define the equation used for its calculation. Specifically, the factor of two which should be present in the numerator is neglected.
19. A. K. Hagan and T. Zuchner, *Anal. Bioanal. Chem.*, 2011, **400**, 2847-2864.

20. A. de Bettencourt-Dias, in *Encyclopedia of Inorganic and Bioinorganic Chemistry*, John Wiley & Sons, Ltd., 2011.
21. G. E. Buono-core, H. Li and B. Marciniak, *Coord. Chem. Rev.*, 1990, **99**, 55-87.
22. P. Atkins and J. de Paula, *Physical Chemistry*, Oxford University Press, Oxford, 8th edn., 2006.
23. J.-C. G. Bünzli and C. Piguet, *Chem. Soc. Rev.*, 2005, **34**, 1048-1077.
24. T. Gunnlaugsson and J. P. Leonard, *Chem. Commun.*, 2005, 3114-3131.
25. C. Görller-Walrand and K. Binnemans, in *Handbook on the Physics and Chemistry of Rare Earths*, eds. K. A. Gschneidner, Jr. and L. Eyring, Elsevier, 1998, vol. 25, pp. 101-264.
26. S. Cotton, *Lanthanides and Actinides*, Oxford University Press, Incorporated, 1991.
27. J.-C. G. Bünzli and G. R. Choppin, *Lanthanide Probes in Life, Chemical, and Earth Sciences: Theory and Practice*, Elsevier, 1989.
28. N. J. Emptage, *Curr. Opin. Pharmacol.*, 2001, **1**, 521-525.
29. J. I. Bruce, D. Parker and D. J. Tozer, *Chem. Commun.*, 2001, 2250-2251.
30. R. S. Dickins, D. Parker, J. I. Bruce and D. J. Tozer, *Dalton Trans.*, 2003, 1264-1271.
31. R. Pal and D. Parker, *Org. Biomol. Chem.*, 2008, **6**, 1020-1033.
32. J. W. Walton, L. D. Bari, D. Parker, G. Pescitelli, H. Puschmann and D. S. Yufit, *Chem. Commun.*, 2011, **47**, 12289-12291.
33. F. S. Richardson, *Inorg. Chem.*, 1980, **19**, 2806-2812.
34. C. M. G. dos Santos, A. J. Harte, S. J. Quinn and T. Gunnlaugsson, *Coord. Chem. Rev.*, 2008, **252**, 2512-2527.
35. S. I. Weissman, *J. Chem. Phys.*, 1942, **10**, 214-217.
36. M. Kasha, *Discussions of the Faraday Society*, 1950, **9**, 14-19.
37. A. P. S. Samuel, J. Xu and K. N. Raymond, *Inorg. Chem.*, 2009, **48**, 687-698.
38. D. Parker, P. Kanthi Senanayake and J. A. Gareth Williams, *J. Chem. Soc., Perkin Trans. 2*, 1998, 2129-2140.
39. A. Beeby, D. Parker and J. A. G. Williams, *J. Chem. Soc., Perkin Trans. 2*, 1996, 1565-1579.
40. D. Parker and J. A. G. Williams, *J. Chem. Soc., Perkin Trans. 2*, 1996, 1581-1586.
41. S. Blair, R. Kataky and D. Parker, *New J. Chem.*, 2002, **26**, 530-535.
42. Y. Amao, I. Okura and T. Miyashita, *Chem. Lett.*, 2000, **29**, 934-935.

43. Y. Amao, I. Okura and T. Miyashita, *Bull. Chem. Soc. Jpn.*, 2000, **73**, 2663-2668.
44. G.-L. Law, R. Pal, L. O. Palsson, D. Parker and K.-L. Wong, *Chem. Commun.*, 2009, 7321-7323.
45. F. Kielar, C. P. Montgomery, E. J. New, D. Parker, R. A. Poole, S. L. Richardson and P. A. Stenson, *Org. Biomol. Chem.*, 2007, **5**, 2975-2982.
46. G.-L. Law, D. Parker, S. L. Richardson and K.-L. Wong, *Dalton Trans.*, 2009, 8481-8484.
47. R. A. Poole, F. Kielar, S. L. Richardson, P. A. Stenson and D. Parker, *Chem. Commun.*, 2006, 4084-4086.
48. S. Ghose, E. Trinquet, M. Laget, H. Bazin and G. Mathis, *J. Alloys Compd.*, 2008, **451**, 35-37.
49. R. S. Dickins, D. Parker, A. S. de Sousa and J. A. G. Williams, *Chem. Commun.*, 1996, 697-698.
50. J. I. Bruce, R. S. Dickins, L. J. Govenlock, T. Gunnlaugsson, S. Lopinski, M. P. Lowe, D. Parker, R. D. Peacock, J. J. B. Perry, S. Aime and M. Botta, *J. Am. Chem. Soc.*, 2000, **122**, 9674-9684.
51. S. E. Plush and T. Gunnlaugsson, *Org. Lett.*, 2007, **9**, 1919-1922.
52. A. Thibon and V. C. Pierre, *Anal. Bioanal. Chem.*, 2009, **394**, 107-120.
53. R. S. Dickins, T. Gunnlaugsson, D. Parker and R. D. Peacock, *Chem. Commun.*, 1998, 1643-1644.
54. S. J. A. Pope and R. H. Laye, *Dalton Trans.*, 2006, 3108-3113.
55. A. Beeby, I. M. Clarkson, R. S. Dickins, S. Faulkner, D. Parker, L. Royle, A. S. de Sousa, J. A. G. Williams and M. Woods, *J. Chem. Soc., Perkin Trans. 2*, 1999, 493-504.
56. Y. Haas and G. Stein, *J. Phys. Chem.*, 1972, **76**, 1093-1104.
57. D. Parker, *Coord. Chem. Rev.*, 2000, **205**, 109-130.
58. D. L. Dexter, *J. Chem. Phys.*, 1953, **21**, 836-850.
59. T. Förster, *Discussions of the Faraday Society*, 1959, **27**, 7-17.
60. N. N. Greenwood and A. Earnshaw, *Chemistry of the Elements*, Butterworth-Heinemann, Oxford ; Boston, 2nd edn., 1997.
61. S. Pandya, J. Yu and D. Parker, *Dalton Trans.*, 2006, 2757-2766.
62. C. K. Luk and F. S. Richardson, *J. Am. Chem. Soc.*, 1975, **97**, 6666-6675.
63. D. Parker, R. S. Dickins, H. Puschmann, C. Crossland and J. A. K. Howard, *Chem. Rev.*, 2002, **102**, 1977-2010.

64. J. Crassous, *Chem. Soc. Rev.*, 2009, **38**, 830-845.

65. J. Crassous, *Chem. Commun.*, 2012, **48**, 9684-9692.

66. S. D. Bonsall, M. Houcheime, D. A. Straus and G. Muller, *Chem. Commun.*, 2007, 3676-3678.

67. K. T. Hua, J. Xu, E. E. Quiroz, S. Lopez, A. J. Ingram, V. A. Johnson, A. R. Tisch, A. de Bettencourt-Dias, D. A. Straus and G. Muller, *Inorg. Chem.*, 2012, **51**, 647-660.

68. F. Stomeo, C. Lincheneau, J. P. Leonard, J. E. O'Brien, R. D. Peacock, C. P. McCoy and T. Gunnlaugsson, *J. Am. Chem. Soc.*, 2009, **131**, 9636-9637.

69. M. Seitz, E. G. Moore, A. J. Ingrarn, G. Muller and K. N. Raymond, *J. Am. Chem. Soc.*, 2007, **129**, 15468-15470.

70. M. Seitz, K. Do, A. J. Ingram, E. G. Moore, G. Muller and K. N. Raymond, *Inorg. Chem.*, 2009, **48**, 8469-8479.

71. A. P. S. Samuel, J. L. Lunkley, G. Muller and K. N. Raymond, *Eur. J. Inorg. Chem.*, 2010, 3343-3347.

72. J. L. Lunkley, D. Shirotani, K. Yamanari, S. Kaizaki and G. Muller, *J. Am. Chem. Soc.*, 2008, **130**, 13814-13815.

73. S. Di Pietro and L. Di Bari, *Inorg. Chem.*, 2012, **51**, 12007-12014.

74. D. Shirotani, T. Suzuki, K. Yamanari and S. Kaizaki, *J. Alloys Compd.*, 2008, **451**, 325-328.

75. D. Shirotani, T. Suzuki and S. Kaizaki, *Inorg. Chem.*, 2006, **45**, 6111-6113.

76. E. J. Corey and J. C. Bailar, *J. Am. Chem. Soc.*, 1959, **81**, 2620-2629.

77. L. Di Bari and P. Salvadori, *ChemPhysChem*, 2011, **12**, 1490-1497.

78. S. Aime, M. Botta, G. Ermondi, E. Terreno, P. L. Anelli, F. Fedeli and F. Uggeri, *Inorg. Chem.*, 1996, **35**, 2726-2736.

79. R. S. Ranganathan, N. Raju, H. Fan, X. Zhang, M. F. Tweedle, J. F. Desreux and V. Jacques, *Inorg. Chem.*, 2002, **41**, 6856-6866.

80. J. A. K. Howard, A. M. Kenwright, J. M. Moloney, D. Parker, M. Woods, M. Port, M. Navet and O. Rousseaux, *Chem. Commun.*, 1998, 1381-1382.

81. M. Woods, S. Aime, M. Botta, J. A. K. Howard, J. M. Moloney, M. Navet, D. Parker, M. Port and O. Rousseaux, *J. Am. Chem. Soc.*, 2000, **122**, 9781-9792.

82. L. Di Bari, G. Pintacuda and P. Salvadori, *Eur. J. Inorg. Chem.*, 2000, **2000**, 75-82.

83. M. Woods, Z. Kovacs, R. Kiraly, E. Brücher, S. Zhang and A. D. Sherry, *Inorg. Chem.*, 2004, **43**, 2845-2851.

84. R. S. Dickins, J. A. K. Howard, C. W. Lehmann, J. Moloney, D. Parker and R. D. Peacock, *Angew. Chem. Int. Ed. Engl.*, 1997, **36**, 521-523.

85. C. L. Maupin, R. S. Dickins, L. G. Govenlock, C. E. Mathieu, D. Parker, J. A. G. Williams and J. P. Riehl, *J. Phys. Chem. A*, 2000, **104**, 6709-6717.

86. R. S. Dickins, J. A. K. Howard, C. L. Maupin, J. M. Moloney, D. Parker, J. P. Riehl, G. Siligardi and J. A. G. Williams, *Chem. Eur. J.*, 1999, **5**, 1095-1105.

87. R. S. Dickins, J. A. K. Howard, J. M. Moloney, D. Parker, R. D. Peacock and G. Siligardi, *Chem. Commun.*, 1997, 1747-1748.

88. R. S. Dickins, J. A. K. Howard, C. L. Maupin, J. M. Moloney, D. Parker, R. D. Peacock, J. P. Riehl and G. Siligardi, *New J. Chem.*, 1998, **22**, 891-899.

89. L. Di Bari, G. Pescitelli, A. D. Sherry and M. Woods, *Inorg. Chem.*, 2005, **44**, 8391-8398.

90. G. Tircso, B. C. Webber, B. E. Kucera, V. G. Young and M. Woods, *Inorg. Chem.*, 2011, **50**, 7966-7979.

91. B. C. Webber and M. Woods, *Inorg. Chem.*, 2012, **51**, 8576-8582.

92. J. I. Bruce, D. Parker, S. Lopinski and R. D. Peacock, *Chirality*, 2002, **14**, 562-567.

93. J. L. Lunkley, D. Shirotani, K. Yamanari, S. Kaizaki and G. Muller, *Inorg. Chem.*, 2011, **50**, 12724-12732.

94. M. Iwamura, Y. Kimura, R. Miyamoto and K. Nozaki, *Inorg. Chem.*, 2012, **51**, 4094-4098.

95. N. R. Kelly, S. Goetz, S. R. Batten and P. E. Kruger, *CrystEngComm*, 2008, **10**, 68-78.

96. J.-C. G. Bünzli, L. J. Charbonniere and R. F. Ziessel, *J. Chem. Soc., Dalton Trans.*, 2000, 1917-1923.

97. H. G. Brittain, *Coord. Chem. Rev.*, 1983, **48**, 243-276.

98. G. L. Hilmes and J. P. Riehl, *Inorg. Chim. Acta*, 1987, **129**, 123-125.

99. F. Song, G. Wei, X. Jiang, F. Li, C. Zhu and Y. Cheng, *Chem. Commun.*, 2013, **49**, 5772-5774.

100. P. Pfeiffer and K. Quehl, *Ber. Dtsch. Chem. Ges.*, 1931, **64**, 2667-2671.

101. P. Pfeiffer and K. Quehl, *Ber. Dtsch. Chem. Ges.*, 1932, **65**, 560-565.

102. H. G. Brittain, *Inorg. Chem.*, 1981, **20**, 3007-3013.

103. I. Grenthe, *J. Am. Chem. Soc.*, 1961, **83**, 360-364.

104. F. Yan and H. G. Brittain, *Polyhedron*, 1982, **1**, 195-199.

105. G. L. Hilmes, J. M. Timper and J. P. Riehl, *Inorg. Chem.*, 1985, **24**, 1721-1723.

106. F. Yan, R. A. Copeland and H. G. Brittain, *Inorg. Chem.*, 1982, **21**, 1180-1185.

107. S. C. J. Meskers and H. P. J. M. Dekkers, *Spectrochim. Acta, Part A*, 1999, **55**, 1837-1855.

108. H. G. Brittain, *J. Chem. Soc., Dalton Trans.*, 1984, 1367-1370.

109. D. M. Kroupa, C. J. Brown, L. M. Heckman and T. A. Hopkins, *J. Phys. Chem. B*, 2012, **116**, 4952-4958.

110. G. Muller, *Dalton Trans.*, 2009, 9692-9707.

111. D. H. Metcalf, S. W. Snyder, J. N. Demas and F. S. Richardson, *J. Am. Chem. Soc.*, 1990, **112**, 5681-5695.

112. D. H. Metcalf, J. M. M. Stewart, S. W. Snyder, C. M. Grisham and F. S. Richardson, *Inorg. Chem.*, 1992, **31**, 2445-2455.

113. D. H. Metcalf, J. P. Bolender, M. S. Driver and F. S. Richardson, *J. Phys. Chem.*, 1993, **97**, 553-564.

114. T. G. Stockman, C. A. Klevickis, G. M. Grisham and F. S. Richardson, *J. Mol. Recognit.*, 1996, **9**, 595-606.

115. J. P. Bolender and F. S. Richardson, *Biophys. Chem.*, 2003, **105**, 293-322.

116. R. B. Rexwinkel, S. C. J. Meskers, H. P. J. M. Dekkers and J. P. Riehl, *J. Phys. Chem.*, 1992, **96**, 5725-5733.

117. R. B. Rexwinkel, S. C. J. Meskers, J. P. Riehl and H. P. J. M. Dekkers, *J. Phys. Chem.*, 1993, **97**, 3875-3884.

118. D. P. Glover-Fischer, D. H. Metcalf, J. P. Bolender and F. S. Richardson, *Chem. Phys.*, 1995, **198**, 207-234.

119. C. L. Maupin, S. C. J. Meskers, H. P. J. M. Dekkers and J. P. Riehl, *J. Phys. Chem. A*, 1998, **102**, 4450-4455.

120. T. A. Hopkins, D. H. Metcalf and F. S. Richardson, *Chirality*, 2008, **20**, 511-523.

121. F. S. Richardson, D. H. Metcalf and D. P. Glover, *J. Phys. Chem.*, 1991, **95**, 6249-6259.

122. S. C. J. Meskers, M. Ubbink, G. W. Canters and H. P. J. M. Dekkers, *J. Phys. Chem.*, 1996, **100**, 17957-17969.

123. S. C. J. Meskers, M. Ubbink, G. W. Canters and H. P. J. M. Dekkers, *J. Biol. Inorg. Chem.*, 1998, **3**, 463-469.

124. S. C. J. Meskers, C. Dennison, G. W. Canters and H. P. J. M. Dekkers, *J. Biol. Inorg. Chem.*, 1998, **3**, 663-670.

125. S. C. J. Meskers and H. P. J. M. Dekkers, *Spectrochim. Acta, Part A*, 1999, **55**, 1857-1874.

126. S. C. J. Meskers and H. P. J. M. Dekkers, *J. Am. Chem. Soc.*, 1998, **120**, 6413-6414.

127. R. S. Dickins, S. Aime, A. S. Batsanov, A. Beeby, M. Botta, J. I. Bruce, J. A. K. Howard, C. S. Love, D. Parker, R. D. Peacock and H. Puschmann, *J. Am. Chem. Soc.*, 2002, **124**, 12697-12705.

128. P. Atkinson, Y. Bretonnière, D. Parker and G. Muller, *Helv. Chim. Acta*, 2005, **88**, 391-405.

129. G. Bobba, S. D. Kean, D. Parker, A. Beeby and G. Baker, *J. Chem. Soc., Perkin Trans. 2*, 2001, 1738-1741.

130. D. G. Smith, R. Pal and D. Parker, *Chem. Eur. J.*, 2012, **18**, 11604-11613.

131. D. G. Smith, B. K. McMahon, R. Pal and D. Parker, *Chem. Commun.*, 2012, **48**, 8520-8522.

132. R. A. Poole, G. Bobba, M. J. Cann, J.-C. Frias, D. Parker and R. D. Peacock, *Org. Biomol. Chem.*, 2005, **3**, 1013-1024.

133. C. P. Montgomery, E. J. New, D. Parker and R. D. Peacock, *Chem. Commun.*, 2008, 4261-4263.

134. E. J. New, Understanding the cellular behaviour of luminescent lanthanide complexes, Ph.D. Thesis, Durham University, 2009.

135. E. J. New, D. Parker and R. D. Peacock, *Dalton Trans.*, 2009, 672-679.

136. D. M. Dias, J. M. C. Teixeira, I. Kuprov, E. J. New, D. Parker and C. F. G. C. Geraldes, *Org. Biomol. Chem.*, 2011, **9**, 5047-5050.

137. G.-L. Law, C. Man, D. Parker and J. W. Walton, *Chem. Commun.*, 2010, **46**, 2391-2393.

138. P. Atkinson, K. S. Findlay, F. Kielar, R. Pal, D. Parker, R. A. Poole, H. Puschmann, S. L. Richardson, P. A. Stenson, A. L. Thompson and J. H. Yu, *Org. Biomol. Chem.*, 2006, **4**, 1707-1722.

139. C. P. Montgomery, Luminescent lanthanide complexes as cellular imaging agents or HTRF assay components, Ph.D. Thesis, Durham University, 2009.

140. K. H. Chalmers, Fluorinated Paramagnetic Probes for 19-F and 1-H MRS/MRI, Ph.D. Thesis, Durham University, 2011.

141. Z. Kovacs and A. D. Sherry, *J. Chem. Soc., Chem. Commun.*, 1995, 185-186.

142. C. Görller-Walrand, E. Huygen, K. Binnemans and L. Fluyt, *J. Phys.: Condens. Matter*, 1994, **6**, 7797.

143. N. L. Anderson and N. G. Anderson, *Mol. Cell. Proteomics*, 2002, **1**, 845-867.

144. C. Gabay and I. Kushner, *N. Engl. J. Med.*, 1999, **340**, 448-454.

145. J. Ghuman, P. A. Zunszain, I. Petitpas, A. A. Bhattacharya, M. Otagiri and S. Curry, *J. Mol. Biol.*, 2005, **353**, 38-52.

146. D. L. Schönfeld, R. B. G. Ravelli, U. Mueller and A. Skerra, *J. Mol. Biol.*, 2008, **384**, 393-405.

147. P. G. Sammes and G. Yahioglu, *Nat. Prod. Rep.*, 1996, **13**, 1-28.

148. S. Sugio, A. Kashima, S. Mochizuki, M. Noda and K. Kobayashi, *Protein Eng.*, 1999, **12**, 439-446.

149. L. Dente, G. Ciliberto and R. Cortese, *Nucleic Acids Res.*, 1985, **13**, 3941-3952.

150. Y. Ye and A. Godzik, *Nucleic Acids Res.*, 2004, **32**, W582-W585.

151. Y. Ye and A. Godzik, *Protein Sci.*, 2004, **13**, 1841-1850.

152. D. Parker, J. W. Walton, L. Lamarque and J. M. Zwier, *Eur. J. Inorg. Chem.*, 2010, **2010**, 3961-3966.

153. G. L. Trainor, *Expert Opin. Drug Discovery*, 2007, **2**, 51-64.

154. K. M. Wasan, D. R. Brocks, S. D. Lee, K. Sachs-Barrable and S. J. Thornton, *Nat. Rev. Drug Discov.*, 2008, **7**, 84-99.

155. F. Hervé, G. Caron, J.-C. Duché, P. Gaillard, N. Abd. Rahman, A. Tsantili-Kakoulidou, P.-A. Carrupt, P. d'Athis, J.-P. Tillement and B. Testa, *Mol. Pharmacol.*, 1998, **54**, 129-138.

156. F. Zsila and Y. Iwao, *Biochim. Biophys. Acta*, 2007, **1770**, 797-809.

157. K. Nishi, T. Ono, T. Nakamura, N. Fukunaga, M. Izumi, H. Watanabe, A. Suenaga, T. Maruyama, Y. Yamagata, S. Curry and M. Otagiri, *J. Biol. Chem.*, 2011, **286**, 14427-14434.

158. D. M. Corsi, C. Platas-Iglesias, H. v. Bekkum and J. A. Peters, *Magn. Reson. Chem.*, 2001, **39**, 723-726.

159. *The Chemistry of Contrast Agents in Medical Magnetic Resonance Imaging*, eds. A. E. Merbach and E. Tóth, Wiley, New York ; Chichester, 2001.

160. Y. Bretonniere, M. J. Cann, D. Parker and R. Slater, *Org. Biomol. Chem.*, 2004, **2**, 1624-1632.

161. R. Pal, A. Beeby and D. Parker, *J. Pharm. Biomed. Anal.*, 2011, **56**, 352-358.

162. S. Colombo, T. Buclin, L. A. Decosterd, A. Telenti, H. Furrer, B. L. Lee, J. Biollaz, C. B. Eap and H. I. V. C. S. Swiss, *Clin. Pharmacol. Ther.*, 2006, **80**, 307-318.

163. D. Parker, *Chem. Rev.*, 1991, **91**, 1441-1457.

164. T. E. Beesley and R. P. W. Scott, *Chiral Chromatography*, Wiley, 1998.

165. J. M. Seco, E. Quiñoá and R. Riguera, *Chem. Rev.*, 2004, **104**, 17-118.

166. S. J. Butler and D. Parker, *Chem. Soc. Rev.*, 2013, **42**, 1652-1666.

167. W. D. McElroy and B. Glass, *Phosphorus Metabolism*, vol. 1, Johns Hopkins University Press, 1951.

168. W. L. F. Armarego and C. Chai, *Purification of Laboratory Chemicals*, Elsevier Science, 2009.

169. R. M. C. Dawson, *Data for Biochemical Research*, Clarendon Press, Oxford, 1959.

170. J. Bjerrum, *Stability Constants of Metal-Ion Complexes, with Solubility Products of Inorganic Substances: Inorganic Ligands*, Chemical Society, London, 1958.

171. P. Atkinson, Y. Bretonniere and D. Parker, *Chem. Commun.*, 2004, 438-439.

172. S. J. Butler, B. K. McMahon, R. Pal, D. Parker and J. W. Walton, *Chem. Eur. J.*, 2013, **19**, 9511-9517.

173. R. Carr, R. Puckrin, B. K. McMahon, R. Pal, D. Parker and L. O. Palsson, *Methods Appl. Fluoresc.*, 2014, in press.

174. J. P. Bolender, A. Meyers, J. Cordaro and R. S. Ries, *Chirality*, 2002, **14**, 456-464.

175. J. R. Lakowicz, *Principles of Fluorescence Spectroscopy*, Springer, New York, 3rd edn., 2006.

176. T. Cordes, J. Vogelsang and P. Tinnefeld, *J. Am. Chem. Soc.*, 2009, **131**, 5018-5019.

177. S. Steenken and P. Neta, *J. Phys. Chem.*, 1979, **83**, 1134-1137.

178. S. Steenken and P. Neta, *J. Phys. Chem.*, 1982, **86**, 3661-3667.

179. C. Gateau, M. Mazzanti, J. Pecaut, F. A. Dunand and L. Helm, *Dalton Trans.*, 2003, 2428-2433.

180. G. Nocton, A. Nonat, C. Gateau and M. Mazzanti, *Helv. Chim. Acta*, 2009, **92**, 2257-2273.

181. J. W. Walton, R. Carr, N. H. Evans, A. M. Funk, A. M. Kenwright, D. Parker, D. S. Yufit, M. Botta, S. De Pinto and K. L. Wong, *Inorg. Chem.*, 2012, **51**, 8042-8056.

182. L. Charbonnière, R. Ziessel, M. Guardigli, A. Roda, N. Sabbatini and M. Cesario, *J. Am. Chem. Soc.*, 2001, **123**, 2436-2437.

183. J. Schlesinger, J. Rajander, J. A. Ihalainen, D. Ramesh, P. Eklund, V. Fagerholm, P. Nuutila and O. Solin, *Inorg. Chem.*, 2011, **50**, 4260-4271.

184. A. S. Craig, I. M. Helps, K. J. Jankowski, D. Parker, N. R. A. Beeley, B. A. Boyce, M. A. W. Eaton, A. T. Millican, K. Millar, A. Phipps, S. K. Rhind, A. Harrison and C. Walker, *J. Chem. Soc., Chem. Commun.*, 1989, 794-796.

185. J. P. L. Cox, A. S. Craig, I. M. Helps, K. J. Jankowski, D. Parker, M. A. W. Eaton, A. T. Millican, K. Millar, N. R. A. Beeley and B. A. Boyce, *J. Chem. Soc., Perkin Trans. 1*, 1990, 2567-2576.

186. N. H. Evans, R. Carr, M. Delbianco, R. Pal, D. S. Yufit and D. Parker, *Dalton Trans.*, 2013, **42**, 15610-15616.

187. *Stereochemical and Stereophysical Behaviour of Macrocycles*, ed. I. Bernal, Elsevier Science, 1987.

188. J. W. Walton, Highly Emissive Europium Complexes, Ph.D. Thesis, Durham University, 2012.

189. K. Wieghardt, U. Bossek, P. Chaudhuri, W. Herrmann, B. C. Menke and J. Weiss, *Inorg. Chem.*, 1982, **21**, 4308-4314.

190. L. Porrès, A. Holland, L.-O. Pålsson, A. Monkman, C. Kemp and A. Beeby, *J. Fluoresc.*, 2006, **16**, 267-273.

191. G. Sheldrick, *Acta. Cryst. Sect. A*, 2008, **64**, 112-122.

192. O. V. Dolomanov, L. J. Bourhis, R. J. Gildea, J. A. K. Howard and H. Puschmann, *J. Appl. Crystallogr.*, 2009, **42**, 339-341.

193. H. Flack, *Acta. Cryst. Sect. A*, 1983, **39**, 876-881.

194. R. W. W. Hooft, L. H. Straver and A. L. Spek, *J. Appl. Crystallogr.*, 2010, **43**, 665-668.

195. J. W. Walton, A. Bourdolle, S. J. Butler, M. Soulie, M. Delbianco, B. K. McMahon, R. Pal, H. Puschmann, J. M. Zwier, L. Lamarque, O. Maury, C. Andraud and D. Parker, *Chem. Commun.*, 2013, **49**, 1600-1602.

196. P. Nantka-Namirski and J. Piechaczek, *Pol. J. Pharmacol. Pharm.*, 1974, **26**, 545-548.

197. P. Nantka-Namirski and J. Piechaczek, *Pol. J. Pharmacol. Pharm.*, 1976, **28**, 89-94.

198. *Br. Pat.*, GB2467012-A; WO2010084090-A1, 2010.

199. Z. Kovacs and A. D. Sherry, *Synthesis*, 1997, 759 - 763.

200. M. L. Gilbert, G. M. Brown, J. E. Elbert and R. A. Sachleben, *Tetrahedron Lett.*, 1993, **34**, 5531-5534.

201. S. Laurent, L. Vander Elst, S. Houzé, N. Guérit and R. N. Muller, *Helv. Chim. Acta*, 2000, **83**, 394-406.

202. H. Lei and J. Atkinson, *J. Org. Chem.*, 2000, **65**, 2560-2567.

APPENDICES

APPENDIX ONE - CRYSTAL DATA

Table A1: Crystal data and structure refinement for (*R*)-[Co.**L**^{37}].

Empirical formula	$C_{19}H_{24}N_3O_6Co$
Formula weight	449.34
Temperature/K	120
Crystal system	monoclinic
Space group	$P2_1$
a/Å	8.9747(7)
b/Å	7.4776(6)
c/Å	15.0100(12)
α/°	90.00
β/°	107.20(3)
γ/°	90.00
Volume/Å^3	962.28(13)
Z	2
ρ_{calc}mg/mm^3	1.551
m/mm^{-1}	0.864
F(000)	468.0
Crystal size/mm^3	0.05 × 0.04 × 0.001
2Θ range for data collection	2.76 to 53°
Index ranges	$-11 \leq h \leq 11$, $-9 \leq k \leq 7$, $-11 \leq l \leq 19$
Reflections collected	6473
Independent reflections	3721[R(int) = 0.0541]
Data/restraints/parameters	3721/1/262
Goodness-of-fit on F^2	1.081
Final R indexes [I>=2σ (I)]	R_1 = 0.0693, wR_2 = 0.1772
Final R indexes [all data]	R_1 = 0.0911, wR_2 = 0.1916
Largest diff. peak/hole / e Å^{-3}	1.18/-1.02
Flack parameter	0.06(4)